



8-2008

Development and Implementation of Mathematical Modeling, Vibration and Acoustic Emission Technique to Correlate *In Vivo* Kinematics, Kinetics and Sound in Total Hip Arthroplasty with Different Bearing Surfaces

Diana Andreeva Glaser
University of Tennessee - Knoxville

Follow this and additional works at: https://trace.tennessee.edu/utk_graddiss



Part of the [Mechanical Engineering Commons](#)

Recommended Citation

Glaser, Diana Andreeva, "Development and Implementation of Mathematical Modeling, Vibration and Acoustic Emission Technique to Correlate *In Vivo* Kinematics, Kinetics and Sound in Total Hip Arthroplasty with Different Bearing Surfaces. " PhD diss., University of Tennessee, 2008.
https://trace.tennessee.edu/utk_graddiss/437

This Dissertation is brought to you for free and open access by the Graduate School at TRACE: Tennessee Research and Creative Exchange. It has been accepted for inclusion in Doctoral Dissertations by an authorized administrator of TRACE: Tennessee Research and Creative Exchange. For more information, please contact trace@utk.edu.

To the Graduate Council:

I am submitting herewith a dissertation written by Diana Andreeva Glaser entitled "Development and Implementation of Mathematical Modeling, Vibration and Acoustic Emission Technique to Correlate *In Vivo* Kinematics, Kinetics and Sound in Total Hip Arthroplasty with Different Bearing Surfaces." I have examined the final electronic copy of this dissertation for form and content and recommend that it be accepted in partial fulfillment of the requirements for the degree of Doctor of Philosophy, with a major in Mechanical Engineering.

Richard D. Komistek, Major Professor

We have read this dissertation and recommend its acceptance:

Mohamed R. Mahfouz, William R. Hamel, Syed K. Islam

Accepted for the Council:

Carolyn R. Hodges

Vice Provost and Dean of the Graduate School

(Original signatures are on file with official student records.)

To the Graduate Council:

I am submitting herewith a dissertation written by Diana Andreeva Glaser entitled "Development and Implementation of Mathematical Modeling, Vibration and Acoustic Emission Technique to Correlate *In Vivo* Kinematics, Kinetics and Sound in Total Hip Arthroplasty with Different Bearing Surfaces." I have examined the final electronic copy of this dissertation for form and content and recommend that it be accepted in partial fulfillment of the requirements for the degree of Doctor of Philosophy with a major in Mechanical Engineering.

Richard D. Komistek
Major Professor

We have read this dissertation
and recommend its acceptance:

Mohamed R. Mahfouz

William R. Hamel

Syed K. Islam

Accepted for the Council:

Carolyn R. Hodges
Vice Provost and Dean of the
Graduate School

(Original signatures are on file with official student records.)

Development and Implementation of
Mathematical Modeling,
Vibration and Acoustic Emission Technique
to Correlate *In Vivo* Kinematics, Kinetics and Sound
in Total Hip Arthroplasty with Different Bearing Surfaces

A Dissertation
Presented for the
Doctor of Philosophy Degree
The University of Tennessee, Knoxville

Diana Andreeva Glaser
August 2008

Copyright © 2008 by Diana A Glaser
All rights reserved.

Dedication

My dissertation is dedicated to my family who supported me on every step of my way. I would like to thank my husband, Thomas Glaser, for giving me so much encouragement and for his assistance whenever he was needed. I would especially like to thank my parents Andrey and Tatiana Gueorguievi who taught me the value of education, and for their belief that I can achieve everything I wish.

Acknowledgments

With great respect, I would like to thank Dr. Richard Komistek, my major professor, for guiding me with immaculate skill, for the countless opportunities he offered me to expand my horizon and for the freedom to pursue various projects without objection. He always motivated me to go a step further and helped me follow my goals. I would like to thank Dr. Mohamed Mahfouz for his advice and thoughtful comments. I owe my most sincere gratitude to Harold Cates MD, who gave me the opportunity to work with his patients and supported me all the way through my research. Thanks particularly to Dr. Hamel for his input and his engagement in student issues. I also would like to express my thanks to Dr. Islam for serving on my committee. My special thanks go to Ada Pfohl and Rebecca Robertson who helped me through the administrative part of my study and work. My warm thanks are due to Monica Schmidt for her advice and support by dealing with hospital and patient issues.

Last but not least, I would like to thank my colleagues and co-students at the University of Tennessee's Center for Musculoskeletal Research, especially Kourtney Henderson and Stuart Deaderick. I would like to thank also the rest of our graduate team for supporting me during my fluoroscopic experiments.

Abstract

The evaluation of Total Hip Arthroplasty (THA) outcome is difficult and invasive methods are often applied. Fluoroscopy has been used as an *in vivo* diagnostic technique to determine separation which may lead to vibration propagation and audible interactions. The objective of this study was to develop a new, non-invasive technique of digitally capturing vibration and sound emissions at the hip joint interface and to correlate those with the hip kinematics derived from fluoroscopy. Additionally, an examination of the role of hip mechanics on walking performance in THA subjects of various bearings surfaces was performed.

In vivo kinematics, kinetics, corresponding vibration and sound measurements of THA were analyzed post-operatively using video-fluoroscopy, mathematical modeling, sound sensors and accelerometers during gait on a treadmill. Twenty-seven subjects (31 hips) with a metal-on-metal, metal-on-polyethylene, ceramic-on-ceramic, ceramic-on-polyethylene or metal-on-metal polyethylene-sandwich THA were analyzed. A data acquisition system was used to amplify the signal and filter out associated frequencies attributed to noise. The sound measurements were correlated to *in vivo* kinematics. A mathematical model of the human extremity was derived to determine *in vivo* bearing and soft-tissue forces.

For all bearings a distinct correlation of a high frequency sound occurring at the time when the femoral head slides back into the acetabular component was observed. Subjects having a hard-on-hard bearing seemed to attenuate a squeaking and/or

impacting sound, while those having polyethylene liner only revealed a knocking sound attributed to impact loading conditions.

For the first time, audible effects can be derived *in vivo* and the examined correlation brings valuable insight into the hip joint performance in an inexpensive and non-invasive manner. This research may allow for a further correlation to be derived between sound and different types of failure mechanisms. Results from this study will give surgeons and engineers a better understanding of *in vivo* mechanics of the hip joint and this way improve the quality of life of THA patients. In addition, the developed technique builds the first milestone in the design and implementation of a cost effective, non-invasive diagnostic technique which has the potential to become a routine diagnosis of joint conditions.

Table of Contents

Chapter 1	Introduction and Previous Work	1
1.1	<i>Different Bearing Surfaces for THA.....</i>	2
1.2	<i>Femoral Head Separation.....</i>	4
1.3	<i>Hip Squeaking.....</i>	6
1.4	<i>Implant Loosening.....</i>	8
1.5	<i>Diagnostic Techniques.....</i>	9
1.6	<i>Acoustic Analysis</i>	11
1.7	<i>Vibration Analysis</i>	13
1.8	<i>Hip Kinetics.....</i>	18
1.9	<i>Ground Reaction Forces.....</i>	20
1.10	<i>Study Propose</i>	22
1.10.1	Study objectives.....	24
1.10.2	Study design	25
1.11	<i>Dissertation Contribution.....</i>	26
Chapter 2	Background.....	29
2.1	<i>Hip Muscles</i>	29
2.1.1	Hip flexors.....	29
2.1.1.1	Iliopsoas.....	29
2.1.1.2	Rectus Femoris.....	30
2.1.1.3	Tensor Fascia Latae	30
2.1.2	Hip extensors.....	31
2.1.2.1	Gluteus.....	31
2.1.2.2	Hamstring	31
2.1.2.3	Hip Ligaments.....	32
2.2	<i>Muscles Activity during Gait Cycle</i>	32
2.2.1	Stance phase.....	32
2.2.1.1	Loading Response LR (0 to 12 percent of gait cycle)	32
2.2.1.2	Midstance (12 to 31 percent of gait cycle).....	34
2.2.1.3	Terminal Stance (31 to 50 percent of gait cycle).....	34
2.2.1.4	Pre-swing (50 to 62 percent of gait cycle)	35
2.2.2	Swing phase	35
2.2.2.1	Initial Swing.....	35
2.2.2.2	Mid-swing.....	36
2.2.2.3	Terminal Swing	36

2.3	<i>Arthritis</i>	36
2.4	<i>Total Hip Arthroplasty</i>	38
Chapter 3	Experimental Set-Up and Data Acquisition	41
3.1	<i>Subjects</i>	41
3.2	<i>Test Preparations</i>	42
3.3	<i>Patient Selection</i>	43
3.4	<i>Fluoroscopy</i>	46
3.4.1	Tracking of several gait cycles using single video-fluoroscope.....	46
3.4.2	The fluoroscopic unit.....	47
3.4.3	Radiation safety	47
3.4.4	Fluoroscopic image capture.....	48
3.5	<i>Force Plate Measurements</i>	49
3.6	<i>The New Acoustic and Vibration Analysis Technique</i>	53
3.7	<i>Data Acquisition - DAQ</i>	55
3.8	<i>Software Synchronization of two Video and multiple Data Acquisition Signals</i>	55
Chapter 4	Data Processing and Analysis	58
4.1	<i>3-D to 2-D Registration Analysis</i>	58
4.1.1	3D reconstruction procedure.....	58
4.1.2	Algorithm.....	59
4.2	<i>Kinematic Analysis</i>	61
4.3	<i>Gait Analysis</i>	63
4.4	<i>Ground Reaction Forces</i>	64
4.5	<i>Vibration and Acoustic Analysis</i>	67
4.5.1	Sound basics	67
4.5.2	Vibration basics	70
4.5.3	Vibration and sound processing.....	71
4.5.3.1	Noise cancellation.....	72
4.5.3.2	Fourier Transform	73
4.5.3.3	Joint transmissibility, impulse response and transfer function	75
4.5.3.4	Wavelet.....	78
4.6	<i>Calibration, Filtering and Error Analysis</i>	83
4.6.1	Distortion correction.....	83
4.6.2	Fluoroscopic error analysis.....	85

4.6.3	Acoustic and vibration measurement calibration and validation.....	86
Chapter 5	3D Mathematical Modeling.....	88
5.1	<i>Introduction</i>	89
5.2	<i>Coupling the measurement reference frames</i>	90
5.3	<i>Skeletal Modeling</i>	90
5.3.1	Model inputs	94
5.3.2	Rotation angles.....	94
5.3.3	Moving contacts.....	96
5.3.4	Muscles and ligaments	97
5.3.5	Kane's dynamics.....	99
5.3.6	Equations of motion	103
5.3.7	Inertial parameters and dimensioning.....	104
Chapter 6	Statistical Analysis	106
Chapter 7	Results.....	107
7.1	<i>Kinematics and Separation</i>	107
7.2	<i>Gait Analysis</i>	112
7.3	<i>3D Kinetics</i>	113
7.4	<i>Ground Reaction Forces</i>	115
7.5	<i>Correlation of Separation with Sound and Vibration</i>	117
7.6	<i>Vibration Analysis</i>	119
Chapter 8	Discussion.....	123
8.1	<i>Kinematic Analysis</i>	126
8.2	<i>Gait Analysis</i>	130
8.3	<i>Kinetic Analysis</i>	131
8.4	<i>Ground Reaction Forces</i>	133
8.5	<i>Correlation of Kinematics, Sound and Vibration</i>	138
8.6	<i>Acoustic and Vibration Technique</i>	141
8.7	<i>Summary</i>	142
Chapter 9	Study Limitations and Future Work	144
	References.....	149

Appendix A: Patient Questionnaire	174
Appendix B: Surgeon’s Questionnaire in Electronical Format	177
Appendix D: Tables.....	183
Appendix C: Figures	199
Vita.....	250

List of Tables

Table 1: Patients' demographics	183
Table 2: Maximum separation, mid range laxity and number of patients with capsular repair	184
Table 3: Analog signal connector pin-out for the force plate	184
Table 4: Gait analysis parameters and symmetry indices for all unilateral patients	185
Table 5: Gait analysis parameters and symmetry indices for all bilateral patients	186
Table 6: Segment dimensions.....	187
Table 7: Mass moment of inertia	188
Table 8: Segment Masses.....	188
Table 9: Patients included in the kinematic and GRF analysis.....	188
Table 10: Significant difference among the different groups	189
Table 11: Resultant forces for the different bearing groups at the joint interactions, and at the muscles and ligaments	189
Table 12: Results for the vertical ground reaction force parameters	190
Table 13: Results for the anterior-posterior (x) ground reaction force parameters	191
Table 14: Results for the medio-lateral (y) ground reaction force parameters.....	192
Table 15: Results for the statistical analysis of the ground reaction forces	193
Table 16: Maximum Vertical Ground Reaction Forces and Location in the Gait Cycle	194
Table 17: Swing, stance and total gait cycle times.....	195
Table 18: Bearing and sound correlation.....	196
Table 19: Comparison of our femoral frequency results to previous research	197

List of Figures

Figure 1: Flow chart of the research plan	199
Figure 2: Research overview.....	200
Figure 3: Osteoarthritis in the Hip (Orthopaedic Associates, 2008).....	200
Figure 4: Schematic diagram of instrumentation for acoustic and vibration analysis combined with fluoroscopic-video-capturing system and ground reaction force measurement.....	201
Figure 5: Fluoroscopy Machine with Treadmill and Subject [left]; Top View of Fluoroscopy Machine, Image of Radiation Source to Image Intensifier [right]..	202
Figure 6: Example fluoroscopic image of a hip joint in a view from AP direction	202
Figure 7: Example fluoroscopic image of a hip joint with the implant components in pose	203
Figure 8: Example fluoroscopic image with overlaid implant components.....	203
Figure 9: Force plate with sensor description (AccuGait, 2005)	203
Figure 10: Application created to read, calibrate, calculate and analyze the signals...	204
Figure 11: Walking direction on top of the force plate	204
Figure 12: PCB Tri-axial accelerometer compared with penny	204
Figure 13: Sound sensor compared with a Quarter.....	205
Figure 14: Interface of the new software for synchronization of video and data acquisition signals	205
Figure 15: An Example for 3-D CAD Model Matching Projected Fluoroscopy Image Silhouette for a knee joint implant.....	206
Figure 16: An Example for 3-D CAD model matching projected fluoroscopy image silhouette for a hip joint implant	206

Figure 17: Full Sequence of Analyzed Images with 3-D Models Overlaid	207
Figure 18: Fluoroscopic image, 3D registered implant components and a 3D view of the hip joint implant pose	207
Figure 19: 3D view of the hip joint implant positions after successful 3D kinematics reconstruction	208
Figure 20: The distance D between the center of the femoral head and the acetabular component is denoted as hip joint separation when it exceeds 0.5mm	208
Figure 21: Example flexion/extension of the hip during the entire gait cycle	209
Figure 22: Example internal/external rotation of the hip during the entire gait cycle ...	209
Figure 23: Example abduction/adduction rotation of the hip during the entire gait	209
Figure 24: Graphical representation of the GRF parameters in x-direction	210
Figure 25: Graphical representation of the GRF parameters in x-direction	210
Figure 26: Graphical representation of the GRF parameters in y-direction	211
Figure 27: Example of STFT signal analysis. Left: Signal in time domain (x-Axis: Time in % of gait cycle starting with toe off, y-Axis: Signal Amplitude); Right: Time-frequency spectrogram (x-Axis: Time in % of gait cycle starting with toe off, y-Axis: Frequency in Hz)	211
Figure 28: Noise profile (top: noise in the time domain, bottom: spectrogram of the noise).....	212
Figure 29: Filtered noise profile (top: noise in the time domain, bottom: spectrogram of the noise).....	212
Figure 30: Diagram of the Fourier Transform and the Short-Time Fourier Transform .	213
Figure 31: Diagram of the Wavelet analysis.....	213
Figure 32: Diagram of the one dimensional DWT analysis for 3 level analysis	214
Figure 33: Different mother wavelets and scaling functions	215

Figure 34: DB6 wavelet applied in the analysis.....	215
Figure 35: Example of signal analysis and decomposition in squeaking and knocking components. Left: Signal in time domain (x-Axis: Time in % of gait cycle starting with toe off, y-Axis: Signal Amplitude); Right: Time-frequency spectrogram (x-Axis: Time in % of gait cycle starting with toe off, y-Axis: Frequency in Hz)	216
Figure 36: Original image of bead-board used for distortion correction (top left), cleaned up bead-board (top right), beads identified from Matlab application (bottom left) and un-warped/corrected bead-board image.....	217
Figure 37: Beam vibration measurement with both accelerometer to test synchronization, cross talk and proper orientation of the axis	217
Figure 38: Signal generated from the calibrator and recorded by the accelerometer..	218
Figure 39: Measured frequency produced by the calibrator	218
Figure 40: Soft tissue movement.....	219
Figure 41: Muscle contractions	219
Figure 42: Coupling of the different measurement reference frames	220
Figure 43: 3D Schematic of the Leg.....	220
Figure 44: Rotation of the foot with respect to the ground during the entire gait cycle	221
Figure 45: Rotation of the ankle with respect to the foot during the entire gait cycle...	221
Figure 46: Rotation of the knee during the entire gait cycle	221
Figure 47: Example ground reaction forces.....	222
Figure 48: Contact point of foot with ground.....	222
Figure 49: Tibio-Femoral Contact During the Stand Phase: contact point on the tibia [left], contact point on the femur [right]	223
Figure 50: AP Position of the knee contact point on the tibia during the stance phase of gait with respect to the central axis of the tibia	223

Figure 51: AP Position of the knee contact point on the tibia during the entire gait cycle with respect to the central axis of the tibia	223
Figure 52: AP and SI position of the knee contact point on the femur during the stance phase of gait with respect to the central axis of the femur	224
Figure 53: AP position of the knee contact point on the femur during the entire gait cycle with respect to the central axis of the femur.....	224
Figure 54: SI position of the knee contact point on the femur during the entire gait cycle with respect to the central axis of the femur	225
Figure 55: AP position of the hip contact point on the femur during the entire gait cycle from the center of the femoral head.....	225
Figure 56: SI position of the hip contact point on the femur during the entire gait cycle from the center of the femoral head.....	225
Figure 57: AP position of the hip contact point on the pelvis during the entire gait cycle from the center of the femoral head.....	226
Figure 58: SI position of the hip contact point on the pelvis during the entire gait cycle from the center of the femoral head.....	226
Figure 59: Change of the length in patellar ligament and quadriceps.	226
Figure 60: Closed loop patellar ligament – patella – quadriceps chain and free body diagram	227
Figure 61: Hip joint capsule.....	227
Figure 62: Schematic representation of the hip joint ligaments as defined in the model	228
Figure 63: Dimension Measurement of CT scanned Cadaver using Rapidform.....	228
Figure 64: Sequential rotations: a) original reference frame, b)-d) sequential rotations in 3-1-2 order, e) original and final orientation of the reference frame.....	229

Figure 65: Average separation (red) and \pm 1SD (standard variation, blue) for a) MOP, b) COP and c) MOM-PS groups	229
Figure 66: Average separation (red) and \pm 1SD (standard variation, blue) for a) MOM Zimmer large head, b) MOM Biomet large head, c) MOM Biomet medium head and d) all MOM groups	230
Figure 67: Average separation (red) and \pm 1SD (standard variation, blue) for a) hard on soft bearings and b) hard-on-hard bearings groups.....	231
Figure 68: The average maximum separation with standard deviation (SD) for all groups	231
Figure 69: Separation for a large femoral head implant	232
Figure 70: The location of the maximum separation for each patient during the entire gait cycle	232
Figure 71: Correlation of separation and sound signal for M/M-PS patient. HS: heel strike, TO: toe-off.....	233
Figure 72: Iliofemoral ligament forces for both fibers and the entire Iliofemoral force (F_IA) for an example patient	233
Figure 73: Ischiofemoral ligament forces for all 6 fibers and the entire ischiofemoral force (F_IP) for an example patient	234
Figure 74: Iliofemoral and the Ischiofemoral ligament forces for an example patient .	234
Figure 75: Patellar ligament, quadriceps and patellar force for an example patient	235
Figure 76: Joint reaction forces for the ankle and the knee as well as ground reaction forces for an example patient.	235
Figure 77: Hip contact forces for the different bearing groups.....	236
Figure 78: Ground reaction forces for the metal-on-polyethylene group – top left: average forces, top right: vertical average force with SD intervals, bottom left:	

average force in x-direction with SD intervals, bottom right: average force in y-direction with SD intervals.	236
Figure 79: Ground reaction forces for the ceramic-on-polyethylene group – top left: average forces, top right: vertical average force with SD intervals, bottom left: average force in x-direction with SD intervals, bottom right: average force in y-direction with SD intervals.	237
Figure 80: Ground reaction forces for the metal-on-metal group – top left: average forces, top right: vertical average force with SD intervals, bottom left: average force in x-direction with SD intervals, bottom right: average force in y-direction with SD intervals.....	237
Figure 81: Ground reaction forces for the metal-on-metal polyethylene-sandwich group – top left: average forces, top right: vertical average force with SD intervals, bottom left: average force in x-direction with SD intervals, bottom right: average force in y-direction with SD intervals.....	238
Figure 82: Ground reaction forces for the ceramic-on-ceramic group – top left: average forces, top right: vertical average force with SD intervals, bottom left: average force in x-direction with SD intervals, bottom right: average force in y-direction with SD intervals.....	238
Figure 83: Correlation of separation (red) and sound (blue) signal for example patients. a) damp knocking, b) and c) knocking, d) and e) squeaking combined with some knocking components. Left: Signal in time domain (x-Axis: Time in % of gait cycle starting with toe off, y-Axis: Signal Amplitude); Right: Time-frequency spectrogram (x-Axis: Time in % of gait cycle, y-Axis: Frequency in Hz).....	239
Figure 84: Signal from accelerometers attached to femur and pelvis, showing the various vibration patterns. HS: heel strike, TO: toe-off	240
Figure 85: Acceleration signal measured on two example patients.....	240
Figure 86: Frequency content	241

Figure 87: Isolated areas of the signal	241
Figure 88: Frequency content of the isolated time interval	241
Figure 89: Waveform identified with MOM patients	242
Figure 90: Frequency content of a MOM patient	242
Figure 91: Pseudospectrum of a MOM patient	242
Figure 92: ‘Rusty door hinge’ signal wave form, FFT and transfer function.....	243
Figure 93: Crepitus signal wave form, FFT and transfer function	243
Figure 94: ‘Rusty door hinge’ signal wavelet analysis function.....	244
Figure 95: Crepitus signal wavelet analysis	244
Figure 96: Signal of a MOM patient: wave form, transfer function and wavelet analysis function	245
Figure 97: Signal of a MOM patient: wave form, transfer function and wavelet analysis function	245
Figure 98: Signal of a MOM patient: wave form, transfer function and wavelet analysis function	245
Figure 99: Signal of a COP patient: wave form, transfer function and wavelet analysis function	246
Figure 100: Signal of a MOM patient with small diameter femoral head: wave form, transfer function and wavelet analysis function	246
Figure 101: Signal of a MOM-PS patient: wave form, transfer function and wavelet analysis function	246
Figure 102: Signal of a MOM-PS patient: wave form, transfer function and wavelet analysis function	247
Figure 103: Signal of a MOP patient: wave form, transfer function and wavelet analysis function	247

Figure 104: Signal of a COC patient: wave form, transfer function and wavelet analysis function 247

Figure 105: Wavelet analysis and denoising for an example signal: approximation and detail coefficients 248

Figure 106: 3-Level wavelet tree and analysis of the (3,1) level..... 249

Nomenclature

g	acceleration of gravity
Hz	Hertz
in	inch
MPa	mega Pascal
MPH	Miles per Hours
mV	milli Volt
N	Newton
pC	pico Coulomb
RMS	Root-mean-square

Abbreviations:

2D	Two dimensional
3D	Three dimensional
AP	Anterior-Posterior
ML	Medial-Lateral
SI	Superior-Inferior
BW	Body Weight
COC	Ceramic on Ceramic

COP	Ceramic on Polyethylene
DAQ	Data Acquisition
DFT	Discrete Fourier Transform
FEM	Finite Element Modeling
FFT	Fast Fourier Transform
HS	Heel Strike
MOM	Metal on Metal
MOM-PS	Metal on Metal with Polyethylene Inner Liner
MOP	Metal on Polyethylene
MS	Mid Stance
OA	Osteoarthritis
PSD	Power Spectral Density
RMS	Root Mean Squared
STFT	Short-Time Fourier Transform
THA	Total Hip Arthroplasty
TO	Toe Off
TS	Terminal Stance
WT	Wavelet Transform

Chapter 1

Introduction and Previous Work

Total hip arthroplasty (THA) has revolutionized the treatment of degenerative joint diseases, namely osteoarthritis (OA), in hips. The procedure restores the physical functioning of the hip and reduces pain in most patients, thus improving their social wellbeing and quality of life (Laupacis et al. 1993). THA has been developed steadily over the past 40 years and is now a very effective procedure performed routinely in the U.S. Studies have yielded excellent results for all surgical approaches including the anterolateral, lateral, posterolateral, and transtrochanteric approach (Wright et al., 2004).

THA is often a result of extreme osteoarthritis (OA) involving replacement of the proximal femur and the acetabulum of the pelvis. OA is a common bone-joint disease caused by the breakdown of articulating cartilage and is generally a consequence of wear, tear, aging or injury to the joints and affects the ability to perform daily activities more than any other disease (AAOS, 2004). In the United States the incidence of OA are estimated to be up to 90% of the population over age of 40 (Jordon et al., 2000).

More than 200,000 THA procedures are performed yearly in the U.S, reporting an 80% success rate at 20 years (AAOS, 2008; JISRF, 2008, Berry et al., 2002a). Currently, improved patient outcomes can be attributed to ongoing improvements in

implant design, surgical technique, fixation methods, prophylactic therapies, preadmission education, and rehabilitation (Mardones et al., 2005).

1.1 Different Bearing Surfaces for THA

Numerous bearing surfaces for hip arthroplasties are currently in use in attempts to maximize the longevity of the implants. One goal of having alternative articulation surfaces is to reduce periprosthetic osteolysis, which is a biological response to foreign particles generated by the corrosion and wear of the implant, oftentimes leading to aseptic loosening (Archibeck et al., 2000). One major cause of osteolysis and joint instability is the response of macrophages to polyethylene wear particles, which occurs rapidly in physically active patients (Learmonth et al., 2007; Wagner and Wagner, 2000). Cross-linked ultra-high-molecular-weight polyethylene has been developed in attempts to reduce this problem, as its use may result in a decreased generation of debris particles. However, long term studies on this material have not been completed, so fracture toughness and ultimate strength could prove to be problematic if used in younger and more active patients (Learmonth et al., 2007; Garino and Vannozzi, 2006). Polyethylene is used in combination with metal and ceramic, with ceramic-on-polyethylene (COP) implants exhibiting smaller wear rates when compared to metal-on-polyethylene (MOP) implants, although no significant decrease in revision rate has been associated with COP use (Archibeck et al., 2000).

Hard-on-hard bearings have been studied as alternatives to polyethylene in attempts to minimize wear particles. Metal-on-metal (MOM) and ceramic-on-ceramic

(COC) bearings are often implanted in younger and/or more active patients because of their low wear rates (Garino, 2004). Metal bearings may produce metal alloy and corrosion particles, thus leading to periprosthetic osteolysis, aseptic loosening, and metal allergy and hypersensitivity (Archibeck et al., 2000; Garino and Vannozzi, 2006). It has also been shown clinically that metal-on-metal (MOM) bearings perform equally well when compared to metal-on-polyethylene (MOP) bearings (Wagner and Wagner, 2000). Ceramic-on-ceramic (COC) bearings have the lowest wear rates of any of the articulation combinations. Combined with the biologically inert nature of the ceramic, wear and osteolysis are nearly nonexistent with the currently implanted materials (Garino, 2004; Boutin et al.; 1988, Garino and Vannozzi, 2006). It has also been previously determined that MOP and COP THA exhibit larger average separation during abduction-adduction motion than COC implants (Dennis et al., 2006). The large separation values observed with MOP articulations could lead to premature polyethylene wear and implant loosening (Dennis et al., 2006). Further, the low separation values observed with COC implants could suggest an advantage with their use.

A variety of THA implant bearings provide surgeons with the opportunity to offer more specialized treatment tailored to the needs of each patient; however, insufficient objective studies currently inhibit surgeons from making optimal bearing combination selections. An in deep analysis and comparison of different bearings with respect to kinematics, kinetics, vibration and sound, has not be performed so far. However, better

understanding of the performance of the different implants may help develop and optimize such bearings for an improved performance and longevity.

1.2 Femoral Head Separation

In the normal hip joint, retention of the femoral head within the acetabulum is provided by numerous supporting soft tissue structures, including the fibrous capsule, acetabular labrum, ligament of the head of the femur (LHF), and the iliofemoral, ischiofemoral, pubofemoral, and transverse acetabular ligaments. During THA, the LHF is surgically removed and a portion of the remaining supporting soft tissue structures are transected or resected to facilitate surgical exposure. It is logical to assume that the kinematics of the implanted hip will be altered when compared to those of the normal hip, since the stabilizing soft tissues structures are distorted at the time of operation. Previous fluoroscopic studies have shown that the femoral head may separate from the medial aspect of the acetabular component during both gait and when performing an active hip abduction-adduction activity (Dennis et al., 2001; Komistek et al., 2002; Lombardi et al., 2000).

Hip joint sliding of the femoral head within the acetabular cup is potentially detrimental and may cause premature polyethylene wear, prosthetic loosening and instability. In a previous study analyzing subjects while performing a hip abduction/adduction maneuver, femoral head sliding from the acetabulum was not observed in subjects with normal hip joints, but occurred in all subjects implanted with an unconstrained metal-on-polyethylene THA (Northcut, 1998).

Hip separation or femoral head sliding within the acetabular cup is the occurrence of the femoral head component sliding away from the center of the acetabular shell component in the supero-lateral direction, while contact between the femoral head and the acetabular cup remains in the supero-lateral area of the polyethylene liner. The design objective for THA is that the adjoining circular surfaces remain in contact and that concentric motion is evident throughout all weight-bearing activities at the hip joint. In the case of femoral head separation, a small space is created between the two surfaces allowing the implant to slide out of its concentric boundary. Previous studies measured separation during swing phase of gait, ab/adduction activity, and a leg drop motion - during this activity the subject stands on a platform and simply lets one leg dangle (Lombardi et al., 2000; Dennis et al., 2001, Komistek et al., 2001).

The presence of femoral head sliding found in those previous analyses may contribute to premature polyethylene wear because of the increased amount of shear force on the polyethylene material during impulse loading cycles. The impulse generated by the collision of two objects has been shown to potentially compromise the structural integrity of mechanical components (Seireg et al., 1973). A simplified kinetic analysis indicated a predicted average increase in hip forces of 289.5 N due to femoral head sliding and secondarily due to the development of impulse loading conditions (Northcut et al., 1998). These increased loads compromise implant fixation, resulting in premature component loosening. Additionally, during sliding, the femoral head often remains in contact and pivots on the polyethylene liner superolaterally, increasing wear in this region.

The impact conditions can also lead to a vibration response of the materials, which can be a significant cause of implant loosening.

Separation may be a major contributor to implant loosening and wear, but a further understanding of the effects of hip separation and the causes of its occurrence has not been previously studied or determined. In this study, a novel method for determining separation has been developed, allowing for an easier, non invasive approach to determine separation which may lead to the cause for it's occurrence and help it's prevention.

1.3 Hip Squeaking

Fluoroscopy has proven to be an accurate methodology for determining *in vivo* motions (Dennis et al., 1996) and enabling the extraction of accurate three-dimensional (3D) joint kinematics unaffected by erroneous skin movements (Dennis et al., 1996; McCoy e al., 1977). Previously, fluoroscopy has been used to determine that the femoral head in THA slides within the acetabular cup, leading to separation of certain aspects of the articular geometry (Northcut, 1998; Dennis et al., 2001; Komistek et al., 2002). This finding has often been referred to as hip separation, where there is a loss of contact area, leaving only an edge contact. Another interesting phenomenon observed primarily in THA patients is the presence of squeaking (Glaser et al., 2008). Mismatched ceramic couples (Morlok et al., 2001), acetabular component malpostion (Walter et al., 2006) and impingement (Eickmann et al., 2003) have been proposed as factors in the development of squeaking. However, not all cases of mismatched and

malpositioned components lead to squeaking. Additionally, squeaking has been observed in properly matched and positioned implants and when no evidence of neck to rim impingement is present (Walter et al., 2006; Jarett et al., 2003; Rothman, 2006). Audible squeaking of a hip replacement remains, therefore, a still unexplained phenomenon. The sliding motion within the acetabular cup, causing a THA to resemble a “ball and socket” joint, would lead to the induction of vibration propagation across the femoral head/acetabular cup interface, possibly leading to audible interactions. It is further hypothesized that the “squeaking” sound mainly occurred in ceramic-on-ceramic THA, quite possibly due to femoral head separation.

Therefore, fluoroscopy can provide the opportunity to correlate sound and vibration with 3D movement, extract contact positions and localize potential sound sources. This movement of the femoral head from the acetabular component and the impact conditions generated from sliding of this mechanism can be a source for acoustic emission observed in THAs (Glaser et al., 2008). Further, this method may allow for answering some important questions:

- Is sound dependent upon the bearing?
- Are acoustics generated through all bearings?
- Is sound an indication for potential hip failure?
- Can a sound analysis be successfully employed to predict THA failure modes, early post-operative?

1.4 Implant Loosening

Despite the success of THA procedures there are still instances of failure. The major complications following total hip replacement that require revision are implant loosening (Garca-Cimbrelo et al., 1997; Ilchmann, 1997; Numair et al., 1997; Taylor et al., 1997), dislocation, instability, fracture and infection (Fiedler and O'Brien, 2003) as well as premature polyethylene wear (Bono et al., 1994; Gross et al., 1997). Recently, studies also found that separation between the acetabulum cup and the femoral head does occur, which may also play a role in complications observed with THA today.

One of the most serious of these common complications is loosening. In a 10 year, post surgery follow-up study, it was estimated that up to 7% and 29% of THA femoral and acetabular components, respectively, become loose (Christie et al., 2000; Georgiou and Cunningham, 2001). While septic loosening is caused by an infection at the tissue surrounding the hip replacement, aseptic loosening is a reaction to many other factors, known and unknown. Some of the investigated reasons are foreign body reaction to wear particles, body enzymes, and sensitivity to implant motions (Lombardi et al., 1989; Archibeck et al., 2000; Krischak et al., 2003) as well as biomechanical properties of the bone and the amount of bone in contact with the implant (Meredith et al., 1997). Lack of bony in-growth on the porous implant surfaces, mechanical properties of the implants, surface finish, bone loss and possible surgeon error may also lead to implant loosening (Engh et al., 1992; Mohler et al., 1995; Rokkum et al., 1999; Nixon et al., 2007).

Since the incidence of aseptic loosening in THA is reported to be as high as 14% in the US (Sharp et al., 1985), a better understanding of the reasons of its occurrence and more effective methods for determination of loosening are required. One possible source of loosening that has not been investigated as of yet is the effect of vibration propagating through bones and implant components. The novel technique of using sound and vibration may help identify new possibilities for evaluating failure modes such as implant loosening.

1.5 Diagnostic Techniques

The assessment of hip joint performance and clinical outcome for subjects following THA is of great importance for surgeons, orthopaedic industry and researchers. Countless previous studies focused on the evaluation of component outcomes (Learmonth et al., 2007; Kearns et al., 2006; Parvizi et al., 2004; Isaac et al., 2007; Gruber et al., 2007; Arbuthnot et al., 2007), and enormous amounts of time and money have been invested in researching methods to improve implant design and performance of replacement joints (Bill et al., 2007). In most cases, the comparison and performance evaluations are based on questionnaires, clinical examination, and static radiographic review (Swanson and Hanna, 2003). Previous gait analyses of subjects implanted with THA have focused on external hip joint angles and the time-distance parameters of speed, stride length, single leg stance time and cadence (Fiedler et al., 2006; Pagnano et al., 2007; Sirianni et al., 2007). Fluoroscopic studies confirmed that the femoral head slides away from the acetabular component during gait and when

performing a hip abduction/adduction activity. This is often referred to as hip separation, where there is a loss of area contact, leaving only a line contact (Northcut et al., 1998; Dennis et al., 2001; Komistek et al., 2002).

In the improvement of implantable joints and in the assessment of the applicability of new materials, the development of replicable, easy to implement, and non-invasive techniques is required to facilitate the reliable analysis and evaluation of joint performance and clinical outcomes. In the field of arthroplasty, which primarily deals with complications related to post-operative pain, material wear, implant loosening and failure, as well as the overall functional and radiological outcome of the implanted joint, diagnosis is often difficult without the aid of invasive investigation methods (Kernohan and Mollan et al., 1982) and relies heavily on the use of diagnostic imaging techniques. In the case of severe pain, malalignment of arthroplasty components, implant dislocation or advanced loosening, the diagnosed joints can be examined using X-ray, computed tomography (CT), diagnostic ultrasound or Magnetic Resonance Imaging (MRI) examination (National Guideline Clearinghouse, 2000; Radke et al., 2004; Blendea et al., 2005; Eisler et al., 2001). However, these methods may not be sufficient for early detection of functional disorders or premature implant loosening (Kernohan and Mollan, 1982; Eisler et al., 2001). Additionally, these images provide a view of the structure in static conditions, without reporting information pertaining to the implant's mechanical and dynamical characteristics.

Therefore, a new non-invasive technique of digitally capturing hip joint vibration and sound emission has been developed for evaluation of hip performance and diagnosis of femoral head sliding of THA in the acetabular cup.

1.6 Acoustic Analysis

Concerns related to evaluation of implants under invasive conditions and the limitations of imaging techniques have led to the development of alternative tools for implant assessment. Attempts to improve implant evaluation techniques began as early as 1902 when Blodgett examined knee sounds using a stethoscope (Blodgett, 1902). He reported knee sounds to be variable in different subjects and a louder sound seemed to occur with increasing age of the patient. His methods, as well as those of Bircher (Bircher, 1913), who correlated sound with the type of injury, and Walters (Walters, 1929), who found certain acoustic emission before any other symptoms were apparent, are subjectively recorded and evaluated without the aid of an objective signal analysis.

Erb (Erb, 1933) first succeeded to record sounds in graphical form, which opened new possibilities for analyzing sounds in a repeatable manner and in much greater detail. Since then, significant development of data-acquisition systems and signal processing techniques (Chu et al., 1978; Huang et al., 2000; Inoue et al., 1986; Jaecques et al., 2004; McCoy et al., 1987; Nagata, 1988; Reddy et al., 1995; Tavathia et al., 1992; Zhang et al., 1994), and adaptive cancellation of muscle interference from the vibration signal (Zhang et al., 1994) has been made.

Early sound emission research has concentrated on the analysis of the knee joint because of the easier access, less muscle and soft tissue and the complementary reduced noise components. Huang (Huang et al., 2000) created a data acquisition system of microphones installed in the tubes of two stethoscopes to measure the discrepancy and the degree of linear relationship between both hip joints. His findings were made under non-weight bearing conditions using a vibratory force applied to the sacrum and were limited to 8 fixed frequencies. Computational techniques, such as the finite element methods (FEM), became available and popular for performing vibration analyses (Jaecques et al., 2004). Those methods provide possibilities of having an overview not only of the resonant frequencies but also of their modal shapes. However, FEM analysis is based on many assumptions pertaining to boundary conditions, bone properties, soft-tissue masses and muscle contributions. Those assumptions strongly influence the system's vibration and can change the natural frequency of the system under evaluation. It has been also shown that implant loosening can be detected through the change in the frequency content (Collier et al., 1993; Jaecques et al., 2004), but no known *in vivo* studies on the implanted hip joint have been conducted to identify the frequencies across the hip joint during weight bearing activities. Therefore, these previous techniques are not suitable for *in vivo*, subject-specific evaluation of joint conditions and provide only a reference for result verification.

In summary, intensive research has been conducted to assess knee sounds and frequencies, but most have failed to interpret and correlate results with a high degree of accuracy. Previous studies have been performed using microphones with or without

stethoscope equipment; however, it has been shown that microphones cannot reliably detect joint frequencies, especially those experiencing strong interference from noise (Mollan et al., 1982), and the signal clearance can be substantially influenced by skin friction. Very few studies have focused on the hip joint because of the additional challenges pertaining to the increased soft tissue material and muscle activities. Those studies were also performed *in vitro*, under non-weight bearing conditions or by applying FEM techniques. Diagnostic accuracy has not been reliably proven so that no applicable clinical tool is available as of today (Kernohan and Mollan, 1982).

The failure associated with the interpretation of the sound emission and possible reasons for occurrence may directly be attributed to the complicity of the sound signal, the unknown noise factors and unknown sound center - the location from which the sound originates. Implementation of joint movement visualization to the measurement of acoustic emission can help to properly localize the exact sound center and the causes for its occurrence. For this reason, a synchronous recording of sound and fluoroscopy may help to interpret and analyze the signal components.

1.7 Vibration Analysis

Mechanical vibration analysis is often used by mechanical engineers to inspect structural integrity, and it possibly can be applied to determine bone mechanical properties, monitor fracture healing and *in vivo* assessment of mechanical properties of bones (Lowet et al., 1993; Lowet et al., 1996; Van Der Perre and Lowet, 1996).

A limited number of experiments pertained to the possibility of correlating implant loosening with vibration analysis during *in vitro* as well as *in vivo* conditions (Georgiou et al., 2001; Van Der Perre, 1984; Rosenstein et al., Collier et al., 1993; Li et al., 1995; Li et al., 1996). In most cases vibration is applied to the femur in the medio-lateral plane with frequencies up to 1000-1200 Hz.

Previous studies have been performed to investigate the vibratory properties of long bones leading to a huge variety in resonance frequency. This shows the complexity of the present problem to find and identify resonant frequencies of the femur and pelvis.

A shaker method has been applied to find the resonance of an excised human normal (220-375 Hz) and securely implanted (230-325 Hz) femur (Rosenstein et al., 1989). Another study has shown that the femoral frequencies varied with removal of a bone from the neck, of the femoral head, and with the re-attachment of the femoral head (Campbell and Jurist, 1971). As expected the frequencies of the intact femur were the largest, but for all test the frequency was determined to be between 750 and 800 Hz. In another study that applied the same technology, a variation of the femoral frequency between 138 and 177 Hz was found (Thomas et al., 1991) and the conclusion was that the axial compression may affect the stiffness of bone and with it affect the resonant frequency. The femur tested under THA conditions revealed no resonance peaks.

The impulse response method is also used to find resonances of the femur but mainly under *in vitro* conditions. The frequencies found with those studies ranged from

250-880 Hz (Khalil et al., 1981) and 200-930 Hz and 280-830 Hz for normal and implanted experimental frequencies, respectively (Couteau et al., 1998 1, 2). A comparison between experimental femoral resonance frequencies found from impact hammer testing and a finite element model (FEM) of the femur results revealed similar numerical results for normal and implanted femur, 290-925 Hz and 265-780 Hz, respectively (Couteau et al., 1998 1, 2). Another FEM study (Jaecques et al., 2004) performed for well cemented, only cemented in the distal region of the stem and “clinically mobile” femur resulted in 300 Hz for the 1st bending mode, 600 (730) Hz for the torsional intact (well cemented) mode and 850-1000 Hz for the 2nd bending mode. The conclusion was made that in the frequency range of the lower vibration modes (below 1000 Hz) the resonance frequency change between intact and well cemented bone is below 50 Hz except for the torsional mode. They also found that the prosthetic vibration modes are in the range of above 2 KHz. Similarly, a different FEM study reported femoral resonant frequencies in the range of 285 Hz to 710 Hz (Taylor et al., 2002).

The variety of the results indicates the complexity of the present problem. Most of the studies were conducted under *in vitro* or during non-weight bearing conditions, but since the behavior of a mechanical system changes with the constraints, the results may be very different when the bone is in its natural environment surrounded by muscles, ligaments, tendons, skin and fat. Some reports show that skin and other soft tissues can dampen out long bone vibration (Nokes, et al., 1984; Nakatsuchi, et al., 1996), while others predict that those have only a modest affect (Tsuchikane, et al.,

1995). It still must be determined if the frequencies are affected, but those concerns do not seem to influence the ability to take acceleration measurements (Rosenstein et al., 1989; Nokes, et al., 1988).

The factors mentioned so far as well as many different others such as stiffness, mass, dimensions, material properties etc. effect the natural frequency of mechanical structures. However, bones with or without implants act similarly regarding physiological factors affecting their properties. For example, frequencies of fractured bones will increase when the bone heals since the stiffness will increase (Markey et al., 1974; Huang et al, 2003, Mollan et al., 1982) and similarly osteoporosis, diabetes and aging influence frequencies in the opposite direction (Jurist, 1970a; Jurist and Cameron, 1969; Jurist, 1970b). Increases in mass, such as those from the muscles, influence resonant frequencies (Denecker and Moberg, 1968), and the frequency can gradually increase by removing muscles from the joint (Tsuchikane, et al., 1995). On the other side, muscles can also create tension and stiffen the joint (Van Der Perre, et al., 1996).

Not only system properties but also experimental setup can have an affect on the measured frequencies. The measurement of resonant real-time frequencies may lead to different results than those obtained using a subsequent FFT analysis of collected acceleration data (Nokes, et al., 1984). Propagated frequencies are transmitted unchanged over the whole structure and only the amplitude should be different. Accelerometer placement should therefore not have influence on the measured frequencies, since those don't change with the location. Nevertheless, there is a dispute regarding this variation factor (Christensen, 1982). Because of differences in the human

body structure, health as well as muscle characteristics and stiffness some researchers found significant differences between diverse people (Rosenstein, et al., 1989). Additionally, implant geometry and fixation affect the structural vibration (Nokes, et al., 1984; Lowet, et al., 1993) and implant loosening has a significant affect on the measured frequency (Li, et al., 1996; Rosenstein et al., 1989). Bones with and without implants have also been shown to significantly change the natural frequency (Rosenstein, et al., 1989; Couteau and Hobatho, 1998).

Many studies have reported the occurrence of separation of the femoral head from the acetabular cup during gait, and it has been hypothesized that the resulting impact from the components coming back together causes impulse generation. The impact resulting from component collision can result in energy dissipation through vibration, which if coincided with the free, natural frequency of the system, could result in resonance. The subsequent amplified oscillations could reach dangerous magnitudes that could potentially damage the system. Furthermore, if vibration from component impact during gait causes resonance within the hip joint, damage to either the implant components or to the bone may occur. One of the most accurate methods would be to place the accelerometers directly on the bone or implant, which will eliminate the error due to soft tissue effects. This was done *in vitro* (Thomas et al., 1991) and *in vivo* (Rubin et al., 2003) by placing an accelerometer directly on the bone using a needle. Because of the invasive nature of this procedure, this test cannot be carried out for many subjects and it will not become a standard procedure for detecting implant loosening, bone fracture, implant failure or separation.

The present study shall give the option to capture vibrations with devices externally attached to the subject, but more importantly synchronize the readings with joint motions and evaluate further applicability of this technique.

1.8 Hip Kinetics

Only few studies, primary pertaining to stability, have included additional muscle forces (Burke et al., 1991; Callaghan et al., 1992). In these studies, however, muscle and joint contact forces were treated as mechanically independent parameters, and the interdependence between muscle activity and joint contact forces (Winter, 1990) was not considered. Musculoskeletal loading conditions at the hip are determined by the joint contact force as well as twenty different muscles surrounding the joint (Pedersen et al., 1997). Although there is strong evidence that muscles are major contributors to femoral loading (Rohlmann et al., 1982; Lu et al., 1997; Duda et al., 1998), the muscle forces acting *in vivo* are hardly accessible. Computer models have been used to predict the musculoskeletal loading conditions in the past (Seireg and Arvikar, 1975; Brand et al., 1986; Komistek et al., 1994; Glitsch and Baumann, 1997; Pedersen et al., 1997; Komistek et al., 1998), but the validation of the results against *in vivo* data remains a difficult issue (Brand et al., 1994).

Due to a lack of appropriate muscle force data, less complex loading conditions tend to be considered *in vitro*. One of the goals of this study was to develop a load profile that better simulates the *in vivo* loading conditions of total hip replacement patients and at the same time considers the relationship between muscle and joint

forces. The development of the load profile was based on a computer model using inverse dynamics of the lower extremities that has to be validated against *in vivo* data. This model was simplified by grouping functionally similar hip muscles and allowed for determination of muscle and joint contact forces throughout gait. The developed model was used in further research to evaluate the loading conditions in patients with different bearing surfaces. To evaluate the functionality of the developed model the hip contact forces for example patients were calculated and compared to the average of the *in vivo* measured forces produced by Bergmann's telemetric hip data (Bergmann et al., 2001; Heller et al., 2005). The final derived load profile included the forces of the rectus femoris muscle during walking and the ligament capsule around the hip.

No known research has been performed to evaluate the kinematics and kinetics of subjects with different bearings THAs during in-vivo, weight-bearing activities. However, such a comparison is useful in identifying the variance and success of the subjects' performance after THA. For example, altered hip loading during weight-bearing activities may result in increased contact and muscle forces, leading to increased separation combined with pain and accelerated wear. Thus, it is logical to assume that gait mechanics would demonstrate a stronger correlation and serve as a better method in the evaluation of THA performance, when compared to other variables previously studied. However, the literature lacks well-designed studies that provide objective comparison of different bearing THAs in major parameters such as kinematics and kinetics. For that reason, the purpose of this study was to examine the role of hip

kinematics and kinetics on walking performance in subjects after THA and to compare the effectiveness of the various bearings.

1.9 Ground Reaction Forces

Total hip arthroplasty (THA) has revolutionized the treatment of degenerative joint diseases, namely osteoarthritis. The procedure restores the physical functionality of the hip and reduces pain in most patients, thus improving their social wellbeing and quality of life (Laupacis et al., 1993). It has been shown that while there is often significant improvement following THA within six months, normal functioning does not return within two years postoperatively (Murray et al., 1975; Murray et al., 1976; Brown et al., 1981, Long et al., 1993). The abnormal gait during this period places unnatural stress on the unaffected leg, which may lead to the subsequent development of osteoarthritis (Arsever et al., 1996, Dekel et al., 1978, Radin et al., 1978; McCrory et al., 2001).

Although commonly utilized patient questionnaires are valuable for evaluating patients' satisfaction with their implants and often offer important information about the functioning of the prosthesis, no objective analysis of the implant performance can be accomplished. Ground reaction forces (GRF) have been extensively used to quantify and analyze the loading of the hip joint during gait in patients with and without implants (Brown et al., 1981, McCrory et al., 2001; Paul, 1996; Giakas and Baltzopoulos, 1997; Leuchte et al., 2007, Murray et al., 1976). The validity of using these forces for analysis has also been established by the significant correlation of the GRF maximum forces

generated and the loading rate with the same variables measured with instrumented implants (Bassey et al., 1997, Park et al., 1999).

Ground reaction forces have been shown to differ in the affected limb of patients who have undergone THA when compared to normal gait (Giakas and Baltzopoulos, 1997, McCrory et al., 2001). The affected hip joint has been shown to exhibit lower peak forces in comparison to normal gait, leaving the unaffected hip joint to sustain higher peak forces. This unbalance persists for at least two years postoperatively (Giakas and Baltzopoulos, 1997, Bassey et al., 1997, McCrory] et al., 2001). It has also been found that the loading rate is significantly greater in the implanted leg than in a healthy control group (McCrory et al., 2001). This identification of abnormal gait characteristics is important in the evaluation of the implant performance.

Ground reaction forces are implemented in the study in two different ways. GRF synchronized with kinematics derived from fluoroscopy in the time domain are necessary for implementation in the inverse dynamic mathematical model to derive joint kinetics. Another application for GRF is the comparison of THA patients among different bearing surfaces as well as between normal and implanted subjects. This can help evaluate the performance of implants while patients are still active and comfortable with their prostheses.

1.10 Study Propose

Kinematic and kinetic characteristics of total hip arthroplasty patients have been evaluated in countless studies and compared to the performance of healthy subjects. No previous study has been performed to evaluate the kinematics, kinetics, vibrations and acoustical emissions of subjects implanted with various bearing surface THA during an *in vivo*, weight-bearing activity. Understanding of the joint mechanics is essential in predicting and evaluating the success of the involved prosthesis. The evaluation and comparison of different implant designs require accurate *in vivo* kinematics and kinetics. Telemetric data is available, but due to the high cost, only few patients can be examined. Additionally, subjects with healthy hips cannot be included into such evaluations and comparisons due to the invasive nature of this method. Many studies have been performed *in vitro* and by using animal experiments, but they often lack on accuracy when compared against *in vivo* data.

The propagation of hip vibrational frequencies and squeaking may be an indicator of undesirable hip conditions and the sound analysis may be suitable for early detection. Vibration, particularly in the range of the resonance frequency can cause pain, bone degeneration and fracture. A further understanding of the physical response resulting from impact during femoral head sliding may lead to valuable insight pertaining to THA failure. The frequency is affected by the quality of the bone surrounding the fixture and the stiffness of the interface between implant and the bone. If a long term study is performed a decrease in frequency over time may indicate a potential failure. Therefore, one of the goals of this study was to investigate if the implementation of

vibration and sound analysis can be applied to human hip joints under *in vivo* conditions. The vibration and sound evaluation across the hip joint may lead to conclusions, if implant design or material may contribute to the increased risk of resonance.

Although separation has been well documented, it has not been correlated to clinical complications or a more in-depth understanding of the cause and effect. Therefore, a synchronized motion and sound data may provide better opportunities for investigating different failure modes of THAs. Measuring the mechanical properties of the bone-implant system using sound and vibration analyses promises to be a non-invasive and simple way of detecting implant loosening, bone fracture and probably identify different wear patterns.

The interpretation of the sound and vibration data is a complicated task involving an in-depth understanding of data acquisition (DAQ) and signal analysis, as well as the mechanical system characteristics. Sounds and vibrations generated through the implant interaction are possibly an outcome of a forced vibration induced by a driving force leading to a dynamic response. This driving force can be associated with the impact following femoral head sliding and the dynamic response may give insight into implant and bone properties and conditions. For this reason, a synchronous recording of sound and fluoroscopy may help to interpret and analyze the signal components. Kinematic analysis using video fluoroscopy has been additionally employed to obtain necessary information about implant movement, to diagnose separation and help interpret the sensor data.

It is critical that the longevity of hip implants is increased, as the aging population and more active lifestyle of the elderly require more durable and long-lasting prostheses (Learmonth et al., 2007). Many of the methods implemented today for evaluation of hip joint performance are based on invasive procedures or diagnostic imaging techniques, which are often not capable to detect early complications. Therefore, a new noninvasive technique of digitally capturing hip joint vibration and sound emission has been developed for evaluation of hip performance and diagnosis of femoral head sliding of THA in the acetabular cup. The implementation of simultaneously captured *in vivo* hip motion allows for verification of the efficiency of the newly developed method.

1.10.1 Study objectives

The fundamental objectives of this study are to methodically investigate and analyze the 3-D *in vivo* kinematic, kinetic, vibration and acoustic characteristics in THA patients with different bearing surfaces and to compare them with each other during a weight-bearing activity. For this vibration and acoustic emission from the joint interaction has to be captured, synchronized to the joint movement, with the aid of externally attached sensors and the sound has to be correlated with the *in vivo* motion and forces of the implanted joint. Kinematics are obtained using fluoroscopy, which is a well established method representing the current state of the art. Additionally, an inverse dynamic mathematical model that better simulates the *in vivo* loading conditions of a "typical" total hip replacement subject and considers the interdependence of muscle and joint forces has to be develop and implemented for patients with different bearing surfaces THAs. For the implementation of all this different components, a new non-

invasive technique of digitally capturing hip joint vibration and sound emission has to be developed for evaluation of hip performance and diagnosis of femoral head sliding of THA in the acetabular cup.

This study represents the first attempt to apply sound and vibration analysis as an impulse excitation technique (Katsuhiko, 2001) for testing hip conditions and for measuring femoral head sliding in the acetabular component of human hip joints by acoustic and vibration means. It is hypothesized that subjects experiencing femoral head separation will induce an associated sound and it is assumed that differing bearing surface material interactions will lead to different types of sounds.

This is the first study to utilize the established method of kinematics, kinetics and sound analysis techniques to evaluate the performance of implants with different bearing surfaces while patients are still active and comfortable with their prostheses. This new technique will help surgeons and biomedical engineering with the implementation of future prosthesis designs and new materials.

1.10.2 Study design

The flow chart shows the different components of the entire study (Figure 1, all tables and figures are located in the appendix) and a detailed overview of the research procedures are shown in the research overview (Figure 2).

1.11 Dissertation Contribution

The key objective of the present research is the synchronous acquisition of hip joint kinematics, kinetics and to correlate this data with vibration and acoustical signals from total hip arthroplasty patients implanted with different bearing surfaces. The novelty of this research project and the contributions made to the fields of orthopaedics and mechanics are anticipated to be as follows:

- This is the first research project conducted to evaluate various bearing surfaces for Total Hip Arthroplasty using the following principles and techniques:
 - kinematics,
 - kinetics,
 - vibration and
 - acoustical emission.
- Previously researchers have tried to clinically evaluate vibration and/or sound emission from hip joints but have failed to isolate the “true” signal among the unwanted signals pertaining to noise and alternative systems. The novel technique of combined implementation of kinematics and DAQ signals will allow for further understanding of the occurrence and source of joint sounds and the correlation of these signals with clinical diagnoses.
- Uniquely, a baseline will also be establish for correlating femoral head separation from the acetabular cup and the acoustic characteristics for THA hips for different bearing surfaces.

- No commercial software was available that is capable to handle the developed set up, including synchronization of two different video sources and data from several DAQ channels. For this reason, a computer algorithm was developed to synchronize numerous signals of different origin also allowing instant review of the recorded data.
- With respect to mathematical modeling of the human lower extremity, only few previous studies attempted to include soft-tissue structures (muscles and ligaments). Also, these previous models were not validated using experimental data under *in vivo* conditions. In this proposed model, a multi-body computational model was developed that could determine *in vivo* mechanics of the implanted and non implanted hip joint and was correlated to experimentally derived forces using a telemetric hip implant. The results from this parametric model could then be correlated to the vibration and acoustic signals to determine if these sound signals represent detrimental conditions that may lead to implant failure.
- The *in vivo* kinematics, kinetics and acoustical data will provide new view and understanding of the hip joint performance after THA and will help engineers, researcher and surgeons to optimize implant design and bearing surfaces.
- Most importantly, this is the first study to comprehensively evaluate hip joint mechanics. The information and procedures used in this proposed study may lead to the development of new non invasive techniques that could be used to clinically diagnose the condition of the human hip joint. These new non invasive

techniques may allow a surgeon to diagnose clinical concerns without the use of radiation attributed to x-rays and/or CT scans.

Chapter 2

Background

It is difficult to fully understand the kinematics and kinetics of the human body. Therefore, an analysis and study of the muscles and ligaments mainly involved in the gait activity was performed. Additionally, an investigation pertaining to the necessity of total hip replacement (THA), surgical approaches utilized with THA and the possible failure modes associated with it were investigated.

2.1 Hip Muscles

This chapter gives a brief description of the muscles and ligaments contributing to the kinetics of the hip during gait.

2.1.1 Hip flexors

2.1.1.1 Iliopsoas

Iliopsoas is a muscle made up of two parts - Iliacus and Psoas Major. Iliacus originates from the inside of the pelvic bone, whereas psoas major originates from the front of vertebrae L1 to L5. The two muscles then insert via their tendons onto the lesser trochanter of the femur. Iliopsoas is the primary flexor of the hip and is very powerful. If the iliacus portion is shortened it can pull the leg into a flexed position or pull the spine forward into a forward bent position. In a society in which individuals do a lot of sitting this is a concern, since the hip flexor remains in a shortened position for extended

periods of time. If that muscle is chronically shortened it can cause movement restrictions and pain syndromes. When the muscle performs a shortening or isotonic contraction it will bring the femur or leg bone toward the trunk – i.e. hip flexion (Virginia University, Courses).

2.1.1.2 Rectus Femoris

Rectus Femoris is the only one of the four quadriceps muscles that crosses two joints (Hip and knee). Rectus Femoris arises from the anterior inferior iliac spine and passes across the hip joint, down the shaft of the femur superficially and attaches to the patellar tendon at the knee. Because of its attachments it crosses two major joints in the lower extremity so it has muscle actions at both joints. If the pelvis is fixed it flexes the hip and extends the knee (important in walking). If the femur is fixed, it can rotate the pelvis forward from its superior aspect (anteversion) (Virginia University, Courses).

2.1.1.3 Tensor Fascia Latae

The tensor fascia latae (in red), arises from the anterior part of the external lip of the iliac crest and the outer surface of the anterior superior iliac spine. It inserts into the iliotibial tract. The iliotibial tract is a heavy fibrous area of the deep fascia of the upper leg. The iliotibial tract, along with the tensor fascia latae and the gluteus muscles, assists in stabilizing the hip and knee joints during standing and walking.(Virginia University, Courses).

2.1.2 Hip extensors

2.1.2.1 Gluteus

The antagonist or opposite muscle to the hip flexor is the large and powerful gluteus maximus. It is the large buttock muscle located posterior to the sacrum. It arises from the posterior aspect of the ilium, the lower and posterior portion of the sacrum, and the side of the coccyx. It attaches at the iliotibial tract along the posterior aspect. It produces hip extension when activated (Virginia University, Courses). Gluteus medius lies between gluteus maximus posteriorly and tensor fasciae latae anteriorly. Much of the muscle is covered by gluteus maximus. Together with gluteus minimus it abducts and medially rotates the hip joint. Gluteus medius and minimus are fundamental in keeping the trunk in an upright position when the contra-lateral foot is raised during walking (Virginia University, Courses).

During walking body weight is transferred from hip joint to hip joint. In order to prevent the toes from scraping on the ground during the swing phase, gluteus medius on the stance side contracts, tilting the pelvis upwards, lifting the leg clear of the ground (Virginia University, Courses).

2.1.2.2 Hamstring

The hamstrings consist of three muscles - biceps femoris, semitendinosus, and semimembranosus. All three have a common origin at the ischial tuberosity. Biceps femoris inserts onto the lateral part of the knee (fibular head and lateral tibial condyle). Semitendinosus and semimembranosus insert onto the medial knee joint and upper

medial part of the tibia. These muscles contribute to hip extension and knee flexion (Virginia University, Courses).

2.1.2.3 Hip Ligaments

The iliofemoral ligament is shaped like a V and is the stronger of the two ligaments. It passes from the anterior inferior iliac spine down onto the line separating the femoral neck from the lesser and greater trochanters. The pubofemoral ligament runs from the pubic region of the pelvis to an area just above the lesser trochanter on the femur (Virginia University, Courses)

2.2 Muscles Activity during Gait Cycle

The movement pattern observed in the lower limbs during walking, are a direct result of the interaction between external forces (joint reaction and ground reaction) and internal forces (produced by muscles and other soft tissue). Knowledge of the ground reaction force is especially helpful to understand how muscle activity and timing contributes to stability and propulsion. Muscle activity is typically studied using electromyography (EMG). EMG records differ between individuals, and differ for a single individual according to variables such as velocity (Virginia University, Courses).

2.2.1 Stance phase

2.2.1.1 Loading Response LR (0 to 12 percent of gait cycle)

Loading response begins with initial contact, the instant the foot contacts the ground. Loading response ends with contra lateral toe-off, when the opposite extremity

leaves the ground. Thus, loading response corresponds to the gait cycle's first period of double limb support. This is a period of extensive muscle activity. The ankle dorsiflexors act eccentrically to prevent slapping of the foot on the ground. The quadriceps act eccentrically to control knee flexion. Hip flexion is controlled by isometric action of the hamstrings (primarily biceps femoris) and gluteus maximus (primarily its lower portion).

In the frontal plane, activity in the hip abductors, tensor fascia latae, and upper portions of the gluteus maximus control drop of the contralateral pelvis, which is relative hip adduction. While activity in the anterior gluteals (gluteus medius and minimus) might appear eccentric, these muscles simultaneously move the hip joint into internal rotation. In a closed chain, this hip rotation causes the pelvis to rotate forward on the opposite side. Thus, gluteus medius activity may be nearly isometric. Also contributing to both internal rotation and extension of the hip joint are the muscles of the adductor group (Virginia University, Courses).

The erector spinae are also active during loading response. Their activity during this period has been characterized classically as a mechanism to stabilize the trunk during weight transfer, and to prevent its forward flexion during the rapid slowing of forward movement which occurs at initial contact. Recent theory attributes to the paraspinal muscles a more active role in producing important trunk and pelvic rotation (Gracovetsky, 1988). The trunk may therefore act as an inverted pendulum converting potential energy to kinetic energy via the loading of the passive elastic components of the spine. Other theory assumes that the trunk may act as an attenuator of ground reaction forces that progress up the kinetic chain (Sartor et al., 1999)

2.2.1.2 Midstance (12 to 31 percent of gait cycle)

Midstance begins with contralateral toe-off and ends when the center of gravity is directly over the referenced foot. This phase, and early terminal stance (the phase discussed next) are the only times in the gait cycle when the body's center of gravity truly lies over the base of support. As the body moves over the stance limb, activity in the foot's intrinsic muscles (which are primarily subtalar supinators) activate to convert the foot into an increasingly rigid structure. This supination force is augmented by activity in the ankle plantar flexors, which act eccentrically to control closed chain ankle dorsiflexion in the form of tibial advancement over the stable foot. The quadriceps act concentrically to initiate knee extension and the hip abductors continue their activity, becoming isometric as they halt contralateral pelvic drop (Virginia University, Courses).

2.2.1.3 Terminal Stance (31 to 50 percent of gait cycle)

Terminal stance begins when the center of gravity is over the supporting foot and ends when the contralateral foot contacts the ground. During terminal stance, around 35 percent of the gait cycle, the heel rises from the ground. Foot intrinsics and ankle plantar flexors continue to function as during mid-stance, becoming isometric at around 35 to 40 percent of the gait cycle, when continued forward momentum in the body's upper part causes the heel to rise from the floor. Similarly, the hip abductors move from eccentric to isometric to concentric activity, elevating the pelvis in preparation for swing. The iliopsoas becomes active, eccentrically controlling the rate of hip extension. The quadriceps are inactive during this phase, as ground reaction forces, as well as activity in the plantar flexors, maintain knee extension (Virginia University, Courses).

2.2.1.4 Pre-swing (50 to 62 percent of gait cycle)

Pre-swing begins at the initial contact of the contralateral foot and ends at toe off, at around 60 percent of the gait cycle. Thus, pre-swing corresponds to the gait cycle's second period of double limb support. Along with loading response, this is a period of widespread muscle activity. The foot is in its most supinated and rigid position. Acting on this rigid base, the plantar flexors act concentrically, producing a propulsive "pushoff." The iliopsoas also contributes to propulsion as it shifts from eccentric to concentric activity which will advance the extremity into swing phase. At typical to faster walking speeds, the rectus femoris also acts in a nearly isometric fashion, to limit knee flexion and augment hip flexion. Only at slower walking speeds, when ground reaction and joint reaction forces are too small to initiate knee flexion, knee flexors like the short head of the biceps femoris or the gracilis actually work to flex the knee directly. The erector spinae are active on the pre-swing side, and produce greater EMG activity than during their previous period of activity during loading response; a vital debate concerns whether this asymmetrical activity functions simply to control unwanted trunk movement or if it helps initiate forward pelvic rotation, through the mechanism of coupled motion, and thereby helps drive the extremity into swing (Virginia University, Courses).

2.2.2 Swing phase

2.2.2.1 Initial Swing

Initial swing begins at toe-off and continues until maximum knee flexion of this activity (60 degrees) occurs. During this very brief phase, the hip flexors and knee extensors (primarily rectus femoris) continue their pre-swing activity. The dorsiflexors

act concentrically to permit the forefoot to clear the ground. While their activity varies widely among individuals, the hip adductors can also assist during pre-swing and initial swing to assist in hip flexion (Virginia University, Courses).

2.2.2.2 Mid-swing

Mid-swing is the period from maximum knee flexion until the tibia is vertical or perpendicular to the ground. Muscle activity virtually ceases except for the dorsiflexors as the extremity's inertia carries it through swing like a pendulum.

2.2.2.3 Terminal Swing

Terminal swing begins when the tibia is vertical and ends at initial contact. The hamstrings (primarily the medial group) act eccentrically to decelerate the swinging extremity, while the dorsiflexors hold the ankle in position for initial contact. Just before the foot touches the ground, the quadriceps and the hip abductors initiate activity, disclosing the existence of a feed forward mechanism by which the body prepares for the large ground reaction its joints will encounter at initial contact (Virginia University, Courses).

2.3 Arthritis

Different forms of arthritis exist which often have different causes. One of the most common forms of arthritis is osteoarthritis (Conaghan, 2008) which is a degenerative joint disease resulting from trauma or infection of the joint, as well as

simply caused by age. Abnormal anatomy as well as abnormal movement patterns might contribute to the early development of osteoarthritis.

Osteoarthritis (OA) is also known as degenerative arthritis and is a clinical condition in which low-grade inflammation results in pain in the joints. OA is caused by irregular wearing of the articular cartilage that covers the joints and acts as a cushion inside joints and destruction or decrease of synovial fluid that lubricates those joints. As a result the bone surfaces become less well protected by cartilage, the joint becomes pitted, eroded and uneven. Eventually, this causes the two bones to scrape against each other, bone on bone contact, and roughening and wearing away of the bones occurs. When this happens, the joint becomes pitted, eroded and uneven resulting is pain, stiffness and instability, and in some cases, motion of the leg may be greatly restricted. As a result the patient experiences significant pain upon weight bearing, including walking and standing, as well as stiffness, instability of the joint and a loss of function and mobility. Further, decreased range of motion may cause regional muscles to atrophy, and ligaments may become more lax (Conaghan, 2008). Additionally, bone spurs, known as osteophytes may also appear at the edge of the bone (Figure 3) which further limits the motion. Osteoarthritis is common and although it most often occurs in patients over the age of 50, it can occur at any age, especially if the joint is in some way damaged by injuries, trauma and bone deformities.

The process of OA is irreversible, and typical treatment of symptoms associated with mild to medium level of osteoarthritis consists of medication or other interventions that can reduce the pain of OA and thereby improve the function of the joint. However,

hip replacement surgery is in severe cases the only prevailing option. Hip surgery can consist of hip resurfacing or total hip replacement (THA), in both cases the degenerated contact is replaced by artificial implants. Whereas THA replaces the entire joint including the femoral head, hip resurfacing reshapes and caps the damaged hip ball with a metal prosthesis. The damaged hip acetabulum is in both cases fitted with a metal prosthesis.

2.4 Total Hip Arthroplasty

In total hip arthroplasty the natural hip joint is replaced by an artificial prosthetic hip. Several different techniques for the incisions exist and are defined by their relation to the gluteus medius. The main approaches include posterior (Hedley et al., 1990, Pellicci et al., 1998, Suh et al., 2004), lateral (Hardinge or Liverpool, Pai, 1997), antero-lateral (Watson-Jones, Wheeless' Textbook of Orthopaedics, a), and anterior (Smith-Petersen, Wheeless' Textbook of Orthopaedics, b) THA.

In the posterior approach the joint is accessed through the back, taking piriformis muscle and the short external rotators off the femur. This approach allows for an excellent access to the acetabulum and preserves the hip abductors. The higher dislocation rate is a major critic point to this approach, but a repair of the capsule can reduce this risk. The lateral approach is also very commonly used and requires elevation of the hip abductors (gluteus medius and gluteus minimus) in order to access the joint. Osteotomy can be used to lift up the abductors of the greater trochanter, followed by a reapplication afterwards using cables. Another option is to divide the

abductors at their tendinous portion, or through the functional tendon and repaired using sutures. The antero-lateral technique approaches the interval between the tensor fasciae latae and the gluteus medius, whereas the anterior approach utilizes a space between the sartorius and tensor fascia latae. The double incision surgery and minimally invasive surgery are used in the hope to reduce soft tissue damage through reducing the size of the incision. Reduced incision may lead to reduced visualization and impair the component positioning accuracy.

There are many hip implant designs available to surgeons on the market and no general agreement exists to which design is best. Therefore, the selection what is best for the patient is left to each particular surgeon based on his/her experience. Most of the THA prosthesis differ in design, size, material and coating but the basic design is similar regardless of the brand. The total hip prosthesis consists of four major parts. A cup replaces the hip socket (acetabulum) which has been reamed out by the surgeon. The acetabular cup is fixed by either bone cement or has a porous outer surface which allows for bone ingrowth. An acetabular liner is placed in the cup and builds the bearing surface for the implant at the pelvis. It is usually plastic, although some new materials such as ceramic and metal are more often implemented now a days. A metal or ceramic ball is used to replace the fractured head of the femur and is placed on a metal femoral stem that is put inside the superior end of the femur where the femoral head has been cut off by the surgeon. The stem is fixed similarly to the acetabular component in a cemented or non-cemented way.

Much time, effort and money is invested into the design of hip joint implants, but still some complications and failures can occur. Overall the metal-on-polyethylene implant has an 80% to 90% survival rate after 25 to 30 years of use in older patients (Berry, et al., 2002a; Berry, et al., 2002b). However, the survival of THAs has been considered to be poor in young patients. The material used for the implant, the size of the femoral head, and the overall design as well as the surgical technique used, affect the performance, the amount of wear the implant undergoes, the likelihood of complication, and the survival rate of the implant itself.

Chapter 3

Experimental Set-Up and Data Acquisition

3.1 Subjects

The hip implant performance of 27 subjects (31 hips) who previously underwent total hip arthroplasty was observed and analyzed in this study. All surgeries were performed by the same fellowship-trained surgeon. Four THAs were implanted with metal-on-polyethylene (MOP, Versys stem-femoral head system, Trilogy acetabular system, Zimmer, Warsaw, IN, USA), six with ceramic-on-polyethylene (COP, Versys stem, TM modular acetabular system, alumina ceramic femoral head, Zimmer, Warsaw, IN, USA), and five with metal-on-metal polyethylene-sandwich (MOM-PS, Versys stem, TM modular acetabular system, Metasul femoral head and acetabular liner, Converge acetabular cup, Zimmer, Warsaw, IN, USA), as well as eleven metal-on-metal THAs (MOM, M2a 38mm head or Magnum Large Metal Articulation 52mm head, Biomet, Warsaw, IN, USA and Metasul LDH, Durom US Acetabular Component, Zimmer, Warsaw, IN, USA). In the MOM case additionally different sizes were examined with 4 hips implanted with Biomet large head (50mm and up), 4 with Biomet medium head (38mm), and 3 Zimmer large head (50mm and up). Additionally, 5 THAs with ceramic-on-ceramic (COC, Accolade TMZF stem, Trident alumina acetabular -femoral head system, Stryker, Kalamazoo, MI, USA) were included in the study (Table 1).

All subjects were analyzed under *in vivo*, weight-bearing conditions using video fluoroscopy and a data acquisition (DAQ) system to determine *in vivo* motion, vibration, sound and forces. The surgeries were performed using a single, posterolateral incision. To control the surgical technique and THA implant functionality in the study, which should help reduce the number of variables, a single, experienced, fellowship-trained surgeon (Dr. Harold E. Cates, Tennessee Orthopaedics Clinic, Knoxville, TN, USA) performed all surgeries.

3.2 Test Preparations

Institutional Review Board (IRB# 897-A) approval was obtained at the University of Tennessee and Parkwest Hospital, Knoxville, TN, USA. A statement of participation, an informed consent form as well as the Accountability Act (HIPPA) privacy form were signed by each person prior to participation. In addition, a survey describing their own opinions on their post-operative experience, their daily activities and overall satisfaction with their current quality of life were filled out by the patients. The designed questionnaire (Appendix A: Patient Questionnaire, page 174) is based on the Western Ontario and McMaster Universities (WOMAC) osteoarthritis index and Harris hip score questions (HSS). Since both pre-designed questionnaires are very detailed only a selective portion of the questions was used to create the questionnaire for this study. The assortment was based on a previous study proving information about the correlation of those questions and the measured range of motion which suggested that

the points allotted in the questionnaires for range of motion are a reasonable accurate estimation from standardized questionnaire (Brian et al., 1996).

A second automated questionnaire for the surgeons was created (Appendix B: Surgeon's Questionnaire in Electronical Format, page 177). This questionnaire has similarly pre-selected questions that can be applied for all patients and will allow a further study and comparison of all patients of a single surgeon and in the entire institution. It can be recommended that it is used as a standard protocol for documenting patient demographics and statistics.

3.3 Patient Selection

There are two basic types of traditional hip arthroplasty surgical techniques; the posterolateral approach, and the anterolateral approach. The posterolateral approach has been suggested to have a higher correlation with dislocation problems than the anterolateral approach, due to the cut of the posterior capsule and short external rotators that stabilizes the joint (Madsen et al., 2004; Schinsky et al., 2003; Weeden et al., 2003). There are no specific studies that were conducted to define the effects of differing surgical approaches on separation. To reduce surgical variance, subject selection was limited to the one surgeon and one surgical technique. In this study the posterolateral approach was selected because it is widely used in the US.

Subjects with MOP, COP, MOM, MOM-PS and COC implants were invited to participate in the study by Dr. Howard E. Cates, through Tennessee Orthopaedics

Clinic, Knoxville, TN, USA. These subjects were recruited from the pool of patients at the clinic via telephone and postal notification. A screening and a patient questionnaire (Appendix A: Patient Questionnaire, page 174) for each potential subject were performed before each experiment to ensure that participant had satisfied the required clinical criteria. Detailed information about the study, potential benefits and any risks were explained thoroughly before the procedure and the option of withdrawing from the study participation was given to each patient at any time.

All subjects had excellent clinical results (Harris Hip Scores HHS > 90 points (Harris et al., 1990)), without pain, functional deficits, or generalized inflammatory conditions in order to ensure quality performance of the requested gait activity. The Harris Hip Score is a rating of how active the subject is with their daily activities, such as tying a shoe, bending down, sitting in a chair, etc. A score of greater than 90 corresponds to a subject who is able to do 90% of their daily activities with little to no difficulty. All subjects demonstrated no evidence of postoperative hip subluxation or dislocation. None of the subjects walked with a detectable limp and all subjects could actively abduct their operated hip against gravity without difficulty. No audible sounds or noises were detected by the subjects with respect to their operated hip joint.

Patients were selected and matched based on gender, age, body weight, height, diagnosis, postoperative time, and any other conditions that might affect experimental results. Additionally, the length of the skin incision, operating time, length of hospitalization, pre- and post-operative HHS (Table 1), intra-operative mid range laxity and capsular repair status were also recorded for the subjects (Table 2). The age of the

subjects was limited to a range between to 35-85 years and their weight had to be less than 300 lbs in order to ensure that the experimental results properly represented the population and allow for proper and safe experimental environment. It was necessary that recruited subjects fulfill all those requirements in order to eliminate potentially confounding variables which could affect kinematic and kinetic comparisons.

All data was either measured before the experiment or taken from the previous clinical documents of the participant. This clinical data was used in a comprehensive comparative correlation with the kinematic, kinetic and vibrational data and helped to better understand the results derived from this research study. Understanding patient's demographics helped to correlate more accurately the mechanical and dynamic characteristics with clinical outcomes.

All subjects performed gait on a level treadmill with different speeds, but for this initial study, only the gait cycle pertaining to slow walking at 0.5 miles/hour was analyzed for each of the subjects. Subjects were given time to become accustomed to walking on a treadmill. All subjects were able to walk comfortably on the treadmill while not holding onto the handrail for support which were in place for safety but not actively utilized. Each subject walked for a minimum of 5 min, with a minimum of 2 sets of data collected.

3.4 Fluoroscopy

THA affects pertaining to the kinematics and kinetics of the hip joint, in subjects during normal daily activities, has been widely investigated in the past. One of the most commonly studied activities is gait. Therefore, in this present study, subjects were analyzed during gait, as it is the predominant weight-bearing activity, and is, a very important aspect of evaluating patient quality of life. Each subject performed normal walking while on a level treadmill, under fluoroscopic surveillance. A fluoroscopic unit and a video camera were used to capture the *in vivo*, weight-bearing movement of the THA as well as the leg motion during the gait activity allowing for the documentation of the relative motion between the femoral and acetabular components (Figure 4). Several steps during the walking activity were captured. For each subject, one single stride from toe-off to the subsequent toe-off was chosen randomly for analysis.

3.4.1 Tracking of several gait cycles using single video-fluoroscope

The hip joint moves during level walking in the gait direction, the sagittal plane, with a horizontal velocity greater than 0.5 miles per hour (MPH) and a changing acceleration. Due to these boundary conditions, it is not possible to track the hip joint during walking because the hip will move out of the field of the fluoroscopic view. For this purpose a treadmill was applied which kept the hip joint in the range of a 12 inch fluoroscope. The speed of the treadmill was adjusted so that it was at a rate that would allow the images to be captured without occurrence of blurring or ghosting.

3.4.2 The fluoroscopic unit

The fluoroscopic machine (Figure 5) was operated by a certified radiation technician. The use of fluoroscopy allows for the formation of a basic projection image, captured by passing pulsated radiation through the subject's joint and onto an image intensifier (usually a ten to twelve inch diameter circle). A high frequency pulsed fluoroscopy unit (OEC 9800, General Electronic Medical Systems, Salt Lake City, Utah, USA), consisting of a C-arm with high resolution intensifier and a high power rotating anode X-ray tube, was used in this study. The fluoroscopic video was captured at 30 frames per-second with a resolution of 720x680 pixels and captured images were saved in tiff format in order to gain the best quality.

3.4.3 Radiation safety

The amount of radiation emitted from pulsated fluoroscopy unit, measured at the maximum setting was 2.4 rad/min (3.6 Rem), which is much less than using a continuous stream of radiation. Each participant was under fluoroscopic surveillance for less than or equal to 2 minutes and only the hip joint (from the fluoroscopy machine) and foot position (from a second camera aimed at the feet for the gait activity) were recorded. Proper shielding was utilized during the experiment and the total exposure level from the fluoroscopy was far below the established limits for the participants. However, a lead apron was worn by the subjects to cover the area below the first rib in order to reduce any possible radiation exposure. Additionally, all the researchers and nurses were required to wear full lead aprons. Procedures were performed until two

successful movements have been acquired, or a fluoroscopic “on-time” of one minute is achieved with a maximum total exposure time of 2 minutes.

3.4.4 Fluoroscopic image capture

Video-fluoroscopy was performed by acquiring a continuous stream of video at a rate of 30 images/second, with an image intensifier of 10 to 12 in. The image intensifier passed the image onto a mirrored system into a camera which recorded the dynamic movement (Figure 5). The femoral stem and acetabular shell appeared as a blackened silhouette on the video screen (Figure 6). Bone and tissues were viewed surrounding the THA implant as lighter gray areas due to better passivity of the radiation. The fluoroscopic video and the real-time video of the subject’s stride were recorded synchronously to a computer. This created a screen view of the subjects gait cycle *in vivo* and *ex vivo*, allowing use of a visual aid in determining what instance of the gait cycle was captured. Specified frames from the fluoroscopic gait videos for each subject were captured and edited using the software package Adobe Premiere Pro™ (Adobe Systems Incorporated, San Jose, CA, USA). Images were taken at heel-strike, 33% of stance phase, 66% of stance phase, toe-off, and at six increments of swing phase for each subject. Additional images were capture if required for more detailed analysis. Approximately, 18 images per subject were captured to represent the entire gait cycle. Gait phases were determined using the synchronized image of the real-time subject gait cycle. Values of 33% and 66% of stance phase were found by calculating the number of frames between heel-strike and toe-off. This value was then divided by three and added

in succession to the first heel-strike value. Swing phases were found by using the time between the toe-off and the next heel-strike in gait.

3.5 Force Plate Measurements

Prior to each fluoroscopic session, subjects were asked to perform under *in vivo*, weight-bearing conditions, one step on a force plate with the foot of the affected leg falling onto the center of a force plate (AccuSway, AMTI, Advanced Mechanical Technology Inc, Arlington, VA, USA). Subjects were asked to walk slowly over the force plate and practiced stepping onto the force plate before data was collected to make the gait more consistent. Couple of trials were collected for each subject at a slow to comfortable speed. In addition the bodyweight of each patient was recorded prior to the procedure.

The standard option of digital data recording via RS-232 interface provides only a low sampling rate possibility and does not allow for synchronization with other equipment included in our DAQ setup, such as accelerometers and sound sensors. For this reason, an analog 8 channel interface was chosen (Figure 4). The force plate consisted of 4 three-axial force sensors mounted in the top plate at each corner. The forces and moments applied on top of the surface were distributed among the four sensors and separated into three orthogonal force components. The load cells produced signals into all 8 channels: 4 vertical measurements and 4 shear force measurements. The Z analog output was pointing down for each corner, and the XDC channel is opposite the global sign convention. For this reason, there were negative

values in the calibration matrix. The global sign convention is given in bold print in Figure 9 (AccuGait, 2005). When the force plate is powered, eight voltage signals are always present at the 10-pin output connector (Table 3).

A manual calibration was performed each time the force plate was in use. For this reason the ZERO button was pressed manually after the force plate warmed up to initiate the autozero routine. The analog output range of the force plate in use was ± 10.0 Volts with auto zeroed values of approximately 0 volts. Although these near zero values are quite small, it was still recommended that these small values are used to eliminate any mean displacement of the outputs (AccuGait, 2005).

The captured 8 channels represent 4 vertical and 4 horizontal sensor readings. The force plate is initially calibrated at AMTI for both digital and analog outputs. The results of this initial analog calibration are the force and moment sensitivities given in a 6 x 8 element array.

$$S = \begin{bmatrix} S_{11} & S_{12} & S_{13} & S_{14} & S_{15} & S_{16} & S_{17} & S_{18} \\ S_{21} & S_{22} & S_{23} & S_{24} & S_{25} & S_{26} & S_{27} & S_{28} \\ S_{31} & S_{32} & S_{33} & S_{34} & S_{35} & S_{36} & S_{37} & S_{38} \\ S_{41} & S_{42} & S_{43} & S_{44} & S_{45} & S_{46} & S_{47} & S_{48} \\ S_{51} & S_{52} & S_{53} & S_{54} & S_{55} & S_{56} & S_{57} & S_{58} \\ S_{61} & S_{62} & S_{63} & S_{64} & S_{65} & S_{66} & S_{67} & S_{68} \end{bmatrix}$$

For the calibration, all eight analog channels should be normalized to 0.0 Volts. For this reason a calibration file was taken before and after each measurement session. This file represented the force plate measurements of all sensors in an unloaded

condition. To normalize each channel, the acquired unloaded value was subtracted from each force plate output signal:

$$\Delta \bar{F}_- = \bar{F}_-(event\ data) - \bar{F}_-(off)$$

$$\bar{F}_- = [Cz \ Dz \ Az \ Bz \ YAC \ XDC \ XAB \ YBD] \text{ (Table 3)}$$

with $\bar{F}_-(event\ data) =$ data set from the desired event

$\bar{F}_-(off)$ = offset value for each channel in unloaded condition

$\Delta \bar{F}_-$ = “offset corrected” acquired data

The recordings of the 8 channels were processed using self developed software based on MATLAB™ (The MathWorks, Inc., MA) using the 6-by-8 sensibility matrix S and the calibrated acquired data $\Delta \bar{F}_-$ (Figure 10). The final 6 outputs included orthogonal three forces medial-lateral (F_x), anterior-posterior (F_y), and vertical (F_z) and three corresponding moments (M_x , M_y , M_z).

Force calculations:

$$F_x = (\Delta Cz * S11) + (\Delta Dz * S12) + (\Delta Az * S13) + (\Delta Bz * S14) \\ + (\Delta YAC * S15) + (\Delta XDC * S16) + (\Delta XAB * S17) + (\Delta YBD * S18)$$

$$F_y = (\Delta Cz * S21) + (\Delta Dz * S22) + (\Delta Az * S23) + (\Delta Bz * S24) \\ + (\Delta YAC * S25) + (\Delta XDC * S26) + (\Delta XAB * S27) + (\Delta YBD * S28)$$

$$F_z = (\Delta C_z * S_{31}) + (\Delta D_z * S_{32}) + (\Delta A_z * S_{33}) + (\Delta B_z * S_{34}) \\ + (\Delta Y_{AC} * S_{35}) + (\Delta X_{DC} * S_{36}) + (\Delta X_{AB} * S_{37}) + (\Delta Y_{BD} * S_{38})$$

Moment calculations:

$$M_x = (\Delta C_z * S_{41}) + (\Delta D_z * S_{42}) + (\Delta A_z * S_{43}) + (\Delta B_z * S_{44}) \\ + (\Delta Y_{AC} * S_{45}) + (\Delta X_{DC} * S_{46}) + (\Delta X_{AB} * S_{47}) + (\Delta Y_{BD} * S_{48})$$

$$M_y = (\Delta C_z * S_{51}) + (\Delta D_z * S_{52}) + (\Delta A_z * S_{53}) + (\Delta B_z * S_{54}) \\ + (\Delta Y_{AC} * S_{55}) + (\Delta X_{DC} * S_{56}) + (\Delta X_{AB} * S_{57}) + (\Delta Y_{BD} * S_{58})$$

$$M_z = (\Delta C_z * S_{61}) + (\Delta D_z * S_{62}) + (\Delta A_z * S_{63}) + (\Delta B_z * S_{64}) \\ + (\Delta Y_{AC} * S_{65}) + (\Delta X_{DC} * S_{66}) + (\Delta X_{AB} * S_{67}) + (\Delta Y_{BD} * S_{68})$$

Measurements were taken at 10,000 samples per second via a data acquisition (DAQ) system using in-house developed software application (Chapter 3.8, page 55). This setup allowed for synchronization of DAQ and video signals.

An application was developed, Figure 10, to calibrate, calculate and plot the resulting force. For the force data a calibration is necessary every time when the force plate is turned on. The calibration reads a signal file, which should be taken prior to every measurement set and creates a zero-file, which is used for calibration for all subsequent experiments until the machine is turned off. There is an option for easy checking of the calibration by using a load file with known weight. This option computes only the 3 forces and 3 moments acting on the force plate. This gives the opportunity prior to starting the experiments to instantly verify the calibration of the device. The analysis option calculates the Ground Reaction Force (GRF) based on a known sensitivity matrix and outputs the results in a data-file as well as plots.

The force plate was placed with the negative x-axis in waling direction, the y-axis pointing in medio-lateral (ML) direction and the positive z-axis is pointing down (Figure 9 and Figure 11).

3.6 The New Acoustic and Vibration Analysis Technique

Acoustic and vibration signals are generated through the impact of two objects. For this reason, the actual subject-specific, *in vivo* hip joint structural and mechanical conditions during weight-bearing activity were used to provide excitation of the pelvis through the impact of the femoral head in the acetabular component.

A non-invasive acoustic and vibration analysis technique (AVT) was developed for the measurement of acoustic and vibration waves in hip joints (Figure 4). The transduction system included a pair of identical three-axial accelerometers and a sound sensor. Accelerometers (Figure 12), used to determine the propagation of vibration signals transmitted across the hip joint, were externally attached at the bone prominence of the greater trochanter and the anterior superior iliac spine, where the soft and muscle tissue layer is the thinnest (Figure 4). The sound sensor (Figure 13) was placed between both accelerometers at the closest distance to the hip joint interface and allowed for capturing sound emissions during the performed activity. All sensors were securely attached using a spica dressing, tight-fitting sleeve-like article of clothing, designed for the purpose of the study, and adjustments to patient size were achieved with integrated Velcro strips (Glaser et al., 2008). The elastic tension was adjusted to maintain a constant and equal compression to all three sensor components. This setup

was found to be optimal for the capturing of strong acoustic signals as well as the exclusion of ambient noise (Campbell and Jurist, 1971, Glaser et al., 2008).

The criteria for selecting the accelerometers were based on their accuracy and size. The accelerometers used for this study have a sensitivity of approximately 10 mV/g and a nearly linear output in the range of 2 to 7,000 Hz on the x-axis and 2 to 10,000 Hz on the y and z axes. Also, the accelerometers used were very small, approximately 0.25 inches cubed (Figure 12). Piezoelectric accelerometers were chosen, which use a spring-mass system to generate a force equivalent to the amplitude and frequency of vibration. The force is applied to a piezoelectric element, producing a charge on its terminals that is proportional to the vibratory motion. Piezoelectric materials are self-generating, therefore, do not require an external power source, but are constrained by low output sensitivity.

The accelerometer and sound transducer (Figure 13) outputs were collected and amplified by a signal conditioner (PCB 583A series 16 channel, PCB Piezotronics, Inc., Depew, NY). A signal conditioner was needed since the piezoelectric devices, accelerometer and sound transducer used in this project have extremely low signals, and a simultaneous signal measurement with signal conditioning was essential for an effective DAQ system to maximize the accuracy, to allow sensors to operate properly and to ensure safety (Glaser et al., 2008). The signal conditioner used in this study included data amplification, sensor excitation, a programmable low-pass filter and programmable gain. Gain was adjusted to 100, which assured highly sensitive measurements. Measurements were taken at 20,000 samples per second and

simultaneously recorded to a laptop station using in-house developed software (Figure 14, Chapter 3.8, page 55). To prevent aliasing - high-frequency components replicated as low-frequency components that distort the genuine signal - the hardware low-pass filter was adjusted to the Nyquist frequency of 10,000 Hz. The Nyquist frequency is defined as half of the highest Fourier frequency component in the sampled signal, here 20,000 Hz (Glaser et al., 2008).

For signal digitizing, the data acquisition (DAQ) system used was a DI-720 Series (DATAQ Instruments, Inc, Akron, OH) 16-bit DAQ system with USB 2.0 Interface (Figure 3) (Glaser et al., 2008).

3.7 Data Acquisition - DAQ

A proper experimental setup can lead to the success of a study or to its impending failure. Data acquisition involves gathering signals from measurement sources and digitizing the signal for storage, analysis, and presentation on a personal computer (PC). The data acquisition (DAQ) system used is a DI-720 Series (DATAQ Instruments, Inc, Akron, OH) 16-bit DAQ system with 32-channels and USB 2.0 Interface (Figure 4).

3.8 Software Synchronization of two Video and multiple Data Acquisition Signals

When data is recorded from many different and independent systems, a proper synchronization of all sources is crucial for the correct evaluation and correlation of the

obtained readings. Data Acquisition (DAQ) systems equipped with several channels are usually capable of recording the majority of signals needed from an engineering point of view, simultaneously. For best synchronization, all electrical signals should be collected using the same data acquisition board to assure the time-stamps for all collected signals are identical.

No known software was available to capture and synchronize two real time audio/video inputs and DAQ signals as required by this study's setup. Synchronization of such systems is usually achieved through triggering. At the beginning of this project a LED light was used for this purpose. The light was connected to one of the DAQ channels, giving a different voltage reading for the on and off states. At the same time, the event of the illuminated light was recorded by the video system and later used as a manual synchronization point.

This procedure was cumbersome and can introduce unwanted errors pertaining to the reliance of humans to properly interpret the signal. The process usually involved two people to operate the video and DAQ capturing mechanisms and makes instant review impossible. For these reasons, a new software package was developed which can synchronously record two real time audio/video signals and all required DAQ signals. It also made instant review of the synchronized data possible (Figure 14).

The main application was written in C Sharp (C#), a Microsoft object-oriented programming language, and controls, displays and records two audio/video inputs and DAQ components. The software used 'ActiveX control' elements provided from the DAQ

hardware and software manufacturer. 'ActiveX controls' are reusable software components, based on the Microsoft Component Object Model (COM). Two separate uncompressed audio/video files were generated, representing the capture of fluoroscopic and foot-movement videos. Additionally, one data file was recorded in the usual manner that includes all DAQ channels.

The advantage of the developed software was that it required only one user to control all system components. The user was able to see, start, stop and review recordings of video and DAQ signals. Because of the automation of the entire procedure, errors and variation due to human interaction could be excluded. Also, no post processing or manual synchronization was required because the recording of all inputs starts within the ten milliseconds. This latency was much smaller than the NTSC (National Television System Committee analog video and television system) frame rate of 30 frames per second of the video signals (approx. one frame per 33 milliseconds) (Glaser et al., 2008).

Chapter 4

Data Processing and Analysis

4.1 3-D to 2-D Registration Analysis

A full 3D analysis of each fluoroscopic series was achieved by fitting the projection of the 3D CAD models of the femur and acetabular cup to the fluoroscopic image.

4.1.1 3D reconstruction procedure

The three-dimensional (3D) CAD (Computer-aided design) models of the implants were obtained from the participating manufactures or were available in the database in our laboratory. Some of the implants had to be laser scanned, using the process of reverse engineering to obtain CAD models from physically present implants. Those 3D CAD models and the 2-D gait fluoroscopy images were overlaid using previously published 3D registration process (Dennis et al., 1996; Mahfouz et al., 2003) and MATLAB™ (The MathWorks, Inc., MA, USA) applications, written at the Center for Musculoskeletal Research, Tennessee (Mahfouz et al., 2003). Individual fluoroscopic frames at specified increments of the gait cycle were captured from the entire fluoroscopic video. Initially, 3D CAD models of the implant components were entered into the two-dimensional (2D) fluoroscopic scene. The scene consisted of a light source (x-ray), an image plane on which to project the fluoroscopic image (image intensifier),

an area to manipulate a 3D model (subject area), and a camera to view the entire scene. Since metallic and ceramic materials do not allow for radiation transmission, the implants were viewed as darkened silhouettes in the fluoroscopic images. Polyethylene absorbs radiation and is therefore essentially transparent in the fluoroscopic images. Therefore, only metal or ceramic shell liners have been used for referencing. The images were projected onto the image plane (Figure 6), and the corresponding implant models of the femoral and acetabular component (Figure 7) were translated and rotated in 3D until the silhouette of the implants precisely match the outline of the darkened implants on the 2-D fluoroscopic images (Figure 8). This procedure is called 3D-to-2D registration process and is an interactive approach, where the operator of the application performs or assists the automated computer algorithm (Figure 15 and Figure 16) (Dennis et al., 1996; Mahfouz et al., 2003).

4.1.2 Algorithm

The relative orientation of hip implant components was then determined in 3D from a single-perspective fluoroscopic image (Mahfouz et al., 2003). A three-dimensional scene of the fluoroscopic unit was created on a Silicon Graphics Indigo (Mountainview, CA, USA) workstation in C++ using the Open Inventor Toolkit (Mountainview, CA, USA) library. AutoCAD™ (San Rafael, CA, USA) is used to extract measurements (Mahfouz et al., 2003). The 3D to 2D registration method contained a combination of a matching algorithm, optimization technique, and user control to create the analysis. Initially, the user manipulated the models into place and then the computer determined an accurate fit. The correct fit was achieved when the silhouettes of the

acetabulum and femoral stem implant components best matched the corresponding components in the fluoroscopic image. The pose of each component was then recorded and measurements of interest were extracted using a CAD-modeling program.

The images are evaluated by a combination of their pixel values (intensity matching score) and edge detection (contour matching score) determined by (Mahfouz et al., 2003):

Intensity Matching Score:

$$\sum_{(x,y)} G(x,y)H(x,y) / \sum_{(x,y)} H(x,y)$$

Contour Matching Score:

$$\sum_{(x,y)} J(x,y)K(x,y) / \sum_{(x,y)} K(x,y)$$

where $G(x, y)$ = input x-ray image

$H(x, y)$ = predicted x-ray image

$J(x, y)$ = input edge-enhanced image

$K(x, y)$ = predicted edge image

When the pixel or contour values matched the silhouette with the CAD model, both scores resulted in their highest values. When both scores are combined, the minimum value allows the algorithm to localize the best possible match. However, due to the symmetry of the hip joint implants two local minimums can result from the

combination of scores. Out of the two scores only one can be possible; therefore the user evaluates the ideal input and finds the true minimum value (Mahfouz et al., 2003).

During THA analysis the user controls were used a majority of the time. Unfortunately, due to the density of the muscle and fat tissue around the hip joint, using the matching and optimization techniques did not always work. The cylindrical symmetry of the acetabular shell models also caused a problem with the algorithm resulting in a continuous run and never finding the perfect match to the silhouette. The acetabular shell models were often manually fit by the trained user.

The applied algorithm is developed and maintained at the Center for Musculoskeletal Research, Tennessee (Mahfouz et al., 2003) and the application is called SAAM.

4.2 Kinematic Analysis

Individual fluoroscopic video frames at specified time intervals were processed as previously described (Figure 17). After each frame was analyzed for a single participant, kinematic curves were produced to describe the motions of the joint during gait.

A local coordinate system was set up on each of the femoral and acetabular components. The measured variables throughout the motion included the femoral and acetabulum 3D rotational and translational kinematics (Figure 18 and Figure 19). The translations basically consisted of the position vectors of the implants, parallel (TX and

TY) and perpendicular (TZ) to the image plane. The rotational orientation is defined by the angles of out-of-plane rotation *XROT* and *YROT* and the *ZROT* of the rotation in the image plane. The relative rotations were calculated based on the Euler angles from the angles of rotation of each implant in the global coordinate system. The relative rotations *XROT*, *YROT* and the *ZROT* of the femoral component with respect to the acetabular component are described by real orthogonal 3x3 rotation matrix *R* by multiplication of the standard matrices *R_{XROT}*, *R_{YROT}* and *R_{ZROT}*. *R* is build by processing the matrix *R_{fem}*, the orientation of the femoral component, and the matrix *R_{pel}*, the orientation of the acetabular component:

$$R = R_{fem} * R_{pel} '$$

Since the acetabular component is fixed with respect to the pelvis the obtained kinematics for the acetabulum was interpreted as the motion of the pelvis. However, the orientation of the acetabular cup, with respect to the pelvis, has to be known. It is dependent upon the surgeon, the surgical technique and the patient anatomy. Since it is not known and the surgeon can only guess the orientation, the average of each rotation has been assumed to be the 'neutral' position of the cup. The rotation of the cup has therefore been normalized by subtracting the mean value of rotation in question from each individual position angle.

The relative motion of the femur and pelvis were then calculated based on the transformation matrices of each rigid body and were subsequently used to determine the distance between the center of the femoral head and the acetabular component. This information was then used to diagnose if separation (sliding within the acetabular

cup) of the femoral head from the acetabular component had occurred (Dennis et al., 2001, Glaser et al., 2007) (Figure 20).

Temporal equations of the femoral and pelvic motions (Figure 21 - Figure 23) were derived from the relative motions by curve fitting, and in vivo kinematic data was analyzed and compared to describe the difference between the THA groups. Finally, the kinematical equations were input into the mathematical model to determine the 3D kinetic results.

4.3 Gait Analysis

All patients performed normal gait on a level treadmill. During this activity their gait performance was observed and recorded. The analyzed parameters were stance time, swing time, step time, and double support time for the implanted and healthy leg. For all patients, each of the above mentioned parameters were measured during 10 steps and averaged for analysis. With regard to the patients having unilateral implants, the absolute value of the symmetry indices (ASI), for the chosen parameters, was calculated. The ASI was used to compare the gait of the implanted and non-implanted limbs and examine the asymmetry in gait (Herzog et al., 1989; Giakas and Baltzopoulos, 1997).

$$ASI = \left| 2 \cdot \frac{X_h - X_i}{X_h + X_i} \right| \cdot 100\%$$

with X_h and X_i = gait variables for the healthy and implanted side, respectively

When the implanted and non-implanted leg are in perfect symmetry, e.g. $X_i = X_h$, the ASI results to zero. The ASI was also calculated for the same parameters in the bilateral patients. The comparison for those patients was carried out between the left and right leg. Acceptable symmetry was determined to occur when $ASI < 10\%$, as previously suggested (Giakas et al., 1997). Since only absolute values are reported for the ASI, the symmetry index (SI) was used to identify which side resulted in higher parameters. The SI was calculated on the same basis as the ASI, but the positive and negative values were taken into account. For unilaterally implanted patients, a positive value for the SI suggests that the parameter is larger in the healthy limb, while for bilateral patients, a positive value for the SI suggests that the parameters is larger in the right limb.

4.4 Ground Reaction Forces

The ground reaction force vectors were filtered with a low pass filter of 1000 Hz and averaged among the trials for each patient and among the different bearing groups – MOP, COP, MOM, MOM-PS, and COC. Comparisons were also established between hard-on-hard bearings (COC, MOM) and hard-on-soft bearings (MOP, COP). The average force, minimum, maximum, and standard deviation SD were determined for each set of averages. Each force was normalized by the corresponding patient's body weight so that comparisons could be performed between different trials, patients, and implant groups.

$$F_{xBW} = F_{event} / F_{BW}$$

with F_{event} = measured and calibrated ground reaction data during the analyzed activity

F_{BW} = measure body weight (BW) for each patient prior to each patient's experimental session

F_{xBW} = times body weight (xBW) - the normalized forces

The maximum peak forces and stance times were determined. Nine vertical (F_z) parameters were selected as descriptors of the ground reaction force components (Figure 24):

F_{z1} = percent time to first maximum force;

F_{z2} = first maximum force;

F_{z3} = percent time to the minimum force;

F_{z4} = minimum force;

F_{z5} = percent time to second maximum force;

F_{z6} = second maximum force;

F_{z7} = average force.

LR = loading rate;

PR = push-off rate.

Six parameters were collected in the anteroposterior (x) direction: time to maximum braking force (F_{x1}), time to zero force (F_{x2}), time to maximum propelling force (F_{x3}), maximum braking force (F_{x4}), maximum propelling force (F_{x5}), and the average force (F_{x6}) (Figure 25).

Five parameters were analyzed in the mediolateral (y) direction: time to first maximum (F_{y1}), time to first minimum (F_{y2}), average force (F_{y3}), first maximum force (F_{y4}), and first minimum force (F_{y5}) (Figure 26).

These parameters were identified as representative descriptors of ground reaction force data that characterize the essential features of the force components (Bates et al., 1983b; McCrory et al., 2001) and have been used in prior studies to investigate the effects of running shoes on ground reaction forces (Bates et al. 1983a), to assess the effects of additional loads (Bates et al. 1987), and to quantify shoe-orthotic interactions (Hamill et al. 1982; Hamill et al., 1990).

The loading rate (LR) was calculated for each patient as the value of the first peak force (F_{z2}) divided by the time from the beginning of stance (heel strike) to the time when the first peak force occurred (F_{z1}) (McCrory et al., 2001).

$$LR = \frac{F_{z2}}{F_{z1}}$$

The push-off rate (PR) was calculated by dividing the magnitude of the second peak force (F_{z6}) evident through push-off by the time from this peak force to the end of the stance phase (toe-off) (F_{z5}) (McCrory et al., 2001).

$$PR = F_{z6} / F_{z5}$$

The overall maximum peak forces and incidence of three or more peaks in the vertical direction were also determined. From the kinetic data collected, the average gait cycle times as well as the percentages of the gait cycle comprised of the stance and swing phases were calculated for each group.

4.5 Vibration and Acoustic Analysis

Vibration and acoustic signals are generated through the impact of two objects (Glaser et al., 2008). The presented method implements the impulse excitation technique (Katsuhiko, 2001). Initially, the femoral head slides within the acetabular component and comes to rest, with respect to translation, causing a standing wave to be generated at impact. Therefore, the actual subject-specific, *in vivo* hip joint dynamical conditions during weight-bearing activity were used to provide excitation of the pelvis through the impact of the femoral head in the acetabular component. The sound generated through the gait cycle was recorded and analyzed (Glaser et al., 2008).

4.5.1 Sound basics

The ear enables humans and animals to hear their environment. The ears help the body to pick up sound waves and vibrations. Sound travels in waves through the air, the ground, and various other substances and can be felt by vibrations generated through the medium. Sound is a longitudinal mechanical wave of any frequency.

Frequency is the number of vibrations produced per second, varies for each sound and is measured in Hertz (Hz). The frequency of a sound wave determines its tone and pitch. Humans cannot hear sounds of every frequency. The range of hearing for a healthy young person is 20 to 20,000 Hz (Cutnell and Johnson, 1998: 466; Acoustics, National Physical Laboratory (NPL), 2003; Caldarelli and Campanella, 2003). Any frequency that is below the human range is known as infrasound, whereas ultrasound is above the range of the human ear.

Sound pressure level (SPL) is given in db SPL and the threshold of hearing is defined close to 0 dB. The threshold of pain is about 135 dB. In this logarithmic scale the power doubles for each 3 dB increase. At the low end of the hearing range the ears lose function due to background noise. Peak sound pressure is 3 dB higher than root-mean-square (RMS) average pressure. SPL normally refers to RMS pressure.

For a non-linear response, distortion will occur. Harmonic distortion means that a pure 1000 Hz input tone results in spurious outputs at 2000 Hz, 3000 Hz, and other integer multiples of the input frequency. Inter-modulation distortion means two input tones at 1000 Hz and 100 Hz result in spurious outputs at 900 Hz, and 1100 Hz, among others.

Sound Pressure Level (SPL) is defined using a reference which is approximately the intensity of 1000 Hz sinusoid that is just barely audible (zero 'phons'). In pressure units:

$$\begin{aligned}
0 \text{ db SPL} &\equiv 0.0002 \mu \text{ bar (micro barometric pressure)} \\
&= 20 \mu \text{ Pa (micro Pascals)} \\
&= 2.9 \times 10^{-9} \text{ PSI (pounds per square inch)}
\end{aligned}$$

In intensity units:

$$I_o = 10^{-16} \frac{W}{cm^2}$$

Since sound is created by a time-varying pressure, sound levels can be computed in dB-SPL by using the average intensity (averaged over at least one period of the lowest frequency contained in the sound). The relationship between sound amplitude and actual loudness is complex (Stevens and Davis, 1983). Loudness is a perceptual dimension while sound amplitude is physical. Since loudness sensitivity is closer to logarithmic than linear in amplitude (especially at moderate to high loudness), decibels are commonly used to represent sound amplitude, especially in spectral displays.

(SPL) or sound level L_p is a logarithmic measure of the RMS pressure (force/area) of a particular noise relative to a reference noise source. It is usually measured in decibels (dB (SPL), dB SPL, or dB SPL).

$$L_p = 10 \log_{10} \left(\frac{p^2}{p_0^2} \right) = 20 \log_{10} \left(\frac{p}{p_0} \right) \text{ dB}$$

with p_0 = the reference sound pressure

p = the root-mean-square sound pressure being measured.

The commonly used reference sound pressure in air is $p_0 = 20 \mu\text{Pa}$ (RMS). In underwater acoustics, the reference sound pressure is $p_0 = 1 \mu\text{Pa}$ (RMS). It can be useful to express sound pressure in this way when dealing with hearing, as the perceived loudness of a sound correlates roughly logarithmically to its sound pressure.

4.5.2 Vibration basics

Induced or forced vibration is used as the source of excitation of impacts. If a force provides more energy to the system than it can dissipate, instabilities may develop in the form of forced induced vibrations and sound radiation. The frequency of the resulting vibration is determined by the natural frequency of the component parts. Waves generated through the vibration of an object are defined as disturbances which are periodic in time and space. In general, waves exhibit no net transport of material, transport energy, have characteristic waveforms, propagate at uniform waveform-independent speed, and have speeds dependent on medium.

In engineering mechanisms with relative motion, impacts and vibrations can induce negative side effects such as wear, friction, squeal (high frequency noise), chatter (low frequency noise) and self-sustained vibration. Vibration is usually a complex phenomenon and contains elements of axial, bending and torsional vibration. Vibration has always been regarded as having a destructive effect on human beings, construction and mechanical systems.

4.5.3 Vibration and sound processing

Through the use of a sound transducer and accelerometers, the *in vivo* capture and analysis of sound signals transmitted across the hip joints was conducted. This acoustic vibration technique (AVT) was also found to be insensitive to ambient noise. Sound signals captured from both, pelvis and femur, were objectively measured in units of millivolts (mV), and were then compared. The measured signals were divided by the sensitivity S_g (mV/g) or S_a ($mV/(m/s^2)$) and converted to acceleration units in g or m/s^2 . Additionally, the applied gain during the measurements was eliminated by dividing the measurements by 100.

The captured signal was then saved in matrix M of size n by m with sampling frequency F_s (m is the number of channels and n is the number of points collected) in ASCII format (American Standard Code for Information Interchange). Each column of the data represented a separate channel. The signal y was saved under each column of the matrix M and then normalized to the range $-1 \leq y \leq 1$ before it was converted, resulting in a sound that later was heard as loud as possible without clipping. The sound duration depended upon the sampling frequency, F_s and, resulted from $(N-1)*1/F_s$ with N representing the length of the signal. After processing the signal with Matlab the data was stored in the variable y and saved to a WAVE file, in an audio format. The data had a sample rate of F_s Hz and was saved as 16-bit, corresponding to the resolution of each sample in a set of digital, audio data.

4.5.3.1 *Noise cancellation*

A number of methods was experimented and applied to reduce the background noise depicted by the developed instrumentation. Quite often there were external noise sources, such as 60 Hz interference from power lines, temperature variations, vibration, and/or tribo-electric noise. There are many approaches to minimize the effects of noise during data analysis. A built in low pass filter was used during recording the data to eliminate frequencies above the Nyquist frequency of 10 kHz, preventing aliasing to occur. During the signal processing, a high-pass filter was applied to cut off all frequencies lower than 100 Hz. This process removes the low frequency noises, which could arise from the fixation of the sensors, unintended shaking, 60 Hz electrical noise and other low frequency noises present during the data collection process.

The power line noise was found in electrical signals due to AC power-line contamination. AC-powered appliances can give off a characteristic hum (often referred to as the "60 cycle hum"), at the multiples of the frequencies of AC power used. Electric hum is an audible oscillation at the frequency of the mains alternating current, which is 60 Hz in the US. The sound often has a heavy harmonic content. The most common way to eliminate the noise is through a 60 Hz notch filter. Because there are inherent variations in the 60 Hz signal, a notch filter is not robust against signal source frequency changes. Instead of this, the low pass filter was applied due to the fact that frequencies lower than 100 Hz were of no interest for the present analysis. It was most important that all AC powered devices were electrically grounded and all devices were attached to the same circuit to prevent extensive and exaggerated electrical noise.

However, the power line noise consisted not only of 60 Hz AC hum, but also distorted harmonics. The higher the harmonic (180, 240, 300 Hz...), the more audible the signal became. Those harmonics were much more difficult to eliminate and may vary with the environment. Before each experimental session, a noise profile was captured and used to identify the present noise components due to the operation of the machine, as well as due to the power line harmonics (Figure 28 and Figure 29). This profile was then later used to filter out the noise from the captured experimental data.

4.5.3.2 *Fourier Transform*

A Fourier Transform (FT) is a mathematical operation that transforms a signal from the time domain to the frequency domain, and vice versa. All signals were captured in the time domain, i.e. the signals were expressed with respect to time, while in the frequency domain, a signal is expressed with respect to frequency. In the time domain the behavior of the signal at every moment in time can be examined. However, it is difficult to use the signal captured at any particular moment of time to predict how the long-term behavior is related to the short-term development of the signal. Therefore, a better way to look at a signal is to view its spectral density (i.e., the Fourier transform of the signal). The Fourier Transform views the signal as a whole. It switches the dimension of time with the dimension of frequency (Figure 30).

The resulting sound was therefore analyzed using a Fourier Transform algorithm. Discrete Fourier Transform (DFT) was used to convert the signals from time to the frequency domain, which enables the analysis of the signal's properties. A DFT is a Fourier Transform applied to digital (discrete) rather than analog (continuous) signals.

An FFT (Fast Fourier Transform) is a faster version of the DFT that can be applied when the number of samples in the signal is a power of two. An FFT computation takes approximately $N * \log^2(N)$ operations, whereas a DFT takes approximately N^2 operations, so the FFT is significantly faster.

$$X(k) = \sum_{j=1}^N x(j) \cdot \omega_N^{(j-1)(k-1)}$$

$$\omega_N = e^{(-2\pi)/N}$$

with $\omega_N =$ an N th root of unity

$k = 1, \dots, N$

$N =$ length of the vector x

The power spectrum is the measurement of the power at various frequencies and can be calculated by:

$$P_{yy} = X * \text{conj}(X) / M$$

where $X =$ DFT of vector x

$M =$ M -point fast Fourier transform (FFT)

$\text{Conj}(X) =$ Complex conjugate of X

An application was developed (Figure 10), capable of analyzing the force, sound and acceleration data simultaneously. For the acceleration and sound analyses, the raw data, as well as filtered and windowed data were displayed in both the time and frequency domain.

When applying the FT to convert the signal to the frequency domain, the time information was lost. Therefore, when reviewing a FT of a signal, it was impossible to detect the occurrence of a particular event. If the signal properties did not change much over time, a stationary signal is detected and this weakness of the analysis becomes less important. However, the signals captured in course of this study contained numerous non-stationary or transitory characteristics: abrupt changes, beginnings and ends of events. These characteristics can be considered as the most important part of the signal since they change with the occurrence of certain events. A Fourier analysis was not capable of detecting them.

It was more beneficial to apply a windowing technique to analyze, using a FT, only a small section of the signal at a time, allowing for the ability to preserve both the time and frequency information. The spectrogram (Figure 27) reveals the portion of a signal's energy of the frequency as it changes over time. It was generated using the short-time Fourier Transform (STFT). Since the spectrogram has the ability to preserve the time information while revealing information about the frequency content, the spectrogram was used to filter and analyze the sound (Figure 30) (Glaser et al., 2008).

4.5.3.3 Joint transmissibility, impulse response and transfer function

To characterize the input-output relationship of the components of the system, the definition of transfer functions can be used. In the particular problem, transfer-function representation was applied because the system was assumed to be linear and time-invariant.

The transfer function of a linear and time-invariant system is defined as the ratio of the Laplace transform of the output (response function) to the Laplace transform of the input (driving function). It relates the output variable to the input variable under the assumption that all initial conditions are zero and uses mathematical modeling and operational methods to express the differential equations. Similarly, the acoustic transmissibility across the hip joint is defined as the ratio of acoustic response signal (Output) to the input force (Input):

$$\text{Transfer Function} = G(s) = \frac{Y(s)}{X(s)}$$

Most importantly, the transfer function is a property of the system and is therefore independent of the magnitude and characteristics of the input. The units to relate the input to the output are included in the transfer function, but no information concerning the physical structure of the system is implemented. Therefore, many physically different systems can be mathematically identical. Probably, the most important characteristic of a transfer function is that once the function is known, the output or the response can be studied for various forms of inputs. This leads to the understanding of the nature of the system and the factors mostly influencing its behavior.

Initially, the transfer function for our model is unknown and must be established experimentally by introducing known inputs to the system and studying the output. Once established, the transfer function allowed for a full description of the dynamic characteristics of the system to be detected.

One method that can be used to find the transfer function of a system is to apply the impulse response theorem. The impulse response is made up of a large number of sinusoids (Fourier components) and when it depicts a dominant ringing, with a given frequency f Hz, it is indicative of a resonance.

The Laplace transform of a unit-impulse function is unity, therefore, the Laplace transform of the output of the system $Y(s) = G(s)$ gives the impulse response of the system, which is defined as

$$L^{-1}[G(s)] = g(t)$$

The function $g(t)$ is called the impulse-response function of the system and represents the response of a linear system to a unit-impulse input when the initial conditions are zero. The Laplace transform of this function generates the transfer function. Therefore, the transfer function and the impulse-response function of a linear, time-invariant system contain the same information about the system dynamics. It was hence possible to obtain complete information about the dynamic characteristics of a system by exciting it with an impulse input and measuring the response. In practice, an impulse input with a very short duration, compared to the significant time constants of the system, can be considered an impulse.

In the present study it was assumed that if separation of the femoral head within the acetabular cup occurs, an impulse is generated. Initially, the femoral head slides within the acetabular component and comes to rest, with respect to translation, causing a standing wave to be generated at impact. This will result in impulse excitation and will

offer valuable information about the system characteristics and its behavior during the executed activity while under *in vivo* weight bearing conditions. Therefore, the actual subject-specific, *in vivo* hip joint dynamical conditions during weight-bearing activity were used to provide excitation of the pelvis through the impact of the femoral head in the acetabular component. The sound generated through the gait cycle was recorded and analyzed.

4.5.3.4 Wavelet

Additionally, wavelet analysis was applied to divide a given function into different frequency components and then each component was analyzed. The wavelet transformation (WT) is a mathematical function, especially powerful when applied to analyze the spectral properties of non-stationary signals such as the ones captured in this study. WT, which is the representation of a function by wavelets, was performed using scaled and translated copies of a finite-length or fast-decaying oscillating waveform which is selected based on the signal characteristics. For representing functions that have discontinuities and sharp peaks, and for accurately deconstructing and reconstructing finite, non-periodic or non-stationary signals the Wavelet analysis seemed to be more suitable than the traditional Fourier transformations. The WT is capable of overcoming the frequency and time resolution problems associated with the short-time Fourier Transform (STFT). The STFT provides some information about when and at what frequencies a signal event occurs, but the precision is only limited and depends on the size of the window. Once a particular size for the time window, the portion of the signal analyzed at a time, is chosen, that window remained the same for

all frequencies. While the STFT provided uniform time resolution for all frequencies, the WT adjusted the time and frequency resolution with the changing frequency: high time resolution and low frequency resolution for high frequencies and high frequency resolution and low time resolution for low frequencies (Figure 30 and Figure 31). The WT was performed using the windowing technique, but the window width was changed for every spectral component and then the transform was computed, which was the most significant characteristic of the wavelet transform.

In the Continuous Wavelet Transform (CWT), a mother wavelet (or analyzing wavelet) was chosen, and then the signal was multiplied by the wavelet function (window), and the transform is computed separately for different segments of the time-domain signal.

The Discrete Wavelet Transform (DWT) analyzed the signal at different frequency bands with different resolutions by decomposing the signal into a (coarse) approximation coefficients and detail coefficients. During the wavelet decomposition (Figure 32) the signal was passed through several band-pass filters to obtain signal components at different band-widths, for subsequent analysis and processing. DWT employed two sets of functions called scaling functions and wavelet functions (Figure 33), which were associated with low-pass and high-pass filters, respectively. The decomposition of the signal into different frequency bands was obtained by successive low-pass and high-pass filtering of the time domain signal and down-sampling the signal after each filtering.

The DFT of the signal x of the length N was defined as:

$$W(j, k) = \sum \sum x(k) 2^{-j/2} \psi(2^{-j} n - k)$$

where $\psi(t)$ = mother wavelet, a time function with finite energy and fast decay.

In the discrete domain, a filter is represented as a set of numbers which represent the impulse response of the filter. The signal was decomposed by successive high-pass and low-pass filtering of the time domain signal, where the filtering operation corresponded to the convolution of the discrete signal x with the filter g or h :

$$y_{high}[k] = \sum_n x[n]g[2k - n]$$

$$y_{low}[k] = \sum_n x[n]h[2k - n]$$

where $y_{high}[k]$ = output of the high pass filter g

$y_{low}[k]$ = output of the low pass filter h

These vectors are obtained by convolving x with the low-pass filter for approximation, and with the high-pass filter for detail, followed by dyadic decimation outputting the detail coefficients cA_j from the low-pass filter and the approximation coefficients cD_j from the high-pass filter. According to Nyquist's rule, half of the samples were discarded. The filter outputs were then down-sampled by 2 (Figure 32). Only half of each filter output was needed to characterize the signal, therefore this process reduced the time resolution by half. On the other side, each output has half the

frequency band of the input so the frequency resolution was doubled. Only the low-frequency sub-bands were successively decomposed into two (finer) sub-bands, while the high-frequency sub-bands were untouched. Therefore, the approximation coefficients (low frequencies) have a high frequency resolution but poor time resolution, while the detail coefficients of level 1 (high frequencies) have a poor frequency resolution but good time resolution. This led to the progressive change in successive levels of the frequency and time resolutions of the detail coefficients (Figure 31).

This decomposition process was repeated on the coarse approximation as necessary to further increase the frequency resolution. This leads to a tree shaped (pyramidal) algorithm with nodes representing a sub-space with different time-frequency localization (Figure 32). The low-frequency sub-band of the last stage was called the approximation coefficients. The combination of approximation coefficients and the detail coefficients of all levels was defined as DWT coefficients. The tree was an array of band-pass filters which separate the input signal into several components. Each of those components carried a single frequency sub-band of the original signal and allowed for detailed analysis of the original signal. This process is called a filter bank and was designed in such a way that sub-bands can be later recombined to recover original signal (synthesis). The reconstructed details and approximations are true components of the original signal and the original signal can be reassembled through the combination of all components:

$$x = A_1 + D_1 = A_2 + D_2 + D_1 = A_3 + D_3 + D_2 + D_1 \dots$$

A variety of different wavelet families have been defined in the literature. The selection of the mother wavelet is important and can define if successful signal decomposition is possible. In this analysis, the 6 coefficient wavelet family (DB6) proposed by Daubechies, 1988 was used (Figure 34). Different mother Wavelet and scaling functions are presented in Figure 33.

The extracted wavelet coefficients provided a compact representation that showed the energy distribution of the signal in time and frequency. Statistics over the set of the wavelet coefficients was applied to further reduce the dimensionality of the extracted feature vectors. The mean of the absolute value of the coefficients in each sub-band provided information about the frequency distribution of the signal. The standard deviation of the coefficients in each sub-band provided information about the amount of change of the frequency distribution. Ratios of the mean values between adjacent sub-bands provided information about the frequency distribution.

The extracted frequency components are studied with a resolution matched to its scale. The term 'scale' corresponds to the inverse of frequency or to the time resolution. The scale can be converted to a pseudo-frequency by computing the center frequency F_c of the wavelet by associating a given wavelet with a purely periodic signal of frequency F_c :

$$F_a = \frac{F_c}{a \cdot \Delta}$$

where F_a = the center frequency of a wavelet in Hz

F_c = the pseudo-frequency corresponding to the scale a , in Hz

a = is a scale

Δ = sampling period.

Optimal examination and interpretation of the measured sound signal was obtained by decomposing the signal into different components best describing its nature (Figure 35) (Glaser et al., 2008). Initially, the signal was separated into coherent and noisy portions. The noise part was eliminated and the remaining portion of the signal was broken down into its main components. Knocking modules are identified as impulse loads; representing very short durations in time pulses with high amplitude peaks (i.e. high-pitched note that usually sweeps steeply upward in pitch) (Figure 35d). The energy released during the transition from static friction to dynamic is transferred to audible sound. Other sound characteristics based on frequency, magnitude, distribution, and the level of occurrence were defined and comparatively analyzed. The classification of the signal into such main components helped the pattern extraction and the structural and mechanical understanding (Glaser et al., 2008).

4.6 Calibration, Filtering and Error Analysis

4.6.1 Distortion correction

Images captured from the fluoroscopy are initially geometrically distorted by an effect called pin cushioning, created by the distance between the x-ray source and the

image intensifier. This effect caused the pixels of the images to concave inwards, so that the images appear to be warped. In order to correct (un-warp) the images, a calibration method was performed using a calibration grid called bead board (Figure 36, top left). Due to the rigid connection of the x-ray source and the image intensifier to the C-arm of the fluoroscope, the same distortion can be applied through the entire image sequence for one fluoroscopic experiment session performed with the same machine.

The bead board consisted of a clear plexi-glass plate with metal beads inserted at a known distance apart from each other in grid format. The bead board fluoroscopic image was used to estimate the geometrical distortion by an algorithm in Matlab™ (The MathWorks, Inc., MA, USA) (Mahfouz et al., 2003). The Matlab code estimated each 2D spatial transform of the four bead bounded blocks throughout the board (Figure 36, top right) and applied a local bilinear mapping model and gray level interpolation method to remove the distortion (Mahfouz et al., 2003). Overall the Matlab process found the digital pixel locations of the beads in the board (state space) and compared it with the known bead distances (Figure 36, bottom left). Afterwards, a transform function was created to calibrate all of the fluoroscopy images from state space back to the true bead board geometries (Figure 36, bottom right). This process was used to un-warp all images taken by the particular fluoroscopy machine and was performed in all images before the three dimensional reconstruction (Mahfouz et al., 2003).

The letter “E” was also placed on the board to observe whether the fluoroscopy unit inverted the images.

4.6.2 Fluoroscopic error analysis

The factors influencing the accuracy of the position reconstruction of the implants are motion blur and the reduction of the image contrast due to bone or soft tissue overlay, thus leading to a reduction of the signal to noise ratio. It is important to estimate the accuracy of the 3D-to-2D registration process, which can be easily performed using static and dynamic tests.

Two previously published error analyses verified the accuracy of the 3D model-fitting process (Dennis et al., 1996, Mahfouz et al., 2003). Threshold analysis of the 2D to 3D registration system have shown that the translational error is approximately 0.1 mm (with exception of the Z-direction) and rotational error approximately 0.4 degrees under ideal conditions. Experiments have been performed by Mahfouz (Mahfouz et al. 2003) to determine this threshold by comparison of values taken from three different setups. One setup included manually placing the implants in known positions in front of the fluoroscopy machine, taking the image, overlaying the image, and comparing the numbers. Another setup involved implanted cadaver legs which were monitored by an Optotrak system (Optotrak, Inc, Cary, NC, USA) as well as the fluoroscopy machine. The final test used real human subjects (Mahfouz et al., 2003).

An error threshold of 0.5 mm was obtained (Mahfouz et al., 2003); therefore, femoral head sliding was predicted to occur if the femoral head-to-acetabular cup distance was greater than 0.5mm.

4.6.3 Acoustic and vibration measurement calibration and validation

To ensure proper operation of the newly developed acoustic and vibration analysis technique, various functionality tests were performed. Accelerometers were mounted to a metal beam fixed on its one end and free on the other. The free end of the beam was displaced and then released. The vibration of the beam was measured with both accelerometers to assure that those are working simultaneously, that the axes are properly orientated and no significant cross-talk between the channels exists (Figure 37). All channels {x,y,z} of the accelerometers {1,2} were measured simultaneously. The beam vibration was executed in z-direction of the sensors, where the accelerometer Az1 was showing in opposite direction than Az2.

Additionally, a calibrated vibration generator, so called shaker, (PCB394CO6, PCB Piezotronics, Inc., Depew, New York, USA) was used to apply a known frequency operation mode and amplitude to the accelerometers. This handheld shaker is a small, self-contained, battery powered, vibration exciter specifically designed to conveniently verify accelerometer and vibration system performance. The used device operated with 1g RMS acceleration at 159.2 Hz. The data was collected and the measured results were compared to the applied signal (Figure 38 and Figure 39).

The noise level in the operating room was captured before and after each experimental session and a low noise-to-signal ratio was ensured. An attempt was made to filter out unwanted vibrations, induced by machinery motor speed and power line frequency, as well as those from soft-tissue movement (Figure 40) and muscles contractions (Figure 41). The effects of the thickness of the soft tissue were found to be

only moderate and have not been considered in the present study. The Tribo-electric effect is when a spurious signal is generated by a charge output accelerometer by the movement of the co-axial cable. Noise from sources such as those associated in the connecting cable was eliminated by proper mounting of the sensors on the testing surface. The sensor itself as well as the cable in a distance of at least 2 inches was securely fixed to the surface. This eliminated, or at least drastically reduced the possibility and the magnitude of any noise that can occur due to accidental shaking or touching of the accelerometer connection cables.

In order to exclude noises generated from friction, rubbing, and gliding of the instrument, great care was taken to apply the sensors firm but not too tight, so that they will not shift during the procedure. Accelerometers are less sensitive than microphones or stethoscopes with respect to those types of noises, which gives additional advantages to the chosen technique.

Chapter 5

3D Mathematical Modeling

Modeling of dynamic systems and analyzing dynamic characteristics is of great importance to the study and understanding of biomechanical systems, since only limited methods are available to obtain the desired information experimentally. A mathematical model of the human body is defined as a set of differential equations that represent the dynamics of the system and are obtained using the physical laws governing the particular system. In the present study, Newton's law was used to define the model; however, Kane's dynamics (Kane et al., 1985, Kane and Levinson, 1996) was applied to simplify the mathematical model and to optimize its performance (Glaser et al., 2007). In contrast to the use of the classical formulation of dynamics with generic equations of motion, Kane's unique method of auxiliary generalized speeds builds compact, customized and computationally efficient algebraic equations. The equations of motion for this model were determined using the symbolic manipulation algorithm Autolev™ (Online Dynamics Inc, Sunnyvale, CA) and Matlab™ (The MathWorks, Inc. Natick, MA). The purpose of this analysis was to compare the force patterns of THA patients with different bearing surfaces. As a final point, the calculated hip contact forces were compared to in-vivo measured forces produced by Bergmann's telemetric hip data (Bergmann et al, 2001).

5.1 Introduction

To solve for a biological system containing of several objects responding dynamically to their environment requires a real-time solution of that virtual system's equations of motion. Generic equations of motion can provide a solution for a system of a single body or an open chain, but such an approach usually severely limits the family of objects that can be simulated. Instead, when customized equations are formulated and solved by a computer symbolic manipulation or specialized numerical routines, new possibilities of analysis of large and complex systems are opened.

The human body is a multi-body system, or a system of rigid bodies interconnected by various joints that make or break contact with each other during the course of the countless different activities. Therefore, the defined model has to take into account the different and changing contact conditions which may include collision, slide, or roll.

This study presents the design of a multi-body system defined with the symbolic manipulator AutolevTM (OnLine Dynamics, Inc., Sunnyvale, CA, USA; Kane and Levinson, 1996), which enables the user to solve for larger multi-body systems. The designed application automatically formulates the equations using a system description: geometry, inter-connections, external forces, inertia properties, and constitutive laws for springs (such as ligaments). Once formulated, the governing equations were passed to a real-time solver formulated in MatlabTM (The MathWorks, Inc. Natick, MA) that determines the solution of the system (Glaser et al., 2007).

5.2 Coupling the measurement reference frames

For the mathematical description of the leg, the kinematics obtained from fluoroscopy and processed with the 3D-to-2D registration and the ground reaction forces are needed as an input. Each of those parameters has been calculated using different techniques with a coordinate system specific for the processing application. For this reason all variable reference frames had to be transferred to the one global reference frame defined in the mathematical model. The mathematical simulation employed the following reference axes orientation, specified as the Newtonian reference frame N : $1>$ is anterior-posterior (AP), $2>$ is superior-inferior (SI) and $3>$ is in medial-lateral (ML) direction, pointing out of the frame. The left hand rotations of SAAM and the opposite Z-axis orientation were considered as data was transferred to the mathematical model (Figure 42).

5.3 Skeletal Modeling

The human body consists of 7 segments representing the stance foot, stance tibia, stance femur, swing foot, swing tibia, swing femur, the head and torso. For a successful simulation of one step during the gait cycle, only one leg is necessary to gather the required parameters. The number of segments included in this model is based on the consideration of the adequate movement by compromising unnecessary complexity. Therefore, only one leg, consisting of the foot, tibia, femur and the pelvis, as well as the spine modeled as a fix point was created, which allowed for the determination of the joint reaction forces of the ankle, knee, hip and spine during gait.

The chosen segments were separated by anatomic points and joint representation such as bottom of the foot, ankle joint, knee joint with rolling, and the hip joint. All body segments were defined to be rigid.

The developed mathematical model was based on an inverse dynamics model of the lower body (Figure 43). Rather than computing constraint forces as an auxiliary process to the forward dynamics problem, this study used the inverse dynamics formulation which allows inputting the motion and outputting the corresponding forces. Additionally, the inverse approach is more stable than the forward solution model and replaces numerical integration of differential equations with repeated algebraic solution of linear equations. These advantages can make the inverse approach significantly faster and more robust computationally than the forward approach.

The mathematical model of the lower extremity, derived during this study, was an open chain system with four bodies and three joints. Each simulation was customized to the specific patient by incorporating the structural properties and the subject specific motion. The present system employed AUTOLEVTM (Schaechter, 1988), (Kane and Levinson, 1999), (Autolev, 2003) for defining the system and a manipulated MatlabTM (The MathWorks, Inc. Natick, MA) based application to perform the symbolic algebra.

The final results provided the three-dimensional interaction resultant forces and moments. Those kinetic values represented the vector sums of forces in muscles, ligaments, and capsules, forces on the joint-contact surface, and the moments engendered by those forces. There are more unknowns than equations of motion, which

makes the problem indeterminate. Therefore, the model was simplified by grouping functionally similar hip muscles, applying the reduction technique. Details on the method of calculating the contact forces for normal have been reported previously (Komistek et al., 1994, 1998; Dennis et al., 1996; Komistek, 2005). Additions were made by including the key components of the quadriceps mechanism: patella ligament, quadriceps muscles and the patello-femoral interactive forces. Also integrated in the model were the hip capsular ligaments, which were modeled as springs (Glaser et al., 2007).

In this way, the system included a whole dynamic chain from the foot through to the spine. Particularly, the foot, tibia, femur and pelvis were modeled as rigid bodies referred to as A , B , C , D , ground was fixed and treated as the stationary Newtonian N reference frame and the patellar ligament, patella and quadriceps were modeled as the frames referred to as L , P and Q similarly to the ligaments of the hip capsule (Figure 43). The coordinate system was setup at the mass center of each analyzed body. The reference axes were oriented anterior-posterior (AP) and superior-inferior (SI) directions referred to as $1>$ and $2>$ directions in free body diagram, whereas the medial-lateral (ML) direction, here axis $3>$, was pointing out of the frame (Figure 43). One whole step from toe-off to toe-off was simulated.

In the 3D space six equations of motions can be formulated for each body, three for the translations and three for the rotations around each axis. The presented model included four rigid bodies and a maximum of 24 equations of motions were used for solving for the same amount of forces and torques. The Forces F_{AI-3} in the Ankle, F_{KI-3} in the Knee, F_{HI-3} in the Hip and F_{SI-3} in the spine and the related torques were solved.

Since the multi-body model has to hold interconnected bodies together and maintain the pertinent constraint conditions, seven constraints equations were embedded into the equations of motion. The ligaments were computed as part of the simulation and fed back as appropriate constraint forces. The constraints associated with the joints of a mechanism that are not broken during the simulated activity are embedded while the constraints associated with a rolling or sliding contact that are subject to change during simulation were treated by using moving contact points. The distal end of the femur was modeled as a rolling cylinder with equal radii on both condyles chosen to be the average radius of the femoral condyles in the sagittal plane and with a length equal to the width of the intercondylar distance. Only one contact point was considered between the femur and the tibia and no lift-off of one of the condyles has been allowed. The femur is assumed to roll along the AP direction. For the rotations at the hip joint, the values obtained from the 3D registration have been used as input. The center of rotation of the femur and the acetabulum was assumed to be the center of the femoral head. The contact forces were transmitted between both bodies through a moving contact point which is aligned with the assumed direction of the resulting force. A contact area was not considered and no contact pressure was calculated. The ankle was assumed to act as a hinge joint. The relative motion between the foot and the ground while in contact (stance phase) was assumed to be a rotation with progressing contact position. During swing, when the foot is off the ground, the progression of the foot is represented through a translation in the sagittal plane, in walking direction.

5.3.1 Model inputs

The inverse dynamics model was derived for the purpose of solving for all significant leg forces and torques that are used to generate the prescript space-time motion. For this reason, the joint kinematics $q_i(t)$ for $i=1,\dots,4$ has to be input into the simulation, since they describe the state of the leg at every instant of time t .

5.3.2 Rotation angles

The rotation angles were obtain from the fluoroscopy video at heel strike, 33% of mid-stance, 66% of mid-stance, toe off, and four images were taken during the swing phase. The kinematics of the knee and hip were obtained from fluoroscopy. Those for the foot and ankle were assumed based on observations. The angles of rotation for the foot with respect to the ground and the ankle were approximated based on observations (Figure 44 - Figure 45). The angle of rotation of the knee was obtained from fluoroscopy data for a healthy subject (Figure 46). The angle of rotation of the hip was obtained from fluoroscopy data for the THA subjects under investigation (Figure 21 - Figure 23). Because the motion data was obtained on different subjects it needed to be scaled in the time, so that the gait activity, which represents one whole step (from toe-off through heel-strike to toe-off), is identical for all joints. There was no data available for knee subjects for the swing time. The knee rotation of this time period needed therefore to be approximated.

The angles of rotation in $N3>$ direction for the foot with respect to the ground and for the ankle were assumed and were not based on real fluoroscopy data, while the

other rotations were assumed to be zero. The angles of rotation for the knee for the stance phase were obtained from fluoroscopy data for a TKA subject. The $NI>$ rotation was assumed to be zero; since it was assumed that lift-off of the condyles did not occur. The angles of rotation of the hip were obtained from fluoroscopy data of the THA subjects.

A ground reaction force F_{AN} (GRF) was applied as an external force at the contact point of the foot with the ground. All equations for the vertical and horizontal components were formulated based on recorded force data, taken specifically for each patient while performing one step on the fixed force plate. For the swing phase the GRF was added as zero (Figure 47).

The relative joint kinematics obtained from fluoroscopy and the ground reaction force data were curve-fit using piecewise functions as splines of order three or higher with the least sum square error. Those functions were entered into the mathematical model as input for the simulation. The developed model gives an accurate 3D representation of the in-vivo kinematics and kinetics for subjects after THA for gait, ensuring that the soft-tissues and interactive forces were modeled correctly.

Only principle moments of inertia were included for each of the rigid bodies. All other inertia values were assumed insignificant. A left human leg from our extensive Computer Tomography scan data collection, which was similar to the size and shape of the subject tested, was used to determine bone mass centers, as well as the origin and

insertion position of the ligaments and muscles (Glaser et al., 2007). Segment inertia parameters were obtained from a study done by De Leva (1996).

5.3.3 Moving contacts

A moving contact point between the foot and the ground was defined, representing the change of the position of the foot during the gait cycle. In the period between heel-strike (HS) and toe-off (TO) the foot is in contact with the ground and the contact point is moving from the heel to the ball of the foot (Figure 48). The initial contact point is on the heel and is defined as *ANO*. The foot progression is the translation of the foot in the walking direction while swing phase of gait when the foot is not in contact with the ground. A step length of 0.5m has been assumed for all patients.

According to the biomechanical feature of the knee and hip, moving contact points between tibia/femur and femur/pelvis were defined, since the femur is sliding posterior-anterior during knee flexion and extension involved into the gait cycle. For the knee joint the minimum distance between the tibia and femur in the sagittal plane of the fluoroscopic images was found for each increment of time during the stance phase. Those points were then evaluated with respect to the central axis of the tibia and the femur, respectively (Figure 49 - Figure 54). After curve-fit, the generated equations were used as a translational input of the contact position into the model.

The moving contact point of the hip joint is measured from the center of the femoral head and is pointing in the direction of the resulting hip force (Figure 55 - Figure 58).

5.3.4 Muscles and ligaments

The quadriceps was attached to the pelvis and the location of the interaction on the pelvis was obtained from CT scans of a female subject. The rotation of the quadriceps with respect to the patella and the orientation of the patella with respect to the patellar ligament were obtained from the defined geometry based on change of the position vectors (Figure 59). Since the system of the patellar ligament, the patella and quadriceps builds a chain without external forces and with insignificant small inertia, only one unknown has to be calculated from the available equations of motion, while the other resulting forces can be simply extracted from the geometrical orientation (Figure 60). When the quadriceps force ($F_{_QD}$) is calculated and therefore considered as given, the patellar ligament force ($F_{_PL}$) and the force applied from the patella on the femur in normal direction ($F_{_PT}$) can be calculated with the following equations:

$$F_{_PL} = F_{_QD} * \frac{\cos(QPQ3)}{\cos(QLP3)}$$

$$F_{_PT} = F_{_PL} * \sin(QLP3) + F_{_QD} * \sin(QPQ3)$$

with $F_{_QD}$ = Quadriceps force

$F_{_PL}$ = Patellar Ligament force

$F_{_PT}$ = Normal force between patella and femur (in 1> direction)

$QPQ3$ = Angle between the patella and quadriceps in the sagittal plane (Figure 60)

$QLP3$ = Angle between patella and patellar ligament in the sagittal plane (Figure 60)

The force applied from the patella on the femur in $2^>$ direction was calculated based on principles of friction and was directed in the opposite direction of the resultant force acting on a body:

$$F_{CP2} = F_{PT} * \mu$$

with F_{CP2} = Force in $2^>$ direction on the femur due to the contact interaction with the patella

μ = coefficient friction

F_{PT} = Normal force between patella and femur (in $1^>$ direction)

The hip ligaments were modeled as springs (Glaser et al., 2007). For the hip capsule (Figure 61), the iliofemoral ligament was built out of 2 fibers (k_{A1} = 97.8 N/mm and k_{A2} = 100.7 N/mm) and the ischiofemoral ligament out of 6 fibers, each with a stiffness of k_P = 6.15 N/mm resulting in a overall stiffness of 36.9 N/mm (Figure 62). A study done by Hewitt (2002) quantified the values of the stiffness coefficients for the hip capsular ligaments via tensile tests on cadaveric specimens, which were subsequently utilized in the present model. The forces of the hip capsular ligaments were calculated based on their change of length with respect to time, which was obtained from the relative position of the bodies using position vectors. The attachment points on the femur and pelvis are fixed in the C and D coordinate system, respectively. The minimum

length was assumed to be the unscratched length of each ligament. Ligaments as well as muscles act only under tension and cannot apply a compressive force. Therefore care was taken that no muscles or ligaments resulted in a negative (compressive) force at any time during the calculations. Some previous research has suggested that ligaments respond to loading in a nonlinear pattern. In the present study ligaments have been considered as linear springs because slow gait, examined in the study, belongs to the normal daily activities. Since ligament forces are considered to be in their physiologic phase during simple unexacting activities, it was assumed to have linearity to predict ligament forces in the mathematical model.

Ligament forces were calculated using position vector information and then input as restrictive forces in the mathematical model.

5.3.5 Kane's dynamics

Kane's method was chosen among the different available techniques for formulating equations of motion for multi-body systems, because of its relative ease of computer based automation and its computational efficiency. Efficiency here combines the possibility to produce equations with the fewest symbolic operations as well as such equations that require the fewest numerical operations for their solution. Using Kane's method and Autolev, a program to symbolically define multi-body dynamic systems and outputs FORTRAN, Matlab and C source code containing the equations of motion, an effective method of defining and solving the multi-body differential equations has been applied.

For both, the Kane's Dynamic Method and the Newton-Euler approach, the first step is to derive expressions for the velocity and the acceleration of each rigid body in the system. Along with geometrical information, the known kinematics enable the velocities and accelerations of all the important points (with mass and where forces are applied) within the system to be computed. The velocities and accelerations $\{\dot{q}_i(t), \ddot{q}_i(t)\}$ were obtained from differentiation of the position vector $q_i(t)$ since the initial conditions $\{q_i(0), \dot{q}_i(0), \ddot{q}_i(0)\}$, $i=1, \dots, n$ are known.

Since the leg geometry and the joint variables q, \dot{q}_i, \ddot{q}_i are known or can be obtained through mathematical calculations, the angular velocity ${}^j\omega^i$, the angular acceleration ${}^j\alpha^i$, and the linear acceleration of the mass center a^{i*} of the i th body are obtained by using those of the $(i-1)$ st body. The angular velocity ${}^j\omega^i$ is a vector that facilitates analysis of motions of the rigid body i in reference frame j :

$${}^j\omega^i = I_1^A \frac{dI_2}{dt} \cdot I_3 + I_2^A \frac{dI_3}{dt} \cdot I_1 + I_3^A \frac{dI_1}{dt} \cdot I_2$$

The angular acceleration ${}^j\alpha^i$ of the rigid body i in the reference frame j is defined as the first derivative with respect to time of ${}^j\omega^i$:

$${}^j\alpha^i = \frac{{}^i d^j \omega^i}{dt}$$

The kinematical equations describe motions, but do not relate the motion to the forces and torques which determine the motion. The kinematical equations are complete when the velocities of all points affected by forces, and all accelerations of mass centers

are known. The kinematics of the system are much easier to describe using local reference frames affixed to each body rather than a global, Cartesian coordinate reference frame.

Using direction cosines, any vector can be expressed in terms of the component vectors of the reference frames. Direction cosines also allow to work simultaneously in multiple frames without continual transformation of positions vectors, velocities and accelerations to a common reference frame. The dot products between unit vectors of different coordinate reference frames build up the elements of the direction cosine matrix. The transformation between two bodies in contact was derived using the Euler angles $\text{Rot}(3>,\theta_3) - \text{Rot}(1>,\theta_1) - \text{Rot}(2>,\theta_2)$. In the matrices, $C\theta_1$ represents $\cos(\theta_1)$, $S\theta_1$ represents $\sin(\theta_1)$, and similarly for the other subscripts:

$$\begin{Bmatrix} J1 > \\ J2 > \\ J3 > \end{Bmatrix} = \begin{bmatrix} C\theta_1 & S\theta_1 & 0 \\ -S\theta_1 & C\theta_1 & 0 \\ 0 & 0 & 1 \end{bmatrix} \begin{bmatrix} 1 & 0 & 0 \\ 0 & C\theta_2 & S\theta_2 \\ 0 & -S\theta_2 & C\theta_2 \end{bmatrix} \begin{bmatrix} C\theta_3 & 0 & -S\theta_3 \\ 0 & 1 & 0 \\ S\theta_3 & 0 & C\theta_3 \end{bmatrix} \begin{Bmatrix} I1 > \\ I2 > \\ I3 > \end{Bmatrix}$$

$$\begin{bmatrix} C\theta_1 \cdot C\theta_3 + S\theta_1 \cdot S\theta_2 \cdot S\theta_3 & S\theta_2 \cdot S\theta_3 \cdot C\theta_1 - S\theta_1 \cdot C\theta_3 & S\theta_3 \cdot C\theta_2 \\ S\theta_1 \cdot C\theta_2 & C\theta_1 \cdot C\theta_2 & -S\theta_2 \\ S\theta_1 \cdot S\theta_2 \cdot C\theta_3 - S\theta_3 \cdot C\theta_1 & S\theta_1 \cdot S\theta_3 + S\theta_2 \cdot C\theta_1 \cdot C\theta_3 & C\theta_2 \cdot C\theta_3 \end{bmatrix} \begin{Bmatrix} I1 > \\ I2 > \\ I3 > \end{Bmatrix}$$

Usually differential calculus is used to derive the dynamic equations. In a kinematic chain of linked rigid bodies, a vectorized method of deriving the accelerations was applied using vector cross products.

To construct the dynamic model of the lower body system S , variables properly describing the configuration of S and variables that specify the location of a reference point and orientation of a reference frame fixed within each body of S were necessary to be defined. These variables may be called configuration variables and represent the generalized coordinates in Lagrange's method. While the set of variables necessary to specify the location and orientation of each body relative to a common ground could be quite large, a set of generalized coordinates is reduced in number:

$$n < 6 * v - (M + m)$$

with

v	=	Number of bodies of S
M	=	Number of configurations constrains
m	=	Number of motion constrains.

This resulted for the present problem of four rigid bodies building the leg system to 24 generalized coordinates.

While Lagrange's method results in differential equations, Kane's method implements generalized speeds (U) leading to significantly compacter equations. Those motion variables are defined as functions that are linear in the configuration variable derivatives. The number of independent generalized speeds that is required to describe the motion of the system in a particular reference frame is resulting in the number of degree of freedom (DOF) of the system in the given reference frame.

5.3.6 Equations of motion

Based on Kane's method of dynamics the system equations of motion were formulated. The basic equation for Kane's method is derived from Newton's 2nd law of motion:

$$F_r + F_r^* = 0, \quad r = 1, \dots, n$$

The equation above defines the sum of generalized active (F_r) and generalized inertial forces (F_r^*) for each generalized speed equal to zero, where

$$F_r^* = m \cdot a$$

Generalized active forces (F_r) are a combination of the constrained and unconstrained generalized active forces, while the generalized inertial forces (F_r^*) are a combination of the constrained and unconstrained generalized inertial forces of the dynamic problem.

$$F_r = \sum_{u=1}^N [{}^J V_{Ur}^I \cdot \underline{F}^I + {}^J \underline{\omega}_{Ur}^I \cdot \underline{T}^I]$$

$$F_r^* = \sum_{u=1}^N [{}^J V_{Ur}^I \cdot \underline{F}^{I*} + {}^J \underline{\omega}_{Ur}^I \cdot \underline{T}^{I*}]$$

with $r =$ the r^{th} degree of freedom

$n =$ total number of degrees of freedom (here 24)

$N =$ number of rigid bodies in the system (here 4)

$Ur =$ the r^{th} generalized coordinate

$I =$	referencing a body
$J =$	coordinate of the fixed reference frame
${}^J\underline{V}_{Ur} =$	partial velocity or partial derivative of the of change in distance between the position and mass center velocity vector in the rigid body
${}^J\underline{\omega}_{Ur} =$	partial angular velocity or the derivative of the orientation of the rigid body
$F^I =$	resultant force acting on the body
$T^I =$	resultant torque acting on the body
$F^{I*} =$	resultant inertia force on the body
$T^{I*} =$	resultant inertia torque on the body

Using position vectors, velocities, and angular velocities along with 24 equations of motion and the input from the kinematic data, generalized forces and generalized inertias were derived.

5.3.7 Inertial parameters and dimensioning

One of the main goals for the conversion to a fully functional three dimensional model was the integration of more accurate constants and dimensions. In order to get more accurate dimensions a measuring method was implemented in the current project

including CT scans from the same segmented cadaver imported to Rapidform 2006 (INUS Technology, Inc., Seoul, South Korea) three-dimensional scanning software, Figure 63. Once each segment was aligned in the correct coordinate system it was dimensioned using a three-dimensional measuring tool. The resulting dimensions can be found in Table 6.

Segment inertia parameters were obtained from a study done by De Leva in 1996 in which he used an improved gamma-ray scanning technique to obtain relative body segment masses, center of masses, and radii of gyration. The equation used for the mass moment of inertia for a given segment was:

$$I = (M \cdot m) \cdot (l \cdot r)^2$$

with $M =$ body mass

$m =$ % body mass of segment

$l =$ segment length in the longitudinal direction

$r =$ radius of gyration of the segment about the considered axis

The resultant segment inertias can be found in Table 7. The segment masses are summarized in Table 8.

Chapter 6

Statistical Analysis

The means of the kinematic and kinetic variables for the different implant groups were compared for statistical significance. The variables were first tested for normal distribution using the Shapiro-Wilk W test. Variables with normal distribution and equal variance were compared using the Student's t-test to test for significant differences between each implant group. This statistical method could be applied since the groups analyzed were randomly selected (e.g. the selected samples were chosen to be independent from each other), so that the study resulted in an independent sample design.

For the obtained kinematic data, student's t-test with a risk level (α -level) of 0.05, which is especially adequate in estimating the mean of a population when the sample size is small, was used to test for significance between the groups. The selected samples were chosen to be independent of each other (e.g., individuals were randomly selected for each group). The statistical analyses were conducted using JMP (V7, SAS Institute Inc., Cary, NC, USA).

Chapter 7

Results

The relevant results from the 3D *in vivo* kinematics and kinetics of the different bearing groups are presented in this chapter together with the findings of the acoustical and vibrational analysis.

7.1 Kinematics and Separation

The kinematics was examined and the separation was diagnosed when femoral head sliding from the acetabular component occurred and measured greater than 0.5mm. Twenty-four out of thirty-one patients were included in the kinematic and separation analyses. A detailed presentation of number of patients included in each analysis is shown in Table 9. Some patients were not included in the kinematic analysis due to the fact that the 3D CAD-models for the implants could not be obtained, either from the manufacturer or as retrievals for creating the CAD models through reverse engineering.

From fluoroscopy, the obtained relative transformations represented the sequential rotation about the three orthogonal axes and displacement transfers starting from an initial position. The sequence order of the rotations was 3, 1, 2 with the axes defined in Figure 43. Rotation occurring around the 3-axis represented a pure flexion/extension. Rotation around the 2-axis was denoted as internal/external rotation,

although it must be noted that this rotation was around the first intermediate 2-axis. Similarly, the rotation around the 3-axis is not a pure abduction/adduction, but rather a rotation around the second intermediate 3-axis (Figure 64).

Values representing the displacement of the femoral head component from the acetabular cup followed similar trends across the patient population. However, these separation values differed across the different bearing groups. The average separation and its variance between the subjects in each group are displayed in Figure 65 to Figure 67 for the each of the patient groups as well as for the hard-on-soft and hard-on-hard groups.

All subjects in this study, except for one subject having a ceramic-on-polyethylene THA, experienced femoral head separation. All groups experienced a high incidence of separation. Significant higher separation magnitudes were observed for the metal-on-polyethylene group than for the two bearings with the lowest separation, ceramic-on-polyethylene and metal-on-polyethylene with polyethylene-inner-liner patients ($p=0.01$; Table 10). The separation values along with the mid-range laxity during surgery and the number of patients that underwent capsular repair are shown in Table 2.

The bearing group demonstrating the highest average maximum separation was metal on polyethylene articulation, with an average value of 3.9mm (1.4-5.6 mm). Also, among all analyzed subjects, a patient with a metal-on-polyethylene articulating surface experienced the highest magnitude of separation, with a value of 5.6 mm. Interestingly,

the separation values never dropped to the state of no-separation and the separation values for each of the subjects in the metal-on-polyethylene group demonstrated multiple periods of rapid change during the stance-phase of gait (Figure 65a). The separation characteristics of each patient did not exhibit a trend over time, but instead appeared to represent a jerky motion.

The metal-on-metal subjects also revealed a high average separation, with a value of 3.0mm (1.7-4.4mm). This increased separation resulted mainly because of the large head prostheses groups which experienced on average large separation with values of 3.2mm (2.5-4.2mm) and 4.1mm (3.8-4.4mm), respectively (Figure 68). The large head implants are not fully spherical and edge contact of the inferior part of the head with the interior surface of the cup occurred during the gait cycle (Figure 69). This design lead to a hinge movement around this edge and resulted in high separation values. In this situation there is a true separation of the medial aspect of both contact surfaces, reducing the contact area to a small region along the rim. The femoral head is therefore pivoting on the peripheral rim of the liner and inferior edge of the femoral head.

The ceramic-on-polyethylene group had, on average, relatively low separation values and these subjects demonstrated much less jerky motion. These subjects also demonstrated similar separation magnitudes during the stance and swing phases of gait (Figure 65b). Separation was routinely not present during heel strike and toe off.

The maximum separation in the group of the metal-on-metal polyethylene sandwich was 2.4mm (Figure 65c), occurring at heel-off, approximately at 20% of the stance phase of gait. Similar to the ceramic-on-polyethylene group, minimal separation values were achieved slightly after heel strike and before toe-off. Interestingly, during the stance phase an additional minimal separation occurred for almost all analyzed patients. Therefore, this group exhibited a M-shaped trend. A correlation between the separation and abduction/adduction curves was observed, which explains the high separation values during the stance phase of the gait cycle (Figure 71). After heel-strike, the analyzed leg was rapidly loaded and experienced an immediate change from adduction to abduction. This condition may have caused the femoral head to slide from the acetabulum component and lead to edge loading conditions, superolaterally.

Interestingly, the group demonstrating very distinctive separation patterns was the large head metal-on-metal patients group (50mm+). In this group, there was a difference between the Zimmer and Biomet implants. Whereas, the trend of the patients in the Zimmer group followed a sinusoid shape with high separation values during stance phase, the Biomet large femoral head group experienced very high separation values during swing and toe-off, which decreased to a no separation condition during mid-stance (Figure 66a and b). In the metal-on-metal group with medium sized femoral heads (38mm), the trend was similar to the trend of the other bearings with small femoral heads (Figure 66c and Figure 65). On average, the subjects with a metal-on-metal articulating surface and a medium femoral head experienced constant separation without any noticeable return to baseline during the entire gait cycle (Figure 66c).

Similarity to the other groups was also observed in the magnitude of separation which was much smaller compared to the groups with large femoral heads.

The maximum separation observed occurred in a metal-on-polyethylene patient, with a value of 5.6mm. On average the ceramic-on-polyethylene (2.1mm (1.0-3.4mm)), the metal-on-metal medium femoral head diameter (2.1mm (1.7-2.6mm)) and the metal-on-metal polyethylene-sandwich (2.1mm (1.4-2.9mm)) groups achieved the same low separation magnitudes (Table 2). However, there was a difference in the intra-group variation with a much smaller standard deviation among the patients in the metal-on-metal groups (Figure 68). A comparison of hard-on-hard bearings which included all metal-on-metal and ceramic-on-ceramic implants to all hard-on-soft bearings such as the metal-on-polyethylene and ceramic-on-polyethylene implants experienced similar average maximum separation values with a slightly lower value for soft bearings (Table 2). It must be considered that the hard-on-hard bearings group, especially the metal-on-metal patients with large femoral head diameter, negatively influenced the results for this group. It was apparent that the hard-on-hard group experienced a lower intra-group variation than the hard-on-soft group, which is even more prominent if the large head metal-on-metal groups were excluded. The only patient who experienced no separation had a ceramic-on-polyethylene implant.

The position of maximum separation in the gait cycle revealed no trend among groups, as separation occurred throughout the entire gait cycle. Also, the probability of occurrence of maximum separation was found to be the same during the swing and stance phases of gait (Figure 70).

7.2 Gait Analysis

Among all patient groups with unilateral implants and all analyzed gait parameters (Table 4), the parameters that did not fulfill the previously established requirement for acceptable symmetry of $ASI < 10\%$ was the swing time for the metal-on-metal and ceramic-on-ceramic bearing groups, and the double support time for all bearing groups. All implant groups revealed a negative symmetry index for the stance time parameter. Negative SI represent higher values for the implanted leg when compared to the healthy one, but for all bearings the SI values for the stance time were under the threshold of 10%. The ASI for stance time and entire step time of gait were low, with values of 3.9% and 1.1%, respectively, suggesting near symmetry in these aspects of the gait cycle. The symmetry indices for the swing and double support phases of gait were higher, with averages of 9.7% and 13.6%, respectively. Only the hard-on-hard bearings exhibited asymmetry for the swing time greater than our threshold. For the double support time, both the hard-on-hard and the soft-on-hard bearings, revealed higher asymmetry values with more favorable results for the THAs with polyethylene liner. For the double support time, both the hard-on-hard and the soft-on-hard bearings, revealed higher asymmetry values with more favorable results for the THAs with polyethylene liner. A significant difference between the ceramic-on-polyethylene group and the metal-on-metal polyethylene sandwich group for the step length was observed. . There was no significant difference detected for all other groups and analyzed parameters.

The analysis of the gait parameters for the bilateral patients (Table 5) resulted surprisingly in relatively higher asymmetries for the most categories. Values considerably greater than the threshold were observed in the hard-on-hard group for the stance time with an ASI of 22%.

7.3 3D Kinetics

The forces acting in the leg were determined for a patient from each bearing group. The forces acting in the iliofemoral and ischiofemoral ligaments are acting almost antipodal because of their location on the anterior and posterior side of the hip capsule (Figure 72 - Figure 74). Interestingly, the ceramic-on-polyethylene group experienced very high iliofemoral forces but low ischiofemoral forces, whereas the metal-on-metal group showed almost the opposite trend (Table 11). The forces acting in the patellar ligament, quadriceps and patella are displayed for an example patient in Figure 75 and were similar in their pattern. A variation in the magnitude was observed with relatively low overall forces in the metal-on-metal with polyethylene-sandwich patient and higher forces in the metal-on-metal group. The results for the patella-quadriceps mechanism for all groups are summarized in Table 11. There are in some short time intervals negative forces, which is not possible since muscles and ligaments cannot act in compression. However, the negative values are small and can be neglected since it is not expected that the bearing forces have been negatively influenced by this artifact of the numerical calculation. Also, these negative forces may be a result of the error of input data, such as the kinematics, leading to an error in force determination.

The interactive forces pertaining to the ground, the ankle and the knee are plotted in Figure 76. The patterns of all forces were similar to those of the applied subject specific ground reaction force, with increased force magnitude as one moves upward from the ground to the spine (Table 11). We hypothesize that this occurred because of the increased muscle activity at the different joints. Ankle forces were determined to be around 10% higher than the ground reaction forces, whereas knee forces were approximately 40% higher compared to the forces acting at the ankle. The highest forces occurred at the hip interaction, which were in general, around 50% higher than the knee forces (Table 11).

The hip bearing contact forces for the patients in the different bearing groups are displayed in Figure 77. The maximum peak force of 2.9 BW and 2.8 BW were found for a metal-on-metal and a ceramic-on-polyethylene patient, respectively, while the metal-on-polyethylene and the metal-on-metal polyethylene-sandwich patients attained lower maximum peak forces of 2.65 and 2.5 BW, respectively. The only patient who didn't experience the typical M-shaped curve for the forces was the metal-on-metal with polyethylene inner liner. All patients except the ceramic-on-polyethylene experienced the maximum peak force during the loading response which is in the first 33% of the stance phase. For the ceramic-on-polyethylene patient the second peak was more dominant than the first.

For all subjects the maximal forces in the joints occurred at around 33% and 66% of the stance phase, which might be due to the influence of the limb loading and the

joint position. Additionally, influences are to be expected from the momentum which appears to be a major contributor to the resultant joint reaction forces.

7.4 Ground Reaction Forces

After processing and evaluating the ground reaction forces collected during the experimental sessions, for the entire gait cycle, the desired parameters in each of the three mutually perpendicular directions were extracted (Table 12 - Table 14). The average ground reaction forces as well as the intra-group variation of the different bearing surface groups are displayed in Figure 78 - Figure 82. The results of the statistical analysis are represented in Table 14. The ground reaction forces in the vertical direction followed, for all patients, the typical bell-shaped curve. However, some patients expressed a vertical force with two peaks (M-shape) and others expressing a pattern with a single, flat region during the stance phase or with three or more peaks. The groups with hard bearings had a higher occurrence of three or more peaks than groups with soft bearings, with 76% and 50% of the vertical GRF curves having three or more peaks, respectively.

The maximum vertical GRF (Table 16) observed occurred in a patient with a COP implant, with a force of 1.31BW occurring at 75% of the stance phase. The bearing group with the lowest average maximum peak vertical GRF was MOM.

The shortest average time to the first vertical peak force (Fz1) was observed in the MOM-PS group to be 29% (19-34%), and the highest was observed in the COP

group to be 36% (33-39%), with the difference categorized as statistically significant ($p=0.02^*$). Additionally, Fz1 was significantly lower in hard bearings than soft bearings ($p=0.03^*$). The shortest average time to the MS force (Fz3) was observed in COC patients to be 48% (45-53%), which was significantly lower than the average values observed in MOP to be 57% (50-68%) and COP to be 55% (51-60%) patients ($p=0.03^*$ and $p=0.04^*$, respectively). There was no statistical significance when comparing the first peak force (Fz2) and the MS (Fz4) force for each group. The lowest average time to the second peak force (Fz5) was observed in COC patients to be 69% (58-76%). This time was significantly lower than that observed in MOP to be 76% (74-79%), COP 77% (75-80%), and MOM-PS 77% (73-82%) patients ($p=0.02^*$, $p=0.01^*$, $p=0.01^*$, respectively). The largest average second peak force (Fz6) was observed in the COP group with 1.03BW and resulted to be significantly different than the force in the MOM group ($p=0.047^*$).

The lowest average loading rate was observed in MOP patients, with a value of 2.36BW/s (2.01-2.57BW/s). The overall lowest loading rate was observed in a MOM-PS patient, with a value of 1.40BW/s. Interestingly, the MOM-PS group also had the highest average loading rate, with a value of 4.58BW/s.

The highest average push-off rate was found to occur in the COP group with a value of 5.79BW/s (3.80-8.24BW/s), which was significantly higher than the COC group 3.17BW/s (1.90-5.65BW/s) ($p=0.033^*$). The overall highest observed push-off rate occurred in a MOM-PS patient, with a value of 9.92 BW/s. The lowest observed push-off rate was noted in a COC patient, with a value of 1.90 BW/s.

The average maximum breaking force (Fx4) in the MOP group was significantly lower than the MOM and the MOM-PS group ($p=0.0288^*$, $p=0.0071^*$, respectively). The COC group had the lowest average maximum propelling force (Fx5), which was significantly lower than the group with the highest, MOM-PS 0.16BW ($p=0.0265^*$). One COP patient exhibited an abnormal pattern for Fx4 and Fx5. All anterior-posterior results can be seen in Table 13. The value of Fy2 for the COP group was the highest of all groups analyzed 39%, while the MOM-PS and COC groups were the lowest with around 30%. One patient with a MOM large head prosthesis did not exhibit the medio-lateral peak at Fy4. All medio-lateral results can be seen in Table 14.

Since each patient was asked to perform the activity with their chosen speed and a comfortable step length, there was a difference in the total time of the entire step (Table 17). However, the swing phase for most of the groups was around 30% of the total gait cycle time and there was no difference between the hard and soft bearing groups.

7.5 Correlation of Separation with Sound and Vibration

The sound signals were examined and compared to the kinematic findings (Glaser et al., 2008). The sound and accelerometer results for each patient differed in magnitude and pattern. The spectrograms of distinct sounds for each of the patients were used to assess frequency excitation (vertical axis) with respect to time (horizontal axis) (Figure 83, right side).

The sound results for each patient differed in magnitude and pattern. Interestingly, there was a distinct correlation of a high frequency sound occurring at the time when the femoral head slid back into the acetabular component. As the femoral component impacted the acetabular cup, the sound sensor revealed a high frequency sound, representing impact conditions (Figure 83, left side). A thud or “clicking” sound was detected for the subject having a metal-on-polyethylene bearing (Figure 83A). Similar, but much more accentuated, was the sound recorded for the ceramic-on-polyethylene patient. Clear and rich “clicking,” combined with some crepitus, was observed for the subject having a metal-on-metal polyethylene sandwich THA (Figure 83C). The subject with a metal-on-metal THA experienced a sound similar to a “rusty door hinge” (Figure 83D). Ceramic-on-ceramic THA subject experienced a “squeaking” sound with certain alterations which was present throughout the entire gait cycle. The ceramic-on-ceramic articulations were considered to be the noisiest, not in terms of amplitude but in terms of sound development over the entire gait cycle. The only subject in this study (with a ceramic-on-polyethylene THA), who did not experience femoral head separation was the only subject without sound generation during the entire gait cycle. Only background noise was audible for this subject, even with very high signal amplification. A list of sounds for each implant type is presented in tabular form for comparative purposes (Table 18) (Glaser et al., 2007).

In all patients, a knocking sound was observed when the femoral ball contacted the acetabulum. This sound is easily identified by its high amplitude (time domain) and high energy (spectrogram) over a small time interval. Squeaking and rolling sounds

were detected when intensive back and forth movement of the femoral head was observed (Glaser et al., 2007).

None of the patients experienced impingement between the neck and the rim of the components during the analyzed activity.

7.6 Vibration Analysis

As described in the previous chapter, correlation between the acceleration signal and the separation characteristics was observed for all analyzed patients. The impact of two objects led to impulse loading conditions. By executing a gait activity, an impulse was generated when femoral head sliding lead to the impact of the femoral head in the acetabular component and was depicted by the attached accelerometers (Figure 84). While under impact loading conditions, the energy is dissipated through propagating vibration, where the frequency of the resulting vibration was determined using the natural frequency of the component parts.

This condition was used to find the *in vivo* natural frequencies of the hip joint system. The acceleration data was converted into the frequency domain and the frequency content was analyzed. The accelerometer signals (Figure 85) were used to examine bone and implant frequencies and to determine distinctive patterns during hip separation. A FFT program analysis calculated the frequencies and differences between the bearing surfaces were found. The frequency results for the femur in our present

study were then compared to previously published data (Table 19). There is no known published data on the natural frequencies of the pelvis.

The vibration signals, for example patients, are shown in Figure 85. The energy released during the transition from static to dynamic friction was transferred to audible sound. The results were usually too noisy to read if a DFT was performed on the entire signal prior to filtering the frequency content (Figure 86). Therefore, important areas of the signal, that could represent effects of interest such as impulses and resonance, were isolated (Figure 87) and analyzed separately (Figure 88). Several intervals per subject were chosen and evaluated in a similar manner.

Interestingly, it was found that certain frequency ranges were excited for all implants; however, for some patients and/or implants, certain frequencies were not present. The reason for this finding may be due to the different bearing surfaces having variable frequencies which were amplified while others remain insignificant.

The magnitude of the vibration found in the subjects when the femoral head separates from the acetabular cup was much larger than for the subject without separation.

The short time Fourier Transforms for a patient in each group are displayed in Figure 83. From the signal in the time domain (Figure 83, left side) and the STFT signal (Figure 83, right side) it was apparent that the click exhibit in the joint produced synchronous impulses in the time domain. In the technical sense, impulse is a physical quantity, referred to a fast-acting force so that the change in momentum produced by

the force happens with no change in time. In reality this is usually interpreted as a high impact forces, occurring over a very short time interval. This resulted in a step change, represented as a fast collision similar to knocking or clicking events. Those signals were generally pulses, characterized by a waveform, representing a decaying sinusoid with a very short duration in time and high amplitude peaks (Figure 87). During an impulse signal, high energy was observed in the STFT, where a large band of frequencies was excited (Figure 83, right side). The frequency spectrum of the click was consistent through the patients, although there was an expected variation in the energy content. Another type of waveform was observed in the metal-on-metal patients (Figure 89, Figure 90) and resulted in a 'rusty door hinge' signal after transformation to audible sound. The pseudo-spectrum was used as an indicator of the presence of sinusoidal components in the signal (Figure 91). The repeatable signal and its sub-harmonics were much better analyzed visibly than in the standard Fourier Transform.

The frequency content and the transfer function for the 'rusty door hinge' signal waveform, calculated for this period of time, are displayed in Figure 92. The creptus was identified as synchronous outbursts of waveforms with lower level when compared to the clicking and knocking events (Figure 93). The wavelet analysis functions for those signals are shown in Figure 94 and Figure 95.

The wavelet analysis pictures are representations of wavelet coefficients of the vector $S(b,a)$ on the open (b,a) half-plane. The a -axis is directed upwards, ensuring that the low frequencies (high scales) remain above the high frequencies. The positive b -axis is directed to the right and represents the time in number of samples:

$$b - scale = t \cdot F_s$$

with t = Time in seconds

F_s = Sampling frequency in Samples/second

The convergence of the straight lines to one point and the repeatability of the signal can be easily observed from the wavelet analysis graphs.

Different signals of the accelerometers on the femur and pelvis, their transfer function and the wavelet analysis function are displayed in Figure 96 - Figure 104.

For one example signal, the original and noise-suppressed functions as well as the approximation and detailed coefficients before and after denoising, are displayed in Figure 105. For the same signal the wavelet tree and the coefficient on level (3,1) are shown in Figure 106.

Chapter 8

Discussion

Total Hip Arthroplasty (THA) is considered to be an effective procedure routinely performed to alleviate pain and loss of function associated with conditions such as osteoarthritis by replacing the hip joint with prosthetic components (Garino and Vannozzi, 2006; Garrellick et al., 1998). More than 200,000 THA procedures are performed annually in the US, and clinical studies indicate an 80% success rate at 20 years (AAOS, 2008; JISRF, 2008, Berry et al., 2002b). Despite the success of THA procedures, there are still instances of failure. The major complications following total hip replacement that require revision are implant loosening (Garcia-Cimbrelo et al., 1997; Ilchmann, 1997; Numair et al., 1997; Taylor et al., 1997), dislocation, instability, fracture (Kavanagh, 1992; Kavanagh et al., 1985) and infection (Fiedler and O'Brien, 2003), as well as premature polyethylene wear (Bono et al., 1994; Gross et al., 1997; Devane et al., 1997; Sochart et al., 1997).

Various implant bearing surfaces are currently used in THA procedures to maximize the longevity of the implants and reduce implant failure rates by minimizing wear, subsequent osteolysis and implant loosening (Harris, 2001; Archibeck et al., 2000; Learmonth et al., 2007; Wagner et al., 2000). Cross-linked ultrahigh-molecular-weight polyethylene has been developed to decrease the number of wear particles (Muratoglu et al., 2001), while hard-on-hard bearing surfaces have been implemented to eliminate the need for polyethylene all together and to further decrease the wear rates.

Metal-on-metal and ceramic-on-ceramic bearings have shown lower wear rates compared to polyethylene bearings but are subject to metal alloy and corrosion particles (MacDonald, 2004) or ceramic fracture (Hannouche et al., 2003).

While different bearing surfaces produce varying wear rates, all bearing surfaces are subject to some degree of wear and femoral head separation (Learmonth et al., 2007; Wagner et al., 2000; Garino, 2004; Dennis et al., 2001, 2006; Komistek et al., 2002, 2004; Lombardi et al., 2000). Comparing separation values of the femoral head from the acetabular component for a variety of commonly used THA bearings gives valuable information regarding the performance of the hip implants *in vivo*.

The present study investigated hip joint kinematics and kinetics of patients implanted with different bearing surface THAs during post-operative gait, and evaluated the influence of the bearing material combination on those parameters. The investigated bearings in this study performed differently, possibly due to unequal surface finishes and the cohesion reaction between the acetabular component and femoral head, which led to the conclusive presumption that those groups may have distinct post-operative gait characteristics. Previous studies have shown that metal-on-metal THAs experience lower separation than subjects implanted with metal-on-polyethylene prosthesis (Komistek et al., 2002) and that patients with THA, having a polyethylene liner experienced higher separation than those with metal or ceramic liners (Dennis et al., 2006). Therefore, it was hypothesized that the bearing material combination would have an effect on the gait kinematics and result in altered hip separation values and hip contact forces, when subjects with different bearings are set directly in to comparison.

The chosen surgeon in this study had similar experience implanting each of the different THA designs and bearing material combinations. Many other parameters were matched between the analyzed groups to reduce the influence of confounding variables on the results and to allow for reliable interpretation of the results.

Countless research studies and many different methods have been employed to analyze kinematic and kinetic performance of implanted and healthy joints. Researchers have utilized *in vitro* cadaveric (Anglin et al., 2008; Robertson and Kelly, 2008), skin markers studies (Soutas-Little et al., 1987; Andriacchi et al., 1998) and *in vivo* roentgen stereophotogrammetric analysis (RSA) (Börlin et al., 2006; The et al., 2008) to predict human joint motion. Telemetric studies were applied to find invasively joint forces under *in vivo* conditions (Bergman et al., 2001; Davy et al., 1988; Taylor et la., 1997, 2002). Video fluoroscopy and mathematical modeling have proven to be highly accurate, non-invasive techniques for the examination of 3D *in vivo* kinematics (Dennis et al., 1996, 2001, 2006; Komistek et al., 2001, 2002; Mahfouz et al., 2003) and kinetics (Komistek et al., 1994, 1998, 2005; Glaser et al., 2007) of implanted or healthy joints and have been successfully deployed for more than 20 years.

The previously applied methods are precise, but often involve invasive approaches that are too complex and/or time intensive to be effectively applied for routinely clinical evaluation of THA performance. Therefore, the development of replicable, easy to implement, and non-invasive techniques is essential to facilitate a reliable evaluation of joint performance and clinical outcomes on a routine basis. The present research involved in addition to the mechanical analysis of THA patients with

different bearings the development of a non-invasive acoustic and vibration analysis technique for more in-depth evaluation of in vivo hip conditions.

8.1 Kinematic Analysis

Recently, studies also found that femoral head sliding between the acetabulum cup and the femoral head, often referred as separation, does occur, which may also play a role in complications observed with THA today (Dennis et al., 2001, 2006; Komistek et al., 2002, 2004; Lombardi et al., 2000; Northcut, 1998). Premature polyethylene wear as a significant cause of THA failure, may be due to increased impulse loading conditions caused by the decrease in contact area as a result of the femoral head sliding (Dennis et al., 2001, 2006; Komistek et al., 2004, Northcut, 1998).

Femoral head sliding was analyzed with the expectation to reflect differences between the THA designs and bearing combinations, as well as to provide a reference for the developed acoustic and vibrational technique for THA evaluation. The hip joint is often described as a ball-socket joint; however, the true motion of the joint deviates when femoral head sliding occurs. Typically, during separation, the large, uniform contact area between femoral head and acetabulum shifts to undesirable edge loading conditions between both components. In this situation there is a separation of the medial aspect of both contact surfaces, reducing the contact area to a small superolateral region. Therefore, the femoral head is often pivoting on the peripheral rim of the liner in extreme cases of hip separation.

A possible concern is that the impact following separation leads to increased loading conditions on the affected side which may cause increased wear and slowed recovery (Northcut, 1998). This assumption is supported also by various telemetric studies (Bergmann et al., 1997, Bergmann et al., 1993, Hodge et al, 1986, Taylor et al., 1997). The impulse generated by the collision of two objects has been shown to potentially compromise the structural integrity of mechanical components (Seireg and Arvikar, 1973) and may lead to premature component loosening and increased wear. Additionally, the long term effects of the correspondingly altered kinematics and kinetics on the intact limb are also unknown (Hurwitz et al., 2001).

It cannot be definitively proven, that separation present in the hip joint will lead to undesirable conditions. However, it is a fact that in subjects with normal hip joints or those implanted with a constrained THA experience, no femoral head sliding from the acetabulum occurs (Dennis et al., 2001, Northcut, 1998). Additional evaluations of subjects implanted with metal-on-polyethylene THA designs during gait similarly experienced femoral head sliding as had been noted during an abduction-adduction maneuver (Komistek et al., 2002, Lombardi et al., 2000). These results suggest that patients implanted with an unconstrained metal-on-polyethylene THA are subjected to inertial forces that produced sliding of the femoral head from the acetabular component during several different dynamic activities.

In the normal hip joint, maintenance of the femoral head within the acetabulum is provided by several soft tissue structures which support the hip joint. During THA, the ligament of the head of the femur is surgically removed and a portion of the remaining

supporting soft tissue structures are transected or resected to allow surgical exposure. Due to the altered stabilizing soft tissue it is logical to assume that the kinematics of the implanted hip may differ from those of the normal hip. Separation of the femoral head from the acetabular component is potentially detrimental and may play a role in complications observed with THA today, including instability, premature polyethylene wear, and prosthetic loosening.

Wear patterns generated in hip joint simulation devices based on telemetry (Bergman et al., 1997; Davy et al., 1988; Taylor et al., 1997) and mathematical modeling (Brand et al., 1982; Komistek et al., 2005; Komistek et al., 1998) do not accurately recreate wear patterns as they are seen in retrieved implants (Clarke et al., 1997; McKellop et al., 1984; Saikko et al., 1993; Wright and Scales, 1977; Seireg and Arvikar, 1973a, b). However, when separation is implemented in the THA simulators, wear patterns generated *in vitro* are consistent with wear patterns from retrieved implants (Nevolos et al., 2000), which indicates that separation may have an effect on wear patterns *in vivo*.

Previous studies have determined that femoral head separation occurred in all subjects implanted with a metal-on-polyethylene THA (Dennis et al., 2001, Komistek et al., 2002, Lombardi et al., 2000), however lower incidence of separation was observed in other bearings (Dennis et al., 2006). The subjects in the present study experienced high separation values regardless of the bearing combination. The average and maximal magnitude of the femoral head separation was similar to published data except in the case of the metal-on-metal implants (Dennis et al., 2006, Komistek et al., 2002).

The difference may be due to the fact that those studies included metal-on-metal implants with a small or medium femoral head diameter. In our study, the large head metal-on-metal THAs experienced larger separations than the medium diameter implants. Also, subjects analyzed in those studies having a metal-on-metal THA were analyzed very early post-operative, and over time, it could be assumed the incidence and magnitude of hip separation increases.

In the present study, a significantly higher magnitude of hip separation was observed in the metal-on-polyethylene group. This group also experienced the largest intra-group variation among the patients suggesting quite inconsistent results when compared to the other groups. The patient with the overall maximum separation magnitude found in this study was also a patient implanted with a metal-on-polyethylene THA. The subjects with large head metal-on-metal also experienced high separation and demonstrated undesirable gait kinematics. These results may be due to the design of the femoral head and are probably less representative for the metal-on-metal group. Interestingly, all groups of THAs with polyethylene liner achieved the same average separation. The variation among the patients in each group was smaller for the hard-on-hard bearings group when compared to those with polyethylene liners group.

Initially, separation was thought to arise only during non-weight bearing activities, such as the swing phase of gait. A high incidence and magnitude of hip separation during the stance phase of gait was later also proven to occur (Dennis et al., 2006). Our study showed that separation can be equally likely present during swing as well as stance phase of gait. It appears that the acetabular component slides away from the

femoral head probably as a result of the change in the abduction-adduction angle and the applied forces while under weight bearing. It is logical to assume that the disturbance of the capsular ligaments as well as of the ligament of the head of the femur may alter the stability of the hip joint. As the pelvis progresses forward, the supporting soft-tissue structures around the hip joint maintain the femoral head within the acetabulum in the normal hip. The altered muscle and ligament structure of a THA patient may allow the femoral head to separate from the acetabulum as the upper body progresses forward and an increased momentum is created around the medio-lateral axis.

8.2 Gait Analysis

The analysis of gait parameters pertaining to the symmetry between implanted and non-implanted hips is important if we are to understand the level of recovery and identify abnormal gait patterns. Furthermore, the identification of abnormal gait characteristics is important in the evaluation of implant performance.

For the step and stance time parameters, the ASI values for all unilateral patient groups and analyzed parameters were lower than the adopted threshold. This indicates a symmetrical performance of both legs as observed in healthy subjects. Asymmetrical values were observed during the double support time. The average SI for the stance time and all patients in this study was determined to be -1.7% and was lower when compared to the previously published value of 3.53% (McCrary et al., 2001). This may be a sign of more complete recovery or better performance of the implants for the

subjects included in this study. Interestingly, the symmetry values for the stance phase determined for this study were negative, meaning the time for stance was longer in the affected leg, when compared to the healthy leg. This is in disagreement with the positive value for the stance-phase symmetry index determined by McCrory (McCrory et al., 2001). Different values for the stance time between the implanted and healthy leg may indicate balance impairments. The increased stance time of the implanted side may be attributed to balance control.

8.3 Kinetic Analysis

Only limited studies have been performed on calculating in-vivo hip joint contact forces, including additional muscle and ligaments forces (Callaghan et al., 1992; Brand et al., 1994). Previous studies have been performed using computer models to predict muscle and joint reaction forces, but these methods have not been successfully validated against in-vivo data and often led to predicted force magnitudes which were much larger than those obtained from telemetric measurements (Winter, 1990).

Therefore, the goal of this portion of the study was to develop a mathematical model for the hip joint that accurately represents the in-vivo loading conditions of THA patients and, at the same time, considers the relationship between muscle and joint forces (Glaser et al., 2007). The developed mathematical model was capable of determining *in vivo* joint reaction forces at the hip, knee and ankle joints during gait for subjects implanted with different bearing surfaces. The mathematical model of the lower extremity was defined as a set of differential equations that represents the dynamics of

the system. Kane's dynamics (Kane et al., 1985, Kane and Levinson, 1996) was applied to simplify the mathematical model and to optimize its performance. This mathematical technique allows solving of a large number of variables through the use of generalized speeds that describe the motion in the system and builds compact, customized and computationally efficient ordinary differential equations.

The developed mathematical model was based on inverse dynamics where the kinematics are used as an input to the system and forces are calculated based on the mathematical formulations of the motions. Precise kinematics was obtained from fluoroscopy to predict the *in vivo* joint motions and contact positions.

The reduction technique was utilized to simplify the model by grouping functionally similar hip muscles. Only 24 unknowns were employed in the system which contained the 24 equations of motions to describe the human lower extremity. This method led to a determinant system of equations and no optimization routines had to be applied to solve for any additional unknowns. The model was capable for solving the muscle and ligament forces directly, along with the joint reaction forces between the foot/ankle, tibia/femur, femur/patella and pelvis/femur, and the torques across each joint. Having a determinant system, lead to only one possible solution, for each increment of time, throughout the gait cycle.

The development of this model of the human lower extremity is important for in depth analysis and evaluation of clinical problems in this area of the human body.

Further development of the model will allow solving for different clinical conditions and building up a comprehensive tool for force analysis of the lower extremity.

A comparison of the current results to those in a telemetric hip reported by Bergmann et al., (2001) demonstrated that the force patterns and the magnitudes were similar. The average predicted forces in our analysis were 2.5-2.9 BW, while Bergmann reported forces from 2.3 to 3.5 BW, under similar conditions (Glaser et al., 2007).

8.4 Ground Reaction Forces

Additionally, the current study analyzed the ground reaction forces occurring during gait of patients with various hip implant bearing surfaces. The ground reaction forces (GRF) were implemented in the developed analysis in two different ways. First, the GRF were measured during the experimental part of the study and were later input into the mathematical model as external forces acting on the ground-foot interaction. Second, the GRF were used to quantify and analyze the loading of the hip joint during gait by applying important representative descriptors of ground reaction force data to characterize the essential features of the force components.

It has been previously demonstrated that a vertical GRF graph with two peaks is characteristic of healthy, young individuals, while a flat top is representative of abnormal gait developed with joint problems (Brown TRM et al., 1981, Gök et al., 2002). It is possible that the patients in the study exhibiting two peaks have responded more naturally to their implants, while those with a lasting flat-topped pattern maintain the

abnormal gait developed before surgery. The higher percentage of occurrence of flat-topped GRF graphs in the implant groups with hard bearings may be a result of abnormal gait achieved with those implants. This continued abnormal gait could promote abnormal loading on numerous joints in the lower extremity, which could result in joint degeneration.

Several selected ground reaction force measures were significantly different for subjects of the different bearing groups. The lowest average maximum peak GRF force of all groups analyzed was observed in the metal-on-metal (MOM) group, which corresponds to the relatively high average maximum separation value seen in the same group. Conversely, the ceramic-on-polyethylene (COP) group exhibited the lowest average maximum separation as well as the highest average maximum GRF force, with the difference in second maximum peak force (F_{z6} parameter) between MOM and COP being statistically significant ($p=0.047^*$). High separation values suggest an exchange from a large, uniform contact area between the femoral head and the acetabulum to undesirable edge-loading conditions during femoral head sliding and may result from residual muscle damage or unnatural gait loading conditions. In this study, high separation values are accompanied by low GRF values, which could reflect additional instability. Our findings are consistent with previous studies where lower GRF values have been shown to occur in the affected hip joint when compared to normal hips (Bassey et al. 1997, Giakas et al. 1997, Long et al. 1993, McCrory et al. 2001). Low vertical GRF have been suggested to result from analgesic gait developed by the patient prior to surgery, which remains until the patient develops the stability and

balance needed to bring the hip back to normal loading levels (Brown et al., 1981). Low GRF values in the affected hip leave larger forces to be sustained by the unaffected limb, which may lead to accelerated degeneration of numerous joints. Furthermore, the combination of high separation values with low GRF values associated with metal-on-polyethylene (MOP) bearing could reflect the maintenance of abnormal loading in the hip joint following THA and the potential for additional joint degeneration and instability. This instability could arise from slower recovery time or implant performance characteristics that may prevent the joint to fully return to normal functionality. The low separation and high GRF in the COP group suggests a return to normal gait loading conditions, which is vital for the recovery of the patient and the success of the implant.

There is a significant difference in time to the first maximum force (F_{z1}) between the group with the lowest F_{z1} , metal-on-metal polyethylene sandwich (MOM-PS), and the group with the highest F_{z1} , COP ($p=0.02^*$). Results of the MOM-PS group are similar to those found for normal subjects. The results for all other groups are similar to previous studies analyzing THA patients (Basseley et al., 1997; McCrory et al, 2001) where F_{z1} was shown to be significantly longer on the affected leg of THA patients when compared to the unaffected leg. The time to the minimum force (F_{z3}) was significantly longer in MOP and COP patients when compared to ceramic-on-ceramic (COC) patients, which may suggest that COC patients may alter their gait in order to reach a point of minimum load faster in order to minimize pain or to maximize stability. The lowest time to second maximum peak force (F_{z5}) was observed in the COC group, and

was significantly lower than the highest value experienced in the COP group, and as well as in the MOP and MOM-PS groups.

The low average loading rate observed in MOP patients could reflect abnormal loading on the affected limb, as it has previously been shown that THA patients do not put weight on their affected legs as quickly as their unaffected legs or as quickly as healthy control subjects (McCrorry et al., 2001). Lower loading rates in the affected limbs of patients with osteoarthritis of the knee, another group afflicted with instability and pain resulting from joint degeneration, have also been observed (Messier et al., 1992). It has been suggested that these lower loading rates could be a result of attempts to reduce osteoarthritic pain. Conversely, the high average loading rate in the hard bearing group could reflect a more complete recovery of these patients, as greater stability would result in their placing weight on the affected joint more quickly. The significantly lower average push-off rate in COC when compared to COP ($p=0.03^*$) may reflect the COC patients' adaptation of their gait in attempts to minimize pain or to maximize stability.

The GRF in the direction of walking (antero-posterior) revealed an initial negative phase corresponding to the exertion of a backward force by the ground on the body, slowing down the forward movement. The subsequent positive phase approaching toe-off relates to the cyclical acceleration in forward movement. The significantly low maximum braking force (F_{x4}) exhibited by the MOP and COP bearing groups and the significantly low maximum propelling force (F_{x5}) observed in the MOP and COC groups could suggest a "stiffer" mode of locomotion (Brown et al., 1981). It has previously been shown that subjects exhibit smaller antero-posterior peak force magnitudes prior to THA

than afterwards, suggesting a stiffer mode of locomotion when instability and pain are more prevalent. This may suggest balance impairments in the studied patients with soft bearings.

Values for the vertical and antero-posterior GRF parameters as well as the stance times analyzed in this study are similar to previous research (Hamill et al., 1990; McCrory et al., 2001). Some results differ due to the slower walking speeds in the current study. The first and second maximum forces were lower than those reported by Long et al. (1993); however, the speed of gait was probably also here different, thus resulting in differing values. A comparison to the results published by Brown et al. for patients with hip implants between 6 and 12 months post-op, resulted in similar values for the first maximum peak force (Brown et al., 1981). The push-off rate in this study ($4.32 \pm 2.04 \text{ BW/s}$) is slightly lower than the reported push-off rate from McCrory ($5.03 \pm 1.74 \text{ BW/s}$); however, this could be a result of the intra and inter-subject variability (McCrory et al., 2001). The average values for the analyzed parameters generated in this study were similar to those of previous research indicating consistency in the measuring techniques and procedures employed during testing.

Interestingly, the COP group was associated with the lowest separation, highest GRF and push-off rate, and an above average loading rate. All of these characteristics could suggest a more complete recovery of the patients in this group, which could be a result of better implant performance and stability in the patients.

No preoperative data was collected on the subjects included in this study. It is therefore unknown if this pattern of walking may be attributed to gait patterns adopted prior to the surgery, when these subjects had severe, painful arthritis in the joint.

8.5 Correlation of Kinematics, Sound and Vibration

The noninvasive technique presented in this paper to digitally capture hip joint sound and vibration emissions was developed for the evaluation of hip performance and for the diagnosis of femoral head sliding in the acetabular cup of patients who have undergone THA (Glaser et al., 2008). The interpretation of the diagnostic sound and vibration data is a complicated task, involving an in-depth understanding of data acquisition and signal analysis, as well as the mechanical system characteristics. Kinematic analysis using video fluoroscopy was used to obtain necessary information about implant movement and to diagnose separation.

Femoral head sliding within the acetabular cup occurs in the majority of THA subjects, and magnitudes of the femoral head separation agree with the findings in our study (Dennis et al., 2001, 2006). A possible concern is that the impact following separation leads to increased loading conditions at the bearing surface interface, especially superolaterally, which may lead to increased wear (Northcut, 1998). However, no studies using experimental techniques, other than fluoroscopy, have been used to detect femoral head sliding so far.

In this study, based on the concept of the impulse excitation method, the established vibration and acoustic techniques provided a more in-depth understanding of the occurrence of femoral head separation from the acetabular cup (Glaser et al., 2007). Among analyzed patients following THA, the sensors were consistently able to detect frequencies propagating across the hip joint. A data acquisition system was used to amplify the signals and filter out unwanted noise generated by undesired frequencies. The signal from the sensor was converted to sound and then correlated with the three-dimensional hip movement obtained from fluoroscopic images and processed with our model-fitting software package. The correlation of the visual exploration using fluoroscopy with audible and vibration emission using a new acoustic and vibration analysis technique (AVT) confirmed and validated the newly developed methodology. Distinct sounds such as clicking or squeaking and a sound similar to a “rusty door hinge” were found and seemed to be associated with the different bearing surfaces involved in the study.

This is the first study to document and correlate visual effects with audible and vibration emission of THA under *in vivo* conditions (Glaser et al., 2007). The sound measured using our newly developed method indicates that the implanted hip components were subjected to variable dynamic loading conditions at the bearing surface interface. Varying magnitudes and frequencies related to different bearing surface materials may have led to different types of sounds associated with these motion patterns. One explanation for separation during stance phase is the immediate change from abduction to adduction after heel-strike, when the analyzed leg is rapidly

loaded. This condition causes the femoral head to slide from the acetabular component, leading to the adverse side effect of edge loading. Another possible cause could be the momentum established by the contralateral leg thrusting forward, while the foot of the leg experiencing separation remains in contact with the ground.

The vibration caused by the ringing of components in the THA system has the potential to damage both prosthetic components, as well as the area of the bone that they are in contact with. Future analysis will determine if our technique can be applied to detect early implant loosening and bone fracture, since those changes will directly affect the propagated frequencies. In summary, these results are promising, and the trends may be used to properly identify and differentiate the frequency content.

Different implant groups were used in this study to validate whether the AVT system is capable of detecting and correlating sound and visual images for varying conditions. Results indicate good correlation with fluoroscopic analysis and great sensitivity for identifying diverse conditions.

In the future, this newly developed methodology may provide information about joint conditions and it is our goal that the AVT technique could be used to extract valuable information that can be used to enhance clinical diagnoses. A further understanding of the physical response resulting from impact during femoral head sliding in addition to a comparison of variable bearing surfaces may lead to valuable insight pertaining to THA failure as well as enable improvements in future implant development.

8.6 Acoustic and Vibration Technique

The desire for a non-invasive method of analysis and clinical evaluation of degenerative joints or those after partial or total replacement led to the foundation of new technologies. The method developed in the present work is based on using the accelerometers as sensors to depict joint interactive signals. The development was supported by the clinical evaluation of requirements and possible implementations as well as the theoretical and scientific examination of potential alternatives.

The idea of analyzing joint vibrations is not new, but the application in this study may be. The evaluation of previous implemented methods of detection and recording systems revealed that acoustic microphones and electronic systems did not fulfill the necessary requirements on frequency range and dynamic sensitivity. Those parameters are essential for proper detection, recording and analysis of vibration emissions generated at the interaction of human joints. After studying all requirements, potential alternatives and possible result outcomes, a practical method was developed by the synthesis of clinical applicability and adaptability together with the scientific possibilities to interpret joint signals. The application of accelerometers proved to fulfill the clinical, practical and scientific requirements set to properly analyze and evaluate human joints as a routine procedure.

The method in this work is capable to capture, store and analyze joint vibration and sound emissions. The applied technique is able to eliminate two of the major

problems associated with the microphone technique: high background and skin friction noise.

Signals from muscle contractions and soft tissue movement were also captured with the applied sensors. Due to their distinct characteristics, the applied analysis technique was capable of detecting and eliminating those interfering signals and the developed acoustic and vibration technique (AVT) was not inhibited from its application as a diagnostic technique.

The developed technique has been proven to detect joint vibration and acoustic emissions, allowing analysis of the measured signal parameters and correlation with the synchronically measured *in vivo* kinematics. The uniqueness of the AVT technique implies not only to its capability for easy and non-invasively implementation in the routine diagnosis of pathological joint conditions, healthy or implanted, but also it provides a cost effective, but valuable diagnostic tool based on the impulses generated at the joint interaction.

8.7 Summary

The present project captured *in vivo* sound and vibration simultaneously with *in vivo* motion of the hip joint during weight-bearing activities. Hip joint forces were accurately obtained from an inverse dynamic mathematical model that better simulated the *in vivo* loading conditions of a "typical" total hip replacement patient and considers the interdependence of muscle and joint forces. In this study, the focus pertained on the

development of a novel, non-invasive technique for digitally capturing hip joint vibration and sound emission for evaluation of hip performance and diagnosis of femoral head sliding in the acetabular cup of THA. For this reason, THA patients with different bearing surfaces were included in the study and compared.

The vibration and sound characteristics depended upon the mechanical characteristics of the implant and the driving forces. Therefore, by analyzing the vibration and sound patterns of patients during dynamic movement, it may be possible to characterize *in vivo* and non-invasively the femoral head, acetabular cup and bone properties.

This is the first study to utilize the established method of kinematics, kinetics and sound analysis techniques to evaluate the performance of implants with different bearing surfaces while patients are still active and comfortable with their prostheses. Sound and frequency identification under *in vivo* conditions for THA generates new possibilities for better understanding of wear and failure modes in THA. This research may allow for a further correlation to be derived between sound and different types of failure mechanisms. This study provides important information for surgeons, researchers and implant developers to better understand the function of the hip joint, help design improved hip joint prosthesis and this way improve the quality of life of THA patients. In addition, the developed technique builds the first milestone in the design and implementation of a cost effective, non-invasive diagnostic technique which has the potential to be implemented in the routine diagnosis of pathological conditions for healthy or implanted joints.

Chapter 9

Study Limitations and Future Work

The limitations of the presented study pertaining to the clinical evaluation of the involved subjects could be related to the small number of patients in each of the groups that were studied. Additionally the study provides only a single time prospective and doesn't follow the subjects over time as their conditions change from pre- to post operatively performance and different recovery stages. It will be important to conduct follow-up studies in the future that involve a greater number of subjects within each group, more surgeons, differing surgical techniques and longer postoperative periods. The findings of the present study must be evaluated in view of the single activity. Therefore, it cannot be definitively concluded that the results from this study in gait will reflect other activities. Also, a more detailed rehabilitation protocol including supervised hip muscle specific strengthening should be implemented. All patients were instructed to follow the same rehabilitation program, leaving the rest of their postoperative rehabilitation to their individual discipline. Closer rehabilitation monitoring is needed to clarify the true differences due to the different bearing surfaces and explain the variability within groups.

We realize that in addition to the bearing combination supplementary factors such as surgical approach and body mass index (BMI), implant positioning and rehabilitation techniques may play a role in hip mechanics. In the present study, an attempt was made to control multiple variables, so that effects of those unwanted

factors on soft tissue support were minimized to provide a clear investigation of the desired parameters. Therefore, it was our goal to use a single, experienced surgeon in the study, and control multiple variables, which should be some of the strengths of this study.

Fluoroscopy has proven to be a precise method for obtaining in vivo, weight-bearing kinematics and determination of the presence of hip joint separation. The mathematical model created for this study has shown results which are in agreement with those of telemetric studies. The implementation of acoustics and vibration analysis in addition to the accurate procedures of kinematic and kinetic evaluation involved in this work enable extensive evaluation of gait characteristics as they have not been studied previously.

Separation associated with the most of the THAs was presumed to lead to decreased contact area and increased contact stresses. If this condition can be associated with wear, it could be determined in a follow-up study, but was not assessed in this present study. While kinematic analyses of patients with and without separation will provide a comparison of the hip joint interaction forces (Glaser et al., 2007), the persistence of the increased wear is difficult to prove and will involved retrieval analysis of failed hips with known separation status.

The results from this study reveal new questions that may be of concern and could be of interest in the development of future hip prostheses: (1) Are the sounds generated, under in vivo conditions for a THA, dependent on the bearing surface and

are these acoustic signals generated for all bearings? (2) Are specific sounds an indicator of potential hip failure? (3) Could this sound analysis be successfully employed to identify THA failure, early post-operative and be used to clinical diagnose conditions pre-operatively?

The new developed AVT technique revealed very promising results. New research possibilities have been discovered and the present work raised important clinical questions. However, this study has to be followed by larger clinical trials to support and extend the preliminary findings in the present work. More patients, different clinical conditions and retrieval studies have to be performed to verify the wide application possibilities of the developed technique, to further improve the method and make it a routine diagnostic technique. To achieve this, the data acquisition system has to be improved with respect to size, handling, storage and design. Most importantly, the signal analysis algorithm and the filtering options have to be improved and optimized. Also it is recommended that more analyzed parameters be included. The noise-to-signal level has to be improved, as well as an automatic mathematical application has to be developed to handle the measured signals and transfer the information to easier understandable and applicable clinical information. With the better understanding of the signals and the improvement of the techniques that may lead to a cost effective diagnostic tool, the synchronization with fluoroscopy will become unnecessary. In this case, a wireless system with a small chip can be developed to capture and store the data. A powerful application will later transfer the data to the personal computer and analyze the recorded signals. Due to the expected size of the tool, the possibility will be

given to collect long-term data during a variety of activities of the daily life or in extreme situations.

In conclusion, a non-invasive technique for capturing vibration and acoustic emission of human joints has been developed. Preliminary results revealed that the analysis of joint vibrations and sound is worthy of further research. Future research could determine if these signals will lead to a better understanding of hip joint mechanics. It is also a goal that this newly developed technology may provide valuable information that could be used to enhance clinical diagnosis and lead to improvements in future bearing selection and implant design development. It is believed that the technique can be applied to diagnose and prevent clinical disorders of the skeletal, muscular and ligament systems and can help to assess the best treatment with respect to efficiency and improved quality of life for patients with joint disorders and/or replacements.

List of References

References

- AAOS, American Academy of Orthopaedic Surgeons. Facts on Hip Replacements.
<http://www.aaos.org/Research/stats/Hip%20Facts.pdf>. Accessed June 2008.
- American Academy of Orthopaedic Surgeons, 2004. Osteoarthritis of the Hip: State of the Condition. <http://www.aaos.org/research/research.asp>. Accessed April 2008.
- AccuGait, User's Manual and Install Guide, Version 1.5, 2005
- Acoustics. National Physical Laboratory (NPL), 2003:
<http://www.npl.co.uk/server.php?show=conWebDoc.2061>. Accessed June 2006.
- American Academy of Orthopaedic Surgeons, 2003. Hip Joint Replacement. In: Fiedler E, O'Brien S (Eds.), Improving musculoskeletal care in America, (IMCA) Information Series, Osteoarthritis of the hip, A compendium of evidence-based information and resources. American Academy of Orthopaedic Surgeons, Rosemont, IL, pp. 4.1-4.54.
- Anglin C, Brimacombe JM, Wilson DR, Masri BA, Greidanus NV, Tonetti J, Hodgson AJ, 2008. Intraoperative vs. weightbearing patellar kinematics in total knee arthroplasty: A cadaveric study. *Clinical Biomechanics* 23(1):60-70.
- Arbuthnot JE, McNicholas MJ, et al, 2007. Total Hip Arthroplasty and the Golfer: A Study of Participation and Performance Before and After Surgery for Osteoarthritis. *Journal of Arthroplasty* 22(4), 549-552.

- Archibeck MJ, Jacobs JJ, Black J, 2000. Alternative Bearing Surfaces in Total Joint Arthroplasty, Biologic Considerations. *Clinical Orthopaedics and Related Research* 379, 12-21.
- Arsever CL, Bole GG, 1986. Experimental osteoarthritis induced by selective myectomy and tendotomy. *Arthritis Rheum* 29, 251-61.
- Banks SA and Hodge WA, 1996. Accurate measurement of three-dimensional knee replacement kinematics using single-plane fluoroscopy. *IEEE Trans Biomed Eng*, 1996, 43(6): 638-49
- Bassey EJ, Littlewood JJ, Taylor SJG, 1997. Relations between compressive axial forces in an instrumented massive femoral implant, ground reaction forces, and integrated electromyographs from vastus lateralis during various 'osteogenic' exercises. *Journal of Biomechanics* 30, 213-23.
- Bates BT, Osternig LR, Sawhill JA and James SL, 1983a. An assessment of subject variability, subject-shoe interaction and the evaluation of running shoes using ground reaction force data. *Journal of Biomechanics* 16, 181-191.
- Bates BT, Osternig LR, Sawhill JA and Hamill J, 1983b. 'Identification of critical ground reaction force variables during running'. In: H. Matsui and K. Kobayashi (eds.), *Biomechanics VIII-B*, Vol. 4B. Champaign, IL: Human Kinetics Publishers. pp. 635-640.
- Bates BT, DeVita P and Hamill J, 1987. The effects of additional load on impact force. *Proceedings of the North American Congress for Biomechanics, Montreal*. pp. 215-216.

- Bergmann G, Graichen F, Rohlmann A, 1997: Hip joint forces during load carrying. Clin Orthop. 335:190-201.
- Bergmann G, Graichen F, Rohlmann A, 1993: Hip joint loading during walking and running, measured in two patients. J Biomech. 26:969-990.
- Bergmann G, 2001. Loading of the Hip Joint: Contact forces, Gait Patterns, Muscle Forces, Activities. Journal of Biomechanics 34(7). cd-rom attachment Hip98.
- Bergmann G, Deuretzbacher G, Heller M, Graichen F, Rohlmann A, Strauss J, Duda GN, 2001. Hip contact forces and gait patterns from routine activities. Journal of Biomechanics 34(7), 859-871.
- Berry DJ, Halasay M, Harmsen WS, et al., 2002a. Abstract: Charnley total hip arthroplasty: follow-up at a minimum of 30 years. 69th Annual Meeting Proceedings, American Academy of Orthopaedic Surgeons, Rosemont, Ill, pp. 635.
- Berry DJ, Harmsen WS, Cabanela ME, et al., 2002b. Twenty-five-year survivorship of two thousand consecutive primary Charnley total hip replacements: factors affecting survivorship of acetabular and femoral components. Journal of Bone and Joint Surgery 84-A(2), 171-177.
- Bills P, Blunt L, Jiang X, 2007. Development of a technique for accurately determining clinical wear in explanted total hip term replacements. Wear 263(7-12), 1133-1137. (Available online).
- Bircher E, 1913. Zur Diagnose der Meniscusluxationen und des Meniscusabrisses. Zentralblatt fuer Chirurgie 40, 1852.

- Blendea S, Eckman K, et al, 2005. Measurements of acetabular cup position and pelvic spatial orientation after total hip arthroplasty using computed tomography/radiography matching. *Computer Aided Surgery* 10(1), 37 – 43.
- Blodgett WE, 1902. Auscultation of the knee joint. *Boston Medical and Surgical Journal* 146, 63-66.
- Bono JV, Sanford L, Toussaint JT, 1994. Severe polyethylene wear in total hip arthroplasty. Observation from retrieved AML PLUS hip implants with an ACS polyethylene liner. *Journal of Arthroplasty* 9 (2), 119-125.
- Börlin N, Röhrli SM, Bragdon CR, 2006. RSA wear measurements with or without markers in total hip arthroplasty. *Journal of Biomechanics* 39(9): 1641-1650.
- Boutin P, Christel P, Dorlot JM, Meunier A, de Roquancourt A, Blanquaert D, Herman S, Sedal L, Witvoet J, 1988. The use of dense alumina-alumina ceramic combination in total hip replacement. *Journal of Biomedical Materials Research* 22(12), 1203–1232.
- Brand RA, Crowninshield RD, Wittcock CE, et al., 1982. A model of lower extremity muscular anatomy. *Journal of Biomechanics* 104, 304.
- Brown TRM, Paul JP, Kelly IG, Hamblen DL, 1981. Biomechanical assessment of patients treated by joint surgery. *Journal of Biomedical Engineering* 3, 297-304.
- Caldarelli DD and Campanella RS, 2003. Ear. *World Book Online Americas Edition*.
- Callaghan JJ, Fulghum CS, Glisson RR, Stranne SK, 1992. The effect of femoral stem geometry on interface motion in uncemented porous-coated total hip prosthesis: *Journal of Bone and Joint Surgery*; 74, 839-848.

- Campbell JN, Jurist JM, 1971. Mechanical impedance of the femur: A preliminary report. *Journal of Biomechanics* 4, 319-322.
- Christensen AB, 1982. Resonance of human tibia, method, reproducibility and effect of transaction. *Acta Orthopaedica Scandinavica* 53, 867.
- Christie MJ, DeBoer DK, Tingstad EM, Capps M, Brinson MF, Trick LW, 2000. Clinical Experience With a Modular Noncemented Femoral Component in Revision Total Hip Arthroplasty. 4- to 7-Year Results. *Journal of Arthroplasty* 15(7): 840-848.
- Chu ML, Gradisar IA, Mostardi R, 1978. A noninvasive electroacoustical evaluation technique of cartilage damage in pathological knee joints. *Medical and Biological Engineering Computing* 16, 437-442.
- Clarke IC, Kabo M, 1997. Wear in total hip replacement. In: Amstutz, H.C. (Ed.), *Total Hip Arthroplasty*. Churchill Livingstone, New York, pp. 535-570.
- Collier RJ, Donarski RJ, et al, 1993. The use of externally applied mechanical vibrations to assess both fractures and hip prosthesis. In: Turner-Smith AR (Ed), *Micromovement in Orthopaedics*. Oxford, pp. 151-163.
- Collier RJ, Donarski RJ, Worley AJ, Lay A, 1993. The use of externally applied mechanical vibrations to assess both fractures and hip prosthesis. In: Turner-Smith AR (Ed.), *Micromovement in Orthopaedics*. University Press, Oxford, pp. 151-163.
- Conaghan, Phillip. Osteoarthritis - National clinical guideline for care and management in adults. Retrieved on April 2008.

- Couteau B, Hobatho MC et al., 1998. Experimental and numerical modal analysis of a normal and implanted human femur. In Proceedings of the 11th Conference of the European Society of Biomechanics. Toulouse, France.
- Couteau B, Hobatho MC et al., 1998. Finite element modeling of the vibrational behavior of the human femur using CT-based individualized geometrical and material properties. *Journal of Biomechanics* 31, 383-386.
- Cutnell JD and Johnson KW. *Physics*. 4th ed. New York: Wiley, 1998: 466.
- Daubechies I, 1988. Orthonormal Bases of Compactly Supported Wavelets. *Communications on Pure and Applied Math*. Vol.41, 909-996.
- Davy DT, Kotzar GM, Brown RH, Heipl KG, Goldberg VM, Heiple KG Jr., Berilla J, Burstein AH, 1988. Telemetric force measurements across the hip after total arthroplasty. *Journal of Bone and Joint Surgery* 70A, 45-50.
- De Leva P, 1996. Adjustments to zatsiorsky-seluyanov's segment inertia parameters. *Journal of Biomechanics* 29, 1223-1230.
- Dekel S, Weissman SL, 1978. Joint changes after overuse and peak overloading of rabbit knees in vivo. *Acta Orthopaedica Scandinavica* 49, 519-28.
- Dencker H, Moberg E, 1968. Diagnosis of soft tissue interposition in shaft fractures of the humerus and femur by measuring the conduction of vibrations across the fracture. *Acta Chirurgica Scandinavica* 134, 540.
- Dennis DA, Komistek RD, Northcut EJ et al, 2001. In vivo determination of Hip Joint Separation and the forces generated due to impact loading conditions. *Journal of Biomechanics* 34, 623-629.

- Dennis DA, Komistek RD, Hoff WA, Gabriel S, 1996. In vivo knee kinematics derived using an inverse perspective technique. *Clinical Orthopaedics and Related Research* 331, 107-117.
- Dennis DA, Komistek RD, Mahfouz MR, 2006. Kinematic evaluation of total hip arthroplasty with various bearing materials. In: Benazzo F, Falez F, Dietrich M (Eds.), *Bioceramics and Alternative Bearings in Joint Arthroplasty: 11th BIOLOX Symposium Proceedings*, pp. 1-92.
- Dennis DA, Komistek RD, Walker S, Cheal, Stiehl JB, 2001. Femoral Condylar Lift-off in Total Knee Arthroplasty. *Journal of Bone and Joint Surgery-British* 83-B, 33-39.
- Devane PA, Horne JG, Martin K, Coldham G, Krause B, 1997. Three dimensional polyethylene wear of a press fit titanium prosthesis. Factors influencing generation of polyethylene debris. *Journal of Arthroplasty* 12 (3), 256-266.
- Eickmann TH, Clarke IC, Gustafson GA, 2003. Squeaking in Ceramic on Ceramic Total Hip. *Ceramics in Orthopaedics* 8. Steinkopf Verlag, Darmstadt.
- Eisler T, Svensson O, et al, 2001. Ultrasound for diagnosis of infection in revision total hip arthroplasty. *Journal of Arthroplasty* 16(8), 1010-1017.
- Engh CA; McGovern TF, Bobyn DJ, Harris W, 1992. A Quantitative Evaluation of Periprosthetic Bone-Remodeling After Cementless Total Hip Arthroplasty. *Journal of Bone and Joint Surgery, Incorporated* 74-A(7): 1009-1020.
- Erb KH, 1933. Ueber die moeglichkeit der registrierung von gelenkgeraeuschen. *Deutsche Z. Chir* 241, 237–245.

Fiedler E, Hildebrand M, Moio KC, Wimmer et al, 2006. MIS approach to THA affects gait differences. Presented at Annual Meeting of American Academy of Orthopaedic Surgeons. Chicago, IL.

Fischer H, Johnson EW, 1960. Analysis of sounds from normal and pathologic knee joints. 3rd International Congress of Physical Medicine, 50-57.

Garcia-Cimbrelo, E., Diez-Vazquez, V., Madero, R., Munuera, L., 1997. Progression of radiolucent lines adjacent to the acetabular component and factors influencing migration after Charnley low-friction total hip. *Journal of Bone and Joint Surgery* 79A, 1373-1380.

Garino JP, 2004. Recommendations for Maximizing Range of Motion. In: Lazennec J, Dietrich M, (Eds.). In *Proceedings of the 9th BIOLOX Symposium on Ceramics in Orthopaedics: Bioceramics in Joint Arthroplasty*, 157-161.

Garino JP, Vannozzi, 2006. Comparison of Clinical Results between Ceramic-Ceramic Bearings and Metal on Polyethylene in Total Hip Arthroplasty. In: Benazzo F, Falez F, Dietrich M, (Eds.). In *Proceedings of the 11th BIOLOX Symposium on Ceramics in Orthopaedics: Bioceramics and Alternative Bearings in Joint Arthroplasty*, 135-139.

Garrellick, G., Maichau, H., Herberts, P., Hansson, E., Axelsson, H., Hansson, T., 1998. Life expectancy and cost utility after total hip replacement. *Clinical Orthopedics* 346, 141.

Georgiou AP, Cunningham JL, 2001. Accurate diagnosis of hip prosthesis loosening using a vibrational technique. *Clinical Biomechanics* 16(4), 315-323.

- Gerogiou AP, Cunningham JL, 2001. Accurate diagnosis of hip prosthesis loosening using a vibrational technique. *Clinical Biomechanics* 16, 315-323.
- Giakas G, Baltzopoulos V, 1997. Time and frequency domain analysis of ground reaction forces during walking: an investigation of variability and symmetry. *Gait Posture* 5,189–97.
- Glaser D, Dennis DA, Komistek RD, Miner TM, 2008. Clicking and Squeaking: In vivo correlation of sound and separation for different bearing surfaces. *J Bone Joint Surg Supplement* (in print).
- Glaser D, Komistek RD, Cates HE, Mahfouz MR, 2007. In vivo comparison of hip mechanics for minimally invasive versus traditional total hip arthroplasty. *Clinical Biomechanics* 23, 127-134.
- Gök H, Ergin S, Yavuzer G. Kinetic and kinematic characteristics of gait in patients with medial knee arthrosis. *Acta Orthop Scand.* 2002;73(6):647-652.
- Gracovetsky, S., 1988. *The spinal engine*. Vienna: Springer
- Gross AE, Dust WN, 1997. Acute polyethylene fracture in an uncemented acetabular cup. *Canadian Journal of Surgery* 40 (4), 310-312.
- Gruber FW, Bock A, Trattnig S, Lintner F, Ritschl P, 2007. Cystic Lesion of the Groin due to Metallosis: A Rare Long-Term Complication of Metal-on-Metal Total Hip Arthroplasty. *Journal of Anthroplasty* 22(6), 923-927. (Available online).
- Hamill J, Bates BT and White CA, 1982. Evaluation of foot orthotic appliances using ground reaction force data. *Proceedings of the Second Biannual Conference of the Canadian Society of Biomechanics, Human Locomotion II.* pp. 74-75.

- Hamill J, McNiven SL, 1990. Reliability of selected ground reaction force parameters during walking. *Hum Mov Sci.* 9:117-131.
- Hannouche D, Nich C, Bizot P, Meunier A, Nizard R, Sedel L, 2003. Fractures of Ceramic Bearings. *Clin Orthop Relat Res.* 417:19-26.
- Harris WH, Sledge CB, 1990. Total hip and total knee replacement. *New England Journal of Medicine*, 323-725.
- Haw-Ming Huang, Ching-Lai Chiu, Ching-Ying Yeh and Sheng-Yang Lee, 2003. Factors influencing the resonance frequency of dental implants. *Journal of Oral and Maxillofacial Surgery* 61(10), 1184-1188.
- Hedley AK, Hendren DH and Mead LP, 1990. A posterior approach to the hip joint with complete posterior capsular and muscular repair. *J Arthroplasty* 5 (Suppl), 57.
- Heller MO, Bergmann G, Kassi JP, Claes L, Haas NP, 2005. Determination of muscle loading at the hip joint for use in pre-clinical testing. *Journal of Biomechanics* 38, 1155-1163.
- Herzog W, Nigg BM, Read LJ, Olsson E, 1989. Asymmetries in ground reaction force patterns in normal human gait. *Med Sci Sport Exer* 21:110-114.
- Hewitt JD, Glisson RR, Guilak AK et al., 2002. The mechanical properties of the human hip capsule ligaments. *Journal of Arthroplasty* 17, 82-89.
- Hodge WA, Fuan RS, Carlson KL, Burgess RG, Harris WH, Mann RW, 1986. Contact pressures in the human hip joint measured in vivo. *Biophysics.* 83:2879-2883.

- Huang X, Kwong KSC, Cheng JCY, 2000. Acoustic Transmission in Normal Human Hips. In Proceedings of the Annual Meeting of the EMBS International Conference. Chicago, IL.
- Ilchmann T, 1997. Radiographic assessment of cup migration and wear after hip replacement. *Acta Orthop Scand Suppl* 276, 1-26.
- Inoue J, Nagata Y, Suzuki K, 1986. Measurement of knee joint sounds by microphone. *Sangyo Ika Daigaku Zasshi* 8(3), 307–316.
- Isaac DL, Forder J, Skyrme A, James S, 2007. The Biomet Bi-Metric Total Hip Arthroplasty and Universal Acetabular Cup: High Polyethylene Failure Rate in the Medium Term. *The Journal of Arthroplasty* 22(5), 697-700.
- Jaecques SVN, Pastrav C, et al, 2004. Analysis of the fixation quality of cementless hip prostheses using a vibrational technique. In Proceedings of the annual ISMA2004 International Conference on Noise and Vibration Engineering. Leuven, Belgium.
- Jarrett CA, Ranawat AS, Bruzzone M, Rodriguez JA, Ranawat CS, 2007. The Squeaking Hip: A Underreported Phenomenon of Ceramic-On-Ceramic Total Hip Arthroplasty. *Journal of Arthroplasty* 22(2), 302.
- JISRF, Joint Implant Surgery & Research Foundation. Total Hip Replacement. http://www.jisrf.org/total_hip_replacement.htm. Accessed June 2008.
- Jordon JM, Kington RS, Lane NE, Nevitt MC, Zhang Y, Sowers MF, et al, 2000. Systemic risk factors for osteoarthritis in: Felson DT (conference chair): Osteoarthritis: New insights. Part I: The disease and its risk factors. *Annals of Internal Medicine* 133, 635-646.

- Jurist JM, 1970. In-Vivo determination of the elastic response of bone II. Ulnar resonant frequency in osteoporotic, diabetic and normal subjects. *Physics in Medicine and Biology* 15(3), 427-434.
- Jurist JM, Cameron JR, 1969. Measurement of bone resonant frequency in-vivo. In *Proceedings of the Second International Conference on Medical Physics*. Boston, MA. pp. 187.
- Jurist JM, Dymond AM, 1970. Reproducibility of ulnar resonant frequency measurement. *Aerospace Medicine* 41(8), 875-878.
- Kane TR and Levinson DA, 1985. *Dynamics: Theory and Applications*. McGraw-Hill, New York.
- Kane TR and Levinson DA, 1996. *Dynamics Online: Theory and Implementation With Autolev*. Online Dynamics, Sunnyvale, CA.
- Katsuhiko Ogata, 2001. *Modern Control Engineering (4th Edition)*. Prentice Hall, NJ.
- Kavanagh BF, 1992. Femoral head fractures associated with total hip arthroplasty. *Orthop Clin North Am* 23:249-257.
- Kavanagh BF, Ilstrup DM, Fitzgerald RH, Fitzgerald RH Jr, 1985. Revision total hip arthroplasty. *J Bone Joint Surg* 67-A :517-526.
- Kearns SR, Jamal B, et al, 2006. Factors affecting survival of uncemented total hip arthroplasty in patients 50 years or younger. *Clinical Orthopaedics and Related Research* 453, 103–109.
- Kernohan WG, Mollan RAB, 1982. Microcomputer analysis of joint vibration. *Journal of Microcomputer Applications* 5(4), 287-288.

- Khalil TB, Viano DC, Taber LA, 1981. Vibrational characteristics of the embalmed human femur. *Journal of Sound and Vibration* 75, 417-436.
- Komistek RD, Stiehl JB, and Paxson RD, 1994: Mathematical model of the human lower extremity. *Biomedical Engineering Recent Developments*, J. Vossoughi, Ed., Washington, DC.: 1098-1101.
- Komistek RD, Stiehl JB, Paxson RD, Soutas-Little, 1998. Mathematical Model of the Lower Extremity Joint Reaction Forces Using Kane's Method of Dynamics: A Technical Note, *Journal of Biomechanics* 31(2): 185-189.
- Komistek RD, Dennis DA, Northcut EJ, Ochoa JA, Ritchie, 2001. In Vivo Determination of Hip Joint Separation and the Forces Generated Due To Impact Loading Conditions. *Journal of Biomechanics* 34, 623-629.
- Komistek RD, Dennis DA, Haas BD, Ochoa JA, Hammill C, 2002. An In Vivo Comparison of Hip Joint Separation for after Metal-on-Metal or Metal-on-Polyethylene THA J. *Bone Joint Surgery* 84:1836-1841.
- Komistek RD, 2005. Special issue on Knee Mechanics. *Journal of Biomechanics* 38(2):195.
- Krischak GD, Nikolaus JW, Zabel T, et al, 2003. Influence of preoperative mechanical bone quality and bone mineral density on aseptic loosening of total hip arthroplasty after seven years. *Clinical Biomechanics* 18, 916-923.
- Laupacis A, Bourne R, Rorabeck C, Feeny D, Wong C, Tugwell P, Leslie K, Bullas R, 1993. The effect of elective total hip replacement on health-related quality of life. *Journal of Bone and Joint Surgery Am* 75, 1619-1626.

- Learmonth ID, Young C, Rorabeck C, 2007. The operation of the century: total hip replacement. *Lancet* 370, 1508-1519. (Available online).
- Leuchte S, Luchs A, Wohlrab D, 2007. Measurement of ground reaction forces after total hip arthroplasty using different surgical approaches. *Z Orthop Ihre Grenzgeb* 145(1), 74-80.
- Li PLS, Jones NB, Gregg PJ, 1995. Loosening of total hip arthroplasty; diagnosis by vibration analysis. The British Editorial Society of Bone and Joint Surgery, *Journal of Bone and Joint Surgery Br* 77(4), 640-644.
- Li PLS, Jones NB, Gregg PJ, 1996. Vibration analysis in the detection of total hip prosthetic loosening. *Medical Engineering and Physics* 18(7), 596-600.
- Lombardi AV, Mallory TH, Vaughn BK, Drouillard P, 1989. Aseptic loosening in total hip arthroplasty secondary to osteolysis induced by wear debris from titanium-alloy modular femoral heads. *J Bone Joint Surg Am.* 71: 1337-1342.
- Lombardi AV, Mallory TH, Dennis DA, Komistek RD, Fada, Northcut EJ, 2000. An In Vivo Determination of Total Hip Arthroplasty Pistoning during Activity. *Journal of Arthroplasty* 15(6), 702-709.
- Long WT, Dorr LD, Healy B, Perry J, 1993. Functional Recovery of Noncemented Total Hip Arthroplasty. *Clinical Orthopaedics and Related Research* 288, 73-77.
- Lowet G, Van Audekercke R, Van Der Perre G, Geusens P, Dequeker J, Lammens J, 1993. The relation between resonant frequencies and torsional stiffness of long bones in vitro. Validation of a simple beam model. *Journal of Biomechanics* 26(6), 689-696.

- Lowet G, Van Der Perre G, 1996. Ultrasound velocity measurement in long bones: measurement method and simulation of ultrasound wave propagation. *Journal of Biomechanics* 29(10), 1255-1262.
- MacDonald SJ, 2004. Metal-on-metal total hip arthroplasty: the concerns. *Clin Orthop Relat Res.* (429):86-93. Review.
- Madsen MS, Ritter MA, Morris HH, et al, 2004. The effect of total hip arthroplasty surgical approach on gait. *Journal of Orthopedic Research* 22, 44-50.
- Mahfouz MR, Hoff WA, Komistek RD, Dennis DA, 2003. A robust method for registration of three-dimensional knee implant models to two-dimensional fluoroscopy images. *IEEE Transactions on Medical Imaging* 22, 1561-1574.
- Mardones R, Pagnano M, Nemanich J, Trousdale R, 2005. Muscle Damage after Total Hip Arthroplasty Done with the Two-incision and Mini-posterior Techniques. *Clinical Orthopaedics and Related Research* 441, 63-67.
- Markey EL, Jurist JM, 1974. Tibial resonant frequency measurements as an index of the strength of fracture union. *Wisconsin Medical Journal* 73(5), S62-S65.
- McCoy GF, McCrea JD, Beverland DE, Kernohan WG, Mollan RA, 1987. Vibration arthrography as a diagnostic aid in disease of the knee. *Journal of Bone and Joint Surgery* 69-B(2), 288–293.
- McGrory BJ, Freiberg AA, Shinar AA, Harris WH, 1996. Correlation of Measured Range of Hip Motion Following Total Hip Arthroplasty and Responses to a Questionnaire. *The Journal of Arthroplasty* 11(5), 565-571.

- McCrary JL, White SC, Lifeso RM, 2001. Vertical ground reaction forces: objective measures of gait following hip arthroplasty. *Gait Posture* 14, 104-109.
- McKellop HA, Clark IC, 1984. Evolution and evaluation of materials-screening machines and joint simulators in predicting in vivo wear phenomena . In: Duchyene P, Hastings GW (eds). *Functional Behavior of Orthopaedic Biomaterials. Applications. Vol II*, CRC Press, Boca Raton FL, pp 51-85.
- Meredith N, Shagaldi F, Alleyne D, et al, 1997. The application of resonance frequency measurements to study the stability of titanium implants during healing in the rabbit tibia. *Clinical Oral Implant Research* 8, 234-243.
- Messier SP, Loeser RF, Hoover JL, et al., 1992. Osteoarthritis of the knee: effects on gait, strength and flexibility. *Arch Phys Med Rehabil.* 73(1):29-36.
- Mizuta, et al, 2002. A radiographic study of hip joint alignment after prosthetic hip arthroplasty. *Acta Med Okayama* 56(3), 159-166.
- Mohler CG, Callaghan JJ, Collis DK, Johnston RC, 1995. Early loosening of the femoral component at the cement-prosthesis interface after total hip replacement. *J Bone Joint Surg Am.* 77: 1315-1322.
- Mollan RAB, McCullagh GC, Wilson RI, 1982. A critical appraisal of auscultation of human joints. *Clinical Orthopaedics and Related Research* 170, 231-237.
- Morlock M, Nassutt R, Janssen R, Willmann G, Honl M, 2001. Mismatched wear couple zirconium oxide and aluminum oxide in total hip arthroplasty. *Journal of Arthroplasty* 16, 8.

- Muratoglu O, Bragdon C, O'Connor D et al., 2001. A novel method of cross-linking UHMWPE to improve wear, reduce oxidation and retain mechanical properties. *J Arthroplasty* 16:149.
- Murray MP, Brewer BJ, Gore DR, Zuege RC, 1975. Kinesiology after McKee-Farrar total hip replacement. A two-year follow-up of one hundred cases. *Journal of Bone and Joint Surgery Am* 57, 337-342.
- Murray MP, Gore DR, Brewer BJ, Zuege RC, Gardner GM, 1976. Comparison of Functional Performance after McKee-Farrar, Charnley, and Müller Total Hip Replacement, a six-month follow-up of one hundred sixty-five cases. *Clinical Orthopaedics and Related Research* 121, 33-43.
- Nagata Y, 1988. Joint-sounds in gonarthrosis - Clinical application of phonoarthrography for the knees. *Journal of UOEH* 10(1) 47-58.
- Nakaktsuchi Y, Tsuchikane A, Nomura A, 1996. The vibrational mode of the tibia and assessment of bone union in experimental fracture healing using the impulse response method. *Medical Engineering and Physics* 18(7), 575-583.
- National Guideline Clearinghouse, 2000. Imaging after total hip arthroplasty (THA). *Radiology* 215, 389-390.
- Nevelos J, Ingham E, Doyle C, Streicher R, Nevelos A, Walter W, Fisher J (2000) Microseparation of the centers of alumina-alumina artificial hip joints during simulator testing produces clinically relevant wear rates and patterns. *J. Arthroplasty* 15:793.
- Nixon M, Taylor G, Sheldon P, Iqbal SJ, Harper W, 2007. Does bone quality predict loosening of cemented total hip replacements? *J Bone Joint Surg [Br]* 89-B:1303-8.

- Nokes L, Mintow-Czyz WJ, Mackie I, et al, 1984. Direct and indirect determination of tibial natural frequency- A comparison of frequency domain analysis and fast fourier transform. *Journal of Biomedical Engineering* 6(1), 45-48.
- Nokes LD, Thorne GC, 1988. Vibrations in orthopedics. *Critical Reviews in Biomedical Engineering* 15(4), 309-349.
- Northcut EJ, 1998. In vivo determination of hip joint separation. Thesis, Colorado School of Mines.
- Numair J., Joshi, A.B., Murphy, J.C., Porter, M.L., Hardinge, K., 1997. Total hip arthroplasty for congenital dysplasia or dislocation of the hip. Survivorship analysis and long term results. *Journal of Bone and Joint Surgery* 79A, 1352-1360.
- Orthopaedic Associates, Education: <http://www.oagb.net>. Accessed June 2008
- Pagnano MW, Leone J, Meneghini RM, et al, 2007. A Prospective Randomized Trial Shows 2-Incision THAs Do Not Recover Quicker Than Mini-Posterior THAs. In *Proceedings of the Annual Meeting of the American Academy of Orthopaedic Surgeons*. San Diego, CA.
- Pai VS (1997). "A comparison of three lateral approaches in primary total hip replacement". *Int Orthop* 21 (6): 393–8.
- Park S, Krebs DE, Mann RW, 1999. Hip muscle co-contraction: evidence from concurrent in vivo pressure measurement and force estimation. *Gait Posture* 10, 211–222.

- Parvizi J, Keisu KS, et al, 2004. Primary total hip arthroplasty with an uncemented femoral component: a long-term study of the Taperloc stem. *Journal of Arthroplasty* 19, 151–156.
- Paul JP, 1966. Forces transmitted by joints in the human body. *Proceedings Institution of Mechanical Engineers* -67 181(Pt 37), 8–15.
- Pedersen DR, Brand RA, Davy DT, 1997. Pelvic muscle and acetabular contact forces during gait. *Journal of Biomechanics* 30(9), 959-965.
- Pellicci PM, Bostrom M and Poss R, 1998. Posterior approach to total hip replacement using enhanced posterior soft tissue repair. *Clin Orthop* 355, 224. Full Text via CrossRef | View Record in Scopus | Cited By in Scopus (99)
- Radin EL, Ehrlich MG, Chernack R, Abernethy P, Paul IL, Rose RM, 1978. Effect of repetitive impulsive loading on the knee joints of rabbits. *Clinical Orthopaedics and Related Research* 131, 288–293.
- Radke S, Kirschner S, et al, 2004. Magnetic resonance imaging criteria of successful core decompression in avascular necrosis of the hip. *Skeletal Radiology* 33(9), 519-23.
- Robertson WJ, Kelly BT, 2008. The Safe Zone for Hip Arthroscopy: A Cadaveric Assessment of Central, Peripheral, and Lateral Compartment Portal Placement. *The Journal of Arthroscopic & Related Surgery* 24(6), Supplement 1: e1
- Reddy NP, Rothschild BM, et al, 1995. Noninvasive acceleration measurements to characterize knee arthritis and chondromalacia. *Ann Biomed Eng* 23, 78–84.

- Rokkum M, Brandt M, Bye K, Hetland KR, Waage S, Reigstad A, 1999. Polyethylene wear, osteolysis and acetabular loosening with an HA-coated hip prosthesis. *J Bone Joint Surg [Br]* 81-B: 582-9.
- Rosenstein AD, McCoy GF, and Bulstrode CJ, 1989. The differentiation of loose and secure femoral implants in total hip replacement using a vibrational technique: an anatomical and pilot study. In *Proceedings of the Institution of Mechanical Engineers* 203, 77-81.
- Rosenstein AD, McCoy GF, Bulstrode CJ, McLardy-Smith PD, Cunningham JL, Turner-Smith AR, 1989. The differentiation of loose and secure femoral implants in total hip replacement using a vibrational technique: an anatomical and pilot clinical study. *Proceedings Institution of Mechanical Engineers Part H: J. Eng. Med.* 203(2), 77-81.
- Rothman RH, 2006. Noisy ceramic hip: Is component malpositioning the problem? 17th AAHKS Annual meeting 2006; Dallas, Texas.
- Rubin C, Pope M, Fritton C, Magnusson M, Hansson T, McLeod K, 2003. Transmissibility of 15-Hertz to 35-Hertz Vibrations to the Human Hip and Lumbar Spine: Determining the Physiologic Feasibility of Delivering Low-Level Anabolic Mechanical Stimuli to Skeletal Regions at Greatest Risk of Fracture Because of Osteoporosis. *Spine* 28(23), 2621-2627.
- Sarojak ME, 1998. Model-fit: an interactive pose determining system. Colorado school of mines. Engineering Thesis, Golden, CO.
- Sartor C, Alderink G, Greenwald H and Elders L, 1999. Critical kinematic events occurring in the trunk during walking. *Human Movement Science* 18(5), 669-679

- Schinsky MF, Nercessian OA, Arons RR, Macaulay W, 2003. Comparison of complications after transtrochanteric and posterolateral approaches for primary total hip Arthroplasty. *The Journal of Arthroplasty* 18(4), 430-434
- Seireg A, Arvikar RJ, 1973. The prediction of muscular load sharing and joint forces in the lower extremities during walking. *Journal of Biomechanics* 8, 89-102.
- Sharp DJ, Porter KM, 1985. The Charnley total hip replacement in patients under 40. *Clinical Orthopedics* 201, 51-56.
- Sirianni LA, Dorr LD, Yun A, et al, 2007. Gait analysis of MIS THR. In Proceedings of the Annual Meeting of the American Academy of Orthopaedic Surgeons. San Diego, CA.
- Sochart DH, Porter ML, 1997. The long term results of Charnley low-friction arthroplasty in young patients what have congenital dislocation, degenerative osteoarthritis, or rheumatoid arthritis. *Journal of Bone and Joint Surgery* 79A, 1599-1617.
- Stevens SS and Davis H, 1983. *Hearing: Its Psychology and Physiology*, American Institute of Physics, for the Acoustical Society of America.
- Swanson TV, Hanna RS, 2003. Advantages of Cementless THA Using Minimally Invasive Surgical Technique. In Proceedings of the Annual Meeting of the American Academy of Orthopaedic Surgeons Meeting. New Orleans, LA.
- Tavathia S, Rangayyan R, et al, 1992. Analysis of knee vibration signals using linear prediction. *IEEE Transactions on Biomedical Engineering* 39, 959–970.

- Taylor JG, Perry JS, Meswania JM, Donaldson N, Walker PS, Cannon SR, 1997. Telemetry of forces from proximal femoral replacements and relevance to fixation. *Journal of Biomechanics* 30: 225-234.
- Taylor WR, Roland E, et al, 2002. Determination of orthotropic bone elastic constants using FEA and modal analysis. *Journal of Biomechanics* 35, 767-773.
- The B, Hosman A, Kootstra J, Kralj-Iglic V, Flivik G, Verdonschot N, Diercks R, 2008. Association between contact hip stress and RSA-measured wear rates in total hip arthroplasties of 31 patients. *Journal of Biomechanics* 41(1): 100-105.
- Thomas AM, Luo DZ, Dunn JW, 1991. Response of human femur to mechanical vibration. *Journal of Biomedical Engineering* 13(1), 58-60.
- Tsuchikane A, Naktsuchi Y, Nomura A, 1995. The influence of joints and soft tissue on the natural frequency of the human tibia using the impulse response method. In *Proceedings of the Institution of Mechanical Engineers Part H* 209(3), 149-155.
- Van der Perre G, 1984. Dynamic analysis of human bones. In: Ducheyne P, Hastings GW (Eds.), *Functional Behavior of Orthopedic Biomaterials* 1. CRC Press, pp. 99-159.
- Van Der Perre G, Lowet G, 1996. In vivo assessment of bone mechanical properties by vibration and ultrasonic wave propagation. *Bone* 18(V1-S1), 29S-35S.
- Virginia Commonwealth University, Courses: http://www.courses.vcu.edu/DANC291-003/unit_6.htm. Accessed February 2005

- Wagner M, Wagner H, 2000. Medium-Term Results of a Modern Metal-on-Metal System in Total Hip Replacement. *Clinical Orthopaedics and Related Research* 379, 123-133.
- Walter WL, O'Toole G, Walter WK, Ellis A, Zicat B, 2006. Squeaking in ceramic-on-ceramic hips; the importance of acetabular component orientation. *Journal of Arthroplasty* 22, 296-503.
- Walters CF, 1929. The value of joint auscultation. *Lancet* i, 920.
- Weeden SH, Paprosky WG, Bowling JW, 2003. The early dislocation rate in primary total hip arthroplasty following the posterior approach with posterior soft-tissue repair. *Journal of Arthroplasty* 18(6), 709-713.
- Wheeless' Textbook of Orthopaedics, a, Duke Orthopaedics. Anterolateral Approach to Hip Joint: (Watson Jones):
http://www.wheelessonline.com/ortho/anterolateral_approach_to_hip_joint_watson_jones. Accessed July 2008.
- Wheeless' Textbook of Orthopaedics, b, Duke Orthopaedics. Anterior Approach to the Hip (Smith Petersen):
http://www.wheelessonline.com/ortho/anterior_approach_to_the_hip_smith_peterson. Accessed July 2008.
- Winter DA, 1990: Biomechanics and motor control of human movement. John Wiley & Sons, Inc., Canada.

Wright JM, Crockett HC, Delgado S, Lyman S, Madsen M, Sculco TP, 2004. Mini-incision total hip arthroplasty. A prospective, controlled investigation with 5-year follow-up evaluation. *Journal of Arthroplasty* 19(5), 538–545.

Wright KWJ, Scales JT (1977) The use of hip joint simulators for the evaluation of wear of total hip prosthesis. In Winter GD, Leray JL, deGroot K (eds). *Evaluation of Biomaterials*. John Wiley, Chichester, 135-146.

Zhang YT, Rangayyan RM, et al, 1994. Adaptive cancellation of muscle contraction interference from knee joint vibration signals. *IEEE Transactions on Biomedical Engineering* 41, 181–191.

Appendix

Appendix A: Patient Questionnaire

Patient Questionnaire			
1 Personal Information:			
1.1	Full name:	1.2	Occupation:
1.3	Date of birth:	1.4	Sex: <input type="radio"/> female <input type="radio"/> male
1.5	Height:	1.6	Weight:
1.7	Implant Side: <input type="radio"/> Right <input type="radio"/> Left <input type="radio"/> Bilateral	1.8	Shoe size:
1.9	Residence City: State:	1.10	Date of surgery:
2 Background:			
2.1	Reason for surgery: <input type="radio"/> injury <input type="radio"/> arthritis <input type="radio"/> wear <input type="radio"/> other _____		
2.2	Have you had any previous surgery? <input type="radio"/> Yes <input type="radio"/> No	Comment:	
2.3	Other implants: <input type="radio"/> none <input type="radio"/> left hip <input type="radio"/> right hip <input type="radio"/> left knee <input type="radio"/> right knee <input type="radio"/> spine <input type="radio"/> left ankle <input type="radio"/> right ankle <input type="radio"/> shoulder <input type="radio"/> other _____		
2.4	Do you have any pre-existing conditions? <input type="radio"/> No <input type="radio"/> Spine <input type="radio"/> Hip <input type="radio"/> Knee <input type="radio"/> Vascular		
	Comment:		
2.5	Are you having any psychological difficulties that may affect how you perform certain activities? <input type="radio"/> No <input type="radio"/> stress <input type="radio"/> depression <input type="radio"/> work-related accident <input type="radio"/> pending lawsuit <input type="radio"/> other _____		
	Comment:		
	Are you experiencing: <input type="radio"/> pain <input type="radio"/> swelling <input type="radio"/> deformity <input type="radio"/> limp <input type="radio"/> other _____		
2.6	<input type="radio"/> none <input type="radio"/> mild <input type="radio"/> moderate <input type="radio"/> severe <input type="radio"/> extreme		
	Comment:		
	<input type="radio"/> occasionally <input type="radio"/> once per week <input type="radio"/> more than once per week		
	<input type="radio"/> daily <input type="radio"/> always		
2.7	Are there any activities that bother you in particular? <input type="radio"/> walking <input type="radio"/> squatting <input type="radio"/> climbing stairs <input type="radio"/> bicycling <input type="radio"/> jumping		
	<input type="radio"/> getting up from chair <input type="radio"/> sitting down in chair <input type="radio"/> other _____		
	Comment:		
3	Are you exercising?	How often? <input type="radio"/> daily <input type="radio"/> weekly <input type="radio"/> monthly <input type="radio"/> other _____	
	<input type="radio"/> Yes <input type="radio"/> No	What type of exercises?	
4	How much physical movement is required for your job?	<input type="radio"/> extensive <input type="radio"/> moderate <input type="radio"/> minimal <input type="radio"/> none	
		How often? <input type="radio"/> daily <input type="radio"/> weekly <input type="radio"/> monthly <input type="radio"/> other _____	
	What type of movement?		
5	Other activities of interest: <input type="radio"/> dancing <input type="radio"/> gardening <input type="radio"/> living on the third floor without an elevator		
	other _____ How often? <input type="radio"/> daily <input type="radio"/> weekly <input type="radio"/> monthly <input type="radio"/> other _____		
6	Your ability to perform basic activities of daily living: (0 - with ease, 1 - with difficulty, 2 - cannot)		
6.1	How difficult is it to cut your toenails on the operated side?	0	1 2
6.2	How difficult is it to put on socks?	0	1 2
6.3	How difficult is it to tie a shoe?	0	1 2

Patients Questions Booklet
Transfer Functions Across the Hip
08/20/07

1/3

Initials _____
Date _____

7 Activity level during the day: Rank the activity of your day from 1-10. (1- mostly sitting and lying, 10 - almost the whole day on foot (standing, walking, running etc.))			
7.1	How active would you describe your day before your implant? 1 2 3 4 5 6 7 8 9 10		
7.2	How active would you describe your day now? 1 2 3 4 5 6 7 8 9 10		
8 Questions about the STIFFNESS around your hip: (0 - no stiffness, 1 - mild stiffness, 2 - moderate stiffness, 3 - severe stiffness, and 4 - extreme stiffness)			
8.1	How severe is your stiffness after first awakening in the morning? 0 1 2 3 4		
8.2	How severe is your stiffness after sitting, lying, or resting later in the day? 0 1 2 3 4		
9 Questions about the PHYSICAL FUNCTION of your hip: For each of the following activities, please indicate the degree of difficulty you are currently experiencing. (0 for no difficulties, 1 for mild difficulties, 2 for moderate difficulties, 3 for severe difficulties, and 4 for extreme difficulties)			
9.1	Bending to the floor to pick up an object? 0 1 2 3 4	9.2	Getting in/out of car? 0 1 2 3 4
9.3	Putting on socks? 0 1 2 3 4	9.4	Taking off socks? 0 1 2 3 4
9.5	Getting in/out of bath? 0 1 2 3 4	9.6	Getting on/off toilet? 0 1 2 3 4
9.7	Going down stairs? 0 1 2 3 4	9.8	Going up stairs? 0 1 2 3 4
9.9	Lying down? 0 1 2 3 4	9.10	Bending? 0 1 2 3 4
9.11	Shopping? 0 1 2 3 4	9.12	Walking on flat ground? 0 1 2 3 4
9.13	Sitting? 0 1 2 3 4	9.14	Standing? 0 1 2 3 4
9.15	Arising from bed? 0 1 2 3 4	9.16	Arising from sitting? 0 1 2 3 4
9.17	Heavy chores? 0 1 2 3 4	9.18	Light chores? 0 1 2 3 4
10 Questions about the PAIN in the hip: For each of the following activities, please indicate the degree of pain you are currently experiencing (0 for no pain, 1 for mild pain, 2 for moderate pain, 3 for severe pain, and 4 for extreme pain)			
9.1	Bending to the floor to pick up an object? 0 1 2 3 4	9.2	Getting in/out of car? 0 1 2 3 4
9.3	Putting on socks? 0 1 2 3 4	9.4	Taking off socks? 0 1 2 3 4
9.5	Getting in/out of bath? 0 1 2 3 4	9.6	Getting on/off toilet? 0 1 2 3 4
9.7	Going down stairs? 0 1 2 3 4	9.8	Going up stairs? 0 1 2 3 4
9.9	Lying down? 0 1 2 3 4	9.10	Bending? 0 1 2 3 4
9.11	Shopping? 0 1 2 3 4	9.12	Walking on flat ground? 0 1 2 3 4
9.13	Sitting? 0 1 2 3 4	9.14	Standing? 0 1 2 3 4
9.15	Arising from bed? 0 1 2 3 4	9.16	Arising from sitting? 0 1 2 3 4
9.17	Heavy chores? 0 1 2 3 4	9.18	Light chores? 0 1 2 3 4
11 How satisfied are you with the outcome of your implant?			
<input type="radio"/> 1- very dissatisfied <input type="radio"/> 2- somewhat dissatisfied <input type="radio"/> 3- neutral <input type="radio"/> 4- somewhat satisfied <input type="radio"/> 5- very satisfied			
Comment:			

12	Does your hip produce any noises or sounds such as clicking or squeaking? <input type="radio"/> yes <input type="radio"/> no	
If yes:		
12.1	What type of noise is produced? <input type="radio"/> squeaking <input type="radio"/> grinding <input type="radio"/> clicking <input type="radio"/> creaking <input type="radio"/> other _____	
12.2	During what activity? <input type="radio"/> walking <input type="radio"/> hiking <input type="radio"/> bicycling <input type="radio"/> jogging <input type="radio"/> squatting <input type="radio"/> jumping <input type="radio"/> ascending stairs <input type="radio"/> descending stairs <input type="radio"/> other _____	
12.3	How often does it occur? <input type="radio"/> constantly <input type="radio"/> regularly <input type="radio"/> occasionally <input type="radio"/> rarely	
12.4	When did it start?	12.5 Has it stopped? <input type="radio"/> yes <input type="radio"/> no
12.6	If it has stopped, when did it occur last?	
12.7	Is there any dependence on any of the following? <input type="radio"/> no <input type="radio"/> after first awakening in the morning <input type="radio"/> after long periods of sitting <input type="radio"/> after extensive activity <input type="radio"/> morning hours <input type="radio"/> afternoon hours <input type="radio"/> at night <input type="radio"/> other _____	
Comment:		
12.8	Were you regularly taking any medication during the time when the noise started? <input type="radio"/> yes <input type="radio"/> no	Comment:
12.9	Are you now taking any medication on a regular basis? <input type="radio"/> yes <input type="radio"/> no	Comment:
13	Is there anything else that bothers / concerns you? <input type="radio"/> yes <input type="radio"/> no	Comment:
Please sign		
Signature _____		Date _____

Appendix B: Surgeon's Questionnaire in Electronical Format

QUESTIONNAIRE FOR SURGEONS

Questionnaire for data collection of THR Patients

All information will be treated as strictly confidential!

1.	Patient data		
1.1	Last Name	<input type="text"/>	First Name <input type="text"/> Initial <input type="text"/>
1.2	Residence of patient	State <input type="text"/>	Country <input type="text"/>
1.3	Date of birth	<input type="text"/>	
1.4	Age at surgery	<input type="text"/>	(years)
1.5	Date of Surgery	<input type="text"/>	
1.6	Follow-Up	<input type="text"/>	(months)
1.7	Height of patient	<input type="text"/>	(in)
1.8	Weight of patient	<input type="text"/>	(lbs)
1.9	Gender	<input type="radio"/> Female <input type="radio"/> Male	
1.10	Harris Hip Scores	Pre-OP <input type="text"/>	Post-OP <input type="text"/>
1.11	Side of Implant	<input type="radio"/> Right <input type="radio"/> Left	
1.12	Diagnosis	<input type="text"/>	
2.	X-Ray availability	Months before/after OP	Weight bearing?
2.1	Pre-OP <input type="radio"/> Yes <input type="radio"/> No	<input type="text"/>	<input type="radio"/> Yes <input type="radio"/> No
2.2	Early Post-OP <input type="radio"/> Yes <input type="radio"/> No	<input type="text"/>	<input type="radio"/> Yes <input type="radio"/> No
2.3	Late Post-OP <input type="radio"/> Yes <input type="radio"/> No	<input type="text"/>	<input type="radio"/> Yes <input type="radio"/> No

3. Medical Issues	
3.1	Other implants <input type="text"/>
3.2	Degenerative joints <input type="text"/>
3.3	Any other pain/ conditions that have not yet been addressed <input type="text"/>
3.4	Activity level
	Pre-OP <input type="text"/> Post-OP <input type="text"/>
4. Circumstances of surgery	
4.1	Hospital name <input type="text"/>
4.2	Name of surgeon <input type="text"/>
4.3	Surgical Approach <input type="text"/> If other, please type in drop-down box to the left
4.4	Incision type <input type="text"/> If other, please type in drop-down box to the left
4.5	Mid-range laxity <input type="text"/> (mm)
4.6	Capsular repair <input type="radio"/> Yes <input type="radio"/> No Comment: <input type="text"/>
4.7	Leg length Affected side <input type="text"/> (in) Unaffected side <input type="text"/> (in)
4.8	Implant position (degrees) Inclination <input type="text"/> Anteversion <input type="text"/> CCD-angle <input type="text"/>
4.9	Fixation <input type="checkbox"/> Cemented <input type="checkbox"/> Non-cemented <input type="checkbox"/> Pressfit (specify)
	Underreaming <input type="text"/>
4.10	Surgery duration <input type="text"/> (min)
4.11	Blood loss <input type="text"/> (cc)
4.12	Blood transfusion <input type="text"/> (cc)
4.13	Complications <input type="radio"/> Yes <input type="radio"/> No Comment: <input type="text"/>

4.	Circumstances of surgery (cont.)		
4.14	Hospitalization	<input type="text"/>	(days)
4.15	Patient satisfaction level	Pre-OP <input type="text"/>	Post-OP <input type="text"/>
5.	Implant system		
5.1	Stem		
	Manufacturer	<input type="text"/>	If other, please type in drop-down box to the left.
	Trade name	<input type="text"/>	
	Component number	<input type="text"/>	
	Stem size	<input type="text"/>	
	Taper type (angle)	<input type="text"/>	
	Material	<input type="text"/>	If other, please type in drop-down box to the left.
	Are samples available?	<input type="radio"/> Yes <input type="radio"/> No	Comment: <input type="text"/>
	Are retrievals available?	<input type="radio"/> Yes <input type="radio"/> No	Comment: <input type="text"/>
	Manufacturing process	<input type="text"/>	
	Surface treatment (blasting)	<input type="text"/>	
	Coating	<input type="text"/>	
5.2	Femoral Ball Head		
	Manufacturer	<input type="text"/>	If other, please type in drop-down box to the left.
	Trade name	<input type="text"/>	
	Component number	<input type="text"/>	
	Ball diameter	<input type="text"/>	(mm)
	Neck length	<input type="text"/>	
	Material	<input type="text"/>	If other, please type in drop-down box to the left.

5.3	Acetabular Liner			
	Manufacturer	<input type="text"/>	If other, please type in drop-down box to the left.	
	Trade name	<input type="text"/>		
	Component number	<input type="text"/>		
	Material	<input type="text"/>	If other, please type in drop-down box to the left	
	Sandwich insert	<input type="radio"/> Yes <input type="radio"/> No	Taper-locked	<input type="radio"/> Yes <input type="radio"/> No
	Are samples available?	<input type="radio"/> Yes <input type="radio"/> No	Comment:	<input type="text"/>
	Are retrievals available?	<input type="radio"/> Yes <input type="radio"/> No	Comment:	<input type="text"/>
5.4	Cup			
	Manufacturer	<input type="text"/>	If other, please type in drop-down box to the left.	
	Trade name	<input type="text"/>		
	Component number	<input type="text"/>		
	Material	<input type="text"/>	If other, please type in drop-down box to the left.	
	Cup size	Inner diameter <input type="text"/> (mm)	Outer diameter <input type="text"/> (mm)	
	Are samples available?	<input type="radio"/> Yes <input type="radio"/> No	Comment:	<input type="text"/>
	Are retrievals available?	<input type="radio"/> Yes <input type="radio"/> No	Comment:	<input type="text"/>
	Manufacturing process	<input type="text"/>		
	Surface treatment (blasting)	<input type="text"/>		
Coating	<input type="text"/>			
6.	Audible Conditions			
6.1	Does the hip produce any audible noise?	<input type="radio"/> Yes	<input type="radio"/> No	
	If yes, please continue			
6.2	When did it start?	<input type="text"/>		

6.	Audible Conditions (cont.)		
6.3	How long has it persisted?	<input type="text"/> (months)	Comment: <input type="text"/>
6.4	How often does it occur?	<input type="text"/>	
6.5	Has it stopped?	<input type="radio"/> Yes <input type="radio"/> No	Comment: <input type="text"/>
6.6	If it has stopped, when did it occur last?	<input type="text"/>	
6.7	During what activity does it usually occur?	<input type="text"/>	If other, please type in drop-down box to the left.
6.8	Is there any dependence on the time of day?	<input type="radio"/> Yes <input type="radio"/> No	Comment: <input type="text"/>
6.9	Could it be reproduced in a doctor's office?	<input type="radio"/> Yes <input type="radio"/> No	
6.10	Type of noise and activity:		
	Noise	Activity	
	<input type="checkbox"/> Squeaking	<input type="text"/>	If other, please type in drop-down box to the left.
	<input type="checkbox"/> Grinding	<input type="text"/>	
	<input type="checkbox"/> Clicking	<input type="text"/>	
	<input type="checkbox"/> Creaking	<input type="text"/>	
	<input type="checkbox"/> Other: <input type="text"/>	<input type="text"/>	
	Any combination of sounds?		
	<input type="checkbox"/> Squeaking	<input type="text"/>	If other, please type in drop-down box to the left.
	<input type="checkbox"/> Grinding		
	<input type="checkbox"/> Clicking		
	<input type="checkbox"/> Creaking		
	<input type="checkbox"/> Other: <input type="text"/>		

Tables

Appendix D: Tables

Table 1: Patients' demographics

Bearing	# of patients	Follow-Up (months)	Age (years) avg SD	Height (m) avg SD	BW (kg) avg SD	BMI - avg SD	HSS-PreOp avg (min-max) SD	HSS-PostOp avg (min-max) SD	Implant	
MOP	4	31	68 6	1.8 0.1	83 17	27 4	44 (29 - 59) 14	98 (95 - 100) 3	Versys femoral stem, TM Modular acetabular cup, Trilogy liner, Zimmer, Warsaw, IN Versys femoral stem, Trilogy acetabular system Zimmer, Warsaw, IN	
COP	6	20	59 7	1.8 0.1	83 17	26 5	51 (40 - 69) 11	93 (73 - 100) 10	Versys femoral stem, TM Modular acetabular cup, alumina ceramic femoral head Zimmer, Warsaw, IN	
MOM	Zimmer (large)	3	7	50 6	1.8 0.0	95 11	29 3	52 (41 - 58) 10	92 (84 - 98) 7	Versys femoral stem, Metasul femoral head, Durom Acetabular component, Zimmer, Warsaw, IN
	Biomet (large)	4	17	43 3	1.8 0.1	100 42	30 10	45 (39 - 55) 8	82 (69 - 94) 14	M2a metal articulation, Biomet, Warsaw, IN
	Biomet (medium)	4	25	58 5	1.7 0.1	88 11	30 3	46 (30 - 61) 13	94 (88 - 100) 5	M2a metal articulation, Biomet, Warsaw, IN
	Overall MOM	11	17	50 8	1.8 0.1	94 25	30 6	47 (30 - 61) 10	89 (69 - 100) 11	
MOM-PS	5	9	52 13	1.8 0.1	96 18	25 4	44 (23 - 63) 16	96 (91 - 100) 5	Versys femoral stem, Converge acetabular cup, Metasul femoral head and liner Zimmer, Warsaw, IN	
COC	5	41	48 10	1.8 0.1	96 18	26 3	44 (27 - 57) 11	90 (65 - 100) 14	Accolade Femoral Stem, Trident acetabular system, alumina femoral head Stryker Kalamazoo, MI	
All Patients	31	22	54 11	1.8 0.1	86 19	27 5	46 (23 - 69) 11	92 (65 - 100) 10		
Hard	21	21	50 9	1.8 0.1	87 21	28 5	46 (23 - 63) 11	91 (65 - 100) 11		
Soft	10	24	63 8	1.8 0.1	83 17	26 5	48 (29 - 69) 12	95 (73 - 100) 8		

Table 2: Maximum separation, mid range laxity and number of patients with capsular repair

Bearing	Subjects	Maximum Separation (mm)			Mid-range Laxity (mm)	Capsular Repair (# patients)	
		avg	(min-max)	SD			
MOP	4	3.9	(1.4 - 5.6)	1.9	2	4	
COP	6	2.1	(1.0 - 3.4)	0.9	1	6	
MOM	Zimmer (large)	4	3.2	(2.5 - 4.2)	0.8	2	3
	Biomet (large)	2	4.1	(3.8 - 4.4)	0.4	1	2
	Biomet (medium)	3	2.1	(1.7 - 2.6)	0.5	2	3
	Overall MOM	9	3.0	(1.7 - 4.4)	1.0	2	8
MOM-PS	5	1.9	(1.4 - 2.4)	0.4	1	4	
All patients	24	2.7	(1.0 - 5.6)	1.2	1	22	
Hard	14	2.6	(1.4 - 4.4)	1.0	2	12	
Soft	10	2.8	(1.0 - 5.6)	1.6	1	10	

Table 3: Analog signal connector pin-out for the force plate

PIN Number	Description	Shorthand Notation
1	Z output from corner C	Cz
2	Z output from corner D	Dz
3	Z output from corner A	Az
4	Z output from corner B	Bz
5	Y output from A and C combined	YAC
6	X output from D and C combined	XDC
7	X output from A and B combined	XAB
8	Y output from B and D combined	YBD
9	Signal reference ground	SGND
10	Chassis ground	GNS

Table 4: Gait analysis parameters and symmetry indices for all unilateral patients

Bearing	Subjects	Average Time (s)										
		Stance					Swing					
		Healthy	Implanted	Difference	Symmetry Index	ASI	Healthy	Implanted	Difference	Symmetry Index	ASI	
MOP	4	1.20	1.21	-0.01	-1.2%	3.9%	0.46	0.46	0.00	0.7%	6.8%	
COP	4	1.80	1.82	-0.02	-0.9%	2.7%	0.62	0.57	0.05	7.3%	8.3%	
MOM	Zimmer (Large)	4	1.77	1.77	0.00	-0.2%	3.9%	0.58	0.59	-0.01	-0.8%	13.2%
	Biomet (Large)	0	-	-	-	-	-	-	-	-	-	
	Biomet (Medium)	4	1.29	1.33	-0.05	-3.8%	5.1%	0.58	0.52	0.06	11.4%	12.2%
	Overall MOM	8	1.53	1.55	-0.02	-2.0%	4.5%	0.58	0.55	0.03	5.3%	12.7%
MOM-PS	5	1.48	1.50	-0.02	-2.0%	4.0%	0.52	0.51	0.01	2.4%	7.5%	
COC	3	1.35	1.36	-0.01	-1.8%	3.7%	0.40	0.39	0.01	5.3%	11.1%	
All	24	1.49	1.51	-0.02	-1.7%	3.9%	0.53	0.51	0.02	4.3%	9.7%	
Hard	16	1.48	1.50	-0.02	-2.0%	4.2%	0.53	0.51	0.02	4.4%	10.8%	
Soft	8	1.50	1.52	-0.02	-1.1%	3.3%	0.54	0.52	0.03	4.0%	7.6%	

Bearing	Subjects	Average Time (s)										
		Step					Double					
		Healthy	Implanted	Difference	Symmetry Index	ASI	Healthy	Implanted	Difference	Symmetry Index	ASI	
MOP	4	1.67	1.67	0.00	0.1%	0.2%	0.37	0.38	-0.01	-2.0%	11.0%	
COP	4	2.41	2.39	0.02	0.7%	1.5%	0.58	0.64	-0.06	-10.1%	13.0%	
MOM	Zimmer (Large)	4	2.35	2.36	-0.01	-0.4%	0.9%	0.57	0.62	-0.05	-9.3%	16.7%
	Biomet (Large)	0	-	-	-	-	-	-	-	-		
	Biomet (Medium)	4	1.86	1.85	0.01	0.4%	0.9%	0.39	0.38	0.01	1.0%	17.0%
	Overall MOM	8	2.11	2.11	0.00	0.0%	0.9%	0.48	0.50	-0.02	-4.2%	16.8%
MOM-PS	5	1.98	2.02	-0.04	-2.1%	2.1%	0.50	0.48	0.02	5.6%	12.8%	
COC	3	1.76	1.75	0.00	0.3%	0.3%	0.46	0.50	-0.04	-6.4%	10.2%	
All	24	2.01	2.02	0.00	-0.3%	1.1%	0.48	0.50	-0.02	-3.1%	13.6%	
Hard	16	2.00	2.01	-0.01	-0.6%	1.2%	0.48	0.49	-0.01	-1.5%	14.3%	
Soft	8	2.04	2.03	0.01	0.4%	0.9%	0.47	0.51	-0.04	-6.1%	12.0%	

Table 5: Gait analysis parameters and symmetry indices for all bilateral patients

Bearing	Average Time (s)											
	Subjects	Stance					Swing					
		Right	Left	Difference	Symmetry Index	ASI	Right	Left	Difference	Symmetry Index	ASI	
MOP	0	-	-	-	-	-	-	-	-	-	-	
COP	2	1.48	1.48	0.00	0.0%	0.9%	0.44	0.46	-0.03	-6.1%	6.1%	
MOM	Zimmer (Large)	0	-	-	-	-	-	-	-	-	-	
	Biomet (Large)	4	1.50	1.40	0.10	7.4%	7.4%	0.45	0.56	-0.11	-24.7%	24.7%
	Biomet (Medium)	0	-	-	-	-	-	-	-	-	-	
	Overall MOM	4	1.50	1.40	0.10	7.4%	7.4%	0.45	0.56	-0.11	-24.7%	24.7%
MOM-PS	0	-	-	-	-	-	-	-	-	-	-	
COC	2	2.04	1.98	0.05	2.8%	3.0%	0.58	0.64	-0.06	-10.6%	10.6%	
All	8	1.63	1.56	0.06	4.4%	4.7%	0.48	0.56	-0.08	-16.5%	16.5%	
Hard	6	1.68	1.59	0.09	5.9%	5.9%	0.50	0.59	-0.09	-20.0%	20.0%	
Soft	2	1.48	1.48	0.00	0.0%	0.9%	0.44	0.46	-0.03	-6.1%	6.1%	

Bearing	Average Time (s)											
	Subjects	Step					Double					
		Right	Left	Difference	Symmetry Index	ASI	Right	Left	Difference	Symmetry Index	ASI	
MOP	0	-	-	-	-	-	-	-	-	-	-	
COP	2	1.92	1.95	-0.03	-1.5%	1.5%	0.50	0.54	-0.04	-12.5%	12.5%	
MOM	Zimmer (Large)	0	-	-	-	-	-	-	-	-	-	
	Biomet (Large)	4	1.95	1.95	0.00	0.0%	0.0%	0.45	0.49	-0.03	-5.5%	16.1%
	Biomet (Medium)	0	-	-	-	-	-	-	-	-	-	
	Overall MOM	4	1.95	1.95	0.00	0.0%	0.0%	0.45	0.49	-0.03	-5.5%	16.1%
MOM-PS	0	-	-	-	-	-	-	-	-	-	-	
COC	2	2.62	2.63	-0.01	-0.4%	0.4%	0.69	0.70	-0.02	-2.6%	4.8%	
All	8	2.11	2.12	-0.01	-0.5%	0.5%	0.52	0.55	-0.03	-6.5%	12.4%	
Hard	6	2.17	2.18	0.00	-0.1%	0.1%	0.53	0.56	-0.03	-4.6%	12.3%	
Soft	2	1.92	1.95	-0.03	-1.5%	1.5%	0.50	0.54	-0.04	-12.5%	12.5%	

Table 6: Segment dimensions

Segment	Landmarks	Direction		
		1(cm)	2(cm)	3(cm)
Foot				
	Ground to tibia/foot	0.000	6.260	0.000
	Toe to heel	21.000	0.000	0.000
	Toe to CM	17.000	5.000	0.000
	Ground to CM	0.000	3.747	0.000
Tibia				
	Ankle to knee	0.158	36.856	1.285
	Ankle to CM	-0.946	26.700	0.000
	Ankle to Hamstring wrapping point	2.11554	34.40260	-1.80960
	Ankle to Hamstring attachment point	0.90694	31.42435	-0.47374
	Ankle to TibTub	-3.444	31.820	1.000
	mid tibial radius (1.35965 cm)			
	top tibial radius			
	Tibial surface (1 direction)	4.92885	0.000	0.000
	Tibial surface (3 direction)	0.000	0.000	7.404
Femur				
	Knee to Femoral ball	0.541	44.817	-5.932
	Knee to top of femur	0.789	42.677	-0.586
	knee to greater tronchanter	0.100	40.315	2.990
	greater tronchanter to lesser Tronchanter	0.141	-2.773	-6.568
	Knee to CM	0.128	28.585	0.089
	greater tronchanter to Iliofem attachment one	-2.209	0.000	-5.506
	greater tronchanter to Iliofem wrapping point one	-2.644	1.043	-7.509
	greater tronchanter to Iliofem attachment point two	-4.000	2.146	-4.072
	greater tronchanter to Iliofem wrapping two	-2.743	3.166	-5.289
	greater tronchanter to Isciolet attachment point	0.187	1.499	-3.214
	greater tronchanter to Isciolet wrapping one	0.320	1.862	-5.947
	greater tronchanter to Isciolet wrapping two	0.240	1.579	-6.064
	greater tronchanter to Isciolet wrapping three	0.101	1.297	-6.269
	greater tronchanter to Isciolet wrapping four	-0.117	1.035	-6.445
	greater tronchanter to Isciolet wrapping five	-0.387	0.797	-6.620
	greater tronchanter to Isciolet wrapping six	-0.740	0.519	-6.794
	Knee to patella contact point	-1.805	1.804	0.054
Femur Radius (1.297 cm)				
Patella				
	Patella to femur contact point			
	Rectus femorus to Patellar ligament attachments	-0.083	4.397	-0.383
	CM to Rectus Femoris attachment	-0.066	2.199	-0.422
CM to Patellar Ligament attachment	0.017	-2.199	0.161	
Pelvis				
	Acetabulum Rad (2.56306 cm)			
	Acetabulum Ref to Iliofemoral attachment site	-2.909	0.456	1.687
	Acetabulum to center of vertebrae	-3.013	11.893	-6.449
	acetabulum to Iliopsoas muscle attachment one (Iliacus)	-0.895	12.846	3.616
	acetabulum to Iliopsoas muscle attachment two (psoas major)	-5.000	17.000	4.403
	Acetabulum to Gluteus muscle attachment	0.658	13.020	2.719
	Acetabulum to Iscioletfemoral attachment one	0.400	-3.500	0.900
	Acetabulum to Iscioletfemoral attachment two	0.700	-2.700	1.000
	Acetabulum to Iscioletfemoral attachment three	0.000	-4.400	0.950
	Acetabulum to Iscioletfemoral attachment four	4.000	-2.000	1.749
	Acetabulum to Iscioletfemoral attachment five	0.000	-1.300	2.100
	Acetabulum to Iscioletfemoral attachment six	-0.200	0.000	2.426
	Acetabulum to Rectus femorus (Quad) attachment site	-2.900	-0.500	1.700
	Acetabulum to CM	0.10380	4.83817	0.42901
	Acetabulum to Gluteus wrapping point	0.01902	8.49210	3.67586
Acetabulum to hamstring attachment	4.57223	-6.28287	0.00000	

Table 7: Mass moment of inertia

Mass Moment of Inertia	I11	I22	I33
Segment	(kg*m ²)	(kg*m ²)	(kg*m ²)
Pelvis	0.048	0.050	0.041
Thigh	0.227	0.044	0.221
Shank	0.030	0.004	0.029
Foot	2.798E-04	6.046E-05	2.436E-04

Table 8: Segment Masses

Segment Masses(based on 62 kg total body mass, Female)	Mass
Segment	Kg
Pelvis	7.731
Thigh	9.164
Shank	2.982
Foot	0.800

Table 9: Patients included in the kinematic and GRF analysis

Bearing	Kinematic Analysis	GRF Analysis
MOP	4	4
COP	6	6
MOM	Zimmer (large)	3
	Biomet (large)	4
	Biomet (medium)	4
	Overall MOM	11
MOM-PS	5	5
COC	0	5
All Patients	24	31
Hard	14	21
Soft	10	10

Table 10: Significant difference among the different groups

Bearing		Separation
MOP	COP	0.01*
	MOM	>0.05
	MOM-PS	0.01*
	COC	>0.05
COP	MOM	>0.05
	MOM-PS	>0.05
	COC	>0.05
MOM	MOM-PS	>0.05
	COC	>0.05
MOM-PS	COC	>0.05
hard	soft	>0.05

Table 11: Resultant forces for the different bearing groups at the joint interactions, and at the muscles and ligaments

Bearing	F_IA (xBW)	F_IP (xBW)	F_PL (N)	F_QD (N)	F_PT (N)	Ankle (xBW)	Knee (xBW)	Hip (xBW)
MOP	1.08	0.34	338	344	132	1.20	1.67	2.65
COP	2.67	0.14	344	360	138	1.34	1.80	2.8
MOM	1.62	0.68	349	354	122	1.31	1.90	2.9
MOM-PS	1.93	0.33	264	272	105	1.32	1.76	2.5

IA: Iliofemoral ligament; IP: Ischiofemoral ligament, PL: patella ligament; QD: quadriceps; PT: patella

Table 12: Results for the vertical ground reaction force parameters

Bearing		MOP	COP	MOM				MOM-PS	COC	All patients	Hard	Soft
				Zimmer (large)	Biomet (large)	Biomet (medium)	Overall MOM					
Subjects		4	6	3	4	4	11	5	5	31	21	10
Fz1	avg	35%	36%	35%	34%	32%	34%	29%	31%	33%	32%	36%
Time to 1st Peak Force (% stance)	min	29%	33%	34%	28%	26%	26%	19%	25%	19%	19%	29%
	max	40%	39%	38%	41%	41%	41%	34%	34%	41%	41%	40%
	SD	5%	3%	3%	6%	6%	5%	6%	4%	5%	5%	4%
Fz2	avg	0.96	1.00	0.94	0.97	0.96	0.96	0.97	0.97	0.97	0.97	0.98
1st Peak Force (BW)	min	0.92	0.88	0.91	0.96	0.93	0.91	0.93	0.91	0.88	0.91	0.88
	max	0.99	1.25	0.98	0.97	1.00	1.00	1.01	1.03	1.25	1.03	1.25
	SD	0.03	0.13	0.03	0.01	0.03	0.03	0.03	0.05	0.06	0.03	0.10
Fz3	avg	57%	55%	52%	56%	52%	53%	51%	48%	53%	52%	56%
Time to MS Force (% stance)	min	50%	51%	46%	50%	45%	45%	44%	45%	44%	44%	50%
	max	68%	60%	58%	59%	57%	59%	64%	53%	68%	64%	68%
	SD	8%	3%	6%	4%	6%	5%	8%	3%	6%	6%	5%
Fz4	avg	0.91	0.96	0.93	0.93	0.95	0.94	0.95	9.35E-01	0.94	0.94	0.94
MS Force (BW)	min	0.86	0.87	0.90	0.83	0.90	0.83	0.89	0.88	0.83	0.83	0.86
	max	0.94	1.17	0.96	0.99	1.01	1.01	1.03	0.96	1.17	1.03	1.17
	SD	0.03	0.11	0.03	0.08	0.04	0.05	0.06	0.03	0.06	0.05	0.09
Fz5	avg	76%	77%	71%	72%	76%	73%	77%	69%	74%	73%	77%
Time to 2nd Peak Force (% stance)	min	74%	75%	63%	69%	71%	63%	73%	58%	58%	58%	74%
	max	79%	80%	79%	75%	80%	80%	82%	76%	82%	82%	80%
	SD	2%	2%	8%	3%	5%	5%	3%	7%	5%	6%	2%
Fz6	avg	0.97	1.03	0.97	0.91	0.96	0.94	0.96	0.96	0.97	0.95	1.00
2nd Peak Force (BW)	min	0.86	0.93	0.96	0.87	0.94	0.87	0.89	0.91	0.86	0.87	0.86
	max	1.07	1.31	1.00	0.95	0.99	1.00	1.00	1.01	1.31	1.01	1.31
	SD	0.10	0.14	0.03	0.04	0.03	0.04	0.04	0.04	0.08	0.04	0.12
Fz7	z	0.67	0.69	0.69	0.67	0.70	0.68	0.69	0.66	0.68	0.68	0.68
Average Force (BW)												
Loading Rate	avg	2.36	3.61	3.18	2.69	3.55	3.14	4.58	3.17	3.37	3.49	3.11
(BW/s)	min	2.01	2.22	2.46	2.10	1.64	1.64	1.40	1.83	1.40	1.40	2.01
	max	2.57	5.18	3.78	3.17	5.47	5.47	10.12	4.96	10.12	10.12	5.18
	SD	0.26	1.05	0.67	0.52	2.14	1.30	3.39	1.32	1.72	1.97	1.03
Push-off Rate	avg	3.54	5.79	4.07	2.95	4.61	3.86	5.31	3.17	4.32	4.04	4.89
(BW/s)	min	2.96	3.80	3.47	2.67	2.35	2.35	1.98	1.90	1.90	1.90	2.96
	max	4.17	8.24	4.64	3.37	8.31	8.31	9.92	5.65	9.92	9.92	8.24
	SD	0.67	1.80	0.59	0.31	2.82	1.75	3.09	1.53	2.04	2.13	1.82

Table 13: Results for the anterior-posterior (x) ground reaction force parameters

Bearing		MOP	COP		MOM			MOM-PS	COC	All patients	Hard	Soft
			Zimmer (large)	Biomet (large)	Biomet (medium)	Overall MOM						
Subjects		4	6	3	4	4	11	5	5	31	21	10
Fx1	avg	29%	26%	21%	24%	24%	23%	24%	21%	24%	23%	28%
Time to Max Braking Force	min	27%	13%	18%	19%	21%	18%	12%	14%	12%	12%	13%
(% stance)	max	31%	30%	26%	32%	28%	32%	37%	27%	37%	37%	31%
	SD	2%	8%	4%	6%	3%	4%	10%	6%	6%	6%	5%
Fx2	avg	0.57	0.56	0.49	0.59	0.53	0.54	0.56	0.51	0.55	0.54	0.56
Time to Zero Force	min	0.52	0.50	0.44	0.54	0.47	0.44	0.51	0.41	0.41	0.41	0.50
(% stance)	max	0.65	0.62	0.57	0.63	0.59	0.63	0.60	0.58	0.65	0.63	0.65
	SD	0.06	0.04	0.07	0.04	0.05	0.06	0.04	0.06	0.06	0.06	0.05
Fx3	avg	82%	83%	82%	83%	84%	83%	82%	80%	82%	82%	82%
Time to Max Propelling Force	min	78%	78%	78%	79%	82%	78%	78%	77%	77%	77%	78%
(% stance)	max	84%	86%	86%	85%	88%	88%	88%	84%	88%	88%	86%
	SD	3%	3%	4%	3%	3%	3%	4%	4%	3%	3%	3%
Fx4	avg	-0.055	-0.065	-0.084	-0.093	-0.077	-0.079	-0.099	-0.085	-0.079	-0.088	-0.061
Max Braking Force	min	-0.061	-0.111	-0.114	-0.137	-0.087	-0.137	-0.119	-0.114	-0.137	-0.137	-0.111
(BW)	max	-0.037	-0.027	-0.063	-0.066	-0.070	-0.027	-0.068	-0.067	-0.027	-0.063	-0.027
	SD	0.012	0.031	0.026	0.031	0.008	0.025	0.019	0.020	0.025	0.021	0.025
Fx5	avg	0.104	0.137	0.137	0.134	0.119	0.129	0.162	0.101	0.128	0.130	0.124
Max Propelling Force	min	0.048	0.117	0.102	0.102	0.103	0.102	0.091	0.045	0.045	0.045	0.048
(BW)	max	0.144	0.195	0.173	0.162	0.128	0.173	0.272	0.154	0.272	0.272	0.195
	SD	0.041	0.030	0.036	0.027	0.011	0.024	0.074	0.040	0.043	0.047	0.036
Fx6	avg	0.004	0.010	0.009	-0.008	0.002	0.000	0.006	-0.001	0.003	0.001	0.008
Average Force	min	-0.011	-0.004	0.008	-0.026	-0.004	-0.026	-0.007	-0.013	-0.026	-0.026	-0.011
(BW)	max	0.011	0.019	0.011	0.012	0.008	0.012	0.025	0.014	0.025	0.025	0.019
	SD	0.010	0.008	0.001	0.016	0.006	0.012	0.013	0.010	0.011	0.012	0.009

Table 14: Results for the medio-lateral (y) ground reaction force parameters

Bearing		MOP	COP	MOM			MOM-PS	COC	All patients	Hard	Soft	
				Zimmer (large)	Biomet (large)	Biomet (medium)	Overall MOM					
Subjects		4	6	3	4	4	11	5	5	31	21	10
Fy1 (% stance)	avg	8%	7%	8%	6%	6%	7%	7%	5%	7%	7%	7%
	min	6%	4%	7%	4%	3%	3%	2%	4%	2%	2%	4%
	max	8%	9%	10%	8%	10%	11%	11%	8%	11%	11%	9%
	SD	1%	2%	2%	2%	3%	3%	4%	2%	2%	3%	2%
Fy2 (% stance)	avg	42%	39%	29%	36%	31%	32%	30%	30%	34%	31%	41%
	min	31%	35%	14%	29%	27%	14%	17%	25%	14%	14%	31%
	max	53%	46%	38%	43%	38%	43%	42%	33%	53%	43%	53%
	SD	9%	5%	13%	7%	4%	8%	9%	3%	8%	7%	7%
Fy3 Average Force (BW)	avg	-0.021	-0.015	-0.022	-0.040	-0.025	-0.030	-0.020	-0.021	-0.023	-0.025	-0.018
	min	-0.032	-0.026	-0.031	-0.066	-0.038	-0.066	-0.038	-0.031	-0.066	-0.066	-0.032
	max	-0.009	-0.001	-0.010	-0.018	-0.010	-0.010	-0.003	-0.012	-0.001	-0.003	-0.001
	SD	0.010	0.010	0.010	0.024	0.011	0.018	0.013	0.007	0.014	0.015	0.010
Fy4 (BW)	avg	0.011	0.017	0.013	0.007	0.005	0.008	0.026	0.007	0.013	0.012	0.015
	min	-0.003	0.001	0.009	0.001	-0.009	-0.009	0.006	0.003	-0.009	-0.009	-0.003
	max	0.018	0.055	0.015	0.009	0.024	0.024	0.084	0.012	0.084	0.084	0.055
	SD	0.009	0.019	0.003	0.005	0.014	0.009	0.032	0.004	0.017	0.018	0.016
Fy5 (BW)	avg	-0.037	-0.034	-0.035	-0.064	-0.050	-0.051	-0.042	-0.055	-0.045	-0.050	-0.035
	min	-0.051	-0.047	-0.042	-0.099	-0.068	-0.099	-0.078	-0.106	-0.106	-0.106	-0.051
	max	-0.021	-0.016	-0.020	-0.032	-0.026	0.020	-0.028	-0.031	-0.016	-0.020	-0.016
	SD	0.016	0.012	0.013	0.030	0.018	0.024	0.020	0.031	0.022	0.024	0.013

Table 15: Results for the statistical analysis of the ground reaction forces

Bearing		Antero-posterior Parameters					Medio-lateral Parameters					Vertical Parameters									
		Fx1	Fx2	Fx3	Fx4	Fx5	Fx6	Fy1	Fy2	Fy3	Fy4	Fy5	Fz1	Fz2	Fz3	Fz4	Fz5	Fz6	Fz7	LR	PR
MOP	COP				>0.05	>0.05		>0.05	>0.05			>0.05		>0.05		>0.05	>0.05				>0.05
	MOM				0.03	>0.05		0.03	>0.05			>0.05		>0.05		>0.05	>0.05				>0.05
	MOM-PS				0.01	0.04		0.02	>0.05			>0.05		>0.05		>0.05	>0.05				>0.05
	COC				>0.05	>0.05		0.02	>0.05			>0.05		0.03		0.02	>0.05				>0.05
COP	MOM				>0.05	>0.05		>0.05	0.05			>0.05		>0.05		>0.05	0.047				>0.05
	MOM-PS	>0.05	>0.05	>0.05	0.02	>0.05	>0.05	0.04	>0.05	>0.05	>0.05	0.02	>0.05	>0.05	>0.05	>0.05	>0.05	>0.05	>0.05	>0.05	>0.05
	COC	>0.05	>0.05	>0.05	>0.05	>0.05	>0.05	0.04	>0.05	>0.05	>0.05	>0.05	>0.05	0.04	>0.05	0.01	>0.05	>0.05	>0.05	>0.05	0.03
MOM	MOM-PS				>0.05	>0.05		>0.05	>0.05			>0.05		>0.05		>0.05	>0.05	>0.05			>0.05
	COC				>0.05	>0.05		>0.05	>0.05			>0.05		>0.05		>0.05	>0.05	>0.05			>0.05
MOM-PS	COC				>0.05	0.03		>0.15	>0.15			>0.05		>0.05		0.01	>0.15	>0.15			>0.15
hard	soft				0.00	>0.05		0.002	>0.15			0.03		>0.05		>0.05	>0.15	>0.15			>0.15

Table 16: Maximum Vertical Ground Reaction Forces and Location in the Gait Cycle

Bearing	Subjects	Maximum Force (BW)			Time to Maximum Force (% stance)			
		avg	(min-max)	SD	avg	(min-max)	SD	
MOP	4	1.01	(0.98 - 1.07)	0.04	58%	(34% - 79%)	24%	
COP	6	1.04	(0.95 - 1.31)	0.14	62%	(33% - 77%)	21%	
MOM	Zimmer (large)	3	0.97	(0.96 - 1.00)	0.03	71%	(63% - 79%)	8%
	Biomet (large)	4	0.98	(0.96 - 0.99)	0.01	46%	(36% - 57%)	10%
	Biomet (medium)	4	0.98	(0.96 - 1.01)	0.02	48%	(32% - 72%)	17%
	Overall MOM	11	0.98	(0.96 - 1.01)	0.02	53%	(32% - 79%)	16%
MOM-PS	5	1.00	(0.97 - 1.03)	0.02	41%	(19% - 77%)	22%	
COC	5	0.99	(0.95 - 1.03)	0.03	47%	(31% - 74%)	17%	
All patients	31	1.00	(0.95 - 1.31)	0.06	53%	(19% - 79%)	19%	
Hard	21	0.98	(0.95 - 1.03)	0.02	49%	(19% - 79%)	18%	
Soft	10	1.03	(0.95 - 1.31)	0.11	61%	(33% - 79%)	21%	

Table 17: Swing, stance and total gait cycle times.

Bearing	# patients	Swing (sec)			Swing (%)			Stance (sec)			Stance (%)			Total Gait			
		avg	(min-max)	SD	avg	(min-max)	SD	avg	(min-max)	SD	avg	(min-max)	SD	avg	(min-max)	SD	
MOP	4	0.5	(0.3 - 0.6)	0.1	28%	(22% - 30%)	4%	1.2	(1.1 - 1.3)	0.1	72%	(70% - 78%)	4%	1.6	(1.5 - 1.9)	0.2	
COP	6	0.7	(0.5 - 1.4)	0.4	29%	(22% - 50%)	11%	1.6	(1.4 - 1.8)	0.2	71%	(50% - 78%)	11%	2.2	(2.0 - 2.8)	0.3	
MOM	Zimmer (large)	3	0.5	(0.4 - 0.6)	0.1	21%	(20% - 23%)	2%	2.0	(1.7 - 2.1)	0.2	79%	(77% - 80%)	2%	2.5	(2.2 - 2.7)	0.3
	Biomet (large)	4	0.4	(0.3 - 0.7)	0.2	25%	(20% - 29%)	4%	1.3	(1.1 - 1.6)	0.3	75%	(71% - 80%)	4%	1.7	(1.4 - 2.3)	0.4
	Biomet (medium)	4	0.6	(0.4 - 0.6)	0.1	29%	(25% - 35%)	4%	1.4	(1.2 - 1.5)	0.2	71%	(65% - 75%)	4%	1.9	(1.8 - 2.1)	0.2
	Overall MOM	11	0.5	(0.3 - 0.7)	0.1	26%	(20% - 35%)	5%	1.5	(1.1 - 2.1)	0.4	74%	(65% - 80%)	5%	2.0	(1.4 - 2.7)	0.5
MOM-PS	5	0.5	(0.3 - 0.7)	0.2	28%	(20% - 35%)	6%	1.4	(1.1 - 1.6)	0.2	72%	(65% - 80%)	6%	1.9	(1.3 - 2.3)	0.4	
COC	5	0.5	(0.3 - 0.7)	0.2	24%	(21% - 26%)	2%	1.6	(0.9 - 2.1)	0.5	76%	(74% - 79%)	2%	2.1	(1.2 - 2.8)	0.6	
All Patients	31	0.5	(0.3 - 1.4)	0.2	27%	(20% - 50%)	6%	1.5	(0.9 - 2.1)	0.3	73%	(50% - 80%)	6%	2.0	(1.2 - 2.8)	0.4	
Hard	21	0.5	(0.3 - 0.7)	0.1	26%	(20% - 35%)	5%	1.5	(0.9 - 2.1)	0.4	74%	(65% - 80%)	5%	2.0	(1.2 - 2.8)	0.5	
Soft	10	0.6	(0.3 - 1.4)	0.3	28%	(22% - 50%)	8%	1.4	(1.1 - 1.8)	0.2	72%	(50% - 78%)	8%	2.0	(1.5 - 2.8)	0.4	

Table 18: Bearing and sound correlation

Sound	Pops / Knocking	Snaps / Thuds	Knocking	Crunching	Grating	Cracking	Squeacking	Duraion of sound
Bearing								
MOP	x	x						isolated
COP	x	x	x	x	x			isolated
MOM-PS	x	x	x	x	x	x		isolated
MOM	x		x	x	x	x	x	sustained
COC	x				x	x	x	sustained

Table 19: Comparison of our femoral frequency results to previous research

	Campbell et al., 1981	Thomas et al., 1990		Khalil et al., 1981	Couteau et al., 1998			
		Normal Experimental	THA		Normal		THA	
					Exp.	FEM	Exp.	FEM
Mode 1	750-800	138-177	None found	250	302	288	278	264
Mode 2	-	-	-	315	353	364	330	324
Mode 3	-	-	-	825	887	819	758	693
Mode 4	-	-	-	879	931	932	832	780
	Rosenstein et al., 1989		Taylor et al., 2002		Jaecques et al., 2004		Present study	
	Normal	THA	Exp.	FEM	Normal FEM	THA	THA Experimental	
Mode 1	220-375	230-325	285	285	300	300	268-495	
Mode 2	-	-	317	324	336	328	368-456	
Mode 3	-	-	521	489	599	730	767-975	
Mode 4	-	-	777	710	844	893		

Figures

Appendix C: Figures

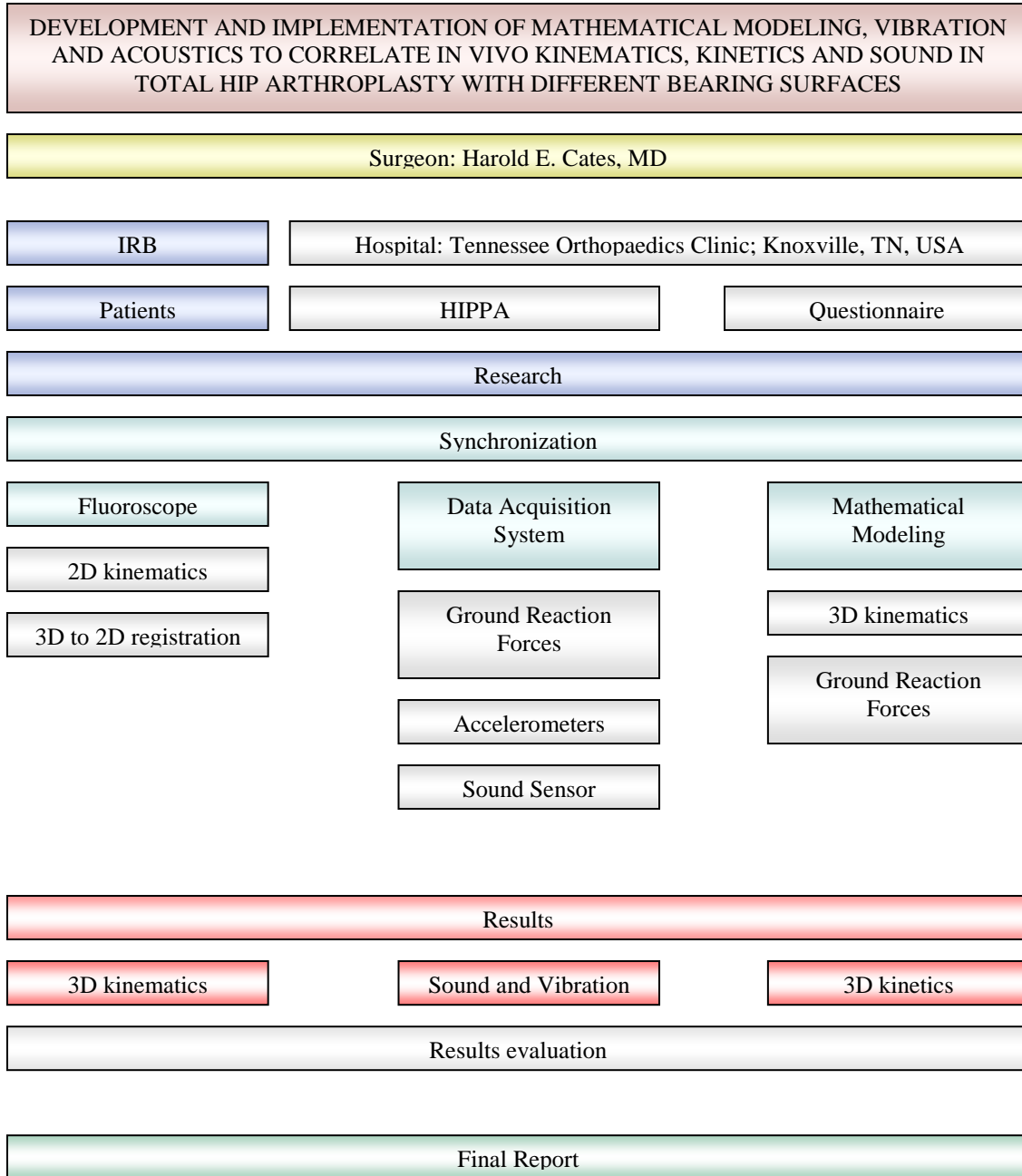


Figure 1: Flow chart of the research plan

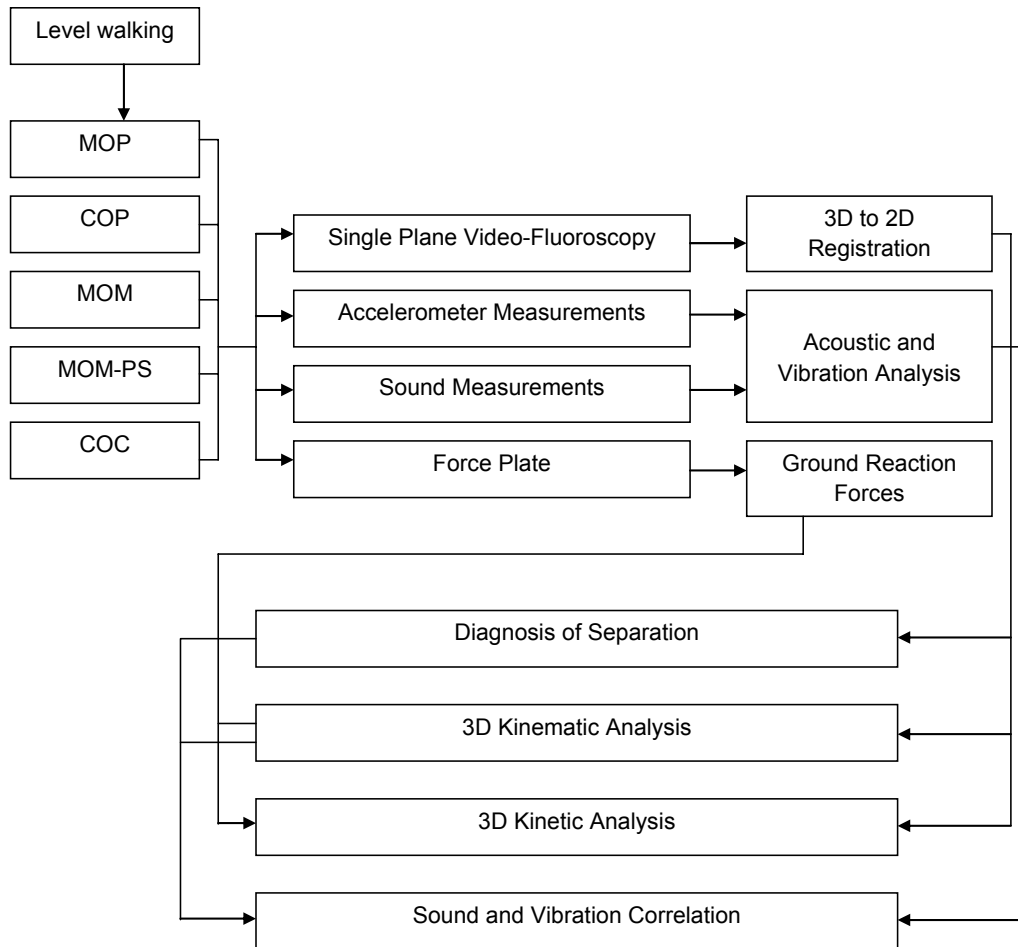


Figure 2: Research overview

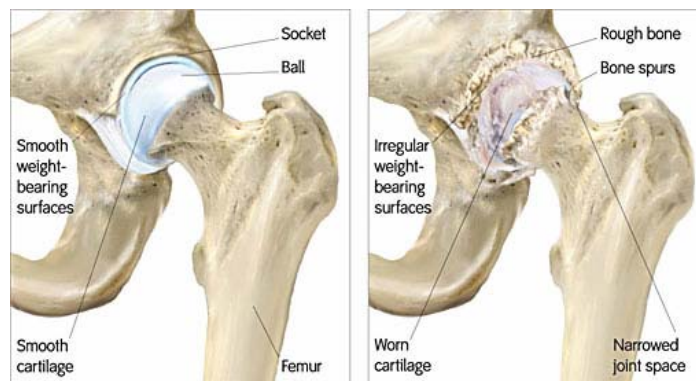


Figure 3: Osteoarthritis in the Hip (Orthopaedic Associates, 2008)

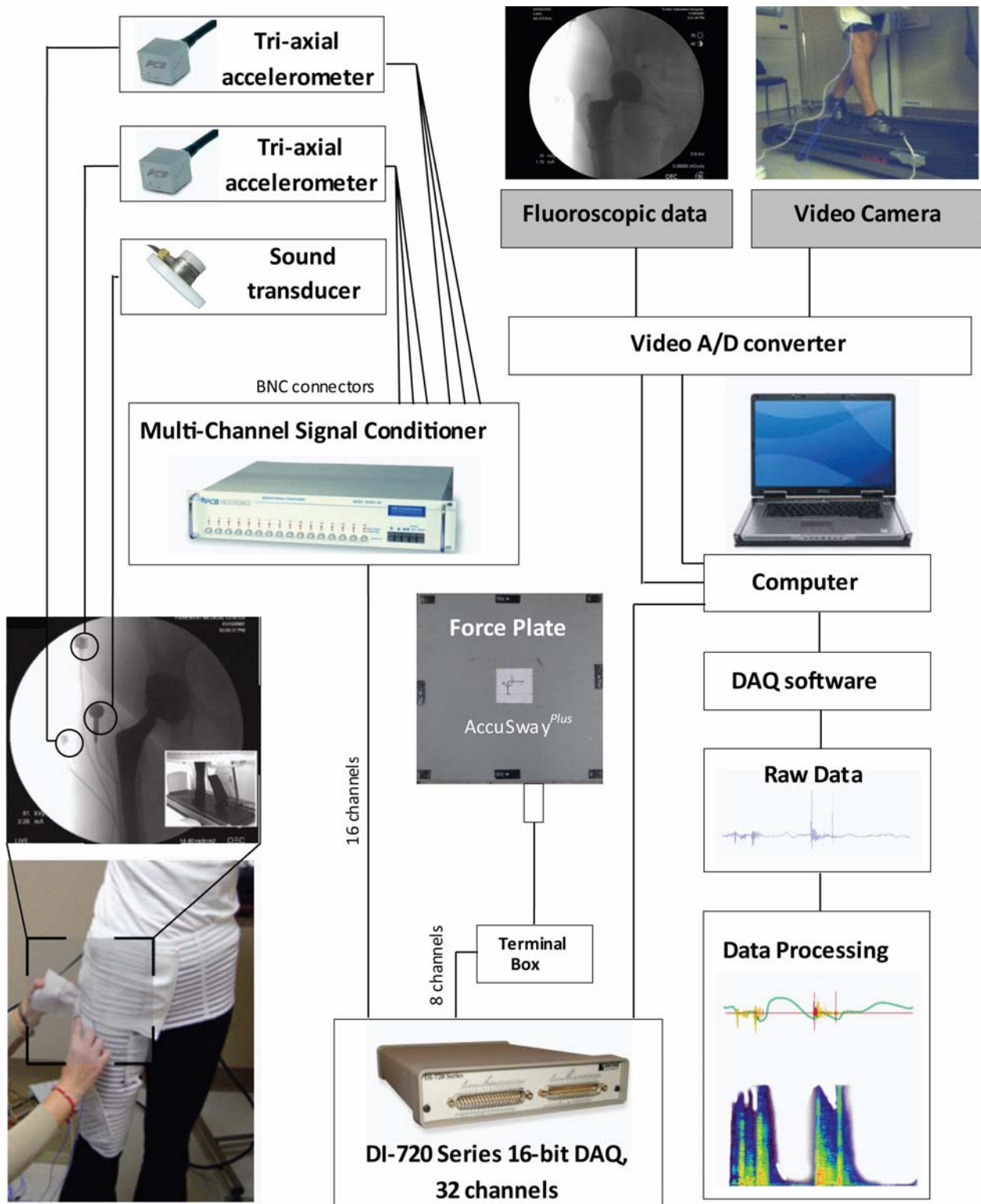


Figure 4: Schematic diagram of instrumentation for acoustic and vibration analysis combined with fluoroscopic-video-capturing system and ground reaction force measurement



Figure 5: Fluoroscopy Machine with Treadmill and Subject [left]; Top View of Fluoroscopy Machine, Image of Radiation Source to Image Intensifier [right]



Figure 6: Example fluoroscopic image of a hip joint in a view from AP direction

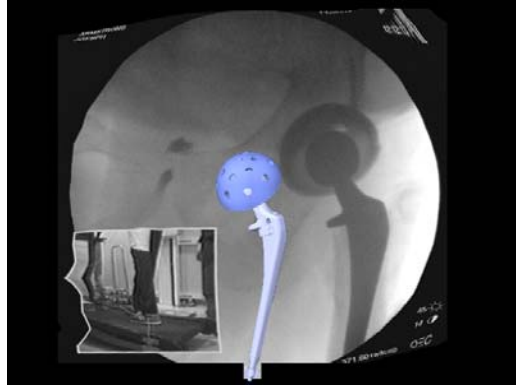


Figure 7: Example fluoroscopic image of a hip joint with the implant components in pose

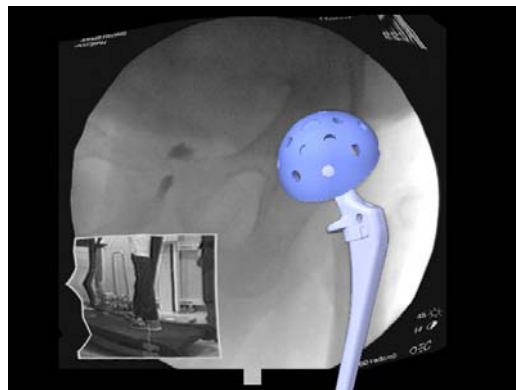


Figure 8: Example fluoroscopic image with overlaid implant components

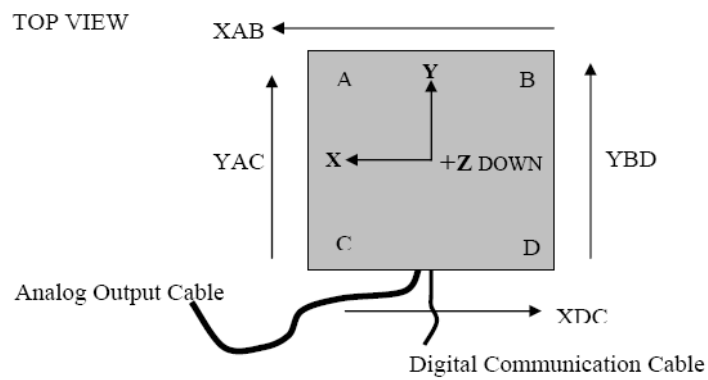


Figure 9: Force plate with sensor description (AccuGait, 2005)

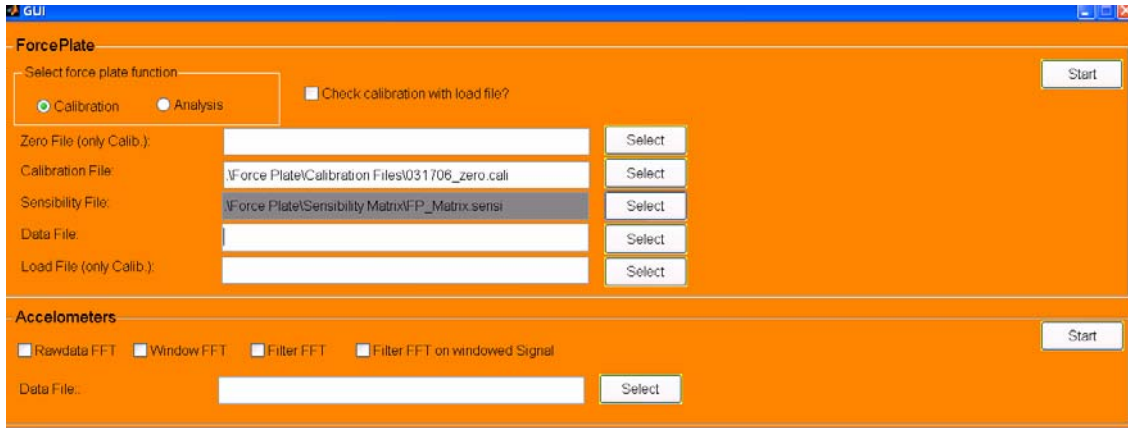


Figure 10: Application created to read, calibrate, calculate and analyze the signals



Figure 11: Walking direction on top of the force plate



Figure 12: PCB Tri-axial accelerometer compared with penny



Figure 13: Sound sensor compared with a Quarter

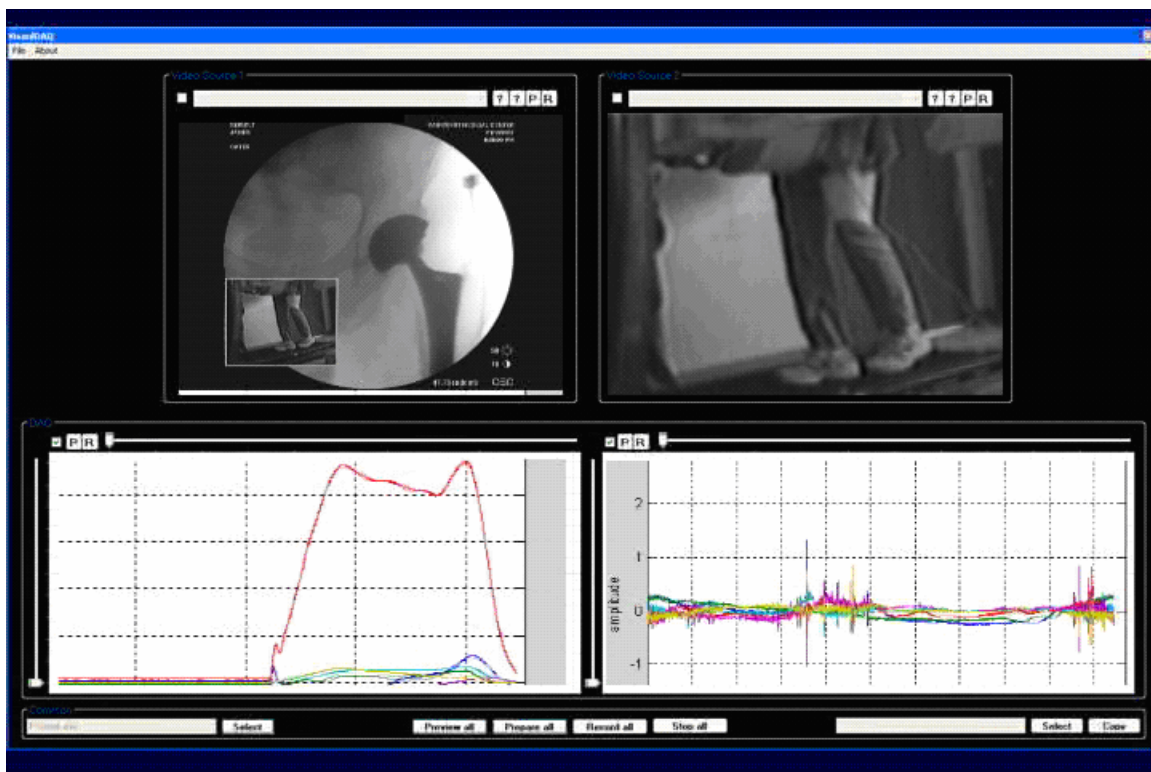


Figure 14: Interface of the new software for synchronization of video and data acquisition signals

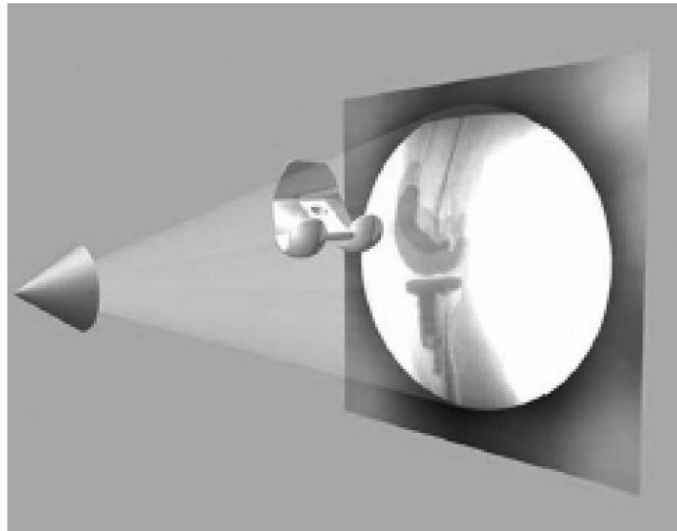


Figure 15: An Example for 3-D CAD Model Matching Projected Fluoroscopy Image Silhouette for a knee joint implant

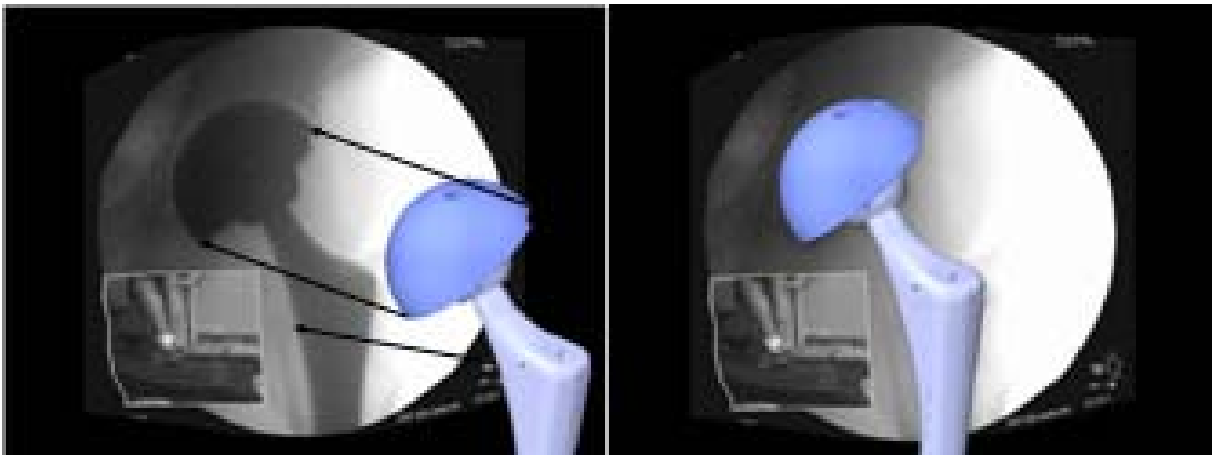


Figure 16: An Example for 3-D CAD model matching projected fluoroscopy image silhouette for a hip joint implant

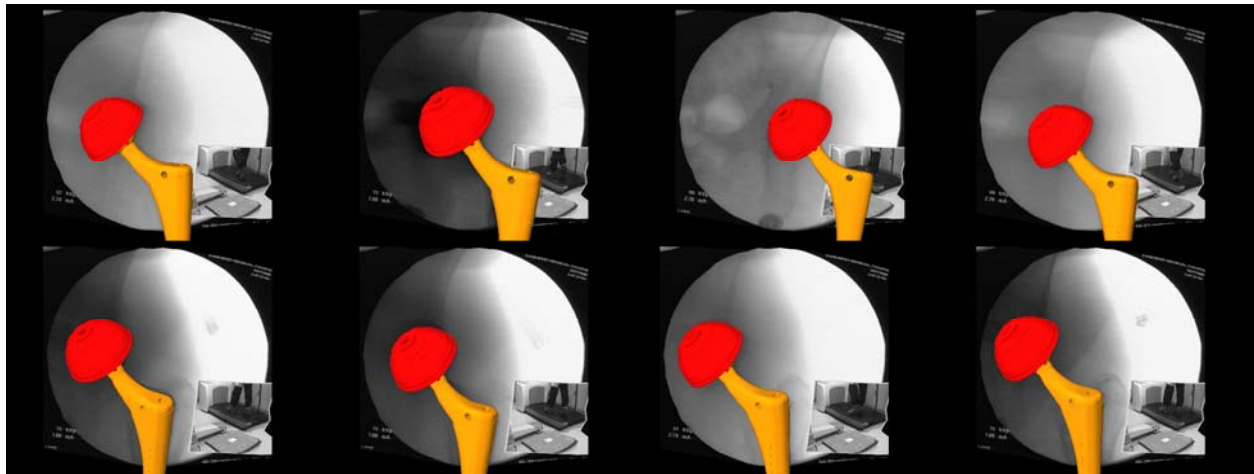


Figure 17: Full Sequence of Analyzed Images with 3-D Models Overlaid

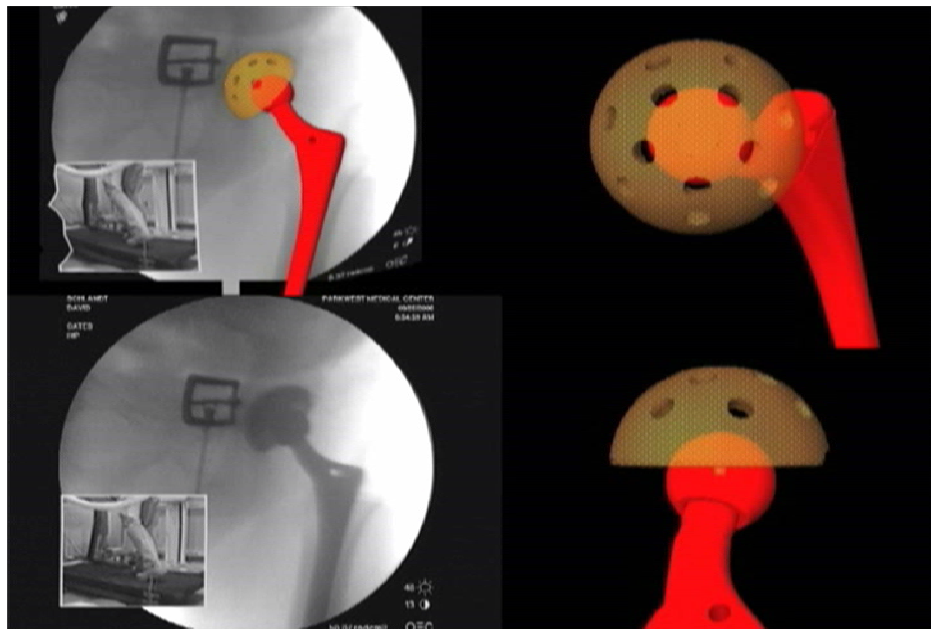


Figure 18: Fluoroscopic image, 3D registered implant components and a 3D view of the hip joint implant pose

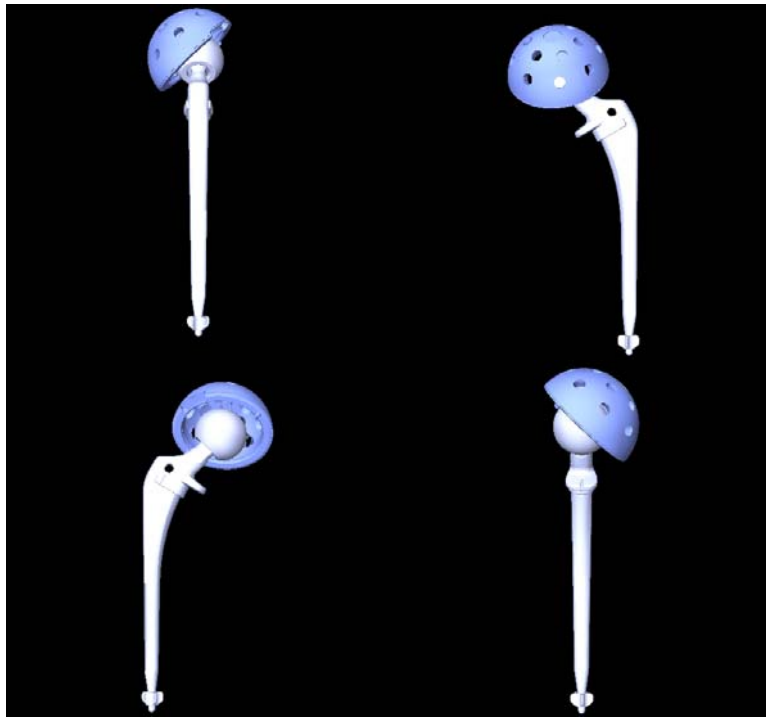


Figure 19: 3D view of the hip joint implant positions after successful 3D kinematics reconstruction

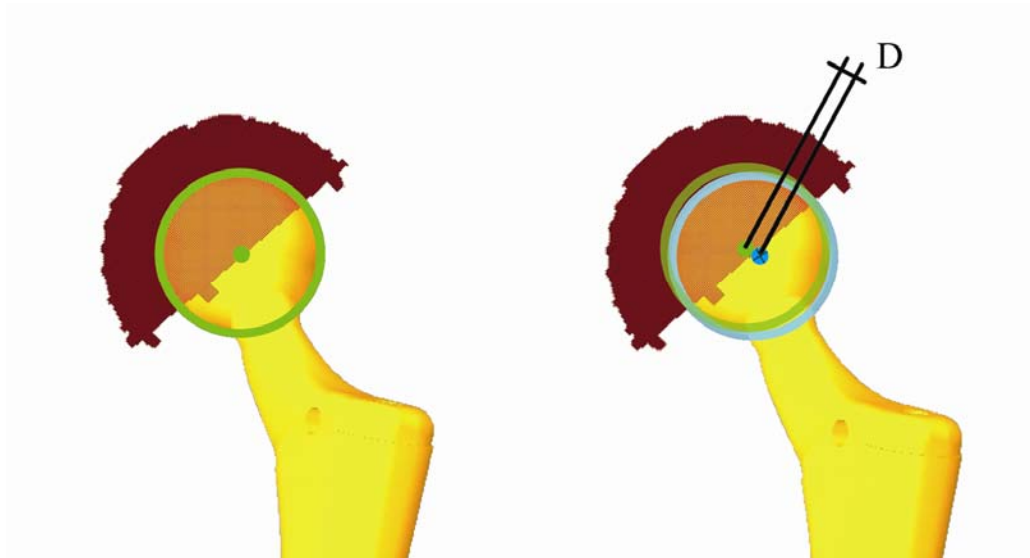


Figure 20: The distance D between the center of the femoral head and the acetabular component is denoted as hip joint separation when it exceeds 0.5mm

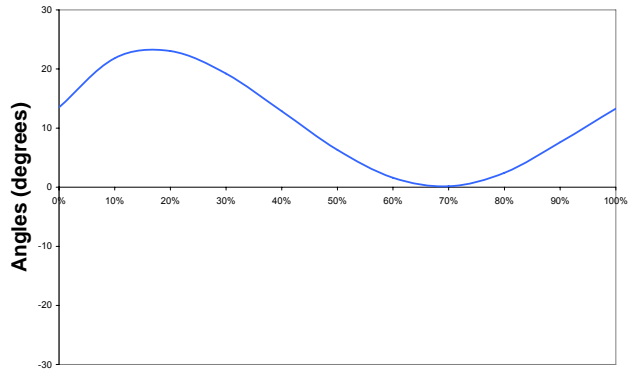


Figure 21: Example flexion/extension of the hip during the entire gait cycle

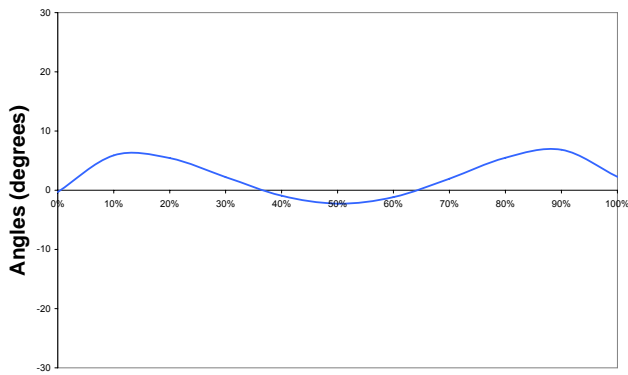


Figure 22: Example internal/external rotation of the hip during the entire gait cycle

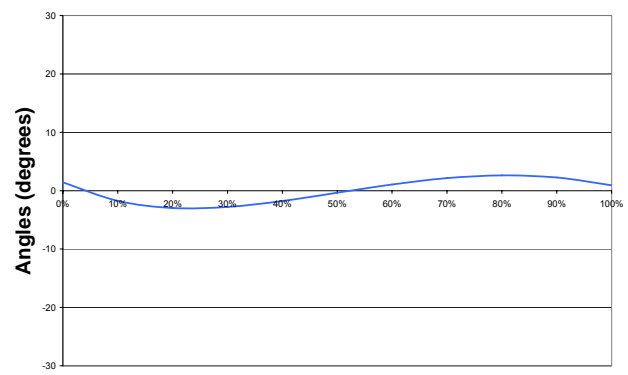


Figure 23: Example abduction/adduction rotation of the hip during the entire gait

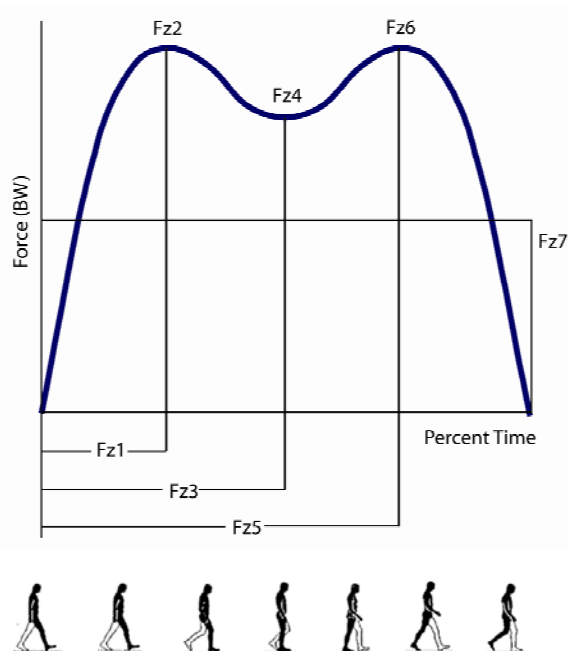


Figure 24: Graphical representation of the GRF parameters in z-direction

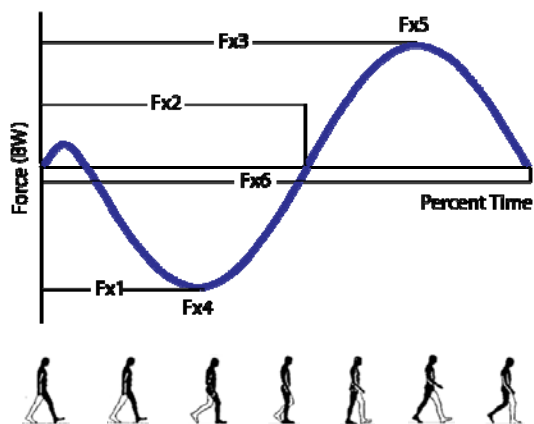


Figure 25: Graphical representation of the GRF parameters in x-direction

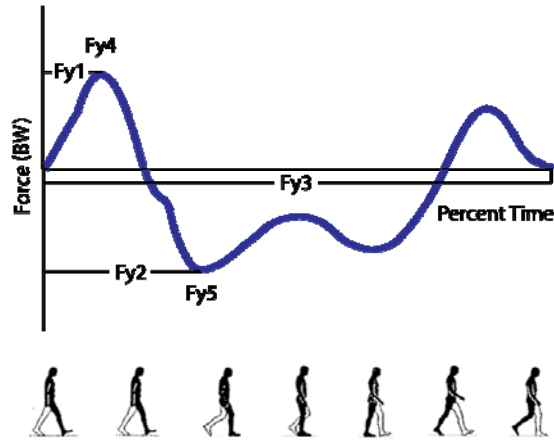


Figure 26: Graphical representation of the GRF parameters in y-direction

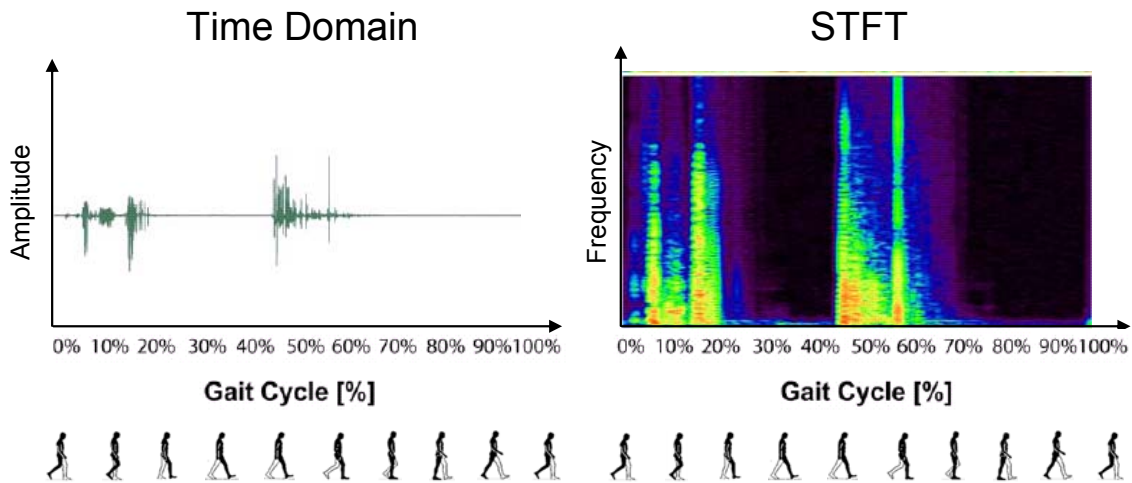


Figure 27: Example of STFT signal analysis. Left: Signal in time domain (x-Axis: Time in % of gait cycle starting with toe off, y-Axis: Signal Amplitude); Right: Time-frequency spectrogram (x-Axis: Time in % of gait cycle starting with toe off, y-Axis: Frequency in Hz)

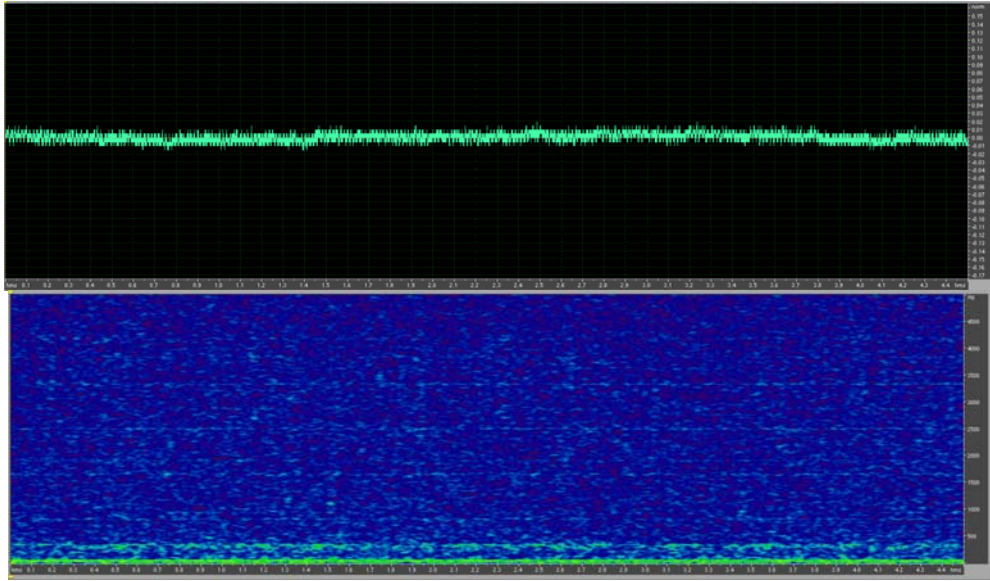


Figure 28: Noise profile (top: noise in the time domain, bottom: spectrogram of the noise)

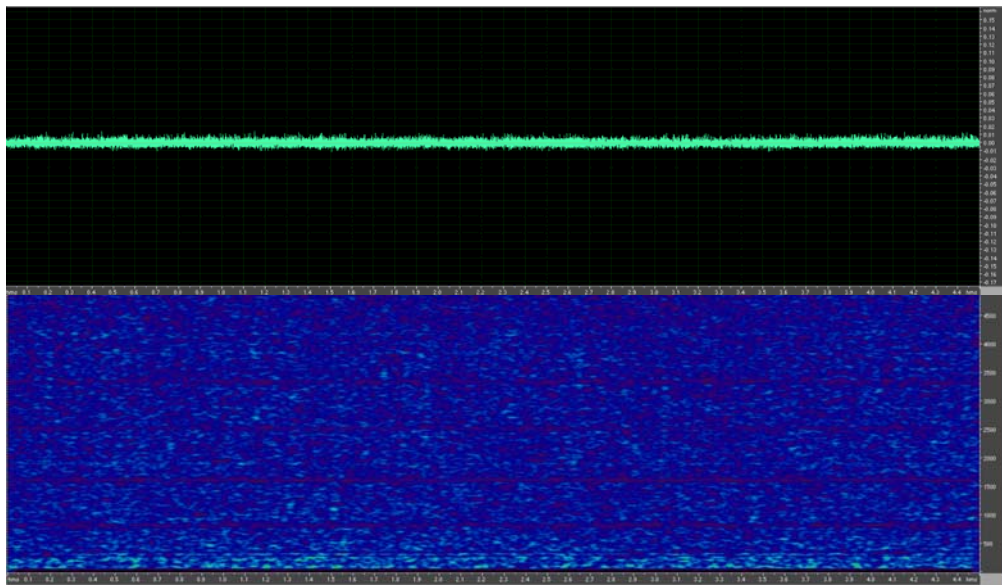


Figure 29: Filtered noise profile (top: noise in the time domain, bottom: spectrogram of the noise)

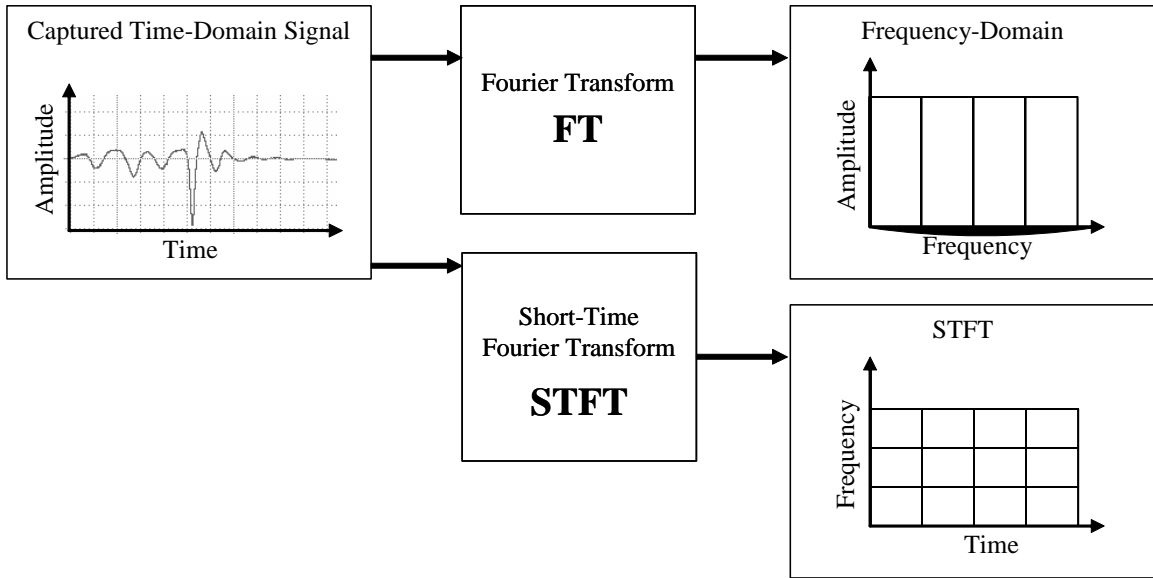


Figure 30: Diagram of the Fourier Transform and the Short-Time Fourier Transform

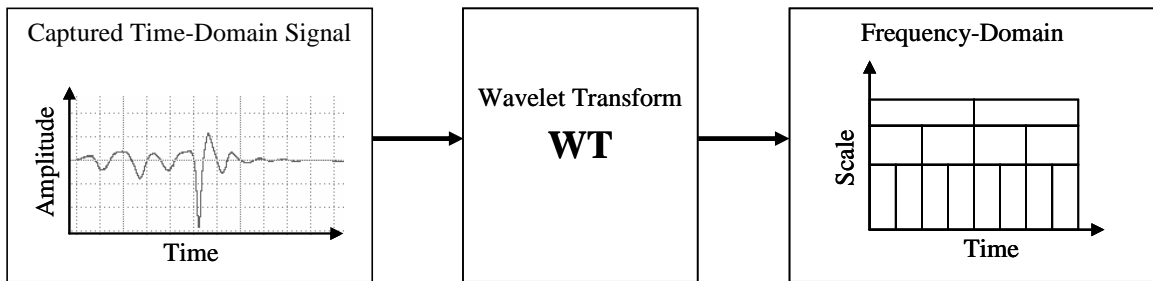


Figure 31: Diagram of the Wavelet analysis

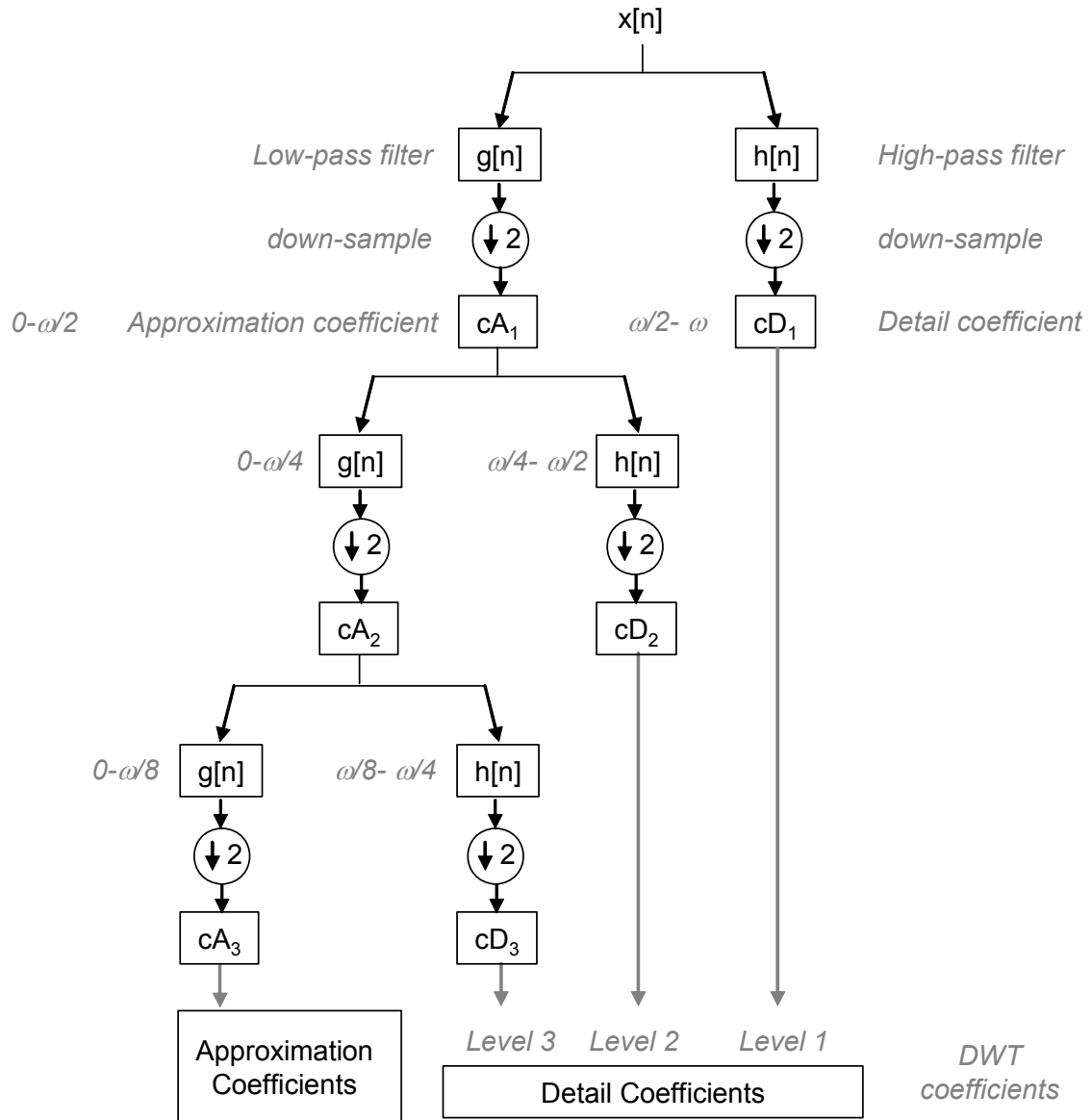


Figure 32: Diagram of the one dimensional DWT analysis for 3 level analysis

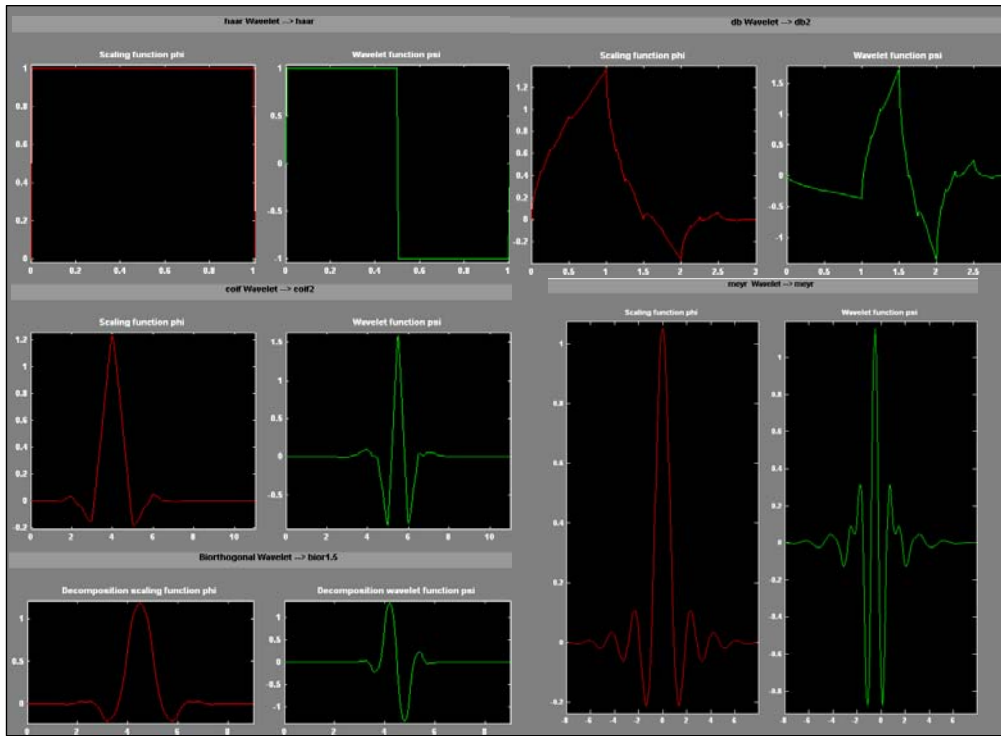


Figure 33: Different mother wavelets and scaling functions

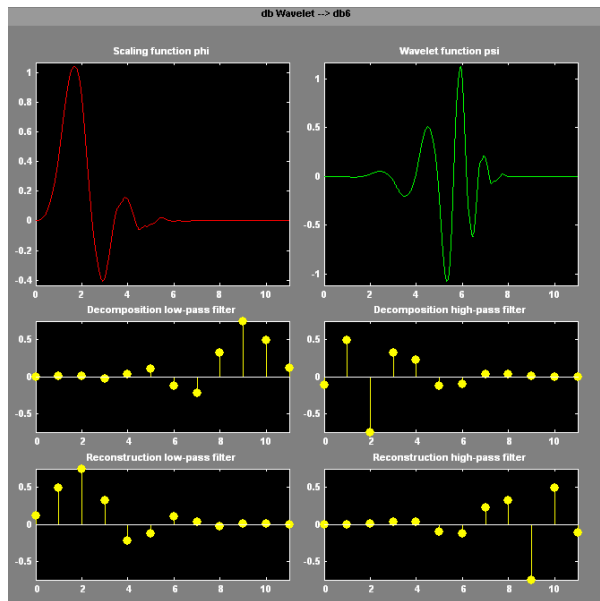
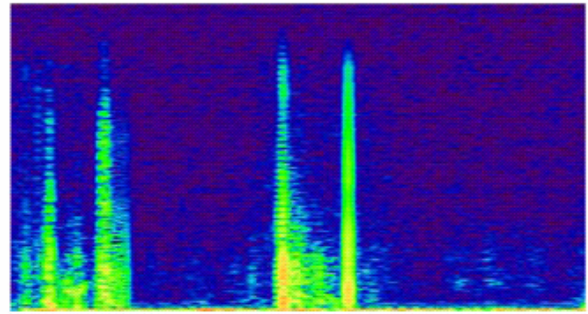
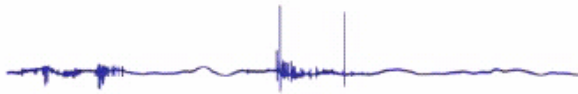
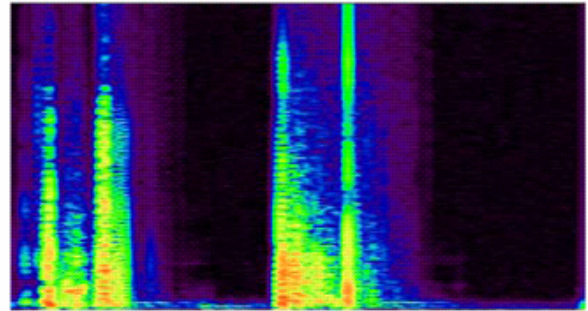
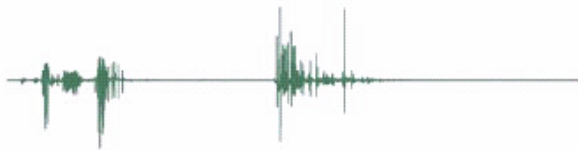


Figure 34: DB6 wavelet applied in the analysis

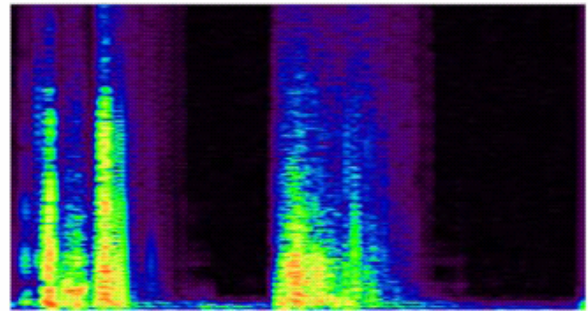
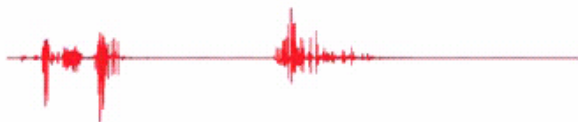
a) Original, noisy signal



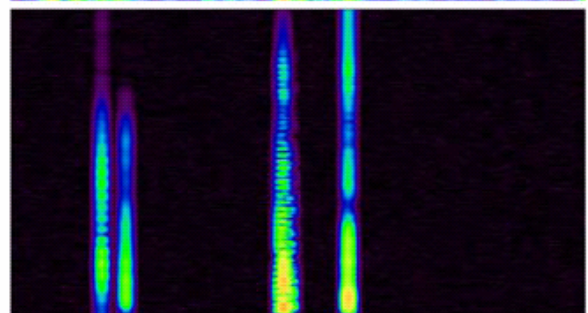
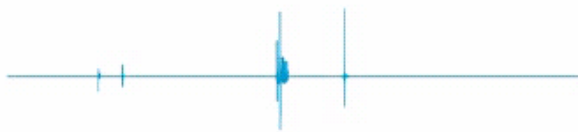
b) Final, amplified signal



c) Final signal, squeaking component



d) Final signal, knocking component



0% 10% 20% 30% 40% 50% 60% 70% 80% 90%100%

Gait Cycle [%]

0% 10% 20% 30% 40% 50% 60% 70% 80% 90%100%

Gait Cycle [%]

Figure 35: Example of signal analysis and decomposition in squeaking and knocking components. Left: Signal in time domain (x-Axis: Time in % of gait cycle starting with toe off, y-Axis: Signal Amplitude); Right: Time-frequency spectrogram (x-Axis: Time in % of gait cycle starting with toe off, y-Axis: Frequency in Hz)

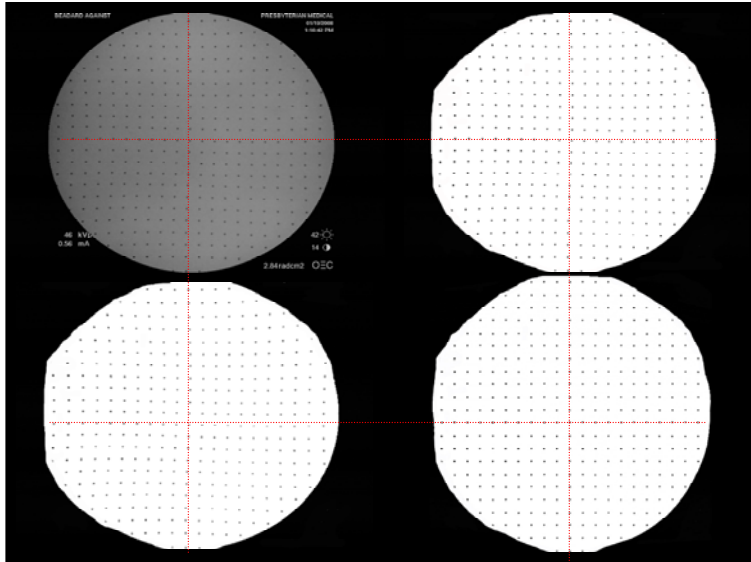


Figure 36: Original image of bead-board used for distortion correction (top left), cleaned up bead-board (top right), beads identified from Matlab application (bottom left) and unwarped/corrected bead-board image

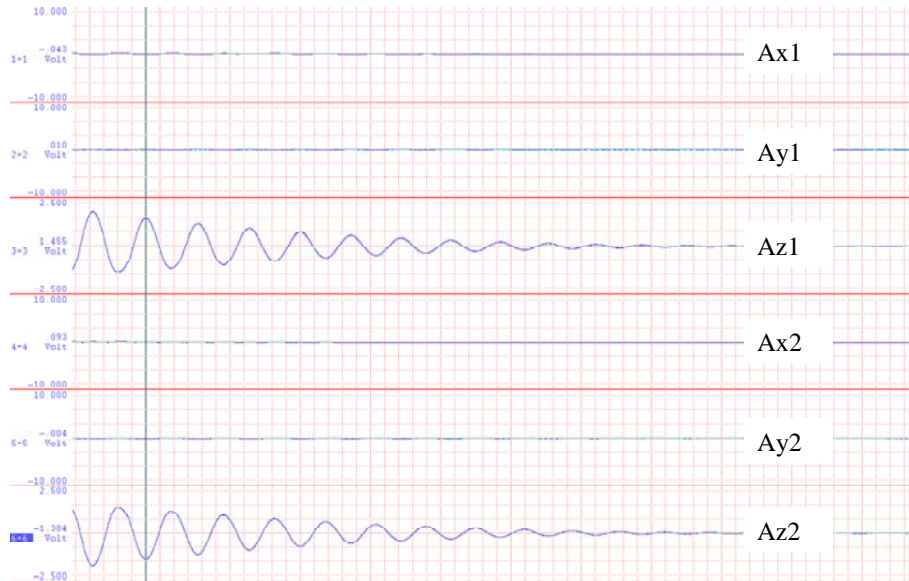


Figure 37: Beam vibration measurement with both accelerometer to test synchronization, cross talk and proper orientation of the axis



Figure 38: Signal generated from the calibrator and recorded by the accelerometer

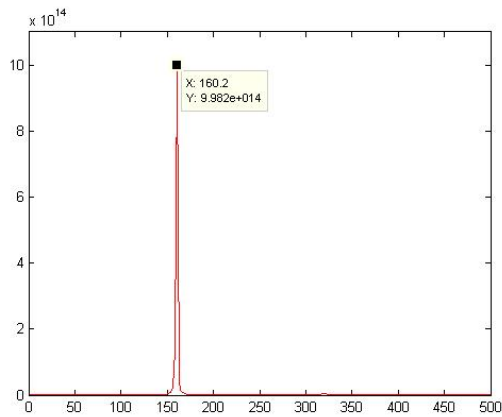


Figure 39: Measured frequency produced by the calibrator

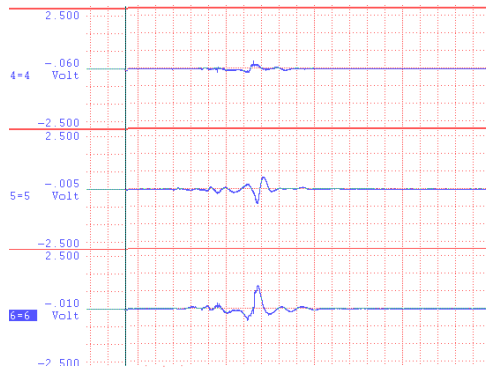


Figure 40: Soft tissue movement

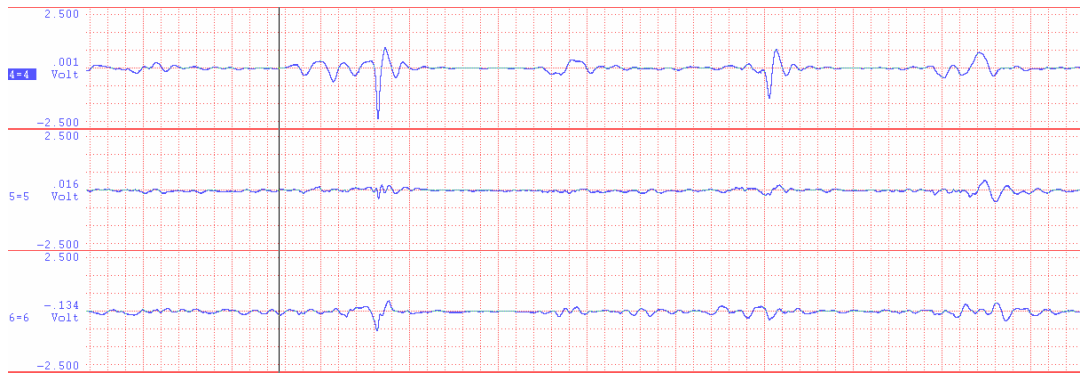


Figure 41: Muscle contractions

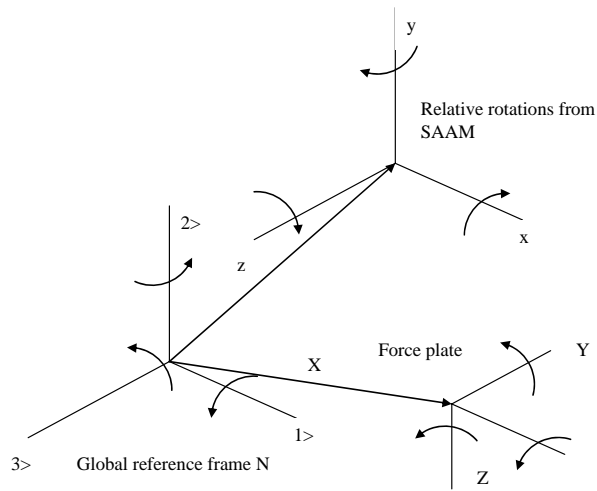


Figure 42: Coupling of the different measurement reference frames

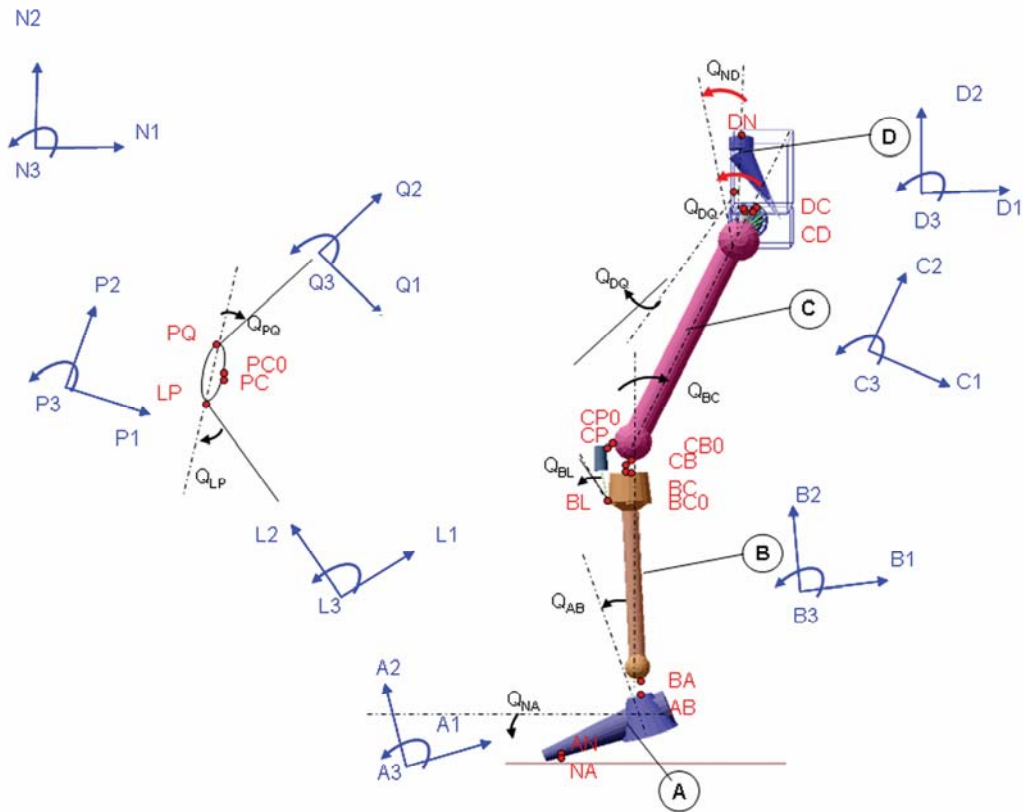


Figure 43: 3D Schematic of the Leg

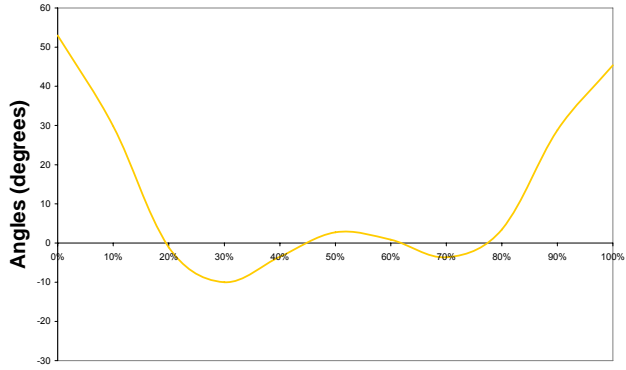


Figure 44: Rotation of the foot with respect to the ground during the entire gait cycle

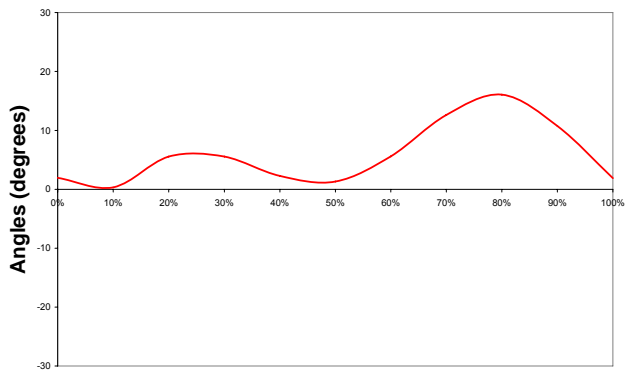


Figure 45: Rotation of the ankle with respect to the foot during the entire gait cycle

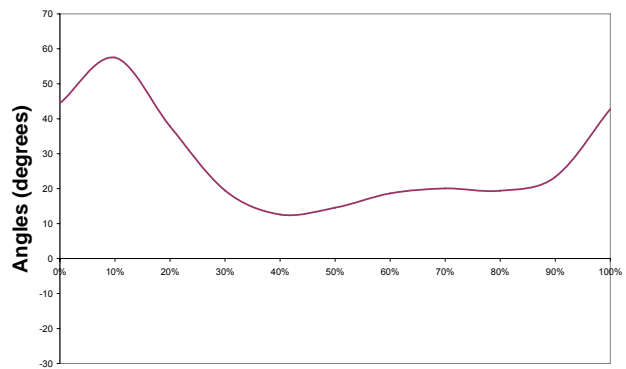


Figure 46: Rotation of the knee during the entire gait cycle

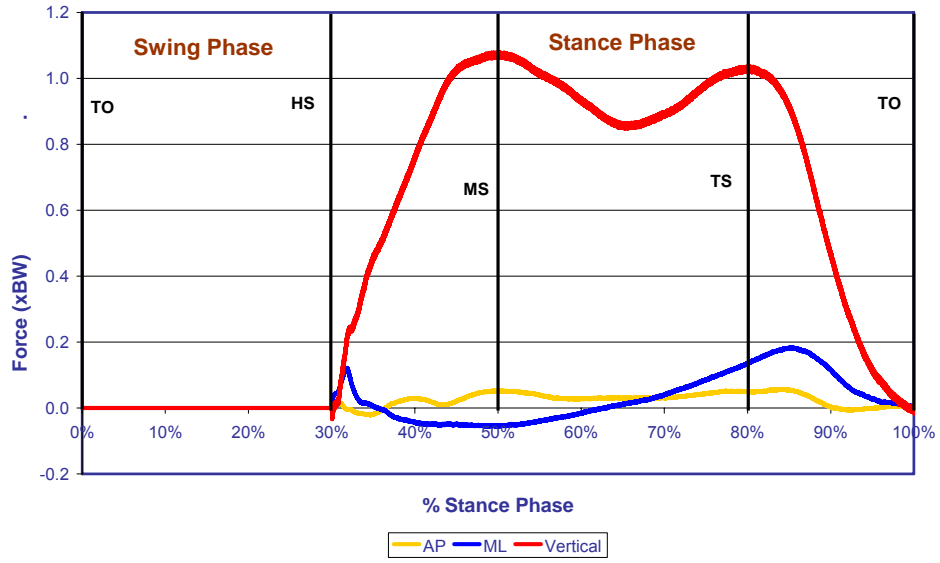


Figure 47: Example ground reaction forces

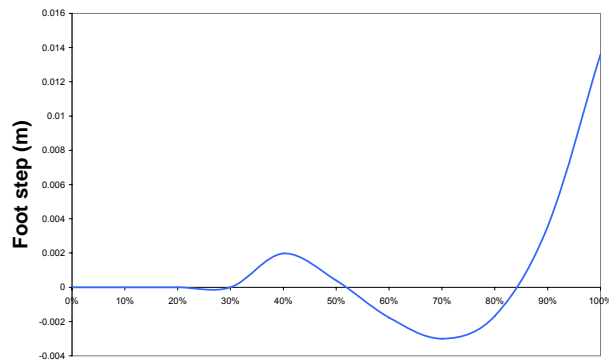


Figure 48: Contact point of foot with ground

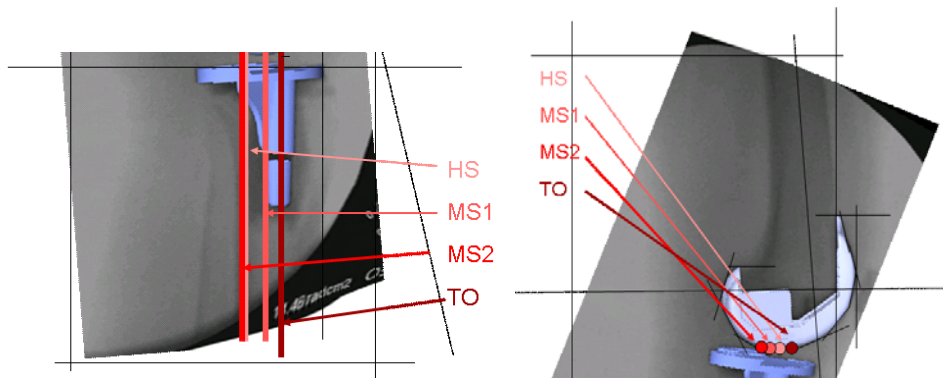


Figure 49: Tibio-Femoral Contact During the Stand Phase: contact point on the tibia [left], contact point on the femur [right]

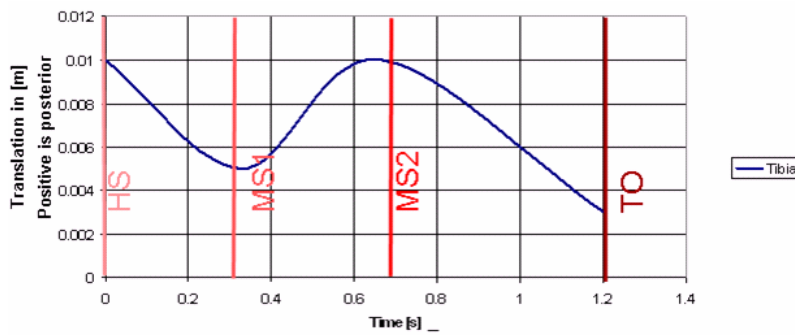


Figure 50: AP Position of the knee contact point on the tibia during the stance phase of gait with respect to the central axis of the tibia

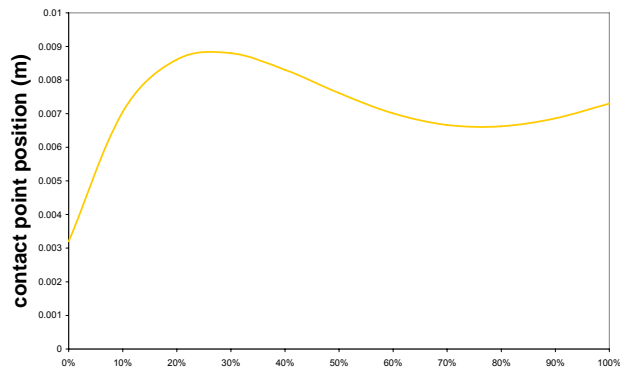


Figure 51: AP Position of the knee contact point on the tibia during the entire gait cycle with respect to the central axis of the tibia

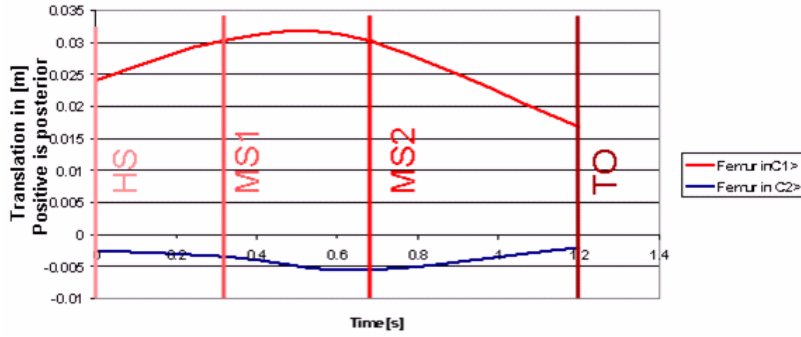


Figure 52: AP and SI position of the knee contact point on the femur during the stance phase of gait with respect to the central axis of the femur

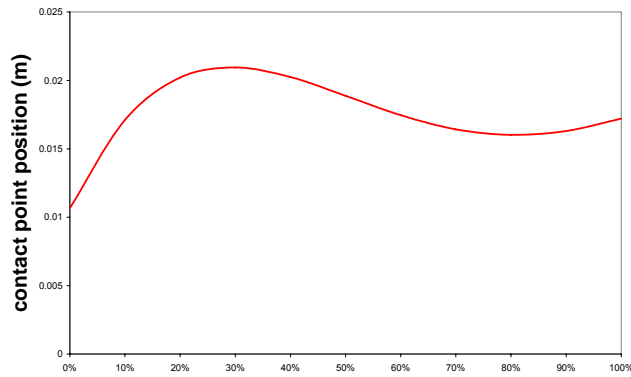


Figure 53: AP position of the knee contact point on the femur during the entire gait cycle with respect to the central axis of the femur

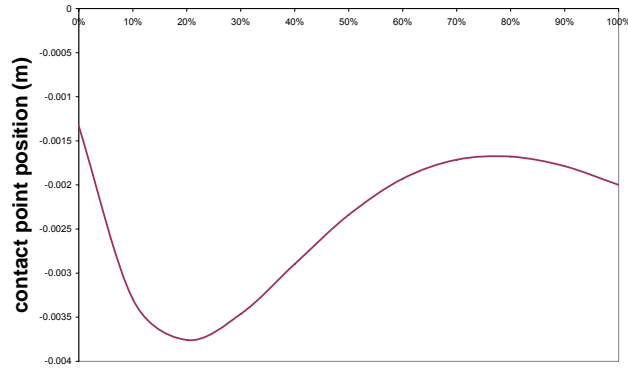


Figure 54: SI position of the knee contact point on the femur during the entire gait cycle with respect to the central axis of the femur

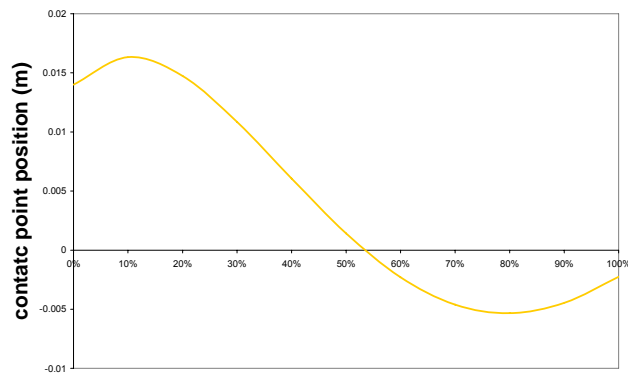


Figure 55: AP position of the hip contact point on the femur during the entire gait cycle from the center of the femoral head

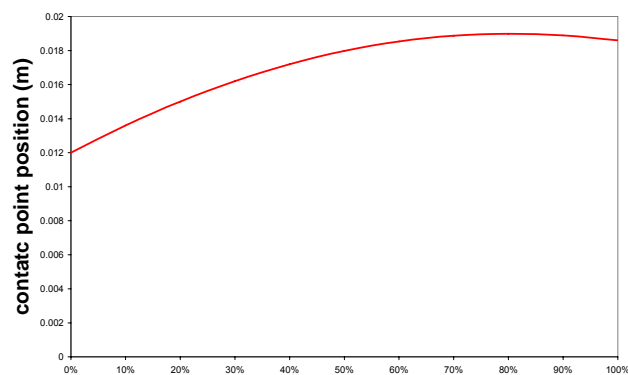


Figure 56: SI position of the hip contact point on the femur during the entire gait cycle from the center of the femoral head

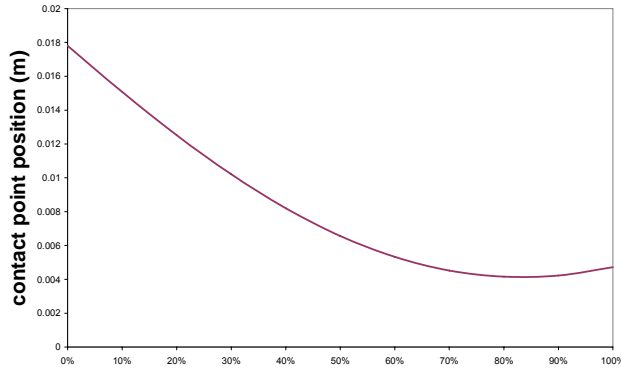


Figure 57: AP position of the hip contact point on the pelvis during the entire gait cycle from the center of the femoral head

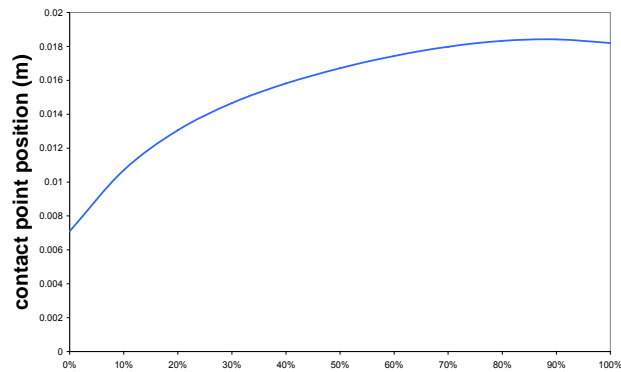


Figure 58: SI position of the hip contact point on the pelvis during the entire gait cycle from the center of the femoral head

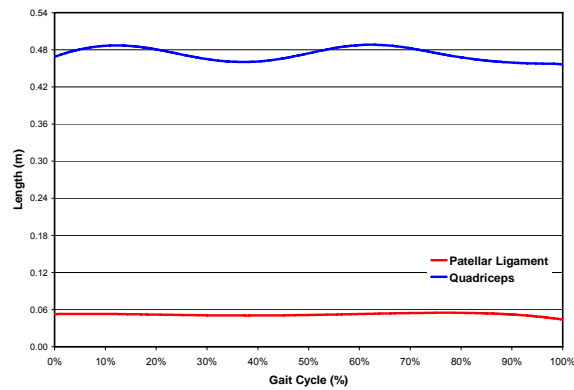


Figure 59: Change of the length in patellar ligament and quadriceps.

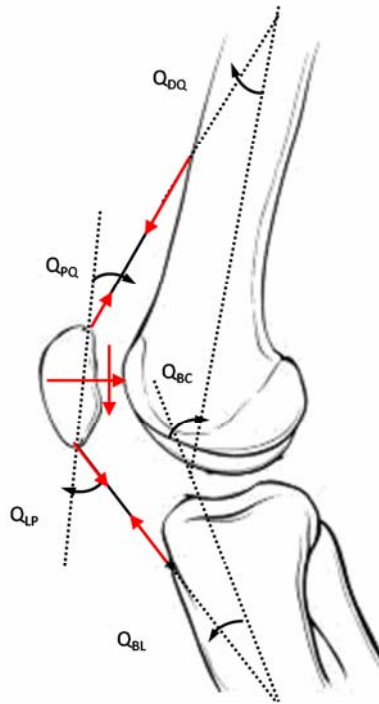


Figure 60: Closed loop patellar ligament – patella – quadriceps chain and free body diagram

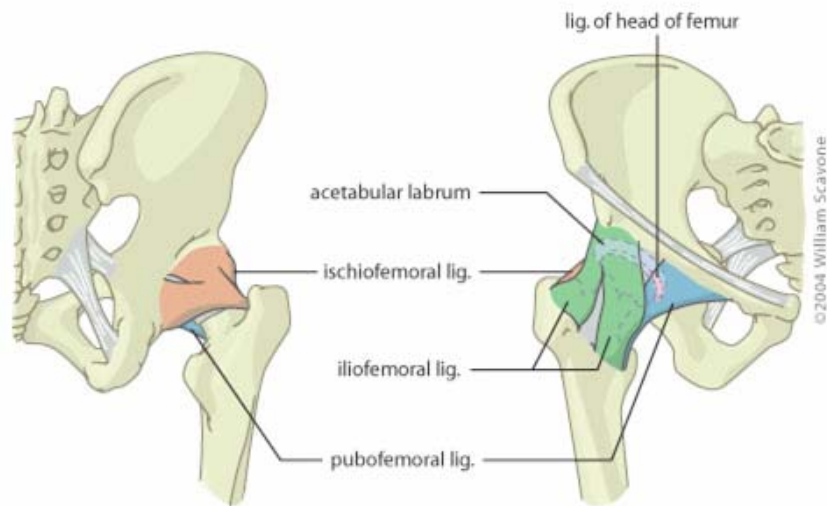


Figure 61: Hip joint capsule

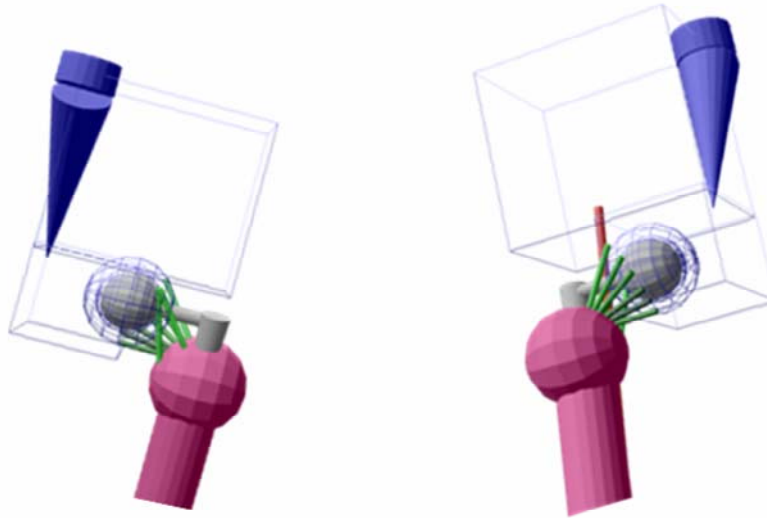


Figure 62: Schematic representation of the hip joint ligaments as defined in the model

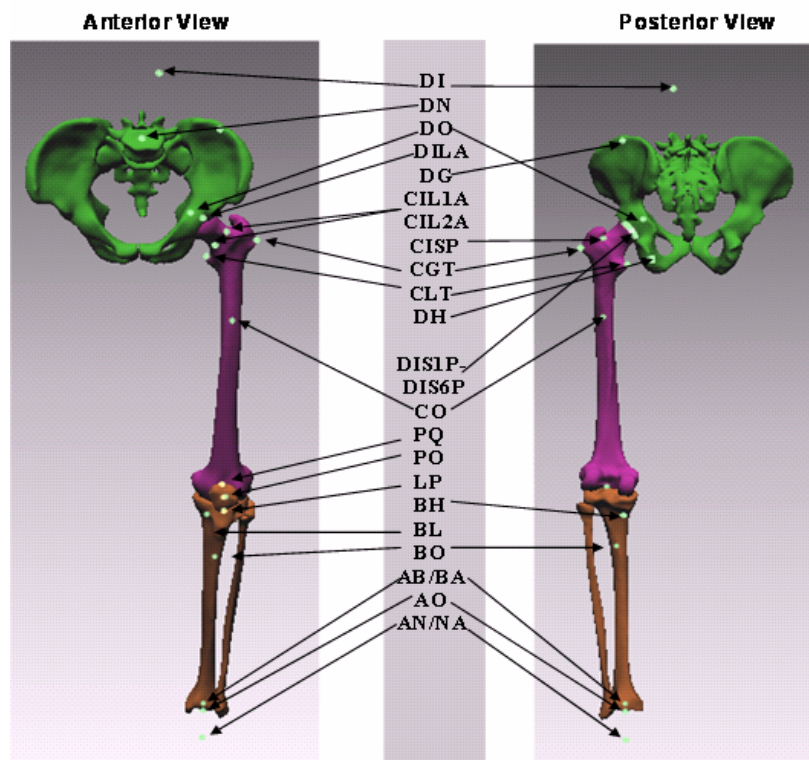


Figure 63: Dimension Measurement of CT scanned Cadaver using Rapidform

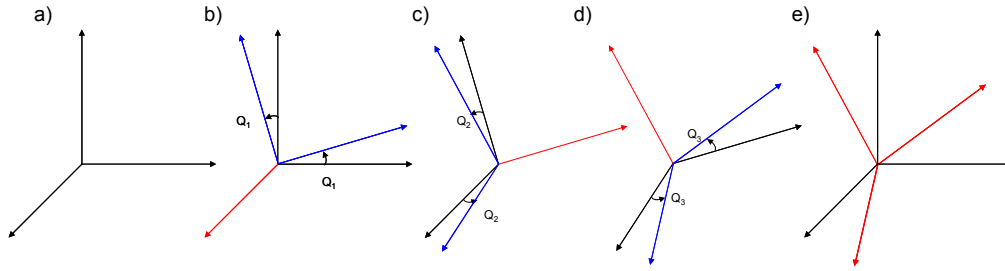


Figure 64: Sequential rotations: a) original reference frame, b)-d) sequential rotations in 3-1-2 order, e) original and final orientation of the reference frame

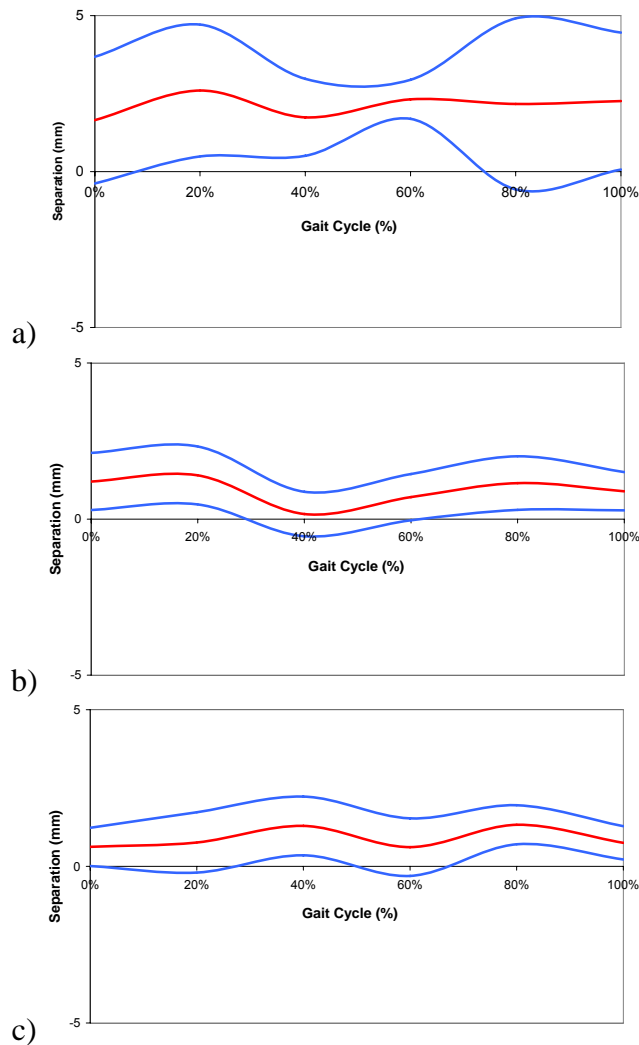


Figure 65: Average separation (red) and ± 1 SD (standard variation, blue) for a) MOP, b) COP and c) MOM-PS groups

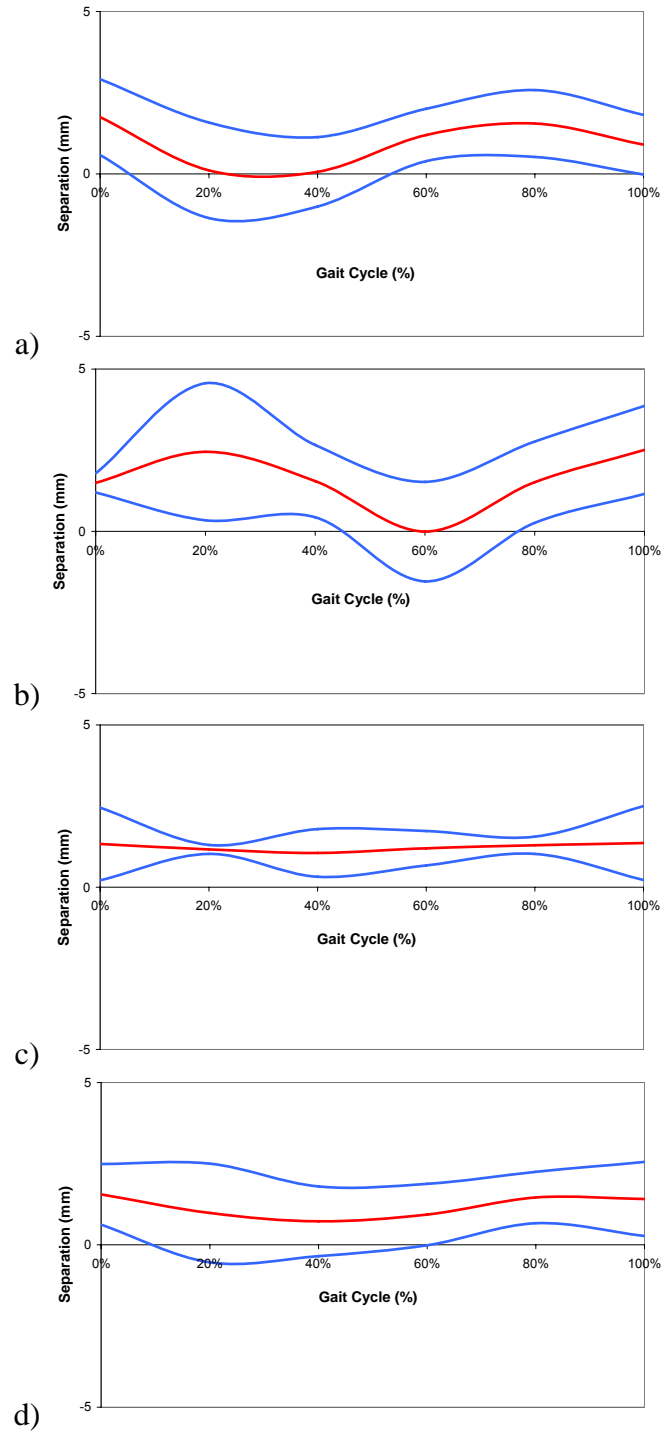


Figure 66: Average separation (red) and ± 1 SD (standard variation, blue) for a) MOM Zimmer large head, b) MOM Biomet large head, c) MOM Biomet medium head and d) all MOM groups

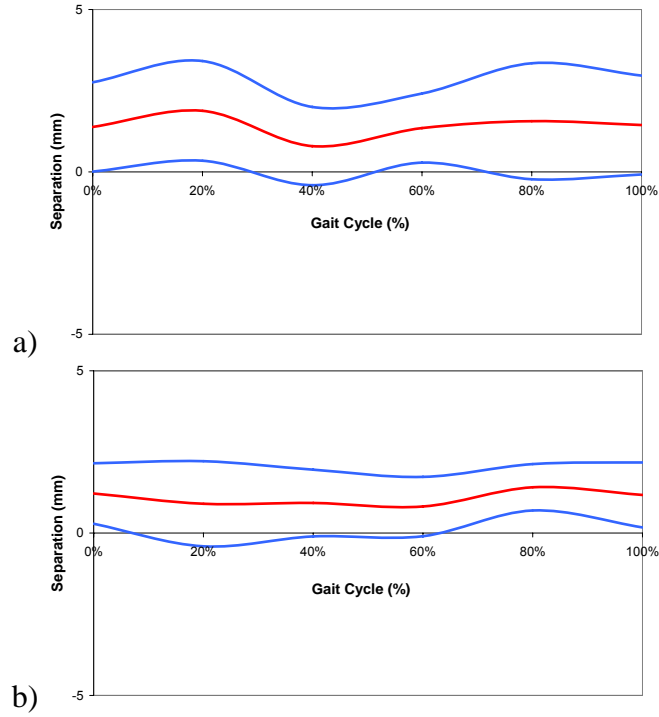


Figure 67: Average separation (red) and ± 1 SD (standard variation, blue) for a) hard on soft bearings and b) hard-on-hard bearings groups

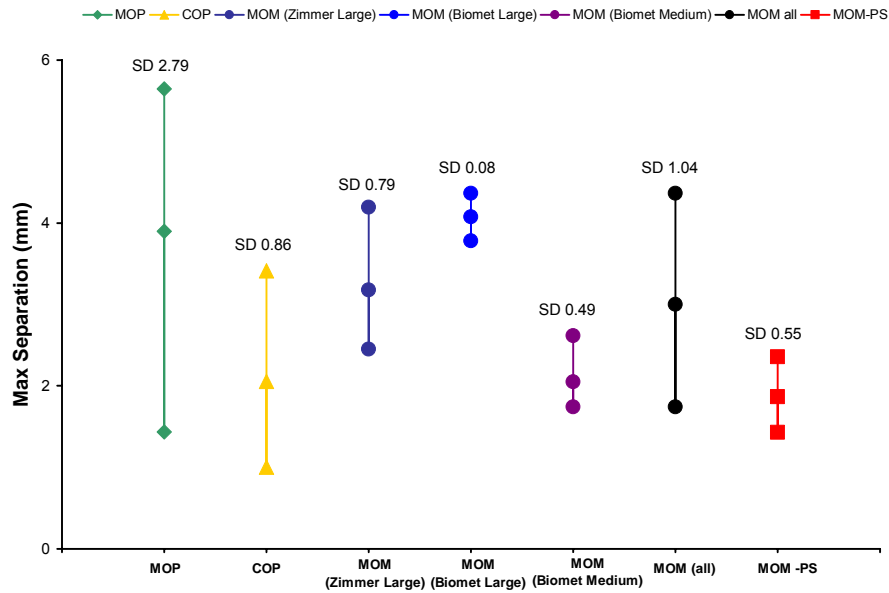


Figure 68: The average maximum separation with standard deviation (SD) for all groups

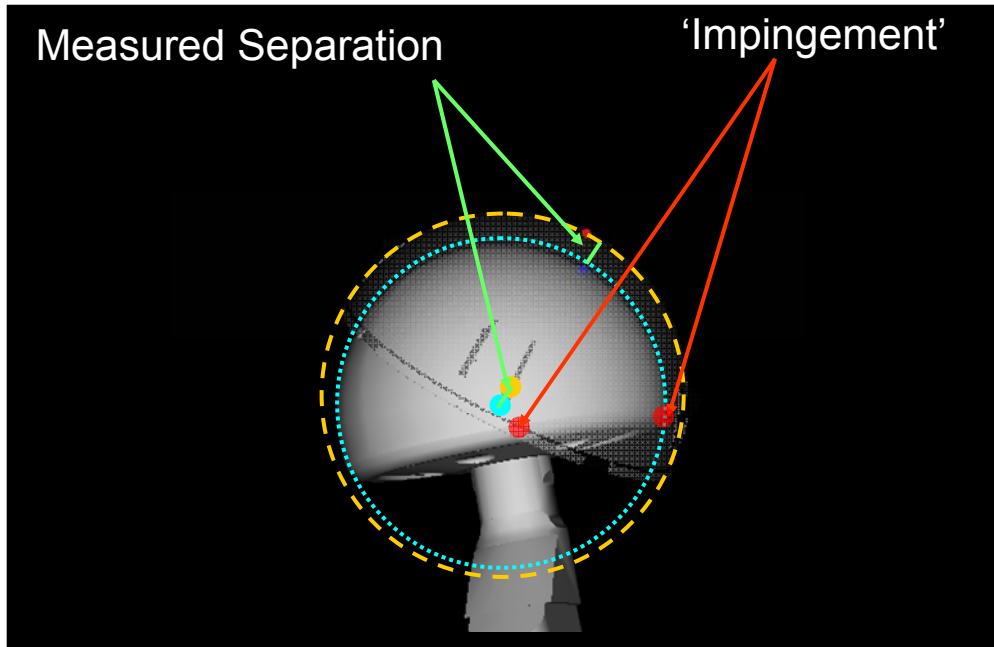


Figure 69: Separation for a large femoral head implant

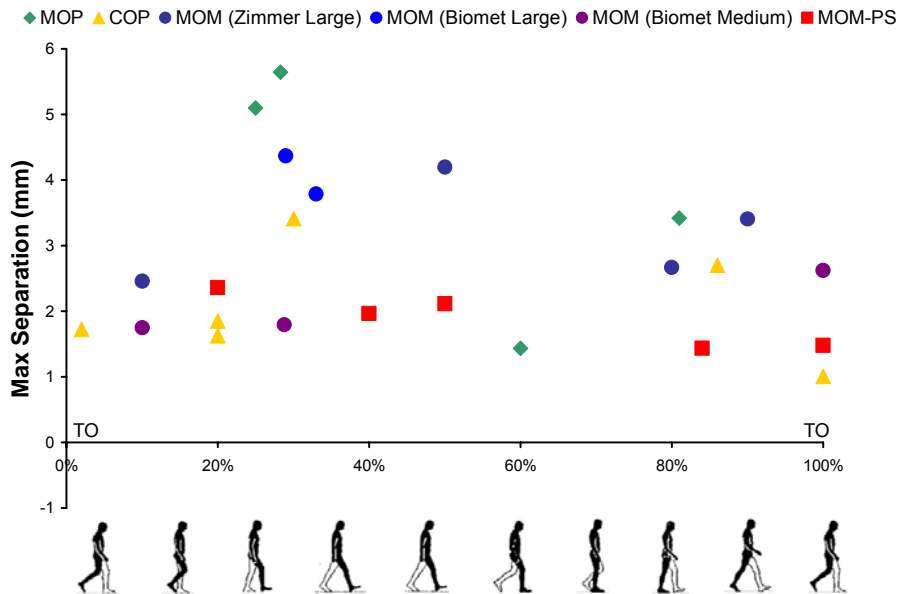


Figure 70: The location of the maximum separation for each patient during the entire gait cycle

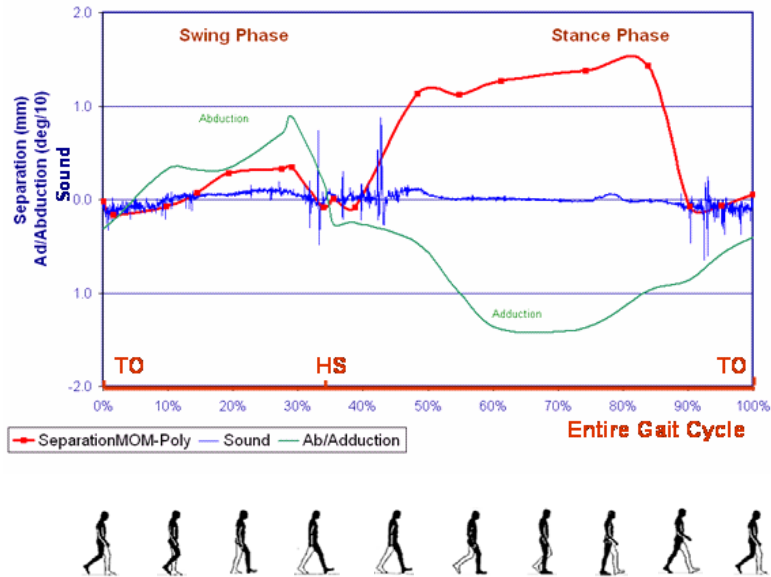


Figure 71: Correlation of separation and sound signal for M/M-PS patient. HS: heel strike, TO: toe-off

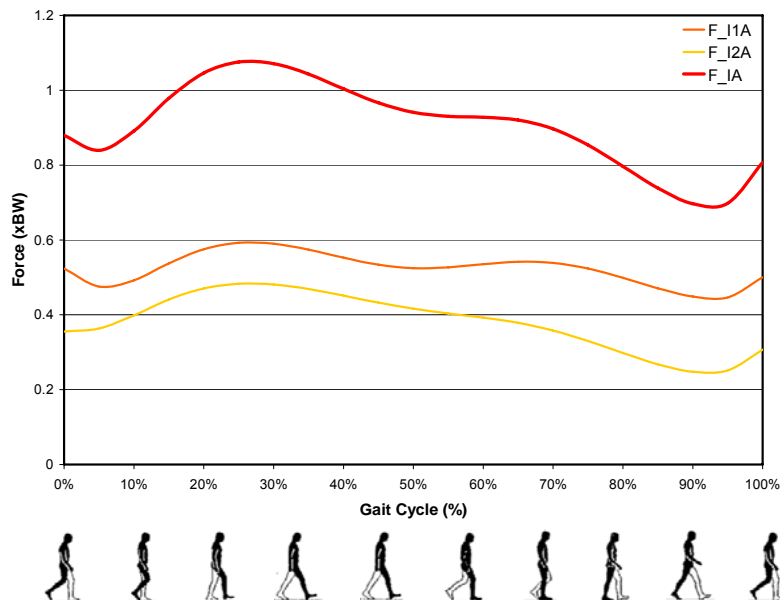


Figure 72: Illofemoral ligament forces for both fibers and the entire Illofemoral force (F_IA) for an example patient

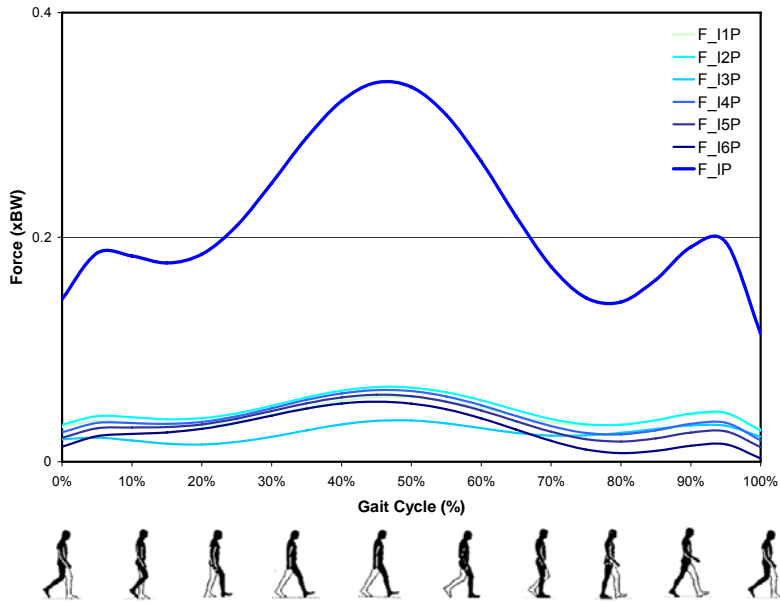


Figure 73: Ischiofemoral ligament forces for all 6 fibers and the entire ischiofemoral force (F_IP) for an example patient

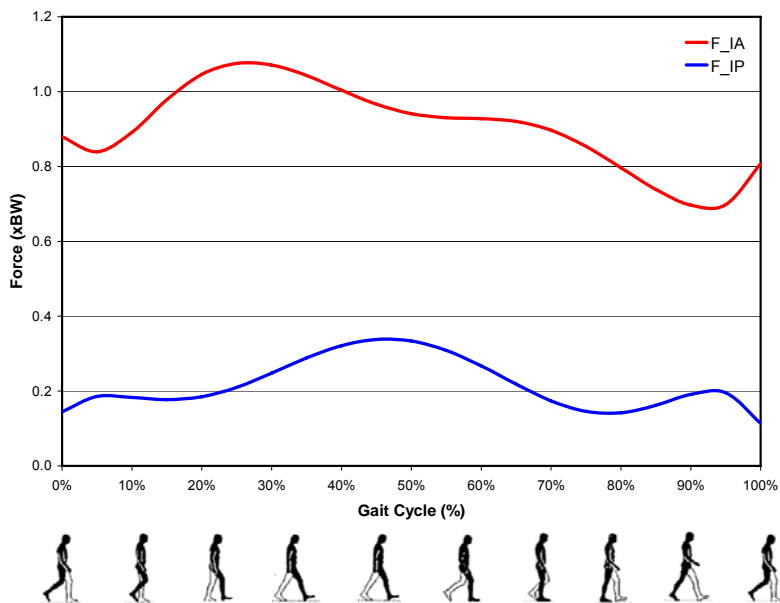


Figure 74: Iliofermal and the Ischiofemoral ligament forces for an example patient

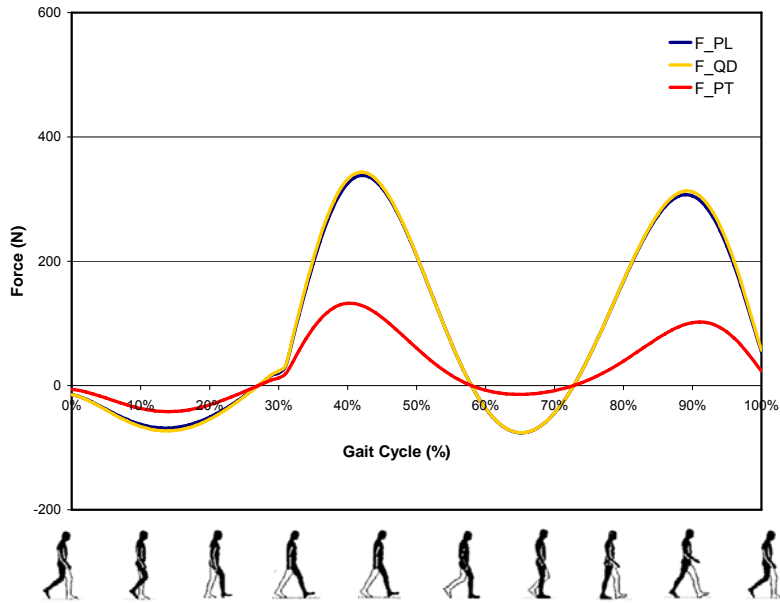


Figure 75: Patellar ligament, quadriceps and patellar force for an example patient

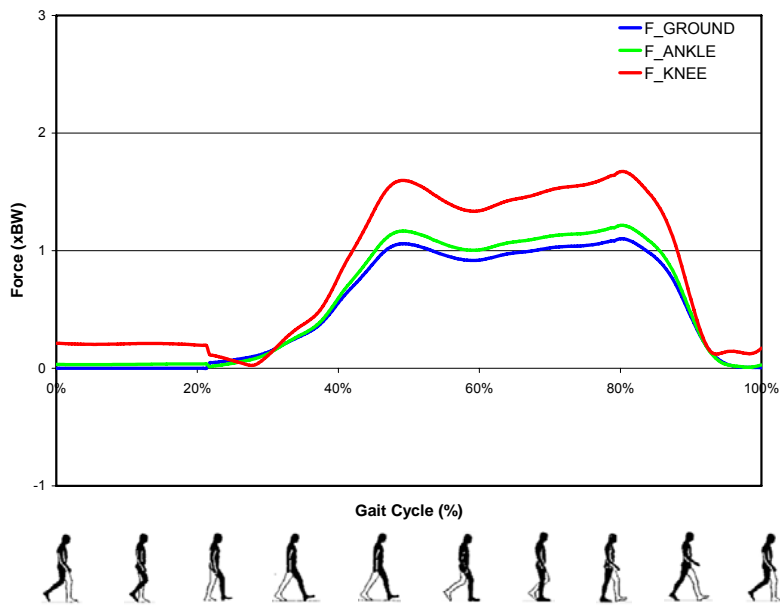


Figure 76: Joint reaction forces for the ankle and the knee as well as ground reaction forces for an example patient.

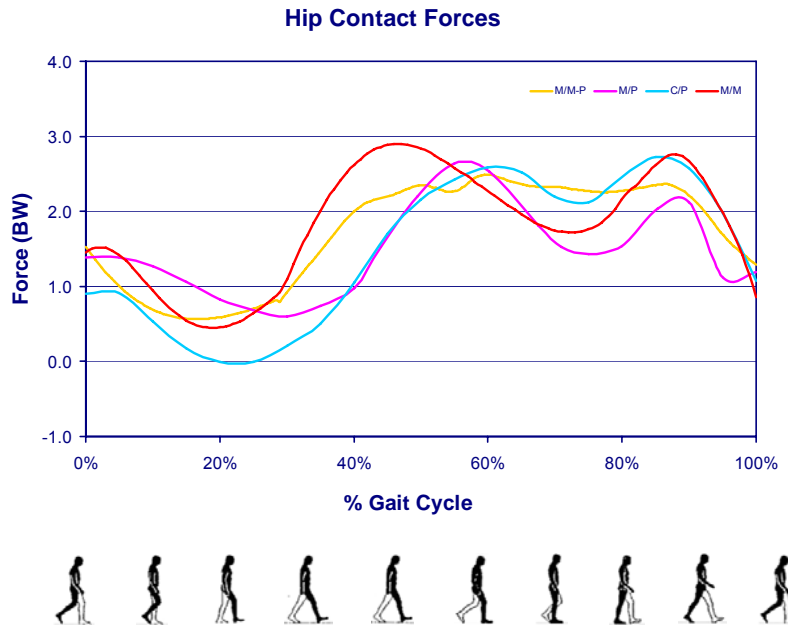


Figure 77: Hip contact forces for the different bearing groups.

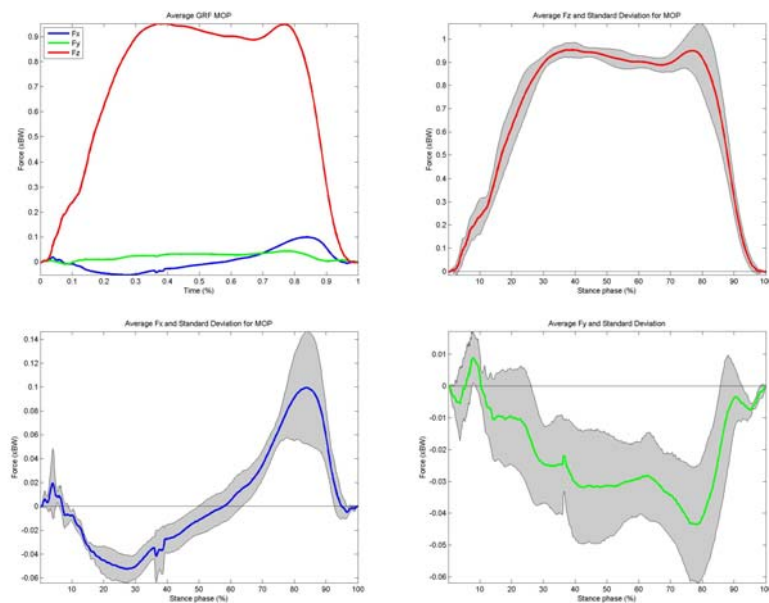


Figure 78: Ground reaction forces for the metal-on-polyethylene group – top left: average forces, top right: vertical average force with SD intervals, bottom left: average force in x-direction with SD intervals, bottom right: average force in y-direction with SD intervals.

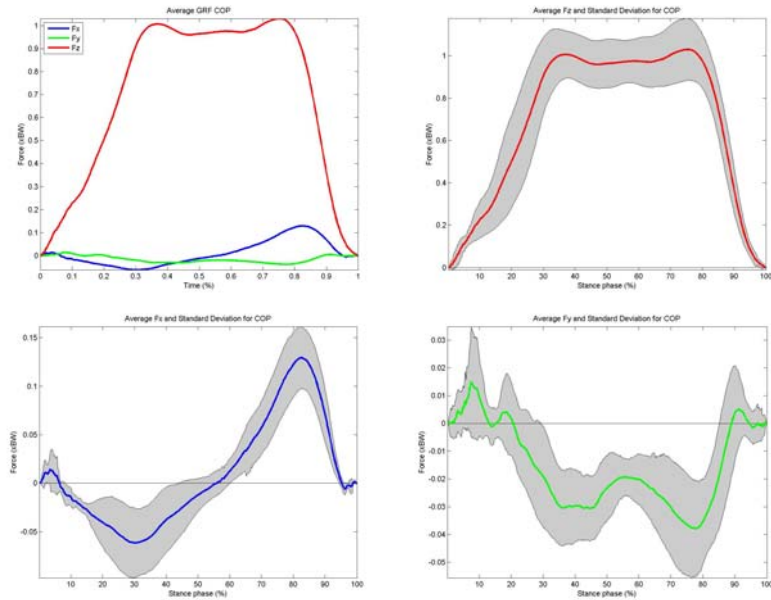


Figure 79: Ground reaction forces for the ceramic-on-polyethylene group – top left: average forces, top right: vertical average force with SD intervals, bottom left: average force in x-direction with SD intervals, bottom right: average force in y-direction with SD intervals.

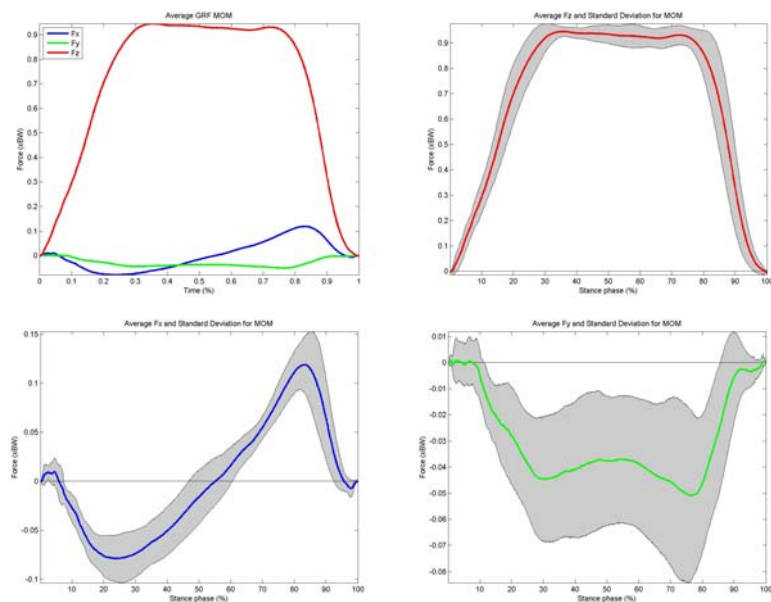


Figure 80: Ground reaction forces for the metal-on-metal group – top left: average forces, top right: vertical average force with SD intervals, bottom left: average force in x-direction with SD intervals, bottom right: average force in y-direction with SD intervals.

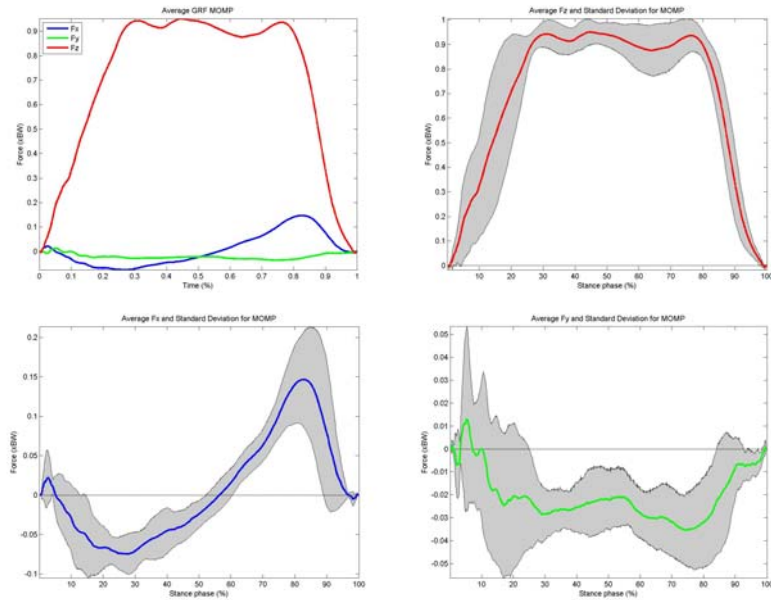


Figure 81: Ground reaction forces for the metal-on-metal polyethylene-sandwich group – top left: average forces, top right: vertical average force with SD intervals, bottom left: average force in x-direction with SD intervals, bottom right: average force in y-direction with SD intervals.

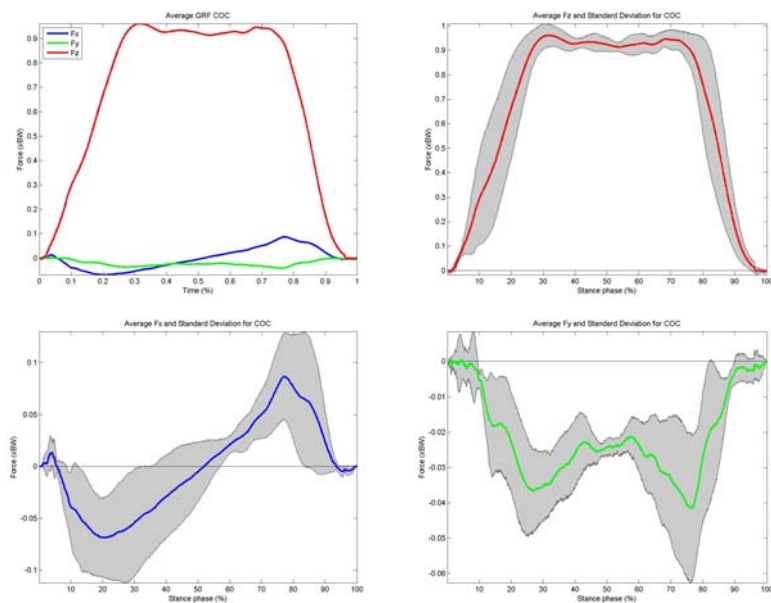


Figure 82: Ground reaction forces for the ceramic-on-ceramic group – top left: average forces, top right: vertical average force with SD intervals, bottom left: average force in x-direction with SD intervals, bottom right: average force in y-direction with SD intervals.

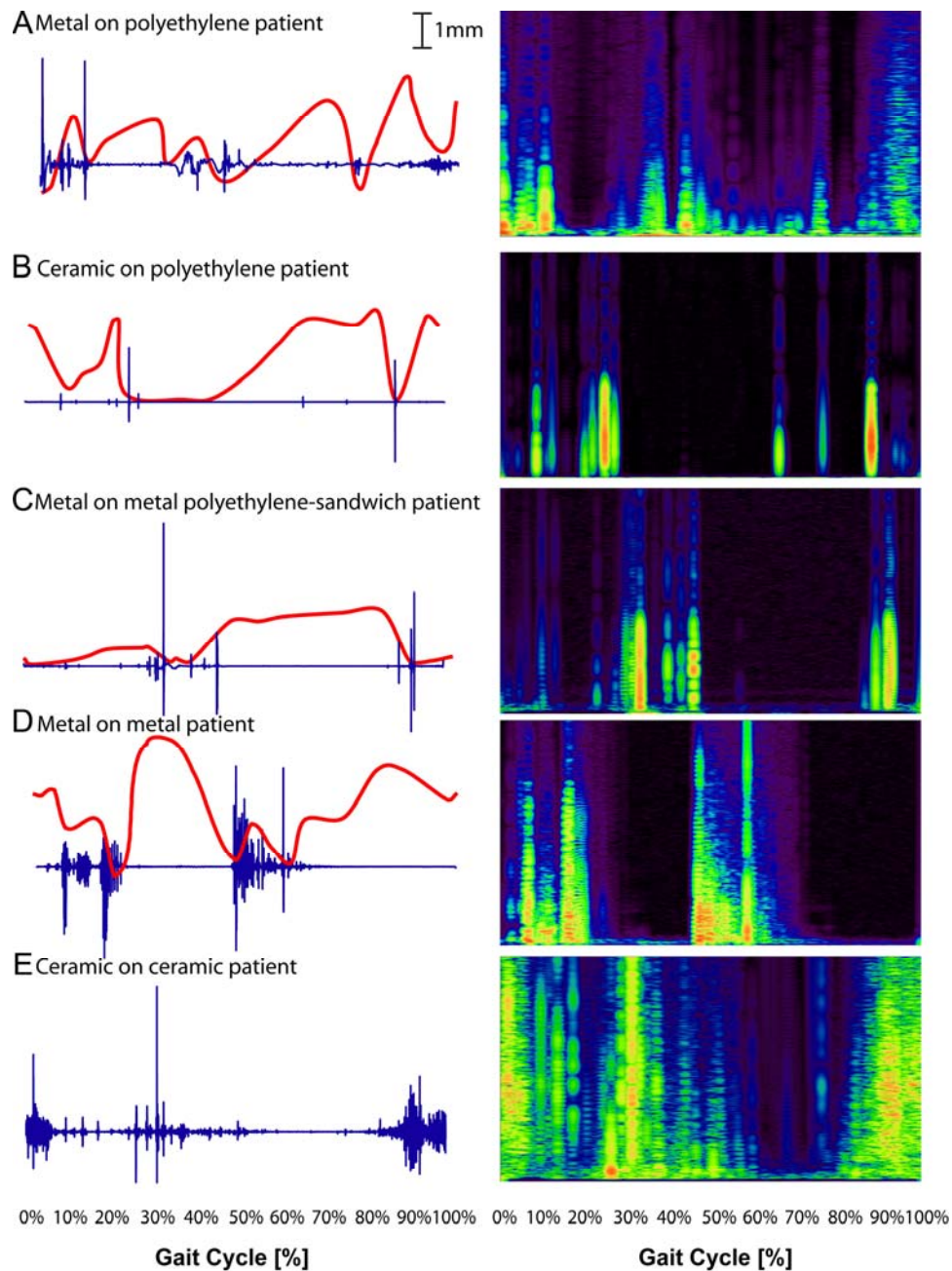


Figure 83: Correlation of separation (red) and sound (blue) signal for example patients. a) damp knocking, b) and c) knocking, d) and e) squeaking combined with some knocking components. Left: Signal in time domain (x-Axis: Time in % of gait cycle starting with toe off, y-Axis: Signal Amplitude); Right: Time-frequency spectrogram (x-Axis: Time in % of gait cycle, y-Axis: Frequency in Hz)

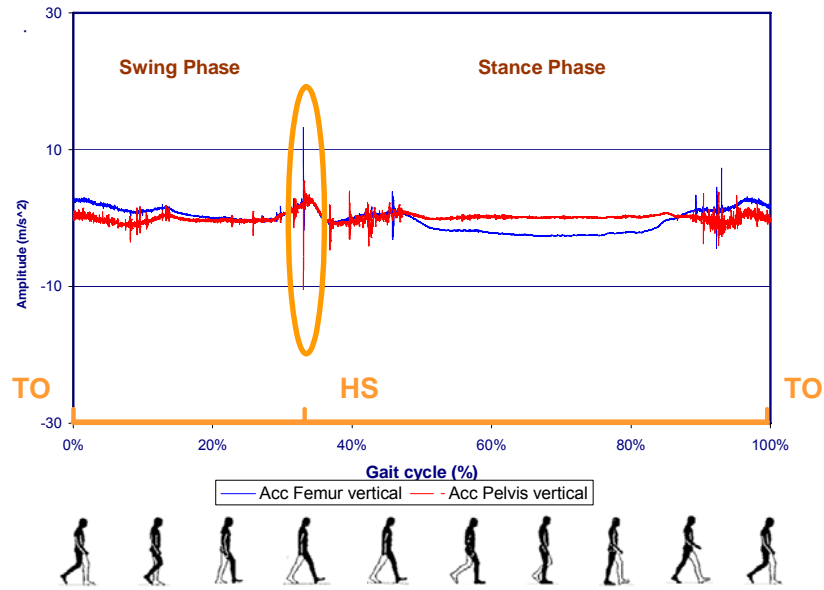


Figure 84: Signal from accelerometers attached to femur and pelvis, showing the various vibration patterns. HS: heel strike, TO: toe-off

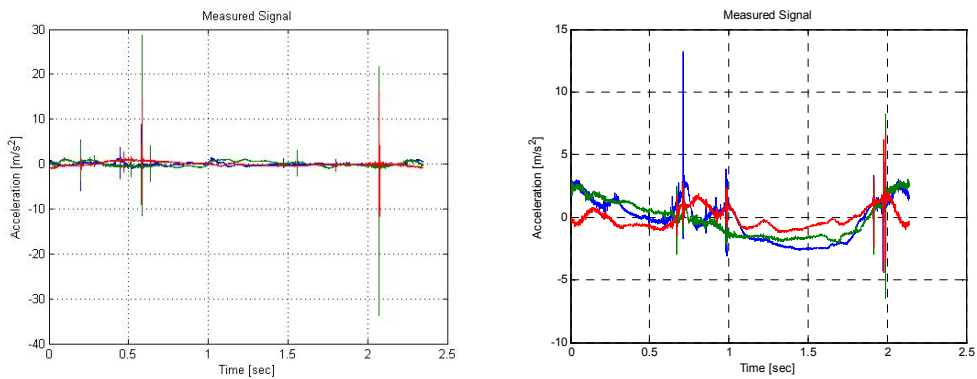


Figure 85: Acceleration signal measured on two example patients

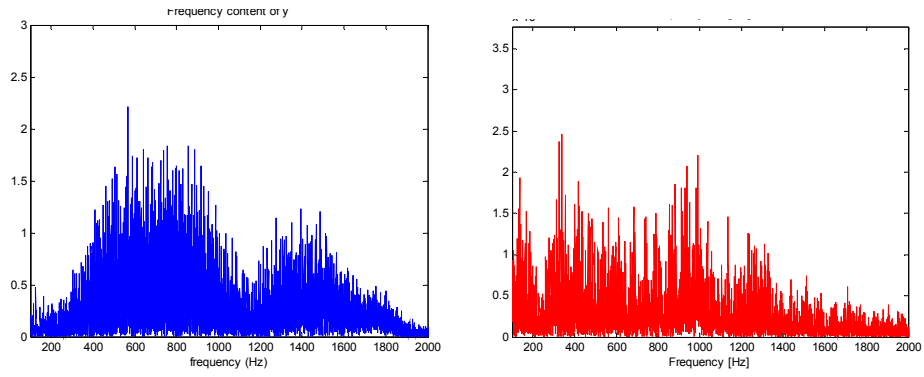


Figure 86: Frequency content

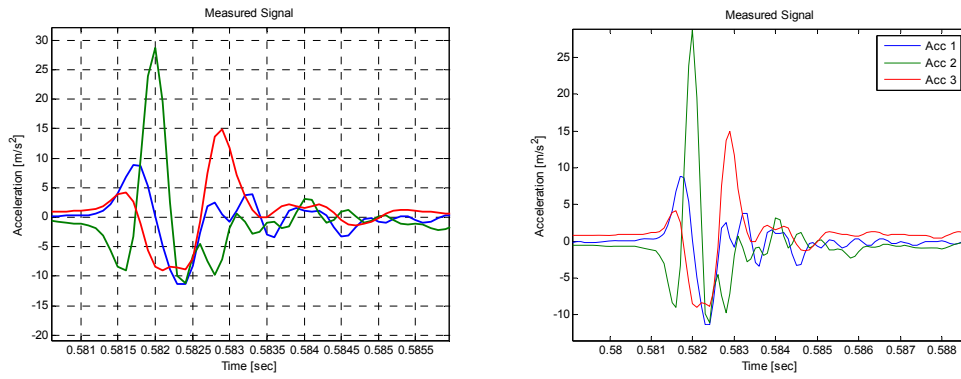


Figure 87: Isolated areas of the signal

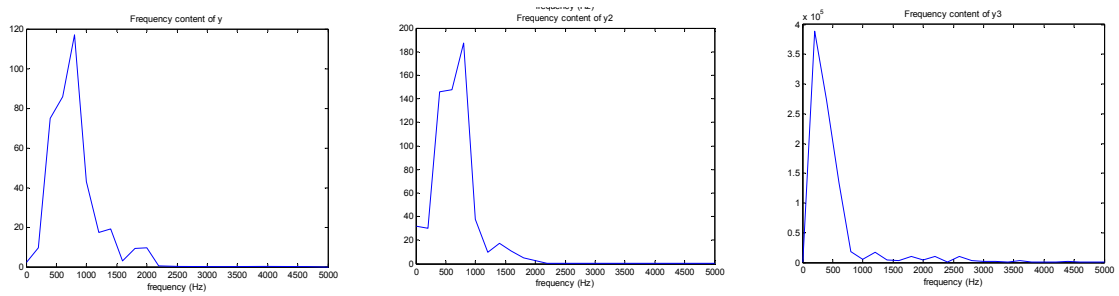


Figure 88: Frequency content of the isolated time interval

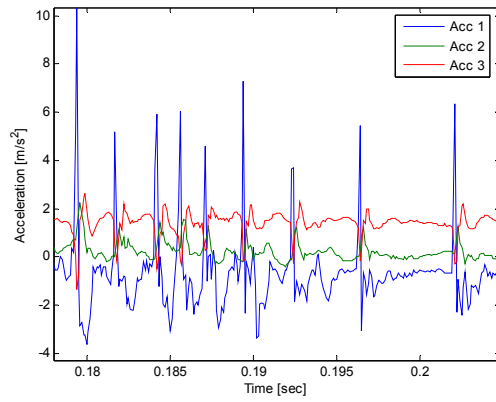


Figure 89: Waveform identified with MOM patients

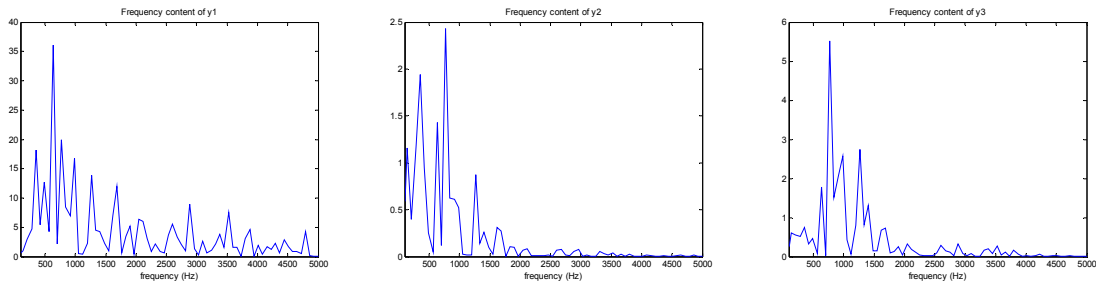


Figure 90: Frequency content of a MOM patient

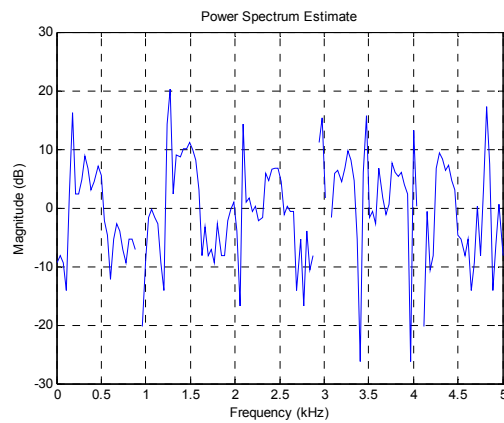


Figure 91: Pseudospectrum of a MOM patient

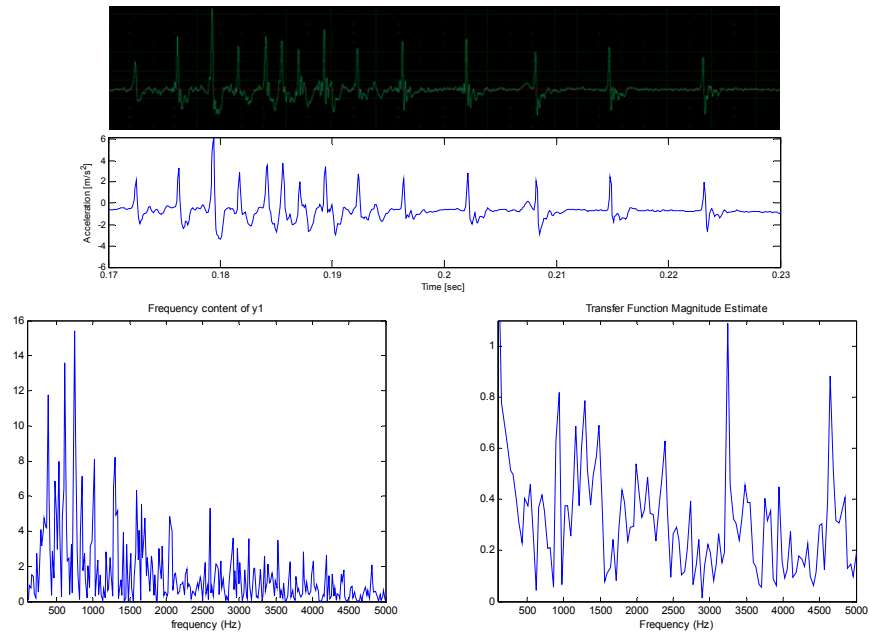


Figure 92: 'Rusty door hinge' signal wave form, FFT and transfer function

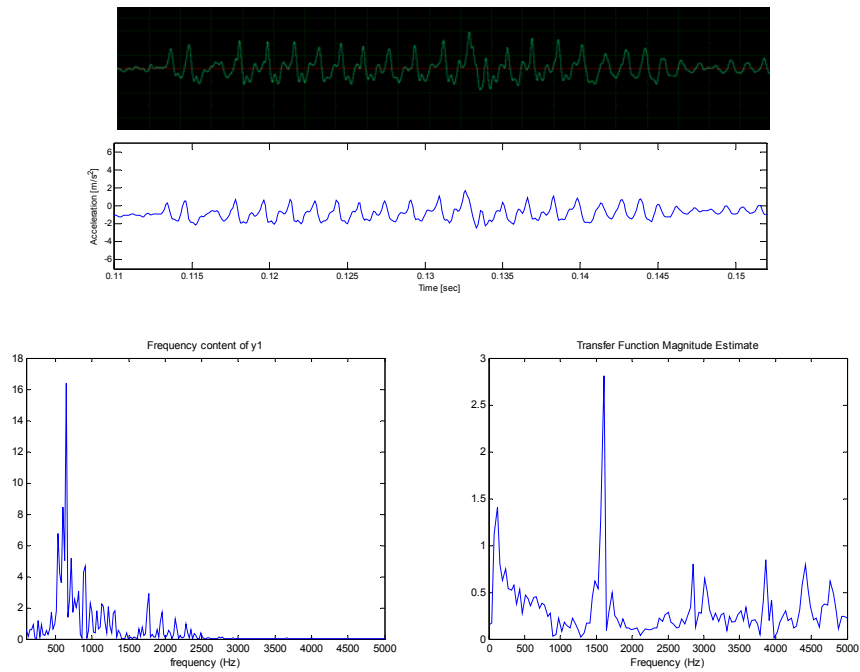


Figure 93: Crepitus signal wave form, FFT and transfer function

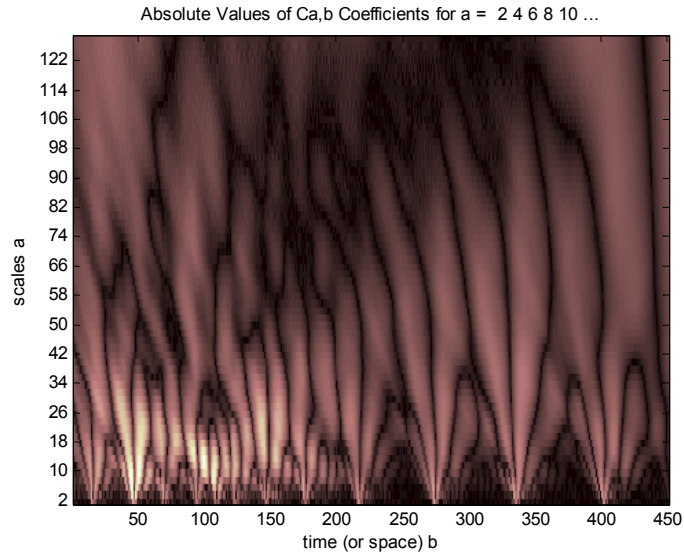


Figure 94: 'Rusty door hinge' signal wavelet analysis function

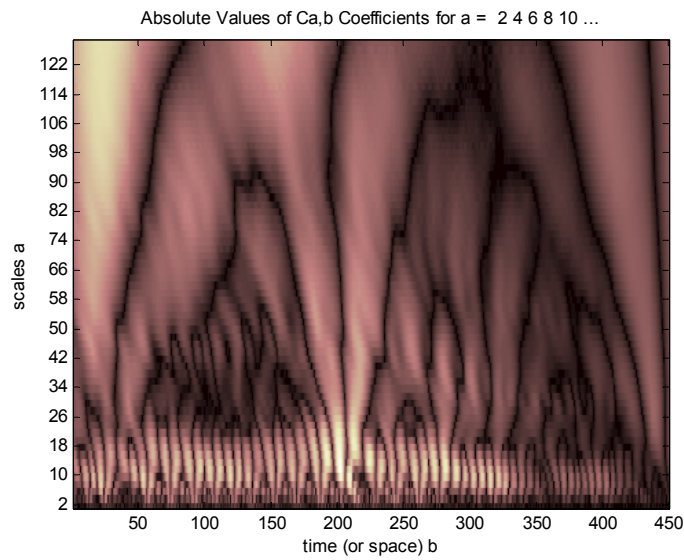


Figure 95: Crepitus signal wavelet analysis

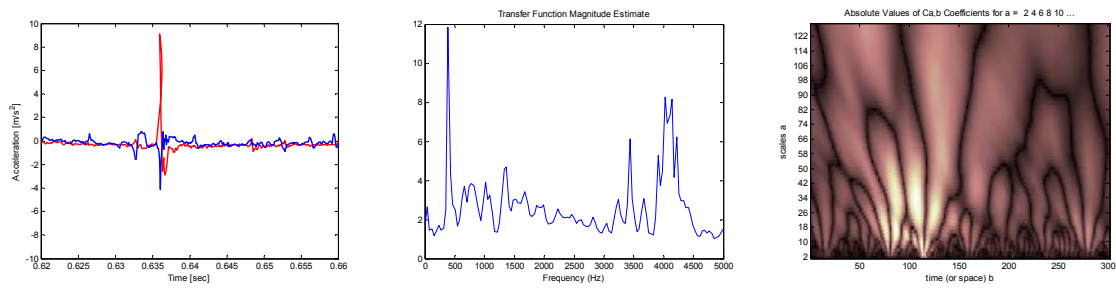


Figure 96: Signal of a MOM patient: wave form, transfer function and wavelet analysis function

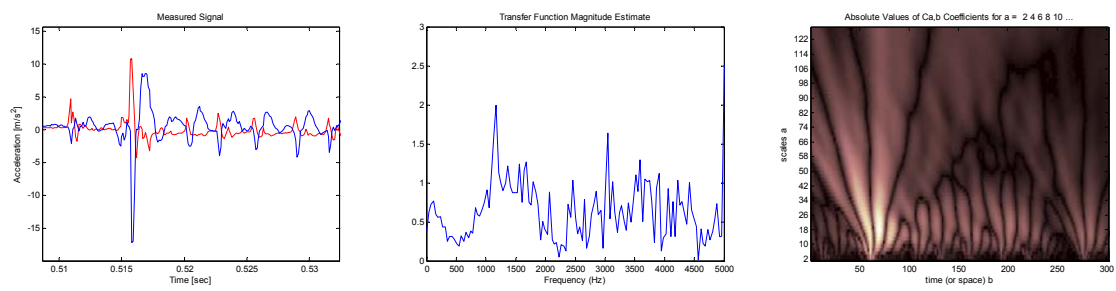


Figure 97: Signal of a MOM patient: wave form, transfer function and wavelet analysis function

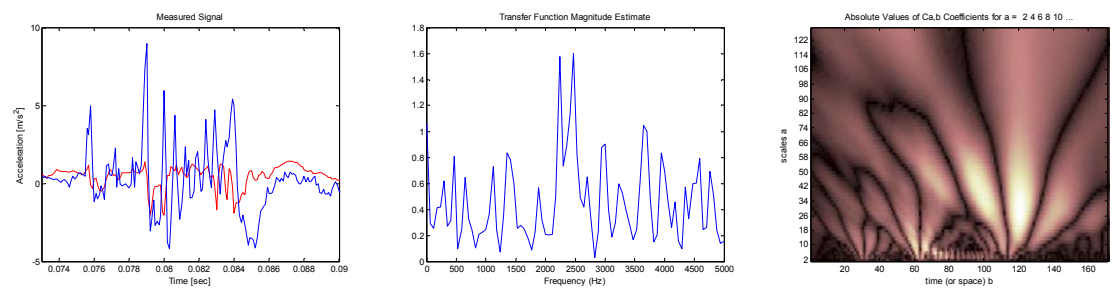


Figure 98: Signal of a MOM patient: wave form, transfer function and wavelet analysis function

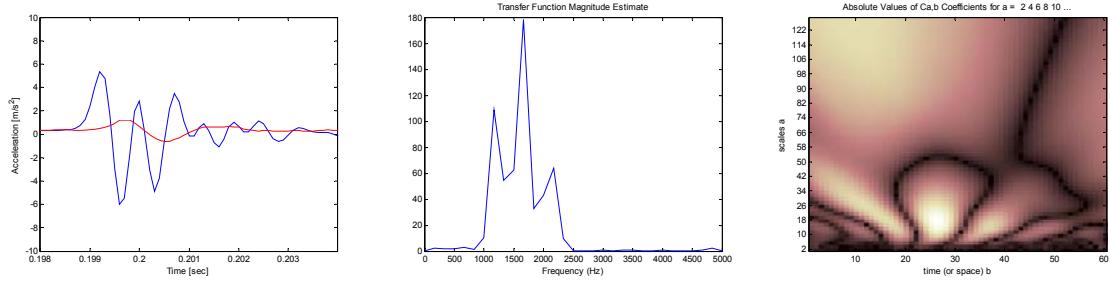


Figure 99: Signal of a COP patient: wave form, transfer function and wavelet analysis function

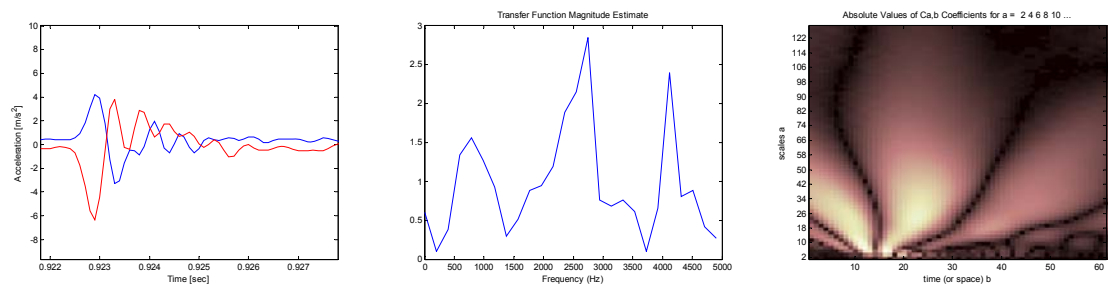


Figure 100: Signal of a MOM patient with small diameter femoral head: wave form, transfer function and wavelet analysis function

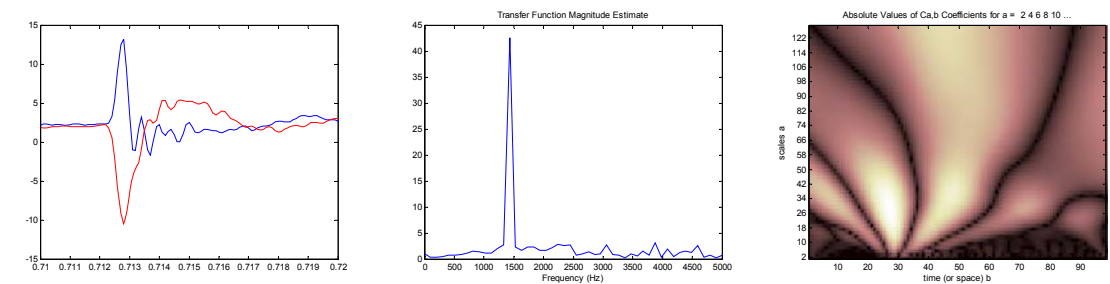


Figure 101: Signal of a MOM-PS patient: wave form, transfer function and wavelet analysis function

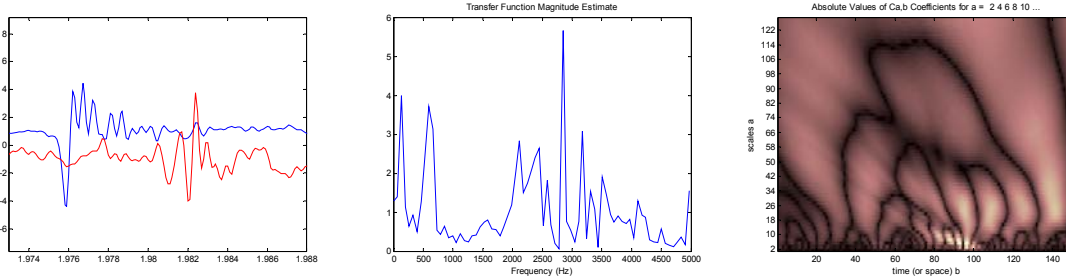


Figure 102: Signal of a MOM-PS patient: wave form, transfer function and wavelet analysis function

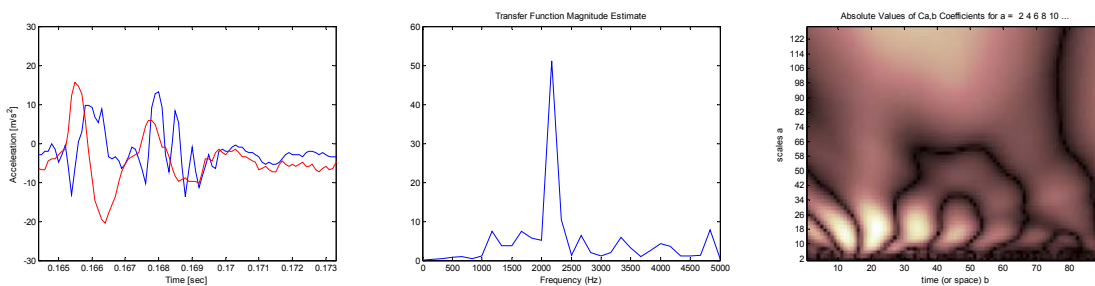


Figure 103: Signal of a MOP patient: wave form, transfer function and wavelet analysis function

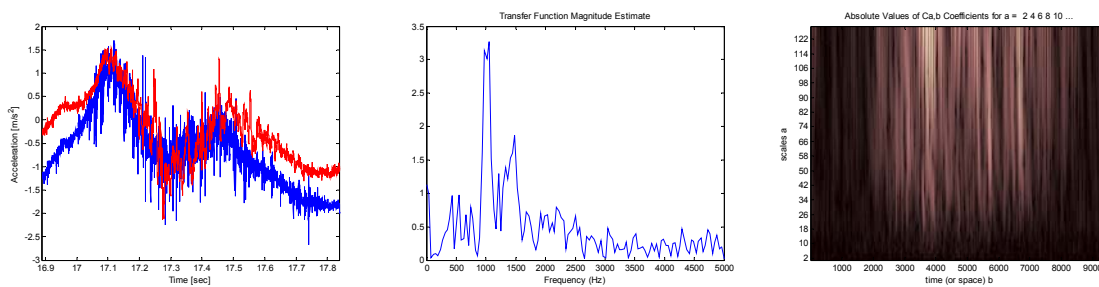


Figure 104: Signal of a COC patient: wave form, transfer function and wavelet analysis function

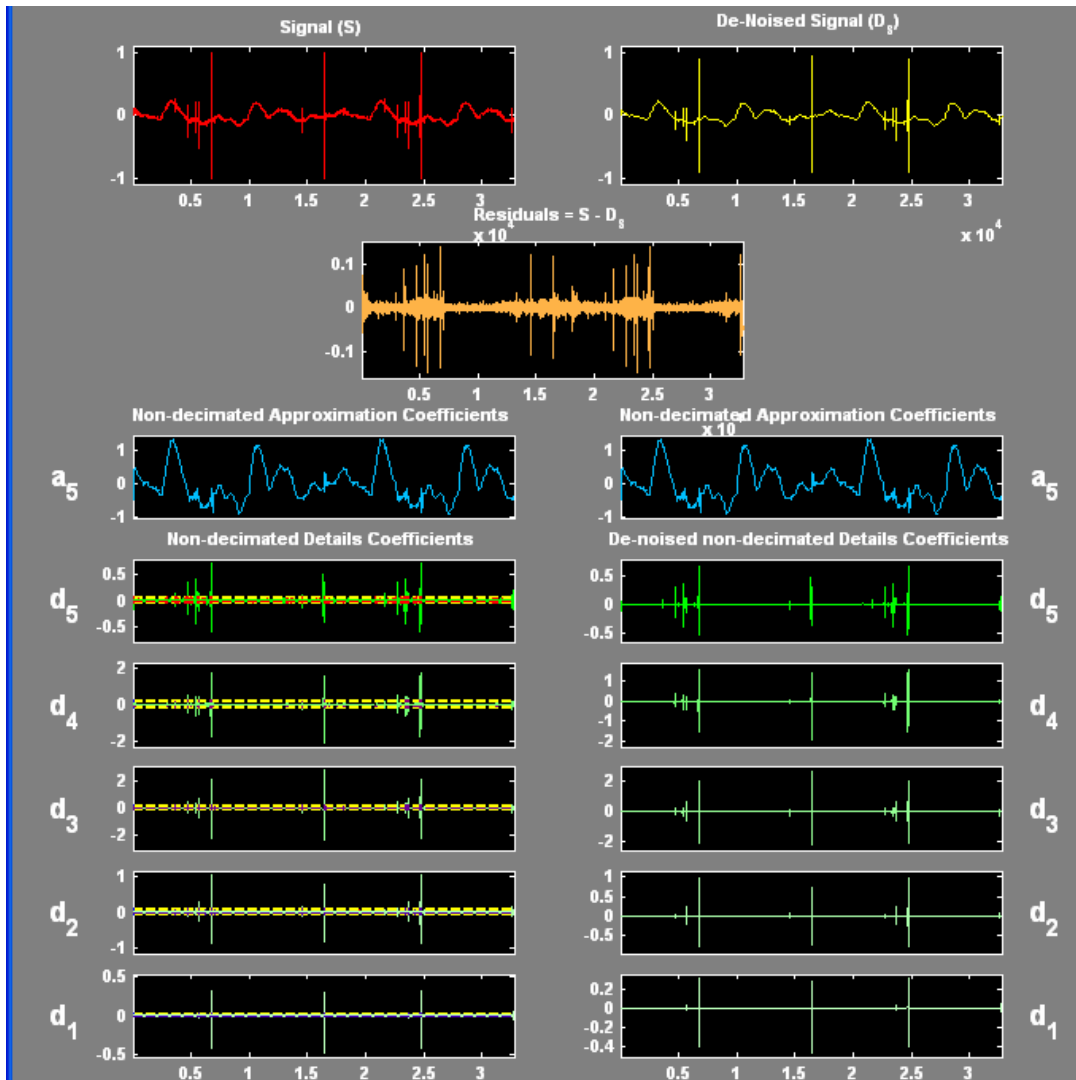


Figure 105: Wavelet analysis and denoising for an example signal: approximation and detail coefficients

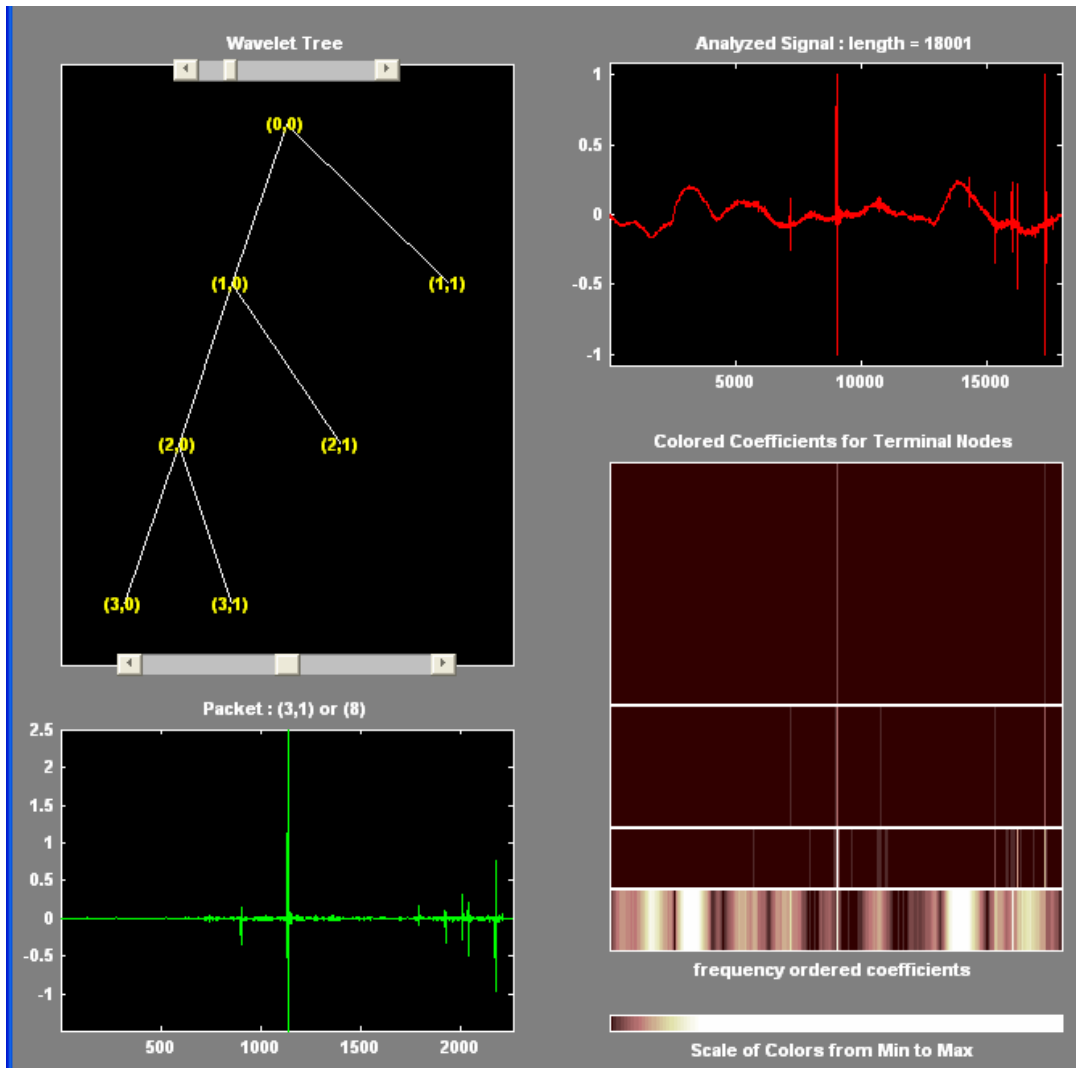


Figure 106: 3-Level wavelet tree and analysis of the (3,1) level

Vita

Diana Andreeva Glaser was born and raised in Sofia, Bulgaria on February 28, 1977. Later she moved to Juelich, Germany, where she graduated from the Zitadelle High School in 1996. She received a Diplom Ingenieur degree (German equivalent of M.S. degree) in Civil Engineering from the RWTH-Aachen Technical University, Germany in 2001. Her thesis, granted by Hochtief AG, Germany, focused on the numerical analysis of the dynamical behavior of a locomotive construction. Afterwards, Diana worked for 3 years as mechanical engineer in the area of static and dynamic analysis. She was involved also in vibration, fatigue and buckling strength analysis. In 2005 Diana was accepted into the Ph.D. program at the University of Tennessee, at which time she also began a graduate research assistantship in the Center for Musculoskeletal Research (CMR). Her Ph.D. program and research work was performed under the supervision of Dr. Richard D. Komistek from the Biomedical Engineering Department. Within the CMR program she was involved in different projects including *in vivo* analysis of hip and knee joint mechanics, 3D patient-specific mathematical modeling, and biomedical applications of DAQ systems. Her personal research in CMR towards the Ph.D. program involved the development and implementation of hip mechanics and a newly developed non-invasive acoustic and vibration analysis method for the evaluation of hip joint performance. She graduated with doctorate degree in Mechanical Engineering from the University of Tennessee in summer 2008.